Issue 2 2022 | Volume 18

The Journal on Advanced Studies in Theoretical and Experimental Physics, including Related Themes from Mathematics

PROGRESS IN PHYSICS

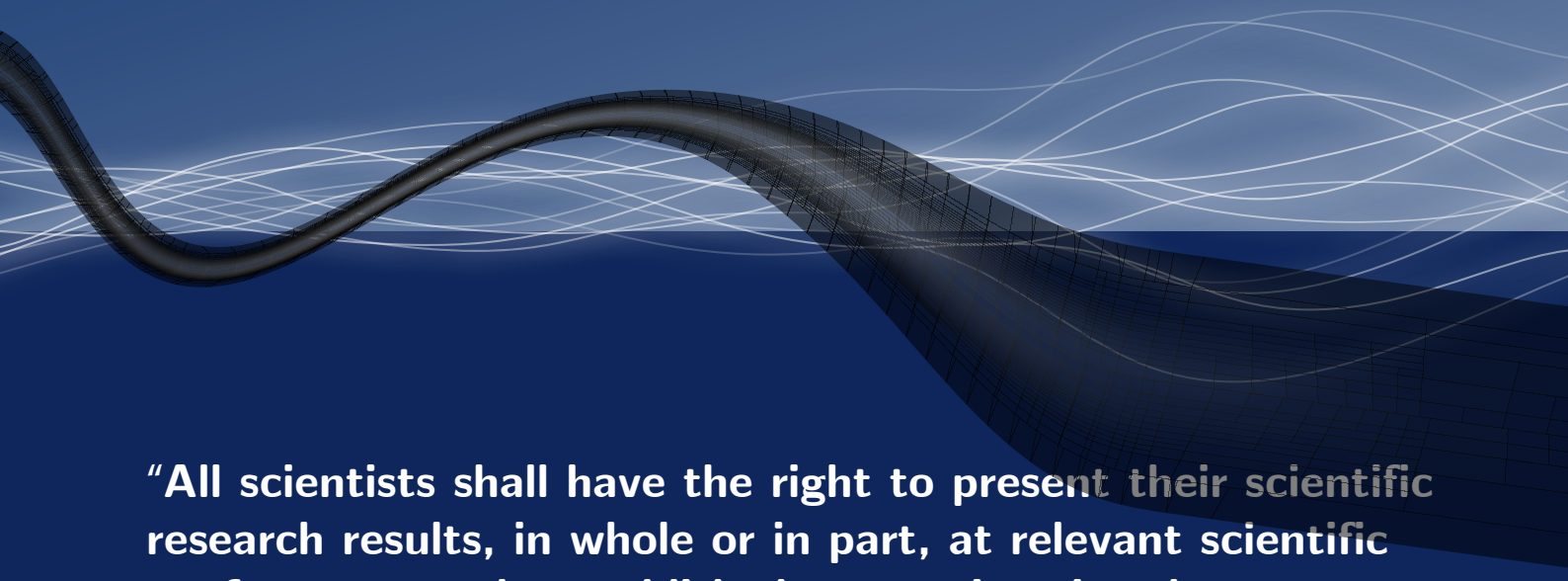

"All scientists shall have the right to present their scientific research results, in whole or in part, at relevant scientific conferences, and to publish the same in printed scientific journals, electronic archives, and any other media." — Declaration of Academic Freedom, Article 8

ISSN 1555-5534

PROGRESS IN PHYSICS

A Scientific Journal on Advanced Studies in Theoretical and Experimental Physics, including Related Themes from Mathematics. This journal is registered with the Library of Congress (DC, USA).

Electronic version of this journal:
http://www.ptep-online.com

Postal Address

Department of Mathematics and Science,
University of New Mexico,
705 Gurley Ave., Gallup, NM 87301, USA

ISSN: 1555-5534 (print)
ISSN: 1555-5615 (online)

Standard Address Number: 297-5092
Printed in the United States of America

October 2022 **Vol. 18, Issue 2**

CONTENTS

Information for Authors

Progress in Physics has been created for rapid publications on advanced studies in theoretical and experimental physics, including related themes from mathematics and astronomy. All submitted papers should be professional, in good English, containing a brief review of a problem and obtained results.

All submissions should be designed in LaTeX format using *Progress in Physics* template. This template can be downloaded from *Progress in Physics* home page http://www.ptep-online.com

Preliminary, authors may submit papers in PDF format. If the paper is accepted, authors can manage LaTeXtyping. Do not send MS Word documents, please: we do not use this software, so unable to read this file format. Incorrectly formatted papers (i.e. not LaTeXwith the template) will not be accepted for publication. Those authors who are unable to prepare their submissions in LaTeXformat can apply to a third-party payable service for LaTeX typing. Our personnel work voluntarily. Authors must assist by conforming to this policy, to make the publication process as easy and fast as possible.

Abstract and the necessary information about author(s) should be included into the papers. To submit a paper, mail the file(s) to the Editor-in-Chief.

All submitted papers should be as brief as possible. Short articles are preferable. Large papers can also be considered. Letters related to the publications in the journal or to the events among the science community can be applied to the section *Letters to Progress in Physics*.

All that has been accepted for the online issue of *Progress in Physics* is printed in the paper version of the journal. To order printed issues, contact the Editors.

Authors retain their rights to use their papers published in *Progress in Physics* as a whole or any part of it in any other publications and in any way they see fit. This copyright agreement shall remain valid even if the authors transfer copyright of their published papers to another party.

Electronic copies of all papers published in *Progress in Physics* are available for free download, copying, and re-distribution, according to the copyright agreement printed on the titlepage of each issue of the journal. This copyright agreement follows the *Budapest Open Initiative* and the *Creative Commons Attribution-Noncommercial-No Derivative Works 2.5 License* declaring that electronic copies of such books and journals should always be accessed for reading, download, and copying for any person, and free of charge.

Consideration and review process does not require any payment from the side of the submitters. Nevertheless the authors of accepted papers are requested to pay the page charges. *Progress in Physics* is a non-profit/academic journal: money collected from the authors cover the cost of printing and distribution of the annual volumes of the journal along the major academic/university libraries of the world. (Look for the current author fee in the online version of *Progress in Physics*.)

How to Couple the Space-Time Curvature With the Yang-Mills Theory

Patrick Marquet
Calais, France. E-mail: patrick.marquet6@wanadoo.fr

We suggest here a new approach to couple space-time curvature with the three fundamental forces (interactions) of the standard model described by the Yang-Mills Theory. This is achieved through the extension of the Einstein tensor in the framework of the Weyl formalism (Weyl-Einstein tensor) which is known to exhibit a particular 4-vector referred to as the Weyl-Einstein vector. The Weyl-Einstein manifold so defined admits a tangent Minkowski space at a given point, where this particular vector asymptotically identifies with the Yang-Mills gauge field vectors. As a result, the Weyl-Einstein tensor implicitly interacts with the particles' masses and fields provided by the Yang-Mills equations. Assuming that the principle of equivalence always holds, a very simple grand unification with gravity could be achieved in this way.

Notations

Space-time Greek indices α, β run from 0, 1, 2, 3 for local coordinates.
Latin indices a, b are the group indices.
Space-time signature is -2.
We assume here that $c = 1$.

Introduction

Fields Φ are used to describe the fundamental particles known in modern physics. In Quantum Electrodynamics such fields associated with these particles must be chosen consistent with the symmetries in nature which include for example the space-time symmetries of Special Relativity. The fields Ψ are either scalars (neutral or charged) with spin-zero/spin-1 particles, or fermions with spin-$\frac{1}{2}$ particles. Initially, it was thought that these symmetries should be global symmetries, not depending on the position in space and time. However, it is well known that the laws of electromagnetism possess another *local symmetry*, in which charge is locally conserved, meaning that charged fields have a phase (in the exponent) that varies freely from point to point. This feat led Yang and Mills to suggest that local symmetries be extended from this U(1) group to non *Abelian symmetries* based on *local* gauge invariance which open the way to unify the electromagnetism, weak and strong interactions: U(1) × SU(2) × SU(3) is today known as the *standard model* elaborated by Glashow, Weinberg, Salam and Ward (1979 Nobel Prize). As we know, this theory implies the existence of *gauge fields* $A_\mu(x)$, which are necessarily part of a new covariant derivative $\mathrm{D}_\mu = \partial_\mu - i\mathrm{e}Am(x)$, where e is a coupling constant (see §2.1). In a curved space-time, the classical theory makes use of the Riemann derivative ∇_μ, and D_μ is thus generalized to $\nabla_\mu - i\mathrm{e}A_\mu(x)$ (see, for example, [1, p. 68]). However, the gauge fields $A_\mu(x)$, do not account for the space-time curvature except in the case of the electromagnetic field alone through the Einstein field equations.

Herein, we tackle this problem in a different way:

a) We start by defining a *Weyl connection* that exhibits a particular 4-vector (Weyl-Einstein vector) which induces extended curvature tensors;

b) From these curvatures is inferred the *Weyl-Einstein tensor* which is conceptually conserved like its standard counterpart which it generalizes;

c) A simple relation is established whereby the Weyl-Einstein 4-vector is asymptotically related to the Yang-Mills field vectors.

All three contributions (electromagnetic, weak and strong interactions) are then permitted to interact with the Weyl-Einstein 4-tensor through their respective gauge field vectors alone. A simple grand unification could be achieved through this particular coupling.

1 The Weyl-Einstein tensor

1.1 The curvatures

1.1.1 General issues

Following Lichnerowicz [2], we start by defining the *symmetric Weyl-Einstein connection* on a semi-metric 4-manifold denoted by $\mathfrak{M}$, i.e.

$$W^\alpha_{\mu\nu} = \Gamma^\alpha_{\mu\nu} - \frac{1}{2}\, g^{\alpha\beta}\left(g_{\mu\beta}J_\nu + g_{\nu\beta}J_\mu - g_{\mu\nu}J_\beta\right) \tag{1.1}$$

or, in another form,

$$W^\alpha_{\mu\nu} = \Gamma^\alpha_{\mu\nu} - \frac{1}{2}\left(\delta^\alpha_\mu J_\nu + \delta^\alpha_\nu J_\mu - g_{\mu\nu}J^\alpha\right). \tag{1.1bis}$$

From the point m in the neighbourhood of the Lorentz manifold denoted (M, g), where $\exists$ is a congruence of differentiable lines such that $\forall m' \in (\mathrm{M}, \mathrm{g})$, we may have the conformal metric

$$ds^2_{\mathrm{W}} = e^J ds^2, \tag{1.1ter}$$

where $J = \int_m^{m'} J_\mu dx^\mu$.

In general, the form $dJ = J_\mu dx^\mu$ is non-integrable. The 4-vector J_μ is referred to as the *Weyl-Einstein vector*.

1.1.2 The Weyl-Einstein 4th rank curvature tensor

With the Weyl connection $W^\alpha_{\mu\nu}$ we construct the *Weyl-Einstein curvature tensor* which is assumed to have the standard form of the Riemann-Christoffel tensor

$$(R^\alpha_{\ \beta\mu\nu})_{\rm W} = \partial_\nu W^\alpha_{\ \beta\mu} - \partial_\mu W^\alpha_{\ \beta\nu} + W^\lambda_{\ \beta\mu} W^\alpha_{\ \lambda\nu} - W^\lambda_{\ \beta\nu} W^\alpha_{\ \lambda\mu}\,. \quad (1.2)$$

Inspection shows that the following identity takes place

$$(R^\rho_{\ \alpha\beta\mu})_{\rm W} + (R^\rho_{\ \mu\alpha\beta})_{\rm W} + (R^\rho_{\ \beta\mu\alpha})_{\rm W} = 0\,. \quad (1.3)$$

Using the Riemann covariant derivative denoted using a semi-colon, the Bianchi identity also reads

$$(R^\rho_{\ \alpha\beta\mu})_{{\rm W}\,;\delta} + (R^\rho_{\ \alpha\delta\beta})_{{\rm W}\,;\mu} + (R^\rho_{\ \alpha\mu\delta})_{{\rm W}\,;\beta} = 0\,. \quad (1.3\text{bis})$$

Let us now express $(R_{\mu\nu\alpha\beta})_{\rm W}$ with the metric connection ∇_β. Setting $(\Gamma^\rho_{\nu\alpha})_{\rm J} = \frac{1}{2}\,(\delta^\rho_\nu J_\alpha + \delta^\rho_\alpha J_\nu - g_{\nu\alpha} J^\rho)$, we obtain

$$\begin{aligned}(R_{\mu\nu\alpha\beta})_{\rm W} = {} & R_{\mu\nu\alpha\beta} + g_{\mu\rho}\nabla_\beta(\Gamma^\rho_{\nu\alpha})_{\rm J} - \\ & - \frac{1}{2}\,g_{\mu\rho}\left[\nabla_\alpha(\Gamma^\rho_{\nu\beta})_{\rm J} + \nabla_\nu(\Gamma^\rho_{\alpha\beta})_{\rm J}\right] + \\ & + g_{\mu\rho}\left[(\Gamma^\rho_{\lambda\beta})_{\rm J}(\Gamma^\lambda_{\nu\alpha})_{\rm J} - (\Gamma^\rho_{\lambda\alpha})_{\rm J}(\Gamma^\lambda_{\nu\beta})_{\rm J}\right] + \\ & + g_{\mu\nu}\left[\partial_\alpha(\Gamma^\rho_{\beta\rho})_{\rm J} - \partial_\beta(\Gamma^\rho_{\alpha\rho})_{\rm J}\right].\end{aligned} \quad (1.4)$$

1.1.3 The Weyl-Einstein 2nd rank tensor

Relation (1.4) eventually leads to the contracted tensor

$$\begin{aligned}(R^\delta_{\ \alpha\beta\delta})_{\rm W} = (R_{\alpha\beta})_{\rm W} = {} & R_{\alpha\beta} + \nabla_\nu(\Gamma^\nu_{\alpha\beta})_{\rm J} - \nabla_\beta(\Gamma^\nu_{\alpha\nu})_{\rm J} + \\ & + (\Gamma^\lambda_{\alpha\beta})_{\rm J}(\Gamma^\nu_{\lambda\nu})_{\rm J} - (\Gamma^\lambda_{\alpha\rho})_{\rm J}(\Gamma^\rho_{\lambda\beta})_{\rm J}\end{aligned}$$

we then have the splitting

$$(R_{\alpha\beta})_{\rm W} = (R_{(\alpha\beta)})_{\rm W} + (R_{[\alpha\beta]})_{\rm W}\,, \quad (1.5)$$

where

$$\begin{aligned}(R_{(\alpha\beta)})_{\rm W} = {} & R_{\alpha\beta} + \nabla_\nu(\Gamma^\nu_{\alpha\beta})_{\rm J} - \frac{1}{2}\left[\nabla_\beta(\Gamma^\nu_{\alpha\nu})_{\rm J} + \nabla_\alpha(\Gamma^\nu_{\beta\nu})_{\rm J}\right] + \\ & + (\Gamma^\lambda_{\alpha\beta})_{\rm J}(\Gamma^\nu_{\lambda\nu})_{\rm J} - (\Gamma^\lambda_{\alpha\rho})_{\rm J}(\Gamma^\rho_{\lambda\beta})_{\rm J}\,,\end{aligned} \quad (1.6)$$

$$(R_{[\alpha\beta]})_{\rm W} = \partial_\alpha(\Gamma^\nu_{\beta\nu})_{\rm J} - \partial_\beta(\Gamma^\nu_{\alpha\nu})_{\rm J}\,. \quad (1.6\text{bis})$$

So forth, we check that $(\Gamma^\rho_{\nu\rho})_{\rm J} = \frac{1}{2}\,(\delta^\rho_\nu J_\rho + \delta^\rho_\rho J_\nu - g_{\nu\rho}J^\rho) = \frac{1}{2}\,(J_\nu + 4J_\nu - J_\nu) = 2J_\nu$. Thus we get

$$(R_{(\alpha\beta)})_{\rm W} = R_{\alpha\beta} - \frac{1}{2}\,(g_{\alpha\beta}\nabla_\nu J^\nu + J_\alpha J_\beta)\,, \quad (1.7)$$

$$(R_{[\alpha\beta]})_{\rm W} = 2\,(\partial_\alpha J_\beta - \partial_\beta J_\alpha) = 2J_{\alpha\beta}\,. \quad (1.8)$$

1.1.4 The Weyl-Einstein curvature scalar

Applying the contraction $R_{\rm W} = g^{\nu\alpha}(R_{\nu\alpha})_{\rm W}$, one obtains

$$\begin{aligned}R_{\rm W} = {} & R - \nabla_\rho\left[g^{\nu\alpha}(\Gamma^\rho_{\nu\alpha})_{\rm J}\right] - \nabla_\rho\left[g^{\nu\rho}(\Gamma^\rho_{\nu\rho})_{\rm J}\right] - \\ & - g^{\nu\alpha}\left[(\Gamma^\rho_{\nu\alpha})_{\rm J}(\Gamma^\nu_{\nu\rho})_{\rm J} - (\Gamma^\lambda_{\nu\rho})_{\rm J}(\Gamma^\rho_{\lambda\alpha})_{\rm J}\right],\end{aligned} \quad (1.9)$$

i.e.,

$$R_{\rm W} = R - \left(\nabla_\rho J^\rho + \frac{1}{2}\,J^2\right). \quad (1.10)$$

1.2 The Weyl-Einstein tensor

Here we omit the subscript $_{\rm W}$ for clarity. Unlike the Riemann-Christoffel curvature tensor, the Weyl curvature tensor is no longer antisymmetric on the pair of indices $\mu\nu$

$$R_{\mu\nu\alpha\beta} + R_{\nu\mu\alpha\beta} = g_{\mu\nu}J_{\alpha\beta}\,, \quad (1.11)$$

or, in another form,

$$R^{\mu\nu}_{\ \ \alpha\beta} + R^{\nu\mu}_{\ \ \alpha\beta} = g^{\mu\nu}J_{\alpha\beta}\,. \quad (1.11\text{bis})$$

Raising the index α in the equation (1.3bis) and contracting on α and μ as well as on μ and δ, we obtain

$$R^{\mu\delta}_{\ \ \beta\mu\,;\delta} + R^{\mu\delta}_{\ \ \mu\delta\,;\beta} = 0\,. \quad (1.12)$$

We next replace $R^{\mu\delta}_{\ \ \delta\beta}$ by its value taken from (1.11bis), and we eventually find

$$R^{\mu\delta}_{\ \ \mu\delta\,;\beta} + 2R^{\mu\delta}_{\ \ \beta\mu\,;\delta} + 2g^{\mu\delta}J_{\delta\beta\,;\mu} = 0\,, \quad (1.13)$$

$$\left(R^{(\delta)}_{\ (\beta)} - \frac{1}{2}\,\delta^\delta_\beta R\right)_{;\delta} = -\,J^\delta_{\ \beta\,;\delta}\,, \quad (1.14)$$

which is just the conservation law for the tensor (re-instating the subscript $_{\rm W}$ and changing the indices)

$$(G_{\alpha\beta})_{\rm W} = (R_{(\alpha\beta)})_{\rm W} - \frac{1}{2}\left(g_{\alpha\beta}R_{\rm W} - 2J_{\alpha\beta}\right). \quad (1.15)$$

We call $(G_{\alpha\beta})_{\rm W}$ the *Weyl-Einstein tensor* expressed with the Riemannian derivatives. Lets us note that $(G_{\alpha\beta})_{\rm W}$ is no longer symmetric. In the pure Riemannian regime, this tensor obviously reduces to the usual Einstein tensor

$$G_{\alpha\beta} = R_{\alpha\beta} - \frac{1}{2}\,g_{\alpha\beta}R\,. \quad (1.16)$$

2 The unification

2.1 A short overview of the Yang-Mills theory

2.1.1 The principle of gauge invariance

Let us recall that a general Lie group G is defined by the representation of a group element denoted U in terms of its generators T^a

$$\mathrm{U} = \exp\left(-i\mathrm{e}\sum_{a=1}^{n}\mathrm{T}^a\mathrm{k}_a\right), \quad (2.1)$$

where e is a coupling constant generalizing the fundamental electronic charge e in the electromagnetic case. The group element U is defined by the values of the N constants k_a, and T^a are hermitian generators satisfying the associated Lie algebra

$$[\mathrm{T}^a,\, \mathrm{T}^b] = i\,\mathrm{C}^{abc}\,\mathrm{T}_c\,, \tag{2.2}$$

where C^{abc} are the real antisymmetric structure constants defining the algebra.

The SU(2) group is defined in terms of the set of all *unitary unimodular matrices* with (2×2) complex elements. The related constraints are known to be

$$\det\|\mathrm{U}\| = 1\,, \tag{2.3}$$

$$\mathrm{U}^{+}\mathrm{U} = \mathrm{U}\mathrm{U}^{+} = \mathrm{I}\,, \tag{2.4}$$

where I is the unit matrix, and U^{+} is the Hermitian conjugate of the matrix U.

2.1.2 Electromagnetism and local gauge invariance U(1)

Consider non-hermitian complex charged scalar fields written in terms of the real fields $\Phi_1(x)$ and $\Phi_2(x)$

$$\Phi(x) = \frac{1}{\sqrt{2}}\,[\Phi_1(x) + i\,\Phi_2(x)]\,, \tag{2.5}$$

$$\Phi^{+}(x) = \frac{1}{\sqrt{2}}\,[\Phi_1(x) - i\,\Phi_2(x)]\,.$$

The classical Lagrangian for this charged scalar field is

$$\mathcal{L} = \partial^{\mu}\Phi^{+}\,\partial_{\mu}\Phi - m^2\Phi^{+}\Phi\,, \tag{2.6}$$

where the first term corresponds to the *kinetic energy* of the scalar field, and the second the *potential energy* of the massive field (mass of the charged particle).

Noether's theorem states that the symmetry of charge conservation is equivalent to the invariance of $\mathcal{L}$ under the group U(1) of continuous phase rotations, specified by a single parameter k.

We then check that this Lagrangian is invariant under the continuous group of phase rotations of Φ called the *global Abelian gauge group* U(1)

$$\Phi(x) \to \Phi(x)\exp i\,\mathrm{k}\,, \tag{2.7}$$

$$\Phi^{+}(x) \to \Phi(x)\exp(-i\,\mathrm{k})\,, \tag{2.7bis}$$

with the real parameter k.

Eqs. (2.7) and (2.7bis) should be true even when the parameter k depends on x^{μ}, thus the phase difference between distinct space-time points is *unobservable*: it is called the *local gauge invariance principle*. However inspection shows that the kinetic energy Lagrangian $\partial^{\mu}\Phi^{+}\partial_{\mu}\Phi$ is not invariant under the local gauge transformation

$$\Phi(x) \to \Phi(x)\exp(-i\,\mathrm{k})\,\mathrm{Q}(x)\,. \tag{2.8}$$

This is because the derivative may now operate on the variable parameter $\mathrm{k}(x)$. To remedy this problem one is forced to introduce a new covariant derivative

$$\mathrm{D}_{\mu} = \partial_{\mu} - i\,\mathrm{e}A_{\mu}(x)\,, \tag{2.9}$$

where Q is the quantity of the charges of the fields Φ which is proportional to the fundamental electronic unit e.

Here, the vector field $A_{\mu}(x)$ transforms as

$$A_{\mu}(x) \to A_{\mu}(x) + \partial_{\mu}\,\mathrm{k}(x)\,. \tag{2.10}$$

Hence, it is also necessary to include a kinetic energy term in $\mathcal{L}$ which takes into account the introduction of the new gauge field $A_{\mu}(x)$. This is achieved by adding the term

$$(\mathcal{L})^{\mathrm{kin}}_{A} = -\frac{1}{4}\,F^{\mu\nu}F_{\mu\nu}\,, \tag{2.11}$$

where we retrieve the electromagnetic field strength tensor

$$F_{\mu\nu} = \partial_{\mu}A_{\nu} - \partial_{\nu}A_{\mu}\,. \tag{2.12}$$

The new Lagrangian is now

$$\mathcal{L} = -\frac{1}{4}\,F^{\mu\nu}F_{\mu\nu} + \mathcal{L}'[\Phi,\, \Phi^{+}\,\mathrm{D}_{\mu}\Phi\,\mathrm{D}_{\mu}\Phi^{+}]\,. \tag{2.13}$$

The tensor $F_{\mu\nu}$ is obviously invariant under the gauge transformation of (2.8), so $(\mathcal{L})^{\mathrm{kin}}_{A}$ is also gauge invariant. This symmetry group is the Abelian group U(1) with a single commuting generator $\mathrm{T}^1 = \mathrm{Q}$ satisfying

$$[\mathrm{T}^1,\, \mathrm{T}^1] = 0\,. \tag{2.14}$$

Unlike the classical theory, the equations of motion are obtained by varying the action $\mathcal{L}$ with respect to A_{μ} for the fixed Φ, i.e.,

$$\partial_{\nu}\left[\frac{\mathcal{L}}{\partial\,(\partial_{\nu}A_{\mu}(x))}\right] - \frac{\partial\mathcal{L}}{\partial A_{\mu}(x)} = 0\,, \tag{2.15}$$

or, in another form,

$$\partial_{\nu}F^{\mu\nu}(x) = \frac{\partial\mathcal{L}}{\partial A_{\mu}(x)}\,. \tag{2.16}$$

From this equation, the current density is easily inferred

$$\mathrm{I}^{\mu}(x) = -\,\frac{1}{\mathrm{e}}\,\frac{\partial\mathcal{L}}{\partial A_{\mu}(x)}\,, \tag{2.17}$$

$$\mathrm{I}^{\mu}(x) = i\left[\Phi^{+}(x)\frac{\partial\mathcal{L}}{\partial\,(\mathrm{D}_{\mu}\Phi^{+})} - \Phi^{\sigma+}(x)\frac{\partial\mathcal{L}}{\mathrm{D}_{\mu}\Phi^{+}}\right], \tag{2.18}$$

which is conserved

$$\partial_{\mu}\mathrm{I}^{\mu} = 0\,. \tag{2.19}$$

The associated charge is given by

$$\mathrm{Q} = \int I^{0}(x)\,d^3x = \int i\left\{\Phi^{+}\,\mathrm{D}_{\mu}\Phi - \mathrm{D}^{\mu}\,\Phi^{+}\Phi\right\}d^3x\,, \tag{2.20}$$

which also remains unchanged with time

$$\frac{d\mathrm{Q}}{dt} = 0\,, \tag{2.21}$$

$$\int \partial x_0\, \mathrm{I}^0(x)\, d^3x = 0\,, \tag{2.22}$$

or, equivalently, $\int \partial_\mu \mathrm{I}^\mu(x)\, d^3x = 0$.

This result is formally equivalent to the classical theory, but it also shows that this new approach remains a particular case of a higher symmetry principle which rules modern physics.

2.2 The unification

2.2.1 The gauge invariance of the Weyl-Einstein connection

If we were to define a Weyl-Einstein covariant derivative just as in (2.9), the connection coefficients $\mathrm{W}^\tau_{\mu\sigma}$ should be invariant under the conformal relation

$$g_{\alpha\beta} \to \mathrm{U}\, g_{\alpha\beta}\,, \tag{2.23}$$

where $U(x) > 0$ is a real scalar. Conformal invariance is here simply achieved by implementing the additional gauge condition

$$J_\mu \to J_\mu - \partial_\mu \mathrm{U} \tag{2.24}$$

as oneself can be easily convinced.

2.2.2 The Weyl-Einstein-Yang-Mills relation

Let us consider the time-like geodesic ds_W spanned by the connexion coefficients $\mathrm{W}^\tau_{\mu\sigma}$ (1.1ter). To this geodesic is associated the 1-form $dJ = J_\mu dx^\mu$. Likewise, we write the Minkowskian line element as ds to which we associate the Yang-Mills 1-form $dA = A_\mu dx^\mu$ where A_μ is the generic term that stands for every gauge field of any of the first three Yang-Mills interactions. A specific unification between the Yang-Mills theory and space-time curvature can be thus achieved through the interaction between the Yang-Mills gauge field and vectors and the Weyl-Einstein vector J_μ. Such a relation can be set so as to maintain the euclidean character of the Yang-Mills theory within the Weyl-Einstein formalism. To this end, we write

$$\frac{dJ}{dA} = 1 + \ln\left(\frac{ds_\mathrm{W}}{ds}\right), \tag{2.25}$$

$$dJ = dA\left[1 + \ln\left(\frac{ds_\mathrm{W}}{ds}\right)\right]. \tag{2.26}$$

When $ds_\mathrm{W} \to ds$, the 4-vector J_μ identifies with the Yang-Mills gauge field vector.

The Yang-Mills physics always takes place in the Minkowski space that is asymptotic to the genuine Weyl-Einstein manifold $\mathfrak{M}$. In this way, the vector J_μ inherent to space-time curvature is regarded as "embedding" all the Yang-Mills gauge fields thereby providing a specific unification as described below.

2.3 Application to the Yang-Mills interactions

2.3.1 The weak interaction (SU(2) symmetry)

Writing classically the group element as

$$\mathrm{U} = \exp\left[\, -i\,\mathrm{h}\,\mathrm{T}^a\,\mathrm{k}_a\right], \qquad a = 1, 2, 3\,, \tag{2.27}$$

with the generators

$$\mathrm{T}^a = \frac{\sigma^a}{2}\,, \tag{2.28}$$

where σ^a are the three 2×2 Pauli spin matrices

$$\sigma^1 = \begin{pmatrix} 0 & 1 \\ 1 & 0 \end{pmatrix},\ \sigma^2 = \begin{pmatrix} 0 & -i \\ i & 0 \end{pmatrix},\ \sigma^3 = \begin{pmatrix} 1 & 0 \\ 0 & -1 \end{pmatrix}, \tag{2.29}$$

which satisfy [4, p. 2]

$$\mathrm{Tr}\left(\frac{\sigma^a}{2}\frac{\sigma^b}{2}\right) = \frac{1}{2}\,\delta^{ab}, \tag{2.30}$$

$$\mathrm{Tr}\,\frac{\sigma^a}{2} = 0\,. \tag{2.31}$$

Here we must introduce three vector gauge fields B^a_μ, which are conveniently represented by the vector field

$$B_\mu(x) = \mathrm{T}^a B_{a\mu}(x)\,. \tag{2.32}$$

The transformation properties of B_μ are obtained from :

$$B_\mu(x) \to B_\mu(x) - \mathrm{T}^a\partial_\mu \mathrm{k}^a(x) + i\,\mathrm{h}\,\mathrm{k}^a(x)\,[\mathrm{T}^a,\, B_\mu(x)]\,, \tag{2.33}$$

where h is the relevant coupling constant.

Here T^a satisfy the commutation relations with different structure constants

$$[\mathrm{T}^a,\, \mathrm{T}^b] = i\,\mathrm{f}^{abc}\,\mathrm{T}_c\,. \tag{2.34}$$

Using (2.30) in (2.33), then multiplying by T^b and taking the trace, we have the transformations laws of the individual gauge field $B^a_\mu(x)$

$$B^a_\mu(x) \to B^a_\mu(x) - \partial_\mu \mathrm{k}^a(x) + \mathrm{h}\,\mathrm{f}^a_{\ bc}\,\mathrm{k}^b(x)\,B^c_\mu(x)\,, \tag{2.35}$$

and the general form of the covariant derivative is

$$D_\mu = \partial_\mu - i\,\mathrm{h}\,B_\mu\,. \tag{2.36}$$

The SU(2) group relevant for matter representation is determined by the generators T^a, so that (2.36) is expressed by

$$\mathrm{D}_\mu = \partial_\mu - i\,\mathrm{h}\,B_{a\mu}\,\mathrm{T}^a, \tag{2.37}$$

where B_μ is here related to J_μ through equation (2.26).

2.3.2 The SU(3) symmetry

We finally illustrate the strong interaction (gluons) by defining the non-Abelian symmetry SU(3) whose elementary group element with 8 real parameters reads

$$\mathrm{U} = \exp\left[-i\,\mathrm{g}\,\frac{\lambda_a}{2}\,\mathrm{k}^a\right], \qquad a = 1,\ldots,8\,. \tag{2.38}$$

The λ^a are the eight Gell-Mann 3×3 Hermitian traceless matrices [5]

$$\lambda_1 = \begin{pmatrix} 0 & 1 & 0 \\ 1 & 0 & 0 \\ 0 & 0 & 0 \end{pmatrix}, \quad \lambda_2 = \begin{pmatrix} 0 & -i & 0 \\ i & 0 & 0 \\ 0 & 0 & 0 \end{pmatrix},$$

$$\lambda_3 = \begin{pmatrix} 1 & 0 & 0 \\ 0 & -1 & 0 \\ 0 & 0 & 0 \end{pmatrix}, \quad \lambda_4 = \begin{pmatrix} 0 & 0 & 1 \\ 0 & 0 & 0 \\ 1 & 0 & 0 \end{pmatrix},$$

$$\lambda_5 = \begin{pmatrix} 0 & 0 & -i \\ 0 & 0 & 0 \\ i & 0 & 0 \end{pmatrix}, \quad \lambda_6 = \begin{pmatrix} 0 & 0 & 0 \\ 0 & 0 & 1 \\ 0 & 1 & 0 \end{pmatrix},$$

$$\lambda_7 = \begin{pmatrix} 0 & 0 & 0 \\ 0 & 0 & -i \\ 0 & i & 0 \end{pmatrix}, \quad \lambda_8 = \begin{pmatrix} 1 & 0 & 0 \\ 0 & 1 & 0 \\ 0 & 0 & -2 \end{pmatrix},$$

and the representation of SU(3) acting on the matter field triplet

$$\psi(x) = \begin{matrix} \psi_1 \\ \psi_2 \\ \psi_3 \end{matrix} \tag{2.39}$$

is just the group element U. Accordingly, the Lagrangian for the SU(3) gauge bosons interacting with the above fermion triplet can be computed to give

$$\mathcal{L} = -\frac{1}{4}\,F^{\mu\nu}{}_k\,F_{\mu\nu}{}^k + i\,{}^\circ\psi_a\,\gamma^\mu_k\left[\partial_\mu - i\,\mathrm{g}\,S^k_\mu\left(\frac{\lambda}{2}\right)^a_{a'}\right]\psi^{a'}, \tag{2.40}$$

where ${}^\circ\psi_a$ is the complex conjugate spinor and where the field strength tensor is

$$F^{\mu\nu}_{\ \ k} = \partial^\mu S^\nu_k(x) + \mathrm{g}\,\mathrm{e}^{lm}_k\,\mathrm{k}_n(x)\,F^\mu_l\,F^\nu_n\,, \quad k,l,n = 1,\ldots,8\,. \tag{2.41}$$

Here, we have the correspondence $S^\mu \to J^\mu$.

2.3.3 Example of the gauge group U(1) × SU(2)

Using (2.29), we can construct explicit examples of the generators T^a needed to describe the transformation of matter multiplet under SU(2) which we will couple with the electromagnetic boson under U(1). We first introduce three vector gauge fields B^a_μ which may be written in the form [6, p. 53, eq. 2.91]

$$B_\mu = \left(\frac{\sigma_a}{2}\right)B^a_\mu = \frac{1}{2}\begin{vmatrix} B^3_\mu & B^1_\mu - i\,B^2_\mu \\ B^1_\mu + i\,B^2_\mu & -B^3_\mu \end{vmatrix}. \tag{2.42}$$

These are the gauge bosons transforming as the adjoint of SU(2) we couple with the gauge boson transforming as U(1).

The kinetic term of the resulting Lagrangian is given by

$$(\mathcal{L})^{\mathrm{kin}} = -\frac{1}{4}\,(B^a_{\mu\nu}\,B_a^{\mu\nu} + F^{\mu\nu}\,F_{\mu\nu})\,. \tag{2.43}$$

Here, the combination $C_\mu = B_\mu + A_\mu$ which takes place in the Euclidean tangent space is identified to the Weyl-Einstein 4-vector J_μ at this point.

All these examples illustrate how the Yang-Mills gauge field vectors actually interact with the Weyl-Einstein 4-vector through equation (2.26).

Conclusion

In this short paper, we have only sketched a possible representation of how space-time curvature can couple with the Yang-Mills Theory in a non-trivial way.

For each type of interaction, we show that the Yang-Mills gauge fields are asymptotically connected to the space-time curvature through the Weyl-Einstein 4-vector. This amounts to state that the first three interactions are defined in the euclidean space-time which is tangent to the Weyl-Einstein manifold at the point where this 4-gauge vector is chosen.

This particular interaction appears as a new coupling between the Weyl-Einstein space-time geometry and the various particles/fields satisfying the Yang-Mills theory. In a sense, such a coupling could be regarded as the realization of a new representation of Einstein's field equations with a source. In the classical General Relativity, the Riemannian field equations disregard the Weyl-Einstein vector and they just display an energy-momentum tensor on the right hand side as a source. The insertion of such a tensor was never entirely satisfactory to Einstein's opinion who always claimed that the right hand side of his equations was somewhat "clumsy". Einstein's argument should not be hastily dismissed: indeed, while his tensor exhibits a conceptually conserved property, the energy-momentum tensor as a source does not, which leaves the theory with a major inconsistency [7]. For a massive tensor, the problem has been cured by introducing the so-called pseudo-tensor that conveniently describes the gravitational field of the mass so that the 4-momentum vector of both matter and its gravity is conserved (for example, the Einstein-Dirac pseudo-density) [8, 9]. Unfortunately by essence, this pseudo-tensor can be transformed away at any point by a change of coordinates that naturally shows the non-localizability of the gravitational energy [10]. At any rate, a pseudo-tensor is not suitable to be represented on the right hand side of the field equations. This is of course a stumbling-block which has plagued General Relativity for more than a century. Moreover, unlike the Einstein tensor, the energy-momentum tensors are mainly antisymmetric and symmetrization is thus always required "afterwards" through the Belinfante procedure. To evade the initial problem one is led to introduce

a vacuum energy-momentum field energy that is "excited" in the vicinity of a mass to produce the gravitational field [11, 12]. Far from the mass, this (real) vacuum energy tensor never vanishes and guarantees the conservation of the source tensor on the right hand side of the field equations. However, several constraints are needed to be implemented which might be viewed as a loss of generality of the theory [13].

Let us note in passing that the most important Einstein solutions are derived from source-free equations as for example the famous Schwarzschild metric [14]. In the frame of our theory, the field equations in the post-Newtonian approximation should certainly deserve further scrutiny which is beyond the scope of this paper. In conclusion, we suggest here to correlate gauge fields so that unification of the three fundamental interactions with Einstein's General Theory of Relativity can be achieved in a very simple way. The principle of equivalence implies that gravity is thus indirectly related to each type of particles described in the Yang-Mills Theory.

Many topics such as the fermion and scalar quantum numbers in the electroweak model, or the spontaneous symmetry breakdown and the Higgs mechanism have not been discussed here.

We are however convinced that the introduction of the Weyl-Einstein formalism in the theory does not conflict with these results, and that it constitutes one of the permissible unifying theory between gauge theories.

Submitted on June 2, 2022

References

1. Hawking S. W., Ellis G. F. R. The Large Scale Structure of Space-Time. Cambridge University Press, 1987.
2. Lichnerowicz A. Les espaces variationnels généralisés. *Annales scientifiques de l'École Normale Supérieure*, série 3, t .62, 1945, 339–384.
3. Weyl H. On generalized Riemann matrices. *Annals of Mathematics*, 1934, v. 35, no. 4, 714–729.
4. Greiner W., Müller B. Gauge Theory of Weak Interaction. Springer-Verlag, 2009.
5. Gell-Mann M. The eightfold way: a theory of strong interaction symmetry. *Cal. Inst. of Technology*, TID 12608 CSTL-20, 1961.
6. Ross G. R. Grand Unified Theories. Benjamin/Cummings Publ. Co., Menlo Park (California), 1985.
7. Landau L., Lifshitz E. The Classical Theory of Fields. Addison-Wesley, Reading, 1962.
8. Tonnelat M. A. Les Théories unitaires de l'Électromagnétisme et de la Gravitation. Gauthier-Villars, Paris, 1965.
9. Dirac P.A.M. General Theory of Relativity. Princeton University Press, 2nd edition, 1975.
10. Straumann N. General Relativity and Relativistic Astrophysics. Springer-Verlag, 1984.
11. Marquet P. The gravitational field: a new approach. *Progress in Physics*, 2013, v. 3, 62–66.
12. Marquet P. Vacuum background field in General Relativity. *Progress in Physics*, 2016, v. 12, 314–316.
13. Marquet. P. Some insights on the nature of the vacuum background field in General Relativity. *Progress in Physics*, 2016, v. 12, 366–367.
14. Kramer D., Stephani H., Hertl E., MacCallum M. Exact Solutions of Einstein's Field Equations. Cambridge University Press, 1979.

Physics of Irrational Numbers

Hartmut Müller

Rome, Italy.
E-mail: hm@interscalar.com

In systems of coupled periodic processes, lasting frequency ratios can cause significant physical effects, which depend on the type of real numbers the ratios are approximating. Rational frequency ratios can cause parametric resonance and amplification, while approaching irrational frequency ratios can avoid them. In this paper we discuss physical effects that can be caused by frequency ratios approximating some irrational algebraic and transcendental numbers. We illustrate this approach on some features of the solar system which are still unexplained.

Introduction

In this paper, we introduce an approach that bases on the physical interpretation of certain statements of the number theory. In modern theoretical physics, numerical ratios usually remain outside the realm of theoretical interest. In this work we try to elucidate the physical meaning of numerical ratios and to show their theoretical and practical importance for resolving some fundamental problems of physics.

One of the unsolved fundamental problems in physics [1] is the stability of systems of a large number of coupled periodic processes, for instance, the stability of planetary systems. If numerous bodies are considered to be gravitationally bound to one another, perturbation models predict long-term highly unstable states [2] that contradict the physical reality of the solar system and thousands of exoplanetary systems.

In our previous publications we have applied our numeric-physical approach to the analysis of the orbital and rotational periods of the planets, planetoids and moons of the solar system and thousands of exoplanets [3] with the conclusion that the avoidance of orbital and rotational parametric resonances by approximation of transcendental ratios can be viewed as a basic forming factor of planetary systems [4].

Another unsolved fundamental problem is the imperishability of motion and interaction, and the inexhaustibility of energy. This question seems to be out of the realms of modern physics. Indeed, until now, all the sources of energy we are currently using – from electricity to radioactivity – were discovered by chance. This fact and the incapacity of inventing new energy sources evidences the lack of comprehention. For instance, the research of the predicted thermonuclear fusion has been going on for 60 years without success [5, 6].

Likewise, the nature of gravitational energy is still a mystery [7]. For instance, what is the propelling force of the orbital motion? Naturally, there is no propelling of orbital motion, the planets are in perpetual free fall. However, the orbital velocity of a planet is very high, 30 kilometers per second in the case of the Earth. The impulse of a planet is therefore enormous and sweeps away everything that gets in its trajectory. Where does this kinetic energy come from? Perhaps, this question seems naive to the physicist who is ready to answer immediately: Besides the primordial kinetic energy of the protoplanetary disk, the potential energy of the gravity field of the star is the source of the kinetic energy of planetary motion. However, this answer only readdresses the question. Then what is the source of gravitational energy? Is it the alleged ability of a mass to curve space-time? Then what causes this ability?

Obviously, the concept of mass is not complete since the numerical values of particle masses still remain a mystery. Where do the observed masses of elementary particles come from? This is the biggest, and oldest, unresolved enigma in fundamental particle physics. There is the widespread, but erroneous, belief that the Higgs boson resolves the origin of particle masses. This is not the case. It merely replaces one set of unknown parameters (particle rest energies) with an equally unknown set of parameters (coupling constants to the Higgs field), so nothing is gained in the fundamental understanding of masses [8].

Is there a hidden inexhaustible source of energy in the universe? Then why can energy not be generated or consumed, but only converted?

The earliest constants of motion discovered were momentum and kinetic energy, which were proposed in the 17^{th} century by René Descartes and Gottfried Leibniz on the basis of collision experiments, and later refined by Euler, Lagrange, d'Alembert and Hamilton. In theoretical physics, Noether's first theorem connects the conservation of energy with the homogeneity of time, supposing that the laws of physics do not change over time. Noether's theorem states that conservation laws apply in a physical system with conservative forces. A conservative force is a force with the property that the total work done in moving a particle between two points is independent of the path taken. Equivalently, if a particle travels in a closed loop, the total work done by a conservative force is zero. In short, a conservative force is a force that conserves energy. Hence, Noether's theorem leads to circular reasoning. It does not explain the cause of energy conservation [9]. Perhaps, no physical principle can explain the origin of energy, because every physical process presupposes the existence of

another physical process that serves as its energy source. This non ending chain of energy converters suggests that the imperishability of motion and interaction, and the inexhaustibility of energy must have a non-physical cause.

Our numeric-physical approach leads us to the conclusion that motion and interaction, including energy as well as other constants of motion are caused by attractors of numeric fields. We illustrate this conclusion on some features of the solar system which are still unexplained.

Theoretical Approach

The starting point of our approach is frequency as obligatory characteristic of a periodic process. As the result of a measurement is always a *ratio* of physical quantities, one can measure only *ratios* of frequencies. This ratio is always a real number. Being a real value, a frequency ratio can approximate an integer, rational, irrational algebraic or transcendental number. In [10] we have shown that the difference between rational, irrational algebraic and transcendental numbers is not only a mathematical task, but it is also an essential aspect of stability in systems of bound periodic processes. For instance, integer frequency ratios, in particular fractions of small integers, make possible parametric resonance that can destabilize such a system [11, 12]. This is why asteroids cannot maintain orbits that are unstable because of their resonance with Jupiter [13]. These orbits form the Kirkwood gaps that are areas in the asteroid belt where asteroids are absent.

According to this idea, irrational ratios should not cause destabilizing resonance interactions, because irrational numbers cannot be represented as a ratio of integers. However, algebraic irrational numbers, being real roots of algebraic equations, can be converted to rational numbers by multiplication. For example, the algebraic irrational number $\sqrt{2} = 1.41421\ldots$ cannot become a frequency scaling factor in real systems of coupled periodic processes, because $\sqrt{2} \cdot \sqrt{2} = 2$ creates the conditions for the occurrence of parametric resonance. Thus, only transcendental ratios can prevent parametric resonance, because they cannot be converted to rational or integer numbers by multiplication. Actually, it is transcendental numbers, that define the preferred frequency ratios which allow to avoid destabilizing resonance [14]. In this way, transcendental frequency ratios sustain the lasting stability of coupled periodic processes. With reference to the evolution of a planetary system and its stability, we may therefore expect that the ratio of any two orbital periods should finally approximate a transcendental number [15].

However, the issue is to clarify the type of number a measured ratio corresponds to. Because of the finite resolution of any measurement, there is no possibility to know it for sure. The obtained value is always an approximation and therefore, it is very important to know the amount of its uncertainty.

It is remarkable that approximation interconnects all types of real numbers – rational, irrational algebraic and transcendental. In 1950, Aleksandr Khinchin [16] made a very important discovery: He could demonstrate that simple continued fractions deliver biunique representations of all real numbers, rational and irrational. Whereas infinite continued fractions represent irrational numbers, finite continued fractions represent always rational numbers. In this way, any irrational number can be approximated by finite continued fractions, which are the convergents and deliver always its nearest and quickest rational approximation.

It is notable that the best rational approximation of an irrational number by a finite continued fraction is not a task of computation, but only an act of termination of the continued fraction recursion. For example, the golden ratio $\phi = (\sqrt{5}+1)/2 = 1.618\ldots$ has a biunique representation as simple continued fraction that contains only the number 1:

$$\phi = 1 + \cfrac{1}{1 + \cfrac{1}{1 + \cfrac{1}{1 + \ldots}}}$$

As the continued fraction of ϕ is periodic, it meets a quadratic equation evidencing that ϕ is algebraic:

$$\phi = 1 + \frac{1}{\phi} \qquad \phi^2 - \phi - 1 = 0$$

In order to save space, in the following we use angle brackets to write down continued fractions, for example the golden ratio $\phi = \langle 1; 1, 1, \ldots \rangle$. So long as the sequence of denominators is considered as infinite, this continued fraction represents the irrational number ϕ. If the continued fraction will be truncated, the sequence of denominators will be finite and we get a convergent that is always the nearest rational approximation of the irrational number ϕ.

In the case of ϕ, the approximation process is very slow because of the small denominators. Only the 10^{th} approximation gives the correct third decimal of ϕ. In fact, the denominators in the continued fraction of ϕ are the smallest possible and consequently, the approximation speed is the lowest possible. The golden ratio ϕ is therefore treated as the 'most irrational' number in the sense that a good approximation of ϕ by rational numbers cannot be given with small quotients. On the contrary, transcendental numbers can be approximated exceptionally well by rational numbers, because their continued fractions contain large denominators and can be truncated with minimum loss of precision. For instance, the simple continued fraction of Archimedes' number $\pi = 3.1415927\ldots = \langle 3; 7, 15, 1, 292, \ldots \rangle$ delivers the following sequence of rational approximations:

$\langle 3 \rangle = 3$
$\langle 3; 7 \rangle = 22/7 = 3.\overline{142857}$
$\langle 3; 7, 15 \rangle = 3.14150943396226$
$\langle 3; 7, 15, 1 \rangle = 3.1415929\ldots$

Already the 2nd approximation delivers the first two decimals correctly. Therefore, 22/7 is a widely used Diophantine approximation of π. The 4th approximation shows already six correct decimals. This special arithmetic property of continued fractions [17] of transcendental numbers has the consequence that transcendental numbers are distributed near by rational numbers of small quotients or close to integers, like $e^3 = 20.08\ldots$ or $\pi^3 = 31.006\ldots$. This can create the impression that complex systems like the solar system provide ratios of physical quantities that approximate rational numbers. More likely, they approximate transcendental numbers [4], which are located close to rational numbers.

Naturally, a continued fraction of π or any other real transcendental number cannot be periodic, otherwise it would meet an algebraic equation. For example, the continued fractions of the algebraic irrationals $\sqrt{2} = \langle 1; 2, 2, 2, \ldots \rangle$ and $\sqrt{3} = \langle 1; 1, 2, 1, 2, \ldots \rangle$ are periodic. In contrast to them, a generalized continued fraction of Euler's number contains all natural numbers in sequence as numerators and denominators and therefore, it cannot be periodic:

$$e = 2 + \cfrac{1}{1 + \cfrac{1}{2 + \cfrac{2}{3 + \cfrac{3}{4 + \ldots}}}}$$

The following generalized continued fraction [18] of π contains all natural numbers factorizing the numerators:

$$\pi = 2 + \cfrac{2}{1 + \cfrac{1 \cdot 2}{1 + \cfrac{2 \cdot 3}{1 + \cfrac{3 \cdot 4}{1 + \ldots}}}}$$

These continued fractions do not only evidence that π and e are not algebraic, but make comprehensible the increase of the approximation speed with every next convergent. In addition, it becomes clear that Archimedes' number π can be approximated faster than Euler's number e.

Among all transcendental numbers, Euler's number $e = 2.71828\ldots$ is unique, because its real power function e^x coincides with its own derivatives. In the consequence, Euler's number allows avoiding parametric resonance between any coupled periodic processes including their derivatives.

Because of this unique property of Euler's number, we expect that periodic processes in real systems prefer frequency ratios close to Euler's number and its roots. The natural logarithms of those frequency ratios are therefore close to integer $0, \pm 1, \pm 2, \ldots$ or rational $\pm 1/2, \pm 1/3, \pm 1/4, \ldots$ values. For rational exponents, the natural exponential function is always transcendental [19]. Since every rational number has a biunique representation as a simple finite continued fraction, we can represent the logarithms of the frequency ratios we are looking for as finite continued fractions:

$$\ln(\omega_A/\omega_B) = \mathcal{F} = \langle n_0; n_1, n_2, \ldots, n_k \rangle \qquad (1)$$

ω_A and ω_B are the angular frequencies of two bound periodic processes A and B avoiding parametric resonance. We use angle brackets for continued fractions. All denominators $n_1, n_2, \ldots, n_k$ of a continued fraction including the free link n_0 are integer numbers. All numerators equal 1. The length of a continued fraction is given by the number k of layers.

The canonical form (all numerators equal 1) does not limit our conclusions, because any continued fraction with partial numerators different from 1 can be transformed into a canonical continued fraction using the Euler equivalent transformation [20]. Therefore, finite canonical continued fractions represent all rational numbers in the sense that there is no rational number that cannot be represented as a finite canonical continued fraction. This universality of canonical continued fractions evidences that the distribution of rational logarithms (1) is fractal. As it is an inherent feature of the number continuum, we call it the *Fundamental Fractal* [14].

The first layer of this fractal is given by the truncated after n_1 continued fractions:

$$\langle n_0; n_1 \rangle = n_0 + \frac{1}{n_1}$$

The denominators n_1 follow the sequence of integer numbers ± 1, ± 2, ± 3 etc. The second layer is given by the truncated after n_2 continued fractions:

$$\langle n_0; n_1, n_2 \rangle = n_0 + \cfrac{1}{n_1 + \cfrac{1}{n_2}}$$

Figure 1 shows the first and the second layer in comparison. As we can see, reciprocal integers $\pm 1/2, \pm 1/3, \pm 1/4, \ldots$ are the attractor points of the fractal. In these points, the distribution density of rational logarithms (1) reaches a local maximum. Integers $0, \pm 1, \pm 2, \ldots$ define the main attractors having the widest ranges. Half logarithms $\pm 1/2$ form smaller attractor ranges, third logarithms $\pm 1/3$ form the next smaller ranges and so forth. Increasing the length of the continued fraction (1), the distribution density of the transcendental frequency ratios ω_A/ω_B is increasing as well. Nevertheless, their distribution is not homogeneous, but fractal. Applying continued fractions and truncating them, we can represent the logarithms $\ln(\omega_A/\omega_B)$ as rational numbers $\langle n_0; n_1, n_2, \ldots, n_k \rangle$ and make visible their fractal distribution.

The linear projection $\mathcal{E} = \exp(\mathcal{F})$ of the fundamental fractal (fig. 1) is a fractal scalar field of transcendental attractors that we call the *Euler field* [3]. Figure 2 (central part) shows the 2D-projection of its first layer. The Euler field is topologically 3-dimensional, a fractal set of embedded

Fig. 1: The distribution of rational logarithms for $k = 1$ (above) and for $k = 2$ (below) in the range $-1 \leqslant \mathcal{F} \leqslant 1$.

spheric equipotential surfaces. The potential difference defines a gradient directed to the center of the field that causes a central force of attraction creating the effect of a field source. Because of the fractal logarithmic hyperbolic metric of the field, also every equipotential surface is an attractor. The logarithmic scalar potential difference $\Delta\mathcal{F}$ of sequent equipotential surfaces equals the difference of sequent continued fractions (1) on a given layer:

$$\Delta\mathcal{F} = \langle n_0; n_1, \ldots, n_k \rangle - \langle n_0; n_1, \ldots, n_k + 1 \rangle$$

Main equipotential surfaces at $k = 0$ correspond with integer logarithms; equipotential surfaces at deeper layers $k > 0$ correspond with rational logarithms.

The Euler field is of pure arithmetic origin, and there is no particular physical mechanism required as field source. Hence, we postulate the universality of the Euler field that should affect any type of physical interaction, regardless of its complexity. Corresponding with (1), the Euler field generates a fractal set of transcendental frequency ratios $\omega_A/\omega_B = \mathcal{E}$ which allow to avoid destabilizing parametric resonance and in this way, provide the lasting stability of periodic processes bound in systems regardless of their complexity. This conclusion we have exemplified [21] in particle physics, astrophysics, geophysics, biophysics and engineering.

In several publications we have shown that the Euler field determines the orbital periods of thousands of exoplanets and large bodies in the solar system [3] as well as their gravitational parameters [4]. Astrophysical and geophysical cycles [22] as well as periodic biophysical processes [10] obey the Euler field. Finally, the Euler field determines the proton-to-electron ratio and the W/Z-to-electron ratio as well as the temperature 2.725 K of the cosmic microwave background radiation [14]. All these findings suggest that the cosmological significance of the Euler field is that of a universal stabilizer.

The radii of the equipotential surfaces of the Euler field $\mathcal{E} = e^{\mathcal{F}}$ are integer and rational powers of Euler's number. However, not only Euler's number $e = 2.71828\ldots$ defines a fractal scalar field of its integer and rational powers, but in general, every prime, irrational and transcendental number does it. While the fundamental fractal (fig. 1) is always the same distribution of rational logarithms, the structure of the corresponding fundamental field changes with the logarithmic base. Here it is important to notice that no fundamental field can be transformed in another by scaling (stretching), because $\log_a(x) - \log_b(x)$ is a nonlinear function of x. In this way, every prime, irrational or transcendental number generates a unique fundamental field of its own integer and rational powers that causes physical effects which are typical for that number. For instance, the golden ratio $\phi = \langle 1; 1, 1, \ldots \rangle$ makes difficult its rational approximation, since its continued fraction does not contain large denominators. Hence, the fundamental field of its integer and rational powers should be a perfect inhibitor of resonance amplification. We propose to name this field after Hippasus of Metapontum who was an ancient Greek philosopher and early follower of Pythagoras, and is widely credited with the discovery of the existence of irrational numbers, and the first proof of the irrationality of the golden ratio. Figure 2 (left part) shows the 2D-projection of the first layer of the Hippasus field $\mathcal{H} = \phi^{\mathcal{F}}$.

Although the golden ratio is irrational, it is a Pisot number, so its powers are getting closer and closer to whole numbers. This is why the Hippasus field can inhibit resonance within small frequency ranges only. Euler's number is not a Pisot number, so that the Euler field permits coupled periodic processes to avoid parametric resonance also over very large frequency ranges. Since the natural logarithm of the golden ratio is close to 1/2, small powers of the golden ratio can approximate main equipotential surfaces of the Euler field. For example, $\phi^2 = 2.618\ldots$ can serve as approximation of $e = 2.718\ldots$ Within small frequency ranges, this circumstance makes the Hippasus field a fast and simplified local approximation of the Euler field. In fact, as the continued fraction of the golden ratio contains only the number 1, approximations of the golden ratio can be achieved faster than approximations of Euler's number, since every extension of its continued fraction requires counting and additional computing. Therefore, systems of coupled periodic processes follow the Hippasus field within small frequency ranges only. For example, several authors [23, 24] have suggested that the Venus-to-Earth orbital period ratio 0.615 approximates the golden ratio $1/\phi = 0.618\ldots$ preventing Earth and Venus from parametric orbital resonance. However, the Hippasus field cannot prevent the whole solar system from orbital resonance. For instance, the Pluto-to-Venus orbital period ratio does not obey a power of the golden ratio, but approximates the 6^{th} power of Euler's number [10]. The 6^{th} power of Euler's number is in the range of the 12^{th} power of the golden ratio that approximates a whole number and hence cannot serve as a scaling factor that prevents parametric resonance.

Obviously, in systems with many coupled periodic processes, the Hippasus field can produce two opposing effects: over small frequency ranges, the Hippasus field can inhibit parametric resonance, but over large frequency ranges, it provides the long-period appearance of resonance amplification.

Furthermore in this paper, we introduce the Archimedes field $\mathcal{A} = \pi^{\mathcal{F}}$. Figure 2 (right part) shows the 2D-projection of its first layer. The radii of the equipotential surfaces of the Archimedes field are integer and rational powers of π.

According to our numeric physical approach, we interpret the fact that circumference / radius = π in the way that the transcendence of π makes possible circular motion. The transcendence of the circumference avoids interruptions and

makes impossible to define the start or endpoint of motion. Furthermore, Archimedes number π makes possible eternal oscillation. This is why it is impossible to *completely* stop oscillations, for example, the thermal oscillations of atoms. According to our approach, the origin of the zero point energy phenomenon lies in the transcendence of π.

Proven by Theodor Schneider [25] in 1937, the perimeter of an ellipse is transcendental. Elliptical or circular motion is the only way to move with acceleration without propulsion. The absence of propulsion makes this motion eternal. In this way, the transcendence of π makes possible eternal accelerated motion. Hence, Archimedes' number appears to be a universal source of kinetic energy and promoter of orbital and rotational motion.

In the framework of our approach, gravity is a physical effect caused by numeric attractors [3]. They cause mass accretion forming a celestial body and determine its movement in space and time. In this way, planets, stars, planetary systems and galaxies are materializations of numeric attractors. These attractors exist long before a star or planet is formed. In order to reach an attractor, the accelerated displacement of matter causes the force conventionally interpreted as gravity. Numeric attractors are primary; mass accretion is secondary. In this way, gravitation is not caused by the body mass, and it is not a physical property of a celestial body at all. We suppose that fundamental numeric attractors cause all types of physical interaction.

As well, the appearance of a field source is only a scaling effect. A field is not created by a charge, but the charge is a scaling effect of the field. The gradient of the field is the force of attraction that indicates the location of the energy source. The attractor is the energy source. Matter falls down to the attractor because in this way it gains energy. This is why the core of a planet is hot. On the contrary, in the assumption that mass is the source of gravity, and in accordance with Newton's shell theorem, the Preliminary Reference Earth Model [26] affirms the *decrease* of the gravity acceleration with the depth. However, this hypothesis is still under discussion. In 1981, Stacey and Holding [27, 28] reported anomalous measures (larger values than expected) of the gravity acceleration in deep mines and boreholes.

According to our approach, the acceleration of free fall should *increase* with the vicinity to the field singularity, but follow the logarithmically hyperbolic fractal metric of the fundamental numeric field. In [29] we have shown that the Euler field reproduces the 3D profile of the Earth's interior confirmed by seismic exploration. As well, the stratification layers in planetary atmospheres follow the Euler field [30].

Are there attractors of the Euler field that coincide with attractors of the Archimedes field? Since $e = 2.71828\ldots$ and $\pi = 3.14159\ldots$ are transcendental, there are no rational powers of these numbers that can produce identical results. Therefore, in general, Archimedes-attractors are different from Euler-attractors. However, some of them are so close to each other that they form common attractors. It is not difficult to compute the exponents of two transcendental numbers that define a common attractor. The ratio of their logarithms is a fractal dimension that equals $\mathrm{D} = \ln\pi = 1.144729\ldots$ Representing D as continued fraction $\langle 1; 7, -11, \ldots\rangle$, we immediately find 8/7 as the first approximation. Consequently, multiples of 8/7 define pairs of Euler-attractors of stability and Archimedes-attractors of motion that are very close to each other. For example, this is valid for $\mathcal{E}\langle 56\rangle$ and $\mathcal{A}\langle 49\rangle$. We will study this and other examples in the paragraph *Exemplary Applications*. Naturally, our description of possible physical effects caused by the fields $\mathcal{A}, \mathcal{E}, \mathcal{H}$ does not claim to be complete.

Exemplary Applications

Let us start with an application of the Euler field that demonstrates its ability of avoiding parametric resonance over extremely large scale-differences. For instance, Venus' distance from Sun approximates the main equipotential surface $\mathcal{E}_e\langle 54\rangle$ of the Euler field of the *electron* that equals the 54^{th} power of Euler's number multiplied by the Compton wavelength of the electron λ_e. The aphelion 0.728213 AU = $1.08939 \cdot 10^{11}$ m delivers the upper approximation:

$$\ln\left(\frac{A_{\mathrm{O}}(Venus)}{\lambda_e}\right) = \ln\left(\frac{1.08939 \cdot 10^{11}\,\mathrm{m}}{3.86159 \cdot 10^{-13}\,\mathrm{m}}\right) = 54.00$$

The perihelion 0.718440 AU = $1.07477 \cdot 10^{11}$ m delivers the lower approximation:

$$\ln\left(\frac{P_{\mathrm{O}}(Venus)}{\lambda_e}\right) = \ln\left(\frac{1.07477 \cdot 10^{11}\,\mathrm{m}}{3.86159 \cdot 10^{-13}\,\mathrm{m}}\right) = 53.98$$

This means that Venus' orbit derives from the Euler field of the electron. In other words, Venus' orbit is of subatomic origin. This is not a random coincidence. Jupiter's distance from Sun approximates the main equipotential surface $\mathcal{E}_e\langle 56\rangle$ of the same electron Euler field. The aphelion 5.45492 AU = $8.160444 \cdot 10^{11}$ m delivers the upper approximation:

$$\ln\left(\frac{A_{\mathrm{O}}(Jupiter)}{\lambda_e}\right) = 56.01$$

The perihelion 4.95029 AU = $7.405528 \cdot 10^{11}$ m delivers the lower approximation:

$$\ln\left(\frac{P_{\mathrm{O}}(Jupiter)}{\lambda_e}\right) = 55.91$$

As well, Jupiter's orbital period 4332.59 days derives from the Euler field of the electron. In fact, it equals the 66^{th} power of Euler's number multiplied by the oscillation period of the electron ($\tau_e = \lambda_e/c = 1.28809 \cdot 10^{-21}$ s is the angular oscillation period of the electron):

$$\ln\left(\frac{T_{\mathrm{O}}(Jupiter)}{2\pi \cdot \tau_e}\right) = \ln\left(\frac{4332.59 \cdot 86400\,\mathrm{s}}{2\pi \cdot 1.28809 \cdot 10^{-21}\,\mathrm{s}}\right) = 66.00$$

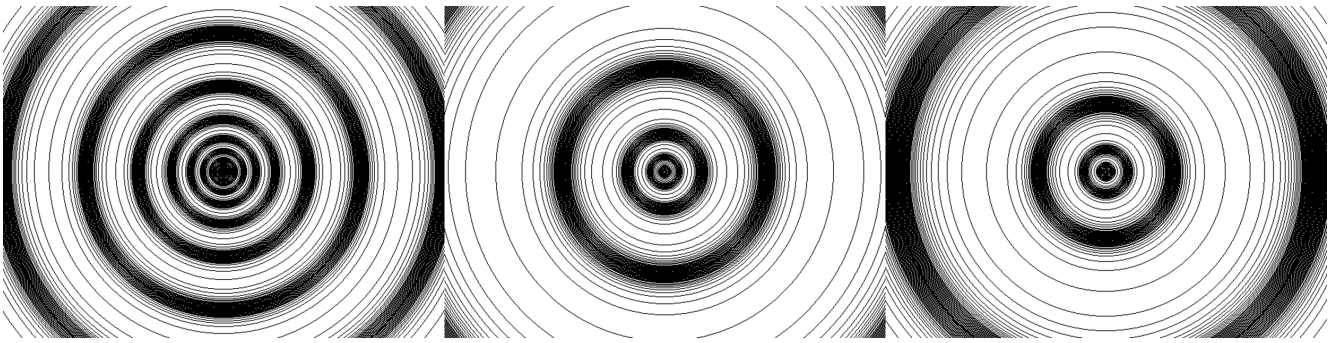

Fig. 2: The image shows the 2D-projection of the first layer ($k = 1$) of equipotential surfaces of the Hippasos Field $\mathcal{H} = \phi^{\mathcal{F}}$ (left), the Euler Field $\mathcal{E} = e^{\mathcal{F}}$ (center), and the Archimedes Field $\mathcal{A} = \pi^{\mathcal{F}}$ (right) of the Fundamental Fractal $\mathcal{F}$. The fields are shown to the same scale.

The same is valid for the orbital period 686.98 days (1.88 years) of the planet Mars that equals the 66^{th} power of Euler's number multiplied by the *angular* oscillation period of the electron:

$$\ln\left(\frac{T_{\mathrm{O}}(Mars)}{\tau_e}\right) = \ln\left(\frac{686.98 \cdot 86400\,\mathrm{s}}{1.28809 \cdot 10^{-21}\,\mathrm{s}}\right) = 66.00$$

Consequently, the ratio of the orbital periods of Jupiter and Mars equals 2π:

$$T_{\mathrm{O}}(Jupiter) = 2\pi \cdot T_{\mathrm{O}}(Mars)$$

This transcendental ratio allows Mars to avoid parametric orbital resonance with Jupiter and evidences that Jupiter and Mars are not planets of different systems, but bound together in the same conservative system (the solar system).

Also the orbital period 224.701 days of Venus derives from the Euler field of the electron, and it is stabilized by the main attractor $\mathcal{E}_e\langle 63\rangle$:

$$\ln\left(\frac{T_{\mathrm{O}}(Venus)}{2\pi \cdot \tau_e}\right) = 63.00$$

The complete (polar) rotational period $T_{\mathrm{R}}(Sun) = 34$ days of the Sun approximates the same attractor:

$$\ln\left(\frac{T_{\mathrm{R}}(Sun)}{\tau_e}\right) = 63.00$$

Consequently, the scaling factor 2π connects the orbital period of Venus with the rotational period of the Sun:

$$T_{\mathrm{O}}(Venus) = 2\pi \cdot T_{\mathrm{R}}(Sun)$$

Needless to say that these numeric relations cannot be derived from Kepler's laws or Newton's law of gravitation. Fig. 3 shows how Archimedes' number bonds together rotational and orbital periods. The scale symmetry of this connection not only reveals the Sun as the engine of planetary motion, but also the special role of Mercury. The connection of its rotation with the orbital motion of the Earth is surprising and encourages further investigation.

In general, orbital periods are stabilized by the Euler field of the electron, and rotational periods by the Euler field of the proton. For instance, the rotational periods of Earth and Mars derive from the angular oscillation period $\tau_p = \lambda_p/c$ of the proton ($\lambda_p = 2.10309 \cdot 10^{-16}$ m is the Compton wavelenght of the proton). They approximate the same attractor $\mathcal{E}_p\langle 67\rangle$. Mars' sidereal rotational period 24.62278 hours delivers the upper approximation:

$$\ln\left(\frac{T_{\mathrm{R}}(Mars)}{\tau_p}\right) = \ln\left(\frac{24.62278 \cdot 3600\,\mathrm{s}}{7.01515 \cdot 10^{-25}\,\mathrm{s}}\right) = 67.01$$

Earth' sidereal rotational period 23.93447 hours delivers the lower approximation:

$$\ln\left(\frac{T_{\mathrm{R}}(Earth)}{\tau_p}\right) = \ln\left(\frac{23.93447 \cdot 3600\,\mathrm{s}}{7.01515 \cdot 10^{-25}\,\mathrm{s}}\right) = 66.98$$

It is notable that the proton-to-electron ratio itself approximates the 7^{th} power of Euler's number and its square root:

$$\ln\left(\frac{\lambda_e}{\lambda_p}\right) = \ln\left(\frac{3.86159 \cdot 10^{-13}\,\mathrm{m}}{2.10309 \cdot 10^{-16}\,\mathrm{m}}\right) \simeq 7 + \frac{1}{2} = \mathcal{E}\langle 7; 2\rangle$$

In the consequence of this potential difference of the proton relative to the electron, the scaling factor $\sqrt{e} = 1.64872\ldots$ connects Euler field attractors of proton stability with similar attractors of electron stability in alternating sequence. In [4] we have applied Khinchine's [16] continued fraction method of approximation to the proton-to-electron ratio.

As we mentioned in the paragraph *Theoretical Approach*, multiples of 8/7 define pairs of Euler-attractors of stability and Archimedes-attractors of motion and energy that are very close to each other. For example, this is valid for $\mathcal{E}_e\langle 56\rangle$ and $\mathcal{A}_e\langle 49\rangle$, because 56/49 = 8/7. This coincidence underlines the significance of the attractor $\mathcal{E}_e\langle 56\rangle$ that determines the orbit of the largest planet in the Solar system. If we apply the exponent 49 to Euler's number, we discover that $\mathcal{E}_e\langle 49\rangle$ corresponds with the radius of the Sun. In this way, the coincidence of $\mathcal{E}_e\langle 56\rangle$ with $\mathcal{A}_e\langle 49\rangle$ identifies the Sun as energy source and Jupiter as main orbital body of the Solar system.

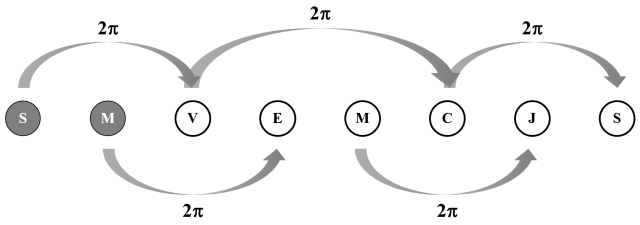

Fig. 3: From left to right: the *rotational* periods of the Sun (S) and Mercury (M), and the *orbital* periods of Venus (V), Earth (E), Mars (M), Ceres (C), Jupiter (J), and Saturn (S), coupled by the scaling factor 2π of the Archimedes field.

Interestingly, it is not the radius of the photosphere that coincides with the equipotential surface $\mathcal{E}_e\langle 49\rangle$, but the radius of the corona. It is noticeable that no complete theory yet exists to account for the extremely high temperature of the corona that reaches up to 20 million Kelvin. Despite great advances in observations and modelling, the problem of solar and stellar heating still remains one of the most challenging problems of space physics [31]. According to our approach, this heating could be a physical effect caused by numeric attractors of the Archimedes field.

Conclusion

According to our numeric-physical approach, numeric fields like $\mathcal{A}, \mathcal{E}$ are primary. Through their physical effects, they not only determine the frequency ratios of elementary particles, but also the setting of orbital and rotational periods in planetary systems. Modern theoretical physics is oriented towards equations, even if they cannot be solved. The language of equations is based on conservation rules, which, however, describe the behavior of model processes under certain ideal conditions of equilibrium. Nevertheless, the search for an equation describing the observed process is often considered a priority task of theoretical research. In this case, as a rule, numerical ratios are considered random. We consider this work to contribute to the idea that great unification in physics cannot be achieved as long as numerical ratios remain outside the realm of theoretical interest.

Acknowledgements

The author is grateful to Leili Khosravi, Veronika Müller, Viktor Panchelyuga, Oleg Kalinin, Viktor Bart and Michael Kauderer for valuable discussions.

Submitted on June 25, 2022

References

1. Hansson J. The 10 Biggest Unsolved Problems in Physics. *International Journal of Modern Physics and Applications*, 2015, v. 1, no. 1, 12–16.
2. Heggie D. C. The Classical Gravitational N-Body Problem. arXiv: astro-ph/0503600v2, 11 Aug 2005.
3. Müller H. Physics of Transcendental Numbers meets Gravitation. *Progress in Physics*, 2021, vol. 17, 83–92.
4. Müller H. Physics of Transcendental Numbers as Forming Factor of the Solar System. *Progress in Physics*, 2022, v. 18, 56–61.
5. Jacquinot J. Fifty years in fusion and the way forward. *Nucl. Fusion*, 2010, v. 50, 014001.
6. Lidsky L. M. The Trouble With Fusion. *MIT Technology Review*, October 1983.
7. Adler R. J. et al. Vacuum catastrophe: An elementary exposition of the cosmological constant problem. *American Journal of Physics*, 1995, v. 63 (7), 620–626.
8. Hansson J. Physical Origin of Elementary Particle Masses. arXiv: 1402.7033v1 [physics.gen-ph] 4 Feb 2014.
9. Brown H. R. Do symmetries "explain" conservation laws? The modern converse Noether theorem vs pragmatism. arXiv:2010.10909v2 [physics.hist-ph] 15 Jun 2021.
10. Müller H. On the Cosmological Significance of Euler's Number. *Progress in Physics*, 2019, v. 15, 17–21.
11. Dombrowski K. Rational Numbers Distribution and Resonance. *Progress in Physics*, 2005, v. 1, no. 1, 65–67.
12. Panchelyuga V.A., Panchelyuga M. S. Resonance and Fractals on the Real Numbers Set. *Progress in Physics*, 2012, v. 8, no. 4, 48–53.
13. Minton D. A., Malhotra R. A record of planet migration in the main asteroid belt. *Nature*, 2009, v. 457, 1109–1111.
14. Müller H. The Physics of Transcendental Numbers. *Progress in Physics*, 2019, vol. 15, 148–155.
15. Müller H. Global Scaling of Planetary Systems. *Progress in Physics*, 2018, v. 14, 99–105.
16. Khintchine A. Continued fractions. University of Chicago Press, Chicago, 1964.
17. Perron O. Die Lehre von den Kettenbrüchen. 1950.
18. Yiu P. The Elementary Mathematical Works of Leonhard Euler. Florida Atlantic University, 1999, pp. 77–78.
19. Hilbert D. Über die Transcendenz der Zahlen e und π. *Mathematische Annalen*, 1893, v. 43, 216–219.
20. Skorobogatko V. Ya. The Theory of Branched Continued Fractions and mathematical Applications. Moscow, Nauka, 1983.
21. Müller H. Global Scaling. The Fundamentals of Interscalar Cosmology. *New Heritage Publishers*, Brooklyn, New York, USA, ISBN 978-0-9981894-0-6, (2018).
22. Müller H. Physics of Transcendental Numbers on the Origin of Astrogeophysical Cycles. *Progress in Physics*, 2021, v. 17, 225–228.
23. Pletser V. Orbital Period Ratios and Fibonacci Numbers in Solar Planetary and Satellite Systems and in Exoplanetary Systems. arXiv: 1803.02828 (2018).
24. Butusov K. P. The Golden Ratio in the solar system. *Problems of Cosmological Research*, vol. 7, Moscow–Leningrad, 1978.
25. Schneider T. Arithmetische Untersuchungen elliptischer Integrale. *Mathematische Annalen*, 1937, v. 113, 1–13.
26. Dziewonski A. M., Anderson D. L. Preliminary reference Earth model. Physics of the Earth and Planetary Interiors, 1981, v. 25, 297–356.
27. Stacey F. D. et al. Constraint on the planetary scale value of the Newtonian gravitational constant from the gravity profile within a mine. *Phys. Rev. D*, 1981, v. 23, 1683.
28. Holding S. C., Stacey F. D., Tuck G. J. Gravity in mines. An investigation of Newton's law. *Phys. Rev. D*, 1986, v. 33, 3487.
29. Müller H. Quantum Gravity Aspects of Global Scaling and the Seismic Profile of the Earth. *Progress in Physics*, 2018, v. 14, 41–45.
30. Müller H. Global Scaling of Planetary Atmospheres. *Progress in Physics*, 2018, v. 14, 66–70.
31. Erdelyi R., Ballai I. Heating of the solar and stellar coronae: a review. *Astronomische Nachrichten*, 2007, v. 328, no. 8, 726–733.

Proposed Laboratory Measurement of the Gravitational Repulsion Predicted by Quantum Celestial Mechanics (QCM)

Franklin Potter

Sciencegems.com, 8642 Marvale Drive, Huntington Beach, CA 92646 USA. E-mail: frank11hb@yahoo.com

Quantum Celestial Mechanics (QCM) predicts the quantization of the orbital angular momentum per unit mass for bodies orbiting a central mass in response to attractive and repulsive gravitational accelerations. Applications to the Solar System, multi-planet exosystems, and to the Pluto system of 5 moons suggest its validity. A laboratory experiment to check this constraint is proposed.

1 Introduction

The gravitational constant G has now been measured by several new techniques, including a dynamic measurement by resonating beams [1] and a simple pendulum laser interferometer [2]. Both methods as well as Advanced LIGO and other gravitational sensors could also measure the repulsive gravitational acceleration predicted by the quantization of angular momentum per unit mass constraint [3] of Quantum Celestial Mechanics (QCM).

Although the Pluto system with its 5 satellites has already been a definitive test of this constraint [4], and its successful applications to the Solar System and numerous multi-planet exosystems have been achieved [5], an Earth-bound laboratory measurement confirmation is preferred.

According to QCM, which is derived from the general relativistic Hamilton-Jacobi equation, the quantization of orbital angular momentum L per unit mass μ constraint of the orbiting body, with quantization integer m, depends upon the total angular momentum L_T for the system of total mass M_T as

$$L/\mu = m\, L_T/M_T\,. \tag{1}$$

Recall that all orbits are equilibrium orbits for Newtonian gravitation for a central mass M and orbit distance r because the radial acceleration

$$\ddot{r} = -\frac{GM}{r^2} + \frac{L^2}{\mu^2\, r^3}\,. \tag{2}$$

But for QCM, the subset of allowed equilibrium orbits are the ones that obey

$$\ddot{r} = -\frac{GM}{r^2} + \frac{m\,(m+1)\,L_T^2}{M_T^2\, r^3} \tag{3}$$

for circular orbits. Therefore, a very small radial displacement from the equilibrium radius r_{eq} of orbit results in an acceleration in the opposite direction.

2 Lab experiment parameters

In order to mimic a Keplerian circular orbit, one would place an ideal rotating metal cylinder of mass M and radius R at a distance r from the gravitational detector. A simple estimation of the parameters for a laboratory scale measurement is made by assuming that the detector is essentially a point mass M_d responding instead of an extended geometrical object. Therefore,

$$r_{eq} = \frac{m\,(m+1)\,L_T^2}{GM\,M_T^2} \approx \frac{m\,(m+1)\,R^4\omega^2 M}{4G\,(M+M_d)^2}\,. \tag{4}$$

Inserting some reasonable values: $M = 5\,\text{kg}$, $R = 5\,\text{cm}$, $M_d = 2\,\text{kg}$, and $m = 1$, the first equilibrium radius will be at $r_{eq} \approx 4781\omega^2$ metre. For $r_{eq} = 1$ metre, i.e. fit in a lab room,

$$\omega \approx 0.0145\,\text{rad/s} \approx 8.3\,\text{rot/hr}\,. \tag{5}$$

By varying the rotation rate ω of the cylinder one can sweep back and forth through several equilibrium radii for $m = 1, 2, 3, ...$ to observe attractive and repulsive accelerations at $r_{eq} = 2r_0, 6r_0, 12r_0, ...$ sensed by the detector, with rapidly decreasing interaction accelerations with increasing r_{eq}.

Acknowledgements

The author thanks Sciencegems.com for support and H. G. Preston for insightful discussions on methods to test Quantum Celestial Mechanics.

Received on August 2, 2022

References

1. Brack T., Balabdaoui F., *et al*. Dynamic measurement of gravitational coupling between resonating beams in the hertz regime. *Nature Physics*, 2022. //doi.org/10.1038/s41567-022-01642-8.
2. Parks H. V. and Faller J. E. A simple pendulum laser interferometer for determining the gravitational constant. *Phil. Trans. A Math. Phys. Eng. Sci.*, 2014, v. 372 (2026).
3. Preston H. G. and Potter F. Exploring large-scale gravitational quantization without $\hbar$ in planetary systems, galaxies, and the Universe. arXiv: gr-qc/0303112.
4. Potter F. Update on Pluto and Its 5 Moons Obeying the Quantization of Angular Momentum per Unit Mass. *Prog. in Phys.*, 2016, v. 12 (1), 56–58.
5. Potter F. Multi-planet exosystems all obey orbital angular momentum quantization per unit mass predicted by Quantum Celestial Mechanics(QCM). *Prog. in Phys.*, 2013, v. 9 (3), 29–30.

An Observational Test of Doppler's Theory Using Solar-System Objects

John "Jack" D. Wilenchik
Phoenix, Arizona, USA. E-mail: wilenchik1@me.com

The scientific community widely accepted Christian Doppler's theory that light Doppler-shifts, even though it was proposed without empirical evidence and never tested on objects with well-known velocities like solar-system planets and moons. I conducted a test of Doppler's theory on a handful of planets and moons (Venus, Ganymede, Europa, and Ceres) using high-resolution data from the Keck Observatory's High Resolution Echelle Spectrometer (HIRES). In doing so, I was careful not to apply the automatic Doppler (heliocentric) corrections for movement of the earth that are normally applied when reducing such data. After comparing the observed shifts to actual velocities given by the NASA/JPL Horizons ephemeris system, I found both observations that agreed and disagreed with their Doppler-predicted values, which is an indication for more expansive tests. I also identified a significant problem with the Doppler explanation for "inclined" spectral lines, which can be found in the spectra of Jupiter and Saturn.

1 Introduction

This year is the 180th anniversary of Christian Doppler's hypothesis that colors of light shift due to movement by the source or observer [4]. Doppler's original paper describing his hypothesis was purely theoretical, and it reached conclusions that were quickly recognized as erroneous in their own time. For example, Doppler suggested that the actual color of every star was white or yellow, and that the stars' apparent colors (red, blue, etc.) were due solely to their radial velocities with respect to the earth [4, §5].* Nevertheless, the last sentence of his original paper proved to be prophetic: in "[t]he distant future," he wrote, his theory would "offer astronomers a welcome means of determining the motions and distances" of distant stars and other objects whose velocities are otherwise "immeasurable." [4, §11].

The instruments of the 19th Century lacked the resolution needed to test Doppler's theory on celestial objects with known velocities, like solar-system planets and moons [8]. As astronomer William Huggins wrote in 1868: "[t]he great relative velocity of light to the known planetary velocities, and to the probable motions of the few stars of which the parallax is known, showed that any alternations of position which might be expected from [Doppler shift] in the lines of the stellar spectra would not exceed a fraction of the interval between the double line D [sodium doublet line D], for that part of the spectrum." [8, p. 530]. "I have devoted much time," Huggins continued, "[and] I hope to accomplish the detection of so small an amount of change... [but] [t]he difficulties of this investigation I have found to be very great..." [*Id.*]. The first astronomer(s) to apply Doppler's theory therefore focused on targets whose velocities could not be rigorously and independently measured, like distant stars and nebulae or gases on the solar surface [7, 8].

But a modern spectrometer like the Keck Observatory's "High Resolution Echelle Spectrometer" (HIRES) is more than capable of performing the "William Huggins Test". I report the results of a test of Doppler's theory on solar-system planets and moons using the shift in their D lines, much like William Huggins intended.

2 Methodology

I searched the Keck Observatory Archive (KOA)† for solar-system data from the HIRES, particularly planets and moons with low axial rotation [11] ‡. The HIRES has a precision on the order of meters per second and has been heavily used in searches for exoplanets; accordingly, its archives contain comparatively few observations of solar-system objects [2,3]. A handful of observations were used: two observations of Venus in 2007 and 2009, one of Ganymede in 2009, one of Europa in 2009, and one of the dwarf planet Ceres in 2005. The data for various observations of Mercury were also considered, but the signal-to-noise ratio was deemed to be too

*In 1868, astronomer William Huggins described Doppler's error as "obvious": "Doppler endeavored...to account for the remarkable differences of colour which some of the binary stars present, and for some other phenomena of heavenly bodies. That Doppler was not correct in making this application of his theory is obvious from the consideration that even if a star could be conceived to be moving with a velocity sufficient to alter its colour sensibly to the eye, still no change of colour would be perceived, for the reason that beyond the visible spectrum, at both extremities, there exists a store of invisible waves which would be at the same time exalted or degraded into visibility, to take the place of the waves which had been raised or lowered in refrangibility by the star's motion. No change of colour, therefore, could take place until the whole of those invisible waves of force had been expended, which would only be the case when the relative motion of the source of light and the observer was several times greater than that of light." [8, p. 530-31].

†The Keck archive can be accessed from //koa.ipac.caltech.edu/cgi-bin/KOA/nph-KOAlogin . The particular datasets used herein are identified in Appendix "A."

‡Rates of rotation were calculated from [1]; or in the case of Venus, also from [6] (indicating that Venus' atmosphere rotates sixty times faster than its surface).

low (and airmass too high) to be included in this exploratory study.

The KOA offers data that has already been reduced and extracted by the Keck Observatory "MAKEE" pipeline ("MAuna Kea Echelle Ex-traction"). However, that pipeline normally applies a "heliocentric correction" of up to around ±30 km/s, which is designed to account for the putative Doppler effect of movement of the earth at the time of observation. MAKEE can be run manually with heliocentric corrections turned "off"; and so I downloaded the same raw science and calibration data that was used to generate the extracted data in the archives, then I re-extracted it using MAKEE without heliocentric corrections. Because I made no effort to account for the effect of the bodies' (or the earth's) axial rotations on Doppler shift, I treated it as a source of error in their calculated radial velocity (see E_{calc} in Table 1). The speed of axial rotation for each object in this study was between ±0.01 and 0.15 km/s, and earth's rotation was estimated at 0.5 km/s, so E_{calc} was never greater than ±0.52 km/s. Putative relativistic effects were calculated to be less than 0.01 km/s and therefore neglected. Finally, the measured Doppler shift in the D lines was compared to radial velocity as given by the NASA/JPL Horizons ephemeris system. More details on methodology are included in Appendix "A."

3 Results

Figure 1 shows plots of the measured and calculated Doppler shifts. While the Sodium absorption lines in Venus' and Ceres' atmospheres appeared at or near their Doppler-predicted positions, the lines in Ganymede and Europa did not. The mean absolute difference (weighted by error) in between measured (Doppler) and calculated (JPL Horizons) velocity for Ganymede and Europa was 9.24 ± 0.72 km/s. These results are also shown in Table 1.

Space-based (Hubble) spectroscopy confirms Na D absorption lines in the atmospheres of both Ganymede and Europa*, which tends to discount telluric interference as a cause for the discrepancy. Its magnitude (9.24 km/s) would also tend to discount atmospheric winds and other internal dynamics.

The discrepancy is less if the lines are compared to the Doppler-predicted shift in solar light reflecting from the body, which is given by:

$$R_{reflect} = R_{helio} + R_{calc} + \frac{R_{helio}R_{calc}}{c} \qquad (1)$$

(where R_{helio} is the object's heliocentric velocity, R_{calc} is its geocentric velocity, and c is the speed of light *in vacuo*)†. However, the bodies' spectra do not show separate lines for reflected light (albedo) and light originating from the object, as Doppler's theory would predict.

*See Observation ID "o51u02040" (Ganymede) and "od9l140m0" (Europa) in the ESA Hubble Science Archive, http://hst.esac.esa.int/ehst/.

†For a derivation of this equation, please see Appendix "B."

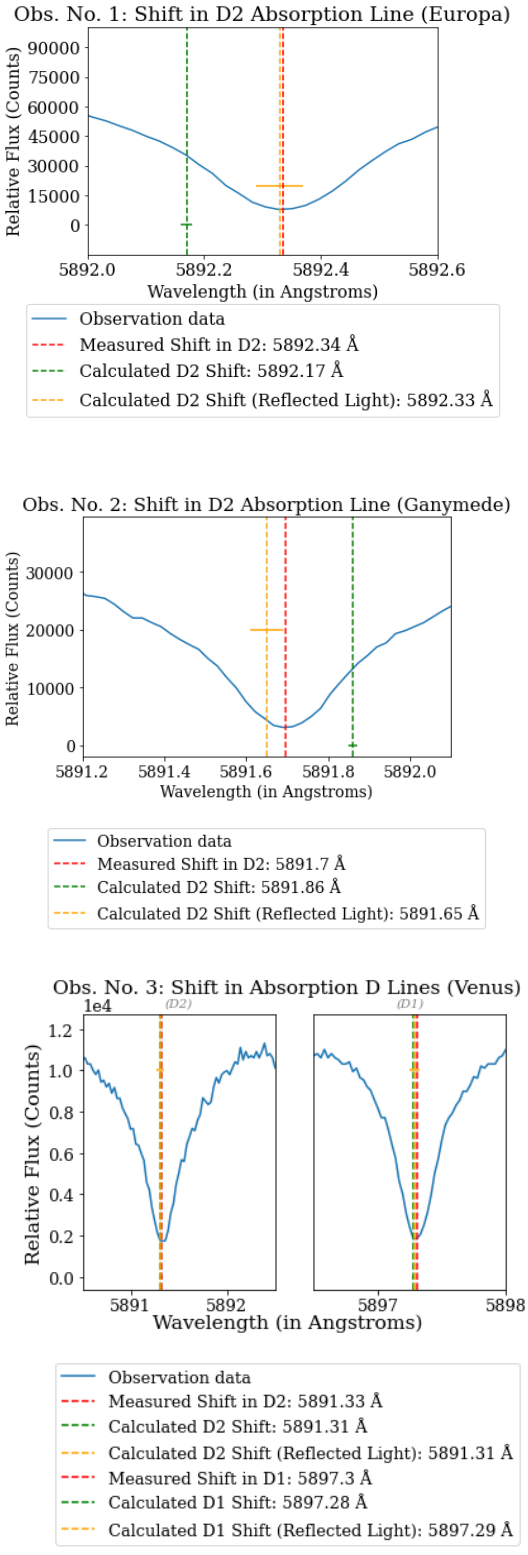

Fig. 1: Plots of the shifts in the D lines (actual and predicted) for the five observations. Error is thinner than the lines, except for the yellow lines (the predicted shifts in albedo), which had more significant error due to the calculated rotation of the sun. (*See also* Table 1.)

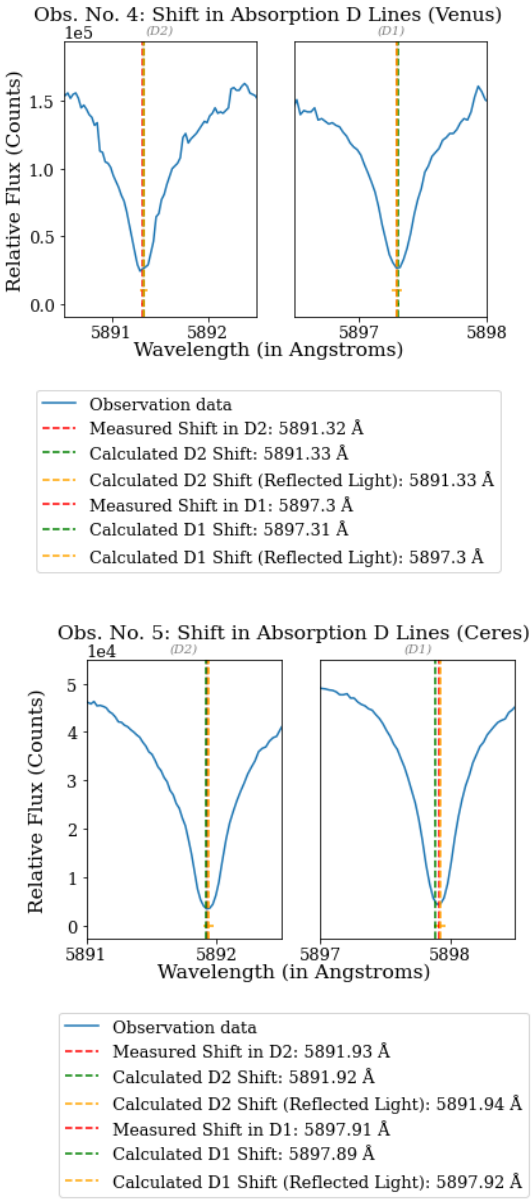

Fig. 1 (cont.)

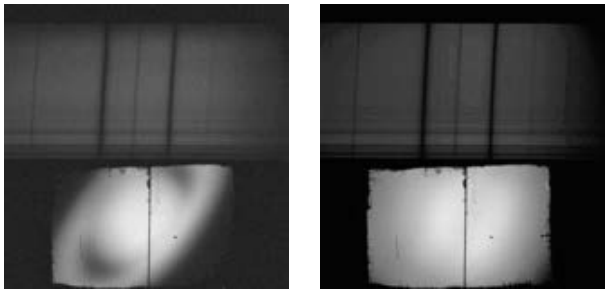

Fig. 2: At top left is an image of the spectrum of Saturn taken on June 25, 2018. Below it is the corresponding camera image of Saturn, which demonstrates the placement of the spectroscopic slit across the face of the planet. At top right is a spectrum of Jupiter taken on June 25, 2018, and below it is the corresponding camera image, which again demonstrates placement of the slit. The linear inclination in both planets' spectra is apparent. (Data source: [10], observations nos. 224 and 225.).

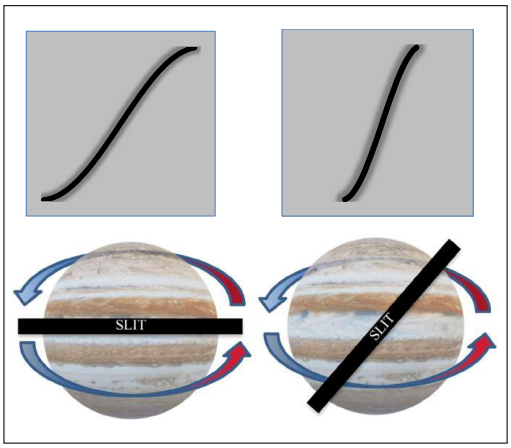

Fig. 3: At top (in gray) are illustrations of the expected sinusoidal pattern of spectral lines that are Doppler-shifted by the rotation of a spherical body. At bottom is shown the corresponding placement of a theoretical spectroscopic "slit" on the planet's surface.

3.1 Concerns with the Doppler modeling of planetary spectral line inclinations

The spectra of Jupiter and Saturn are known to be "tilted", or to exhibit a linear inclination (Figure 2). Historically, the cause of this inclination was deemed to be Doppler shift due to each planet's rotation about its own axis [5, 9]. However, the radial velocities of points across a spherical rotating body should exhibit a curved, sinusoidal pattern (Figure 3). The observed "tilt" is always linear, which suggests a cause other than Doppler shift.

4 Conclusion

Christian Doppler's theory that light Doppler-shifts was accepted and widely applied without an observational test on solar-system planets and moons, due to historical limitations on the resolution of available spectrometers. This "Huggins Test" used a small sample of modern high-resolution spectroscopic observations but nevertheless turned up observations that were inconsistent with their Doppler-predicted values. Further, there is substantial doubt concerning whether the inclined spectral lines of bodies like Jupiter and Saturn can be reasonably explained as a Doppler effect caused by their axial rotation. These results support conducting more expansive tests of the Doppler theory, using modern high-

resolution spectroscopy on solar-system objects with well-known velocities.

Disclosures

No outside funding was received to assist with the preparation of this article, and the author declares no conflicts of interest.

Supplemental Documents

A Python script that will reproduce my data reduction and analysis is available on Zenodo, (doi:10.5281/zenodo.6240436) as "Doppler_Test.py". [11].

Data Availability

The data underlying the results presented in this paper are fully contained on Zenodo [11]. They are also available from their original sources on the Keck Observatory Archive, https://www2.keck.hawaii.edu/koa/public/koa.php.

Acknowledgments

This research made use of the Keck Observatory Archive - (KOA), which is operated by the W. M. Keck Observatory and the NASA Exoplanet Science Institute (NExScI), under contract with the National Aeronautics and Space Administration. Profound thanks go to Dr. Zach Cano for his invaluable advice and assistance, as well as to Dr. Francisco Pina, Dr. Rafael Brahm and Dr. Christina Thöne.

Received on August 11, 2022

References

1. Cox A. Allen's Astrophysical Quantities, 4th Ed. Springer, 1999.
2. Vogt S., Allen S., Bigelow B., Bresee L., Brown B., Cantrall T., Conrad A., Couture M., Delaney C., Epps H., Hilyard D., Horn E., Jern N., Kanto D., Keane M., Kibrick R., Lewis J., Osborne J., Pardeilhan G., Pfister T., Ricketts T., Robinson L., Stover R., Tucker D., Ward J. & Wei M. HIRES: the high resolution echelle spectrometer on the Keck 10-m telescope. *Proc. SPIE* 2198, Instrumentation in Astronomy VIII, 1994. doi:10.1117/12.176725.
3. Butler R., Vogt S., Laughlin G., Burt J., Rivera E., Tuomi M., Teske J., Arriagada P., Diaz M., Holden B. & Keiser S. The LCES HIRES/Keck Precision Radial Velocity Exoplanet Survey. *AJ*, 2017, v. 153, 5. doi:10.3847/1538-3881/aa66ca.
4. Doppler C. Über das farbige Licht der Doppelsterne (Concerning the Coloured Light of Double Stars). *Royal Bohemian Society Of Sciences*, 1842. https://bit.ly/3qpUJpc.
5. Giver L. Line Inclinations in Equatorial Spectra of Jupiter and Saturn. *Astrophysical Journal*, 1964, v. 139, 727. doi:10.1086/147798.
6. Horinouchi T., Hayashi Y., Watanabe S., Yamada M., Yamazaki A., Kouyama T., Taguchi M., Fukuhara T., Takagi M., Ogohara K., Murakami S., Peralta J., Limaye S., Imamura T., Nakamura M., Sato T. & Satoh T. How waves and turbulence maintain the super-rotation of Venus' atmosphere. *Science*, 2020, v. 368, 405–409. doi:10.1126/science.aaz4439.
7. Huggins W. VII. Further observations on the spectra of the sun, and of some of the stars and nebulæ, with an attempt to determine therefrom whether these bodies are moving towards or from the earth. *Proc. R. Soc. London Ser. I*, 1868a, v. 16, 382–386. doi:10.1098/rspl.1867.0080.
8. Huggins W. XXI. Further observations on the spectra of some the stars and nebulæ, with an attempt to determine therefrom whether these bodies are moving towards or from the earth, also observations on the spectra of the sun and of comet II. *Phil. Trans. R. Soc. London, Ser. I*, 1868b, 158, p. 529–565. doi:10.1098/rstl.1868.0022.
9. Moore J. Spectroscopic Observations of the Rotation of Saturn. *Publications Of The Astronomical Society Of The Pacific*, 1939, v. 51, 274. doi:10.1086/125081.
10. Schmidt C. Rapid Imaging Planetary Spectrograph: 2018 Mercury Exosphere Data [Dataset, version 1]. *Zenodo*, 2019. doi:10.5281/zenodo.3588493.
11. Wilenchik J. An Observational Test of Doppler's Theory Using Solar System Objects [Dataset, version 2]. *Zenodo*, 2022. doi:10.5281/zenodo.6240436.

Appendix "A"

Version 6.4 of "MAKEE" was used to extract and reduce the Keck Archive data. The version of MAKEE that was used is dated May 2019 and available for download from: https://sites.astro.caltech.edu/~tb/makee/makee_6.4-2019.tar.gz.

MAKEE was run in a command terminal using Ubuntu 20.04.3 LTS. The MAKEE pipeline requires at least four "FITS" (Flexible Image Transport System) images to reduce and calibrate data: an image of the object; an image to find the "trace" of the echelle orders (which can simply be the image itself, although a star is often used); flat image(s); and an image of the arc lamp for wavelength calibration. Each image in the Keck Observatory Archive (KOA) is assigned a unique "KOAID." The KOAID for each of the raw science and calibration images used in this paper (as well as the CCD and orders extracted) are listed in Table 2.

To remove the heliocentric correction, MAKEE was run using the "-nohc" option. The "-koa" option was also used, which outputs the processed data into ".tbl" files. Finally, in order to run MAKEE, the user must specify a CCD number to be extracted (using the "ccd=*" argument). The final command for processing each observation was "makee [Object.fits] [Trace.fits] [Flat.fits] [Arc.fits] ccd = [CCD No.] -nohc -koa." An optional "log=*.txt" argument sends the command-line output into a "*.txt" file.

After running MAKEE, the region of the Sodium D lines (5890 – 5900 Å) was identified in the extracted orders. The wavelength, flux and error spectrum in the region of the D line(s) was then manually extracted into a ".csv" file (which is contained in the Zenodo depository and named "*_full.csv" for each observation). In Observations No. 1 and 2 (Europa and Ganymede), the D1 line fell beyond the extracted orders, and so only the D2 lines were used. The D lines in Observation No. 5 fell across two different orders; and so the data in Order #7 was used for the D1 line and part of the D2 line, with the remaining data for the D2 line coming from Order #6. Postscript images of the orders for all extractions can be found in the "logs" folder on Zenodo, along with the MAKEE command-line output logs.

Table 1: Summary of Observation Data and Results. (All velocities in km/s.)

Observation No.	**1**	**2**	**3**	**4**	**5**
Target Name	Europa	Ganymede	Venus	Venus	Ceres
Epoch (UT)	12/13/09 4:56	12/11/09 4:53	6/6/07 5:32	1/7/09 4:33	6/17/05 5:54
Exposure (sec)	30	20	500	500	300
Keck Image ID	HI.20091213.17797	HI.20091211.17597	HI.20070606.19972	HI.20090107.16390	HI.20050617.21254
R_{calc}	+30.05	+14.29	-14.04	-12.78	+16.89
E_{calc}	±0.51	±0.51	±0.52	±0.52	±0.51
$R_{Doppler}$	+40.34	+6.09	-13.62	-13.88	+18.25
$E_{Doppler}$	±0.03	±0.05	±0.17	±0.36	±0.48
$\Delta_{Doppler}$	+10.29	-9.20	+0.42	-1.10	+1.36
$E_{\Delta Doppler}$	±0.51	±0.51	±0.55	±0.63	±0.70
R_{helio}	+7.83	-10.91	+0.23	-0.23	+1.43
E_{helio}	±1.99	±1.99	±2.00	±2.00	±1.99
$R_{reflect}$	+37.82	+3.38	-13.81	-13.01	+18.32
$E_{reflect}$	±2.05	±2.05	±2.07	±2.07	±2.05
$\Delta_{reflect}$	+2.52	+2.71	+0.19	-0.87	-0.07
$E_{\Delta reflect}$	±2.05	±2.05	±2.07	±2.10	±2.11
A	1.52	1.47	1.72	1.76	1.25

Legend

R_{calc} = the target object's calculated geocentric velocity at the date and time of observation, from the NASA/JPL Horizons ephemeris system.

E_{calc} = uncertainty in the target's calculated geocentric velocity, due to axial rotation of the earth and target body.

$R_{Doppler}$ = Doppler-measured radial velocity.

$E_{Doppler}$ = uncertainty in the Doppler-measured radial velocity (see Appendix "A" for methodology).

$\Delta_{Doppler}$ = $(R_{Doppler} - R_{calc})$, i.e. the discrepancy in between Doppler-measured velocity ($R_{Doppler}$) and Horizons-calculated velocity (R_{calc}).

$E_{\Delta Doppler}$ = uncertainty in $\Delta_{Doppler}$, i.e. $\sqrt{(E_{calc})^2 + (E_{Doppler})^2}$.

R_{helio} = target object's calculated heliocentric velocity, based on the NASA/JPL Horizons ephemeris system.

E_{helio} = error in the object's heliocentric velocity due to rotation of the sun and target (which were combined in quadrature). Solar rotation was estimated at $]pm1.99$ km/s (based on values from [1]. I used a solar equatorial circumference of 2.720984 million miles, then divided by a rotation period of 26.24 days, to obtain a rotational velocity at the solar equator of 1992.86 m/s.)

$R_{reflect}$ = predicted Doppler shift of solar light reflecting from the target, given by $(R_{calc} + R_{helio})$.

$E_{reflect}$ = error in $R_{reflect}$, i.e. $\sqrt{(E_{calc})^2 + (E_{helio})^2}$.

$\Delta_{reflect}$ = $R_{Doppler} - R_{reflect}$, i.e. the difference in between Doppler-measured velocity ($R_{Doppler}$) and predicted Doppler shift in solar light reflecting form the target ($R_{reflect}$).

$E_{\Delta reflect}$ = uncertainty in $\Delta_{reflect}$, i.e. $\sqrt{(E_{helio})^2 + (E_{Doppler})^2 + (E_{calc})^2}$.

A = averaged airmass (as reported in the image's FITS header).

Table 2: Keck Observatory Archive Datasets

Observation No.	1 (Europa)	2 (Ganymede)	3 (Venus)	4 (Venus)	5 (Ceres)
Object KOIAD	HI.20091213.17797	HI.20091211.17597	HI.20070606.19972	HI.20090107.16390	HI.20050617.21254
Trace (star) ID	HI.20091213.08389	HI.20091211.10571	HI.20070607.01296	HI.20090107.16390	HI.20050616.06005
Flat KOAID	HI.20091213.13363	HI.20091211.13478	HI.20070606.17769	HI.20090107.15456	HI.20050617.19496
Arc KOAID	HI.20091213.10643	HI.20091211.12272	HI.20070606.16831	HI.20090107.01375	HI.20050617.11120
CCD	3	3	2	2	2
Order(s)	11	11	13	13	6,7

To calculate the parameters for a Gaussian fit to each of the Sodium D lines, the "curve_fit" function in Python's SciPy package was used ("SciPy: Scientific Library for Python" version 1.7.3). The error spectrum in the MAKEE-generated data tables (column #7, "Error") was input as "sigma" in the "curve_fit" routine. This produced parameters for the best-fit Gaussian function for each D line, as well as an estimated covariance. The standard deviation in the Gaussian centerline was calculated from the covariance; and this standard deviation was used for error in the measured Doppler shift of each D line. Finally, for those observations in which both D lines could be detected, an average of the two shifts was calculated (weighted by error) to reach a final Doppler shift; and the errors in the shift of each D line were combined in quadrature to reach final error values.

Final shifts were recorded as $R_{Doppler}$ in Table 1, and final errors were recorded as $E_{Doppler}$. The Python code used for these calculations is included in the "Zenodo" depository (as "Doppler_Test.py"), and when run it will reproduce the data analysis and figures used in this paper. Python version 3.9.7 was used.

Appendix "B"

The equation for finding the predicted Doppler shift in solar spectra that are being reflected from a target under observation from the earth ($R_{reflect}$), and expressed in terms of velocity (km/s), is:

$$R_{reflect} = R_{helio} + R_{calc} + \frac{R_{helio}R_{calc}}{c} \tag{2}$$

where R_{helio} is the target's heliocentric velocity, R_{calc} is its geocentric velocity, and c is the speed of light *in vacuo*. To derive this equation, we start with the general Doppler equation for wavelength as a function of radial velocity, which represents the initial Doppler-shifted wavelength of solar light reaching the target (λ_{helio}):

$$\lambda_{helio} = \frac{R_{helio}}{c}\,\lambda_0 + \lambda_0 \tag{3}$$

where λ_0 the target's wavelength at rest. To determine the final observed wavelength after light reflects from the target ($\lambda_{observed}$), we must apply a second Doppler shift to account for the target's geocentric velocity:

$$\lambda_{observed} = \frac{R_{calc}}{c}\,\lambda_{helio} + \lambda_{helio} \tag{4}$$

$$\lambda_{observed} = \lambda_{helio}\left(\frac{R_{calc}}{c} + 1\right). \tag{5}$$

Finally, in order to express the observed wavelength as a shift in velocity ($R_{reflect}$), and as a function of the target's heliocentric and geocentric velocities, we must again use the Doppler equation (this time solved for radial velocity) and make the proper substitutions for $\lambda_{observed}$ and λ_{helio}:

$$R_{reflect} = \left(\frac{\lambda_{observed} - \lambda_0}{\lambda_0}\right) c \tag{6}$$

$$R_{reflect} = \left(\frac{\lambda_{helio}\left(\frac{R_{calc}}{c} + 1\right) - \lambda_0}{\lambda_0}\right) c \tag{7}$$

$$R_{reflect} = \left(\frac{\left(\frac{R_{helio}\,\lambda_0}{c} + \lambda_0\right)\left(\frac{R_{calc}}{c} + 1\right) - \lambda_0}{\lambda_0}\right) c \tag{8}$$

$$R_{reflect} = \left(\frac{R_{helio}}{c} + 1\right)(R_{calc} + c) - c \tag{9}$$

$$R_{reflect} = R_{helio} + R_{calc} + \frac{R_{helio}R_{calc}}{c}\,. \tag{10}$$

On Action in the Spacetime Continuum

Pierre A. Millette

E-mail: pierre.millette@uottawa.ca, Ottawa, Canada

In this paper, we investigate the role of action $\mathcal{S}$ in the Spacetime Continuum (*STC*) as provided by the Elastodynamics of the Spacetime Continuum (*STCED*). We find that energy applies to three-dimensional space, while action applies to four-dimensional spacetime. Planck's reduced constant $\hbar$ corresponds to an elementary quantum of action S_0, with action units being the same as those of angular momentum. We thus find that action is the fundamental four-dimensional spacetime scalar quantity corresponding to energy for three-dimensional space. This helps explain why equations of motion in the Spacetime Continuum are determined by minimizing action, not energy, using the principle of least (or stationary) action. The contribution of a path, in the path integral formulation of quantum mechanics and quantum field theory, depends on the number of elementary quanta of action S_0 in the path.

1 Introduction

In this paper, we investigate the role of action $\mathcal{S}$ in the Spacetime Continuum (*STC*) as provided by the Elastodynamics of the Spacetime Continuum (*STCED*) [1–3]. *STCED* is a natural extension of Einstein's General Theory of Relativity which blends continuum mechanical and general relativistic descriptions of the Spacetime Continuum. The introduction of strains in the Spacetime Continuum as a result of the energy-momentum stress tensor allows us to use, by analogy, results from continuum mechanics, in particular the stress-strain relation, to provide a better understanding of the general relativistic spacetime.

2 Elastodynamics of the Spacetime Continuum

The stress-strain relation for an isotropic and homogeneous Spacetime Continuum is given by [1, 3]

$$2\bar{\mu}_0\,\varepsilon^{\mu\nu} + \bar{\lambda}_0\,g^{\mu\nu}\varepsilon = T^{\mu\nu} \tag{1}$$

where $\bar{\lambda}_0$ and $\bar{\mu}_0$ are the Lamé elastic constants of the Spacetime Continuum: $\bar{\mu}_0$ is the shear modulus (the resistance of the Spacetime Continuum to *distortions*) and $\bar{\lambda}_0$ is expressed in terms of $\bar{\kappa}_0$, the bulk modulus (the resistance of the Spacetime Continuum to *dilatations*), in a four-dimensional continuum as:

$$\bar{\lambda}_0 = \bar{\kappa}_0 - \tfrac{1}{2}\,\bar{\mu}_0\,. \tag{2}$$

$T^{\mu\nu}$ is the general relativistic energy-momentum stress tensor, $\varepsilon^{\mu\nu}$ the Spacetime Continuum strain tensor resulting from the stresses, and

$$\varepsilon = \varepsilon^{\alpha}{}_{\alpha}\,, \tag{3}$$

the trace of the strain tensor obtained by contraction, is the volume dilatation ε defined as the change in volume per original volume [4, see pp. 149–152] and is an invariant of the strain tensor. It should be noted that the structure of (1) is similar to that of the field equations of general relativity,

$$R^{\mu\nu} - \tfrac{1}{2}\,g^{\mu\nu}R = -\varkappa\,T^{\mu\nu} \tag{4}$$

where $R^{\mu\nu}$ is the Ricci curvature tensor, R is its trace, $\varkappa = 8\pi G/c^4$ and G is the gravitational constant (see [2, Ch. 2] for more details).

In *STCED*, as shown in [1, 3], energy propagates in the Spacetime Continuum as wave-like *deformations* which can be decomposed into *dilatations* and *distortions*. *Dilatations* involve an invariant change in volume of the Spacetime Continuum which is the source of the associated rest-mass energy density of the deformation. On the other hand, *distortions* correspond to a change of shape (shearing) of the Spacetime Continuum without a change in volume and are thus massless.

Thus deformations propagate in the Spacetime Continuum by longitudinal (*dilatation*) and transverse (*distortion*) wave displacements. This provides a natural explanation for wave-particle duality, with the massless transverse mode corresponding to the wave aspects of the deformations and the massive longitudinal mode corresponding to the particle aspects of the deformations.

The rest-mass energy density of the longitudinal mode is given by [1, see Eq. (32)]

$$\rho c^2 = 4\bar{\kappa}_0\varepsilon \tag{5}$$

where ρ is the rest-mass density, c is the speed of light, $\bar{\kappa}_0$ is the bulk modulus of the *STC* as seen previously, and ε is the volume dilatation given by (3).

3 Action in the Spacetime Continuum

In a previous paper [5], we considered dislocations in the Spacetime Continuum as a framework for quantum physics. In a subsequent paper [6], we expressed Planck's constant in terms of the Burgers spacetime dislocation constant b_0, given by

$$\hbar = \frac{\bar{\kappa}_0\,b_0^4}{c}\,, \tag{6}$$

where $\bar{\kappa}_0$ is the Spacetime Continuum bulk modulus, b_0 is the Burgers spacetime dislocation constant, c is the speed of light

in vacuo and $\hbar$ is Planck's reduced constant. This equation can be considered to be a definition of Planck's reduced constant $\hbar$. We consider this equation in greater detail.

On the right-hand side of the equation, we have the Spacetime Continuum bulk modulus constant $\bar{\kappa}_0$ in units of energy density [J m^{-3}], that is energy per 3-D volume. We can multiply $\bar{\kappa}_0$ by a 3-D volume to convert it to energy. However, $\bar{\kappa}_0$ is a Spacetime Continuum constant. We need a conversion in terms of the 4-D spacetime volume.

The right-hand side of (6) also includes the term b_0^4 which can be taken to be the 4-D volume of a four-dimensional elementary hypercube of side $b_0 = 1.616 \times 10^{-35}$ m. This 4-D hypervolume has units of [m^4] while the four-dimensional Spacetime Continuum hypervolume consists of three space dimensions and one time dimension with units [m^3 s]. This requires that one of the four-dimensional hypercube dimensions b_0 be divided by c to convert it to a time elementary dimension $t_0 = b_0/c = 5.39 \times 10^{-44}$ s as is observed in (6). Eq. (6) can thus be written as

$$\hbar = \bar{\kappa}_0 \, b_0^3 \, \frac{b_0}{c} = \bar{\kappa}_0 \, b_0^3 \, t_0 = \bar{\kappa}_0 \, V_0^{STC} \tag{7}$$

where V_0^{STC} is the four-dimensional elementary Spacetime Continuum hypervolume and $\hbar$ has units of [J s] which are units of action $\mathcal{S}$.

Hence multiplying $\bar{\kappa}_0$ by a 3-D space volume converts it to energy, while multiplying it by a 4-D spacetime volume converts it to action. Energy applies to three-dimensional space, while action applies to four-dimensional spacetime. From (7), we see that Planck's reduced constant corresponds to an elementary quantum of action S_0:

$$\hbar = \bar{\kappa}_0 \, V_0^{STC} = S_0 \tag{8}$$

which has units of [J s]. Action units are the same as those of angular momentum, but this equivalence is accidental. The basic nature of $\hbar$ is an action, not an angular momentum. Calling $\hbar$ a "spin" quantity is an unfortunate misnomer from the early days of quantum mechanics. It needs to be called more appropriately an action quantity, i.e. the fundamental quantum of action of the Spacetime Continuum.

We thus find that action is the fundamental four-dimensional spacetime scalar quantity corresponding to energy for three-dimensional space. This helps explain why equations of motion in the Spacetime Continuum are determined by minimizing action, not energy, using the principle of least (or stationary) action given by

$$\delta \mathcal{S} = 0 \tag{9}$$

where the action $\mathcal{S}$ is expressed in terms of the Lagrangian L of the system as

$$\mathcal{S} = \int_{t_1}^{t_2} L\left(q(t), \dot{q}(t), t\right) \, dt \tag{10}$$

where $q = (q_1, q_2, ..., q_N)$ are the N generalized coordinates defining the configuration of the system and $\dot{q}$ denotes the time derivative of q.

In Lagrangian field theory, the action is written in terms of the Lagrangian density $\mathcal{L}$ specified in terms of one or more fields $\phi(x)$ and their derivatives $\partial_\mu \phi$ as [7, see p. 15ff]

$$\mathcal{S} = \int_{x_1}^{x_2} \mathcal{L}\left(\phi(x), \partial_\mu \phi\right) \, d^4 x \, . \tag{11}$$

The path integral formulation of quantum mechanics and quantum field theory is a generalization of the action principle of classical mechanics [8]. Interestingly enough, Feynman who developed this formulation [9]

> ... belie[ved] that the path integral captures the fundamental physics, and that hamiltonians and Hilbert space are merely mathematical methods for evaluating path integrals. [10, see p. 143]

In *STCED*, the path integral between two points x_1 and x_2 can be understood to be equivalent to the different possible wave paths between the two points.

The propagation amplitude $G(x_2; x_1)$ between the points x_1 and x_2 is determined from the path integral using the appropriate action for the system under consideration. One can see that since the contribution of a path is proportional to $e^{i\mathcal{S}/\hbar}$ [10, see p. 146], then, from (8), it is equivalent to $e^{i\mathcal{S}/S_0}$. In other words, the contribution of a path depends on the number of elementary quanta of action S_0 in the path.

The quantization of action implied by the above, points to the approach required to achieve quantization of path integrals in quantum physics. Coupled with the understanding that equations of motion in the Spacetime Continuum are determined by minimizing action as per (9) provides an indication for its potential application to the development of a quantized theory of path integrals.

4 Discussion and conclusion

In this paper, we have investigated the role of action $\mathcal{S}$ in the Spacetime Continuum as provided by the Elastodynamics of the Spacetime Continuum (*STCED*). We have found that multiplying the Spacetime Continuum bulk modulus constant $\bar{\kappa}_0$ by a 3-D space volume converts it to energy, while multiplying it by a 4-D spacetime volume converts it to action. Hence energy applies to three-dimensional space, while action applies to four-dimensional spacetime. Planck's reduced constant $\hbar$ corresponds to an elementary quantum of action S_0, with action units being the same as those of angular momentum. We thus find that action is the fundamental four-dimensional spacetime scalar quantity corresponding to energy for three-dimensional space. This helps explain why equations of motion in the Spacetime Continuum are determined by minimizing action, not energy, using the principle of least (or stationary) action. In particular, the contribution of a path, in the path integral formulation of quantum mechanics and quantum

field theory, depends on the number of elementary quanta of action S_0 in the path.

Received on August 24, 2022

References

1. Millette P. A. Elastodynamics of the Spacetime Continuum. *The Abraham Zelmanov Journal*, 2012, vol. 5, 221–277.
2. Millette P. A. Elastodynamics of the Spacetime Continuum: A Spacetime Physics Theory of Gravitation, Electromagnetism and Quantum Physics. American Research Press, Rehoboth, NM, 2017.
3. Millette P. A. Elastodynamics of the Spacetime Continuum, Second Expanded Edition. American Research Press, Rehoboth, NM, 2019.
4. Segel L. A. Mathematics Applied to Continuum Mechanics. Dover Publications, New York, 1987.
5. Millette P. A. Dislocations in the Spacetime Continuum: Framework for Quantum Physics. *Progress in Physics*, 2015, vol. 11 (4), 287–307.
6. Millette P. A. The Burgers Spacetime Dislocation Constant b_0 and the Derivation of Planck's Constant. *Progress in Physics*, 2015, vol. 11 (4), 313–316.
7. Peskin M. E., Schroeder D. V. An Introduction to Quantum Field Theory. Westview Press, Boulder, CO, 1995.
8. Padmanabhan T. Quantum Field Theory: The Why, What and How. Springer, Cham, CH, 2016.
9. Feynman R. P. Space-Time Approach to Non-Relativistic Quantum Mechanics. *Rev. Mod. Phys.*, 1948, v. 20, 367–387. Reprinted in Schwinger, J., ed. Selected Papers on Quantum Electrodynamics. Dover Publications, New York, 1958, pp 321–341.
10. Stone M. The Physics of Quantum Fields. Springer-Verlag, New York, 2000.

Black Hole Universe – A Complete Structure of the Entire Spacetime

T. X. Zhang

Department of Physics, Alabama A&M University, Normal, Alabama 35762. E-mail: tianxi.zhang@aamu.edu

A complete hierarchically layered structure of the entire spacetime is established in accordance with the black hole universe model that the author comprehensively developed on the basis of the three fundamentals without any other hypothetical entities: (1) Newton's cosmological principle (CP) of spacetime homogeneity and isotropy in a large scale, (2) Einstein's general theory of relativity (GR) that describes the effect of matter on spacetime, and (3) Zhang's principle of spacetime black hole equivalence (SBHEP) that postulates spacetimes and black holes to be equivalent (i.e. a black hole wraps a spacetime and a spacetime encloses a black hole). This alternative cosmological model not only explains all the observations of the universe without relying on any other hypothetical entities, but also overcomes all the cosmic difficulties based on the well-developed physics. Our universe is a black hole or spacetime and the observed starlike, massive, and/or supermassive black holes are child universes or subspacetimes of our black hole universe. The author's previous studies have fully and self-consistently described and explained various aspects of black hole universe such as its origin, structure, expansion, evolution, acceleration, emission, entropy, cosmic microwave background radiation, and so on. This study, by constructing the inside of the child universes of our black hole universe, to further develop a complete structure of the entire spacetime and provide us a complete new view to the inside of a black hole and a unique solution of the spacetime singularity.

1 Introduction

A physical cosmology is a branch of study in physics and astrophysics for the physical origin and evolution of the universe. A successful cosmological model should be simple, significant, and complete. Simplicity of a cosmological model refers to that the model is straight-forward and can simply and fully describe the universe based on the currently well-developed laws and theories of physics and astrophysics without making hypotheses that not only are non-testable but also violate the laws of physics and astrophysics. Significance of a cosmological model refers to that the model is important and can significantly explain all the observations of the universe and overcome all the cosmic problems without having any difficulty or without relying on any hypothetical entities. Completeness of a cosmological model refers to that the model is in its totality/entirety and can completely interpret the origin and evolution of development of the entire spacetime rather than only a finite part of the infinite universe or spacetime.

The standard big bang model of the universe (BBU) was developed on the two solid bases: (1) Einstein's general relativity (GR) that describes the effect of matter on spacetime [1] and (2) Newton's cosmological principle (CP) of spacetime isotropy and homogeneity. The Einsteinian field equation given in GR along with the Friedmann-Lemaitre-Robertson-Walker (FLRW) metric of spacetime derived from CP leads to the Friedmann equation (FE) that governs the development and dynamics of the universe [2]. The big bang theory has made incredible successes in explaining the universe, but there exist innumerable problems and difficulties. Solutions of these problems and difficulties severely rely on an increasing number of hypothetical entities (HEs) such as dark matter, dark energy, inflation, big bang singularity, and so on [3]. Therefore, BBU consists of GR, CP, and innumerable HEs, i.e. BBU = {GR, CP, HE, HE, HE,....} (see the blue part of Figure 1). Although it has only two bases (GR and CP), the BBU is neither simple and significant because of severely relying on an increasing number of HEs, which have not yet been and may never be tested or falsified, nor complete because of being finite and thus having unknown (or unable to answer) outside and prehistory.

Recently, the author has developed a new physical cosmology called black hole universe (BHU) [4-5]. Instead of making many HEs as the BBU did, the BHU proposes a new principle to the cosmology - the Principle of Spacetime Black Hole Equivalence (SBHEP) [6] - in an attempt to explain all the existing observations of the universe and overcome all the existing problems and difficulties. Standing on the three bases (GR, CP, and SBHEP), this new cosmological theory - BHU = {GR, CP, SBHEP} (see the red part of Figure 1) - can fully explain the universe in various aspects as well as to conquer all the cosmic problems according to the well-developed physics neither making any other HEs nor including any other unsolved difficulties [7-12]. GR and CP are common to both BBU and BHU. The BBU stands on two legs unstably so that it needs many crutches (or HEs) for support, while the BHU stands on three legs stably without needing any other props. In the BHU, a single SBHEP simply removes all of those innumerable HEs made in the BBU.

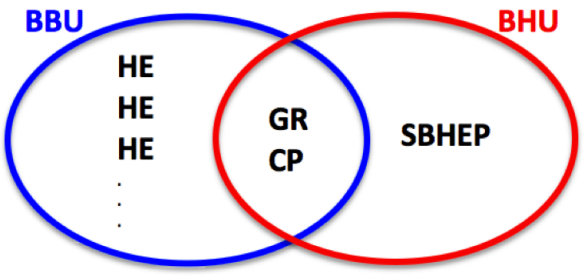

Fig. 1: The BBU versus the BHU [6, 12]. The BBU is developed on the basis of GR and CP with innumerable HEs to explain observations and overcome cosmic problems and difficulties. The BHU is developed on the basis of GR, CP and SBHEP. With one more base, SBHEP, the BHU can also perfectly explain all the existing observations of the universe and meantime overcome the cosmic problems and difficulties in terms of the well-developed physics without needing any other HEs.

The BHU is simple and significant because it does not rely on any HEs, but can fully explain the observations of the universe and overcome the cosmic problems and difficulties in terms of well-developed physics. It is also complete because the entire spacetime is infinite without unknown outside and prehistory. In the previous studies, the author has comprehensively explained various aspects of the universe, including its origin, structure, evolution, expansion, acceleration, cosmic microwave background (CMB) radiation, entropy, emissions of dynamic starlike, massive, and supermassive black holes such as gamma ray bursts, X-ray flares from galactic centers, and quasars, and so on [5-12]. However, the structure of the entire spacetime previously developed was only down to the level of the child universes of our black hole universe, i.e. the observed starlike, massive, and/or supermassive black holes. This study extends the structure of the entire spacetime into the deep insides of the child universes. This effort will provide us a complete structure of the entire spacetime and meantime shows us a brand new view to the insides of black holes, which may solve the black hole singularity issue.

2 Complete structure of the entire spacetime

According to the black hole model of the universe, our four-dimensional (4D) spacetime universe is a black hole, which is an extremely suppermassive and has been fully expanded with mass about a half hundred sextillions of solar masses, radius about forty-three hundred Mpc (or one Hubble length), and surface gravitational field about one third nanometer per second square [5-6]. All the inside, currently observed, starlike, massive, and/or supermassive black holes are subspacetimes (or child universes) of our black hole universe. Figure 2 shows the two-level or layer structure of any sized black hole or spacetime, including our black hole universe, and its child black holes. A black hole is a spacetime and its child black holes are its subspacetimes. For our black hole universe, the child universes or subspacetimes are the observed starlike, massive, and/or supermassive black holes. This hierarchically layered structure of spacetimes and subspacetimes genuinely overcomes the horizon problem, which was identified to exist in the big bang model of the universe primarily by Charles Misner in 1960s [13] and solved by Alan Guth in 1980s with the hypothesis of cosmic inflation [14] according to a field that does not correspond to any physical field. Therefore, in the black hole model of the universe, there does not exist the horizon problem at all. The scale of a black hole or spacetime should be much larger than that of its child black holes or subspacetimes.

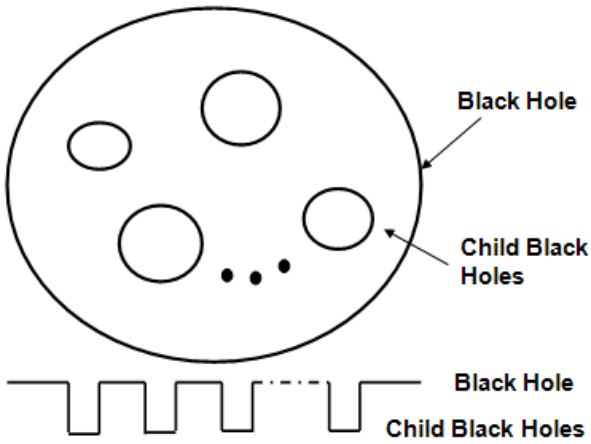

Fig. 2: The two-level or layer structure of a black hole or spacetime. Inside a black hole or spacetime, there are a number of child black holes or subspacetimes. For an example, inside our black hole universe, there are a number of child black hole universes or subspacetimes, which are the observed starlike, massive, and/or supermassive black holes.

Inside a black hole or spacetime, there are a number of child black holes or subspacetimes rather than singularity at the center as described conventionally. Outside a black hole or spacetime, there are a number of parallel sister black holes or spacetimes. Figure 3 shows a three-level or layer structure of a black hole or spacetime with both its inside and outside. The black hole or spacetime and all the parallel sister black holes or spacetimes are child black holes or subspacetimes of the mother black hole. Here, for the sketch to be simple, we have only drawn, inside each black hole or spacetime, three child black holes or subspacetimes. For our black hole universe, the observed starlike, massive, and/or supermassive black holes are its child universes or subspacetimes. The outside parallel universes are its sister universes. Our black hole universe and all the parallel sister universes are child universes or subspacetimes of the mother universe. Figure 4 sketches the four layers of the black hole universe from the child universe up to the grandmother universe which contains the aunt universes, mother universe, sister universes, cousin universes, our universe itself, child universes, and niece uni-

verses. Here again for the sketch to be simple, we only drew three universes for each layer. If the whole space is finite, then the matter in the whole space is finite and thus the number of layers is finite. Otherwise, it has infinite layers and the outermost layer corresponds to the limit of zero degree for the absolute temperature, zero for the density, and infinity for the radius and mass. A complete cosmological model suggests that the entire universe or spacetime must be infinite. For the black hole universe model to appropriately explain CMB, we favored and suggested that the entire spacetime to be infinite and eternal and include infinite universes, which are layered hierarchically [7].

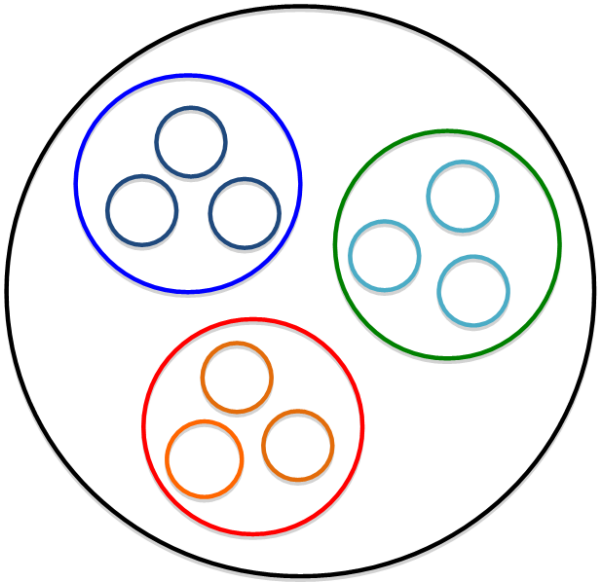

Fig. 3: The three-level or layer structure of a black hole or spacetime. Inside a black hole or spacetime (e.g. the one coded as green), there are a number of child black holes or subspacetimes. Outside the black hole or spacetime, there are a number of sister black holes (e.g., the ones coded as blue and red, respectively). Inside each of sister black holes, there are also a number of its child black holes. The black hole and all sister black holes are all the child black holes or subspacetimes of the mother black hole (coded as black). For our black hole universe, its inside has a number of the child black hole universes or subspacetimes, which are the observed starlike, massive, and/or supermassive black holes. Its outside has a number of sister black hole universes. Our black hole universe and all sister black hole universes are child black hole universes of the mother black hole universe.

For the infinite entire spacetime (called the grand universe), it has infinite layers [5-6, 12]. Figure 5 shows the infinite hierarchically layered structure of the infinite entire spacetime. The top layer is the entire spacetime, i.e. the grand universe, whose mass (M), radius (R), and entropy (S) are infinitely large; while the density (ρ) and temperature (T) (hence pressure) are infinitely small. The bottom layer is the layer of child universes, which are finite, referring to the

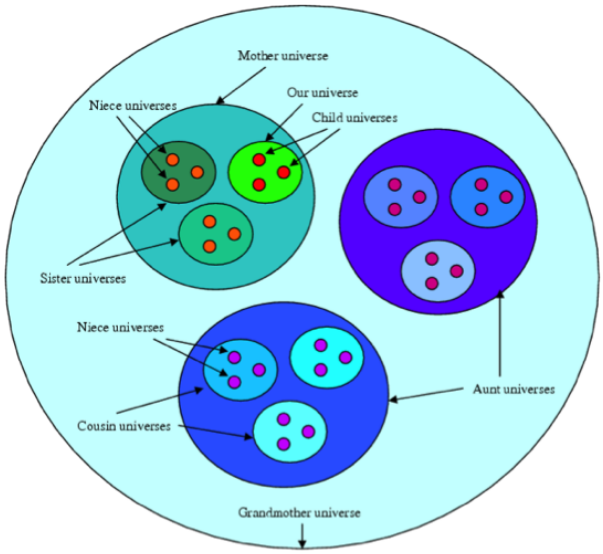

Fig. 4: The four-level or layer structure of our black hole universe up to the grandmother universe [5]. Inside our universe, there are a number of child universes, which are the observed starlike, massive, and/or supermassive black holes. Outside our universe, there are a number of sister universes who also have their own child universes named as niece universes. Our universe and all sister universes are child universes or subspacetimes of the mother universes. Parallel to the mother universe, there are a number of aunt universes who also have their child and grandchild universes or subspacetimes. The mother universe and all aunt universes are child universes or subspacetimes of the grandmother universe.

observed starlike, massive, and/or supermassive black holes. The second layer from the bottom is our universe. The child universe is a subspacetime of our universe; our universe is a subspacetime of the mother universe; the mother universe is a subspacetime of the grandmother universe, and so on. This infinitely layered structure of the entire spacetime can also be represented by using the mathematical set concepts as U = {...{F, F, F, ...{G, G, G, ...{A, A, A, ...{S, S, S, ...{C, C, C, ..., C}}}}...}. Here the child universes (also the niece universes) are null sets (i.e. C = { } and N = { }); the sister universes are sets of niece universes, S = {N, N, N, ...N}; our universe is a set of child universes, O = {C, C, C, ..., C}; the mother universe is the set of our universe and sister universes, M = {S, S, S, ..., O}; the aunt universes are sets of cousin universes, A = {Co, Co, Co, ..., Co}; the grandmother universe is the set of aunt universes and the mother universe, G = {A, A, A, ..., M}; and so on. The grand universe or the entire spacetime U is the grand set of all universes.

This previously developed infinitely layered structure of the infinite entire universe may not be complete, since it does not give what there are inside the child black hole universes. The structure of the entire universe shown in Figure 5 is only from the grand universe down to the child universes, which are currently observed starlike, massive, and/or supermassive

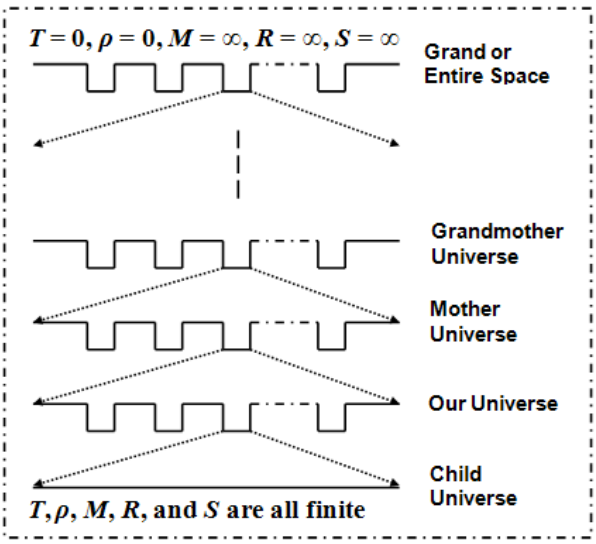

Fig. 5: The hierarchically layered structure of the entire universe, previously developed [6, 12]. It is incomplete because the bottom layer is only down to the child universes, suggested to be empty spacetimes or null sets. The child universes are subspacetimes of the universe in which we live in. Similarly, our universe is a subspacetime of the mother universe, and so on. The top or outmost layer is the entire space of all subspacetimes.

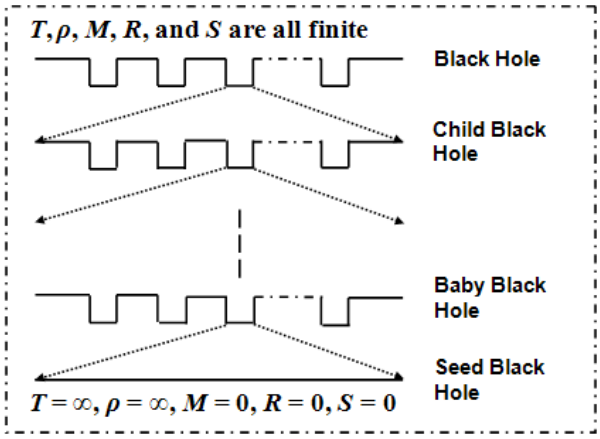

Fig. 6: The hierarchically layered structure of black holes or child black hole universes. Inside any sized black hole or spacetime, which is homogeneous and isotropic in the large or spacetime scale according to Newton's cosmological principle, there are a number of child black holes or subspacetimes. Inside a child black hole, there are a number of grandchild black holes, and so on in analogy. The bottommost is the seed black holes, which are infinitely small and are child black holes or subspacetime of a baby black holes.

blackholes. To have a complete structure of the entire spacetime, we need construct the inside of the child universes. According to Figure 2, any sized black hole or spacetime has a number of its child black holes or subspacetimes, like our black hole universe that has a great number of starlike, massive, and/or supermassive black holes as the child black hole universes. Therefore, inside a starlike, massive, or supermassive black hole, there may be in general a number of child black holes; inside a child black hole, there may be a number of grandchild black holes, and so on (see Figure 6). The innermost or bottommost layer is called seed black holes, which are infinitely small in size, mass, and entropy, but have infinitely large density, temperature, and pressure. The seed black holes are the child black holes of a baby black hole. This infinitely layered structure for the inside of a black hole or a spacetime can also be represented by using the mathematical set concepts. A black hole is a set of child black holes; a child black hole is a set of grandchild black holes, and so on in analogy. The baby black hole is a set of seed black holes, which are represented as null sets. A seed black hole has infinitely small mass, radius, and entropy, but infinitely large density, temperature, and pressure.

This hierarchically layered structure of a black hole provides us a completely new view to the inside of a black hole. At present, on what the inside of a black hole is, it is still an unsolved big open mysterious question in physics, since the Einsteinian general relativity is failed to be applicable to describe the inside of a black hole. Conventionally, most of scientists believe that matter once falling into a black hole will be gravitationally collapsed or drawn to the center point and form a dreaded singularity, where the known laws of physics break down and thus the picture of a black hole inside can be no longer trusted. As the matter inside a black hole is all drawn to the singular point at the center, there should be no matter and hence empty within the event horizon, except for the singular point at the center, which contains all matter of the black hole and thus has infinite density and temperature (see Figure 7). The matter density may be represented as the delta function of the radial distance. A recent notable study suggests that black hole are holograms [15]. This black hole holographic hypothesis considers a black hole as a holographic projection from a flat system of quantum particles that remains gravity-free. Though it may solve the clash between general relativity and quantum mechanics, the hologram model of black hole is still not fully understood. According to the black hole universe model, spacetime and black hole are equivalent. Our universe is a black hole and the observed starlike, massive, and/or supermassive black holes are subspacetimes of our 4D spacetime universe. The Einsteinian general relativity, a theory that describes the effect of matter on spacetime, is applicable to also describe the matter effect on a subspacetime, i.e. the inside of a black hole. The matter inside a black hole does not fall into the center point to form a singular point, but may form a number of child black holes or subspacetimes, which have scales much smaller than the black hole. The infinitely layered structure of a black hole as shown in Figure 6 shows the inside of a black hole to be infinite asymptotically singular spacetmes.

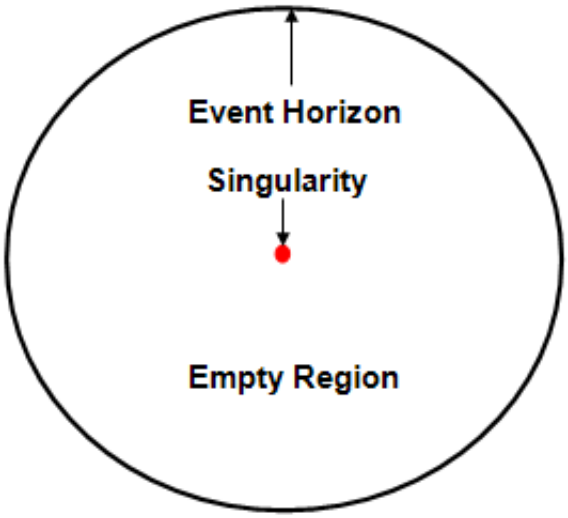

Fig. 7: The singularity of black hole. Conventionally, the matter falling into a black hole will be gravitationally collapsed or drawn to the center point and form a dreaded singularity, where the matter density goes to infinity. This will leads to the most interior region of a black hole does not have matter or is an empty space.

Considering the starlike, massive, and/or supermassive black holes to be child universes of our black hole universe, we can have the hierarchically layered structure of a child black hole universe from the hierarchically layered structure of a black hole given by Figure 6 through replacing the words "Black Hole" by "Child Universe", "Child Black Hole" by "Grandchild Universe", "Baby Black Hole" by "Baby Universe", and "Seed Black Hole" by "Seed Universe", and so on in analogy (see Figure 8). Then, combining Figure 5, which shows the infinite hierarchically layered structure of the entire spacetime that the author previously developed with the bottommost layer to be the child universes, with Figure 8, which shows the infinite hierarchically layered structure of the child universe, we can obtain the complete structure of the entire spacetime as shown in Figure 9. The top layer is the entire spacetime (or grand universe), whose mass, radius, and entropy are infinitely large; while the density, temperature, and pressure are infinitely small. The bottom layer is the layer of seed universes, whose mass, radius, and entropy are infinitely small; while the density, temperature, and pressure are infinitely large. The second layer from the bottom is the layer of baby universe. It is the mother universe of the seed universe. Infinitely going up in analogy, we have the layer of grandchild universes which are child universes or subspacetimes of the child universe of our universe. Our universe is a subspacetime of the mother universe; the mother universe is a subspacetime of the grandmother universe; and so on. This infinitely layered complete structure of the entire spacetime can also be represented by using the mathematical set concepts as U = {...{F, F, F, ...{G, G, G, ...{A, A, A, ...{S, S, S, ...{C, C, C, ..., {Gc, Gc, Gc, ...{....{Ba, Ba, Ba, ...{Se, Se, Se, ...} }...}}}}}}...}. The radii or masses of these universes, from the entire spacetime or grand universe to the seed universes, can be $\{\infty^{\infty}$, ..., ∞^{N}, ..., ∞^{2}, ∞^{1}, ..., M^{N}, ..., M^{2}, M, 1, M^{-1}, M^{-2}, ..., M^{-N}, ..., ∞^{-1}, ∞^{-2}, ..., ∞^{-N}, ..., $\infty^{-\infty}\}$ or simply say from infinitely large ∞^{∞} to infinitely small $\infty^{-\infty}$. This clear structure or picture of the entire spacetime exhibits the completeness of the black hole universe model. Any cosmological model without clearly describing its outside and inside cannot be a complete cosmology. Our next paper will establish the full origin and evolution of the entire spacetime and further give a full description not only to the present universe, but also its past and future or pre- and post-histories.

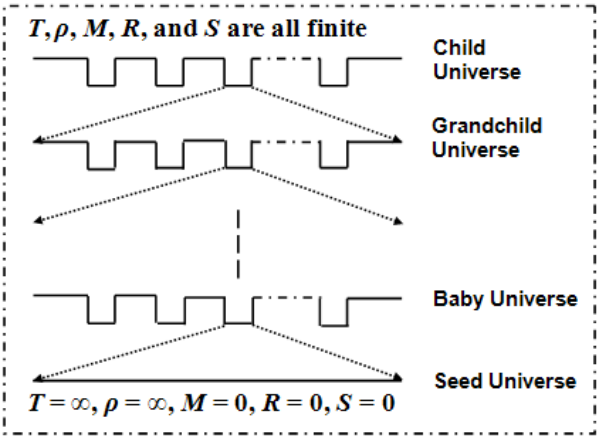

Fig. 8: The hierarchically layered structure of a child universe. Inside a child universe, there are a number of grandchild universes; inside a grandchild universe, there are a number of grand-grandchild universes; and so on in analogy. The bottommost layer is the level of seed universes, which are child universes or subspacetimes of a baby universe.

3 Summary

This study has established a complete structure for the infinite entire spacetime to be infinite hierarchically layered. First, we have constructed the internal structure of black holes or child universes as shown in Figure 6 or Figure 8. Then, we have combined the infinite hierarchically layered structure for the inside of child universes shown in Figure 8 with the previously developed infinite hierarchically layered structure of the entire spacetime that was only down to the child universes shown in Figure 5 to form the complete structure of the entire spacetime that is down to the infinitely small seed universes shown in Figure 9. The top layer is the entire spacetime, i.e. the grand universe, which has infinitely large mass, radius, and entropy and infinitely small density, temperature, and pressure. The bottom layer is the layer of seed universes, which has infinitely small mass, radius, and entropy and infinitely large density, temperature, and pressure. From the infinitely large top layer of the entire spacetime or the grand

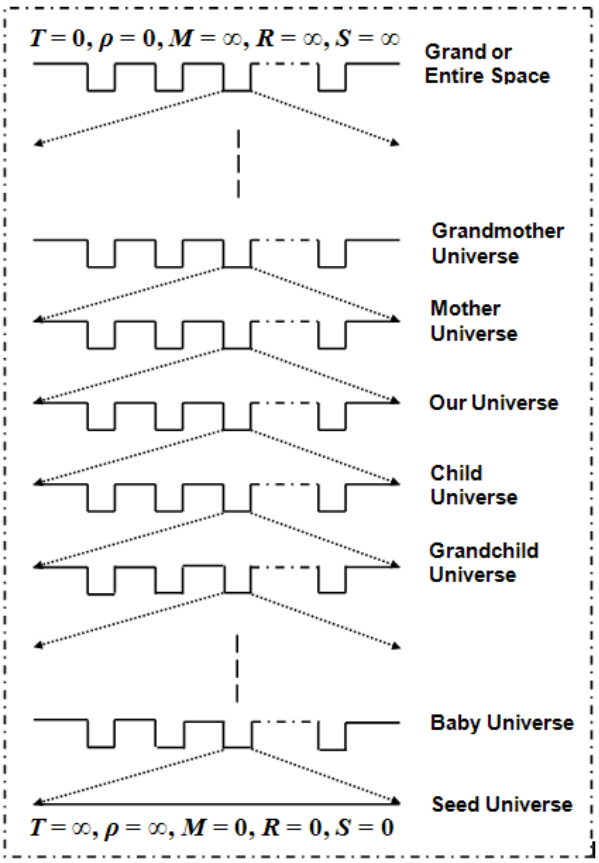

Fig. 9: The complete structure of the entire spacetime. The top or outermost layer is the entire spacetime, which is infinitely large. The bottom or innermost layer is the seed universe, which is infinitely small. The second layer from the bottom is the baby universe, which is the mother universe of the seed universe. Infinitely going up or out in analogy, they are grandchild, child, and our universes. Our universe is a subspacetime of the mother universe; the mother universe is a subspacetime of the grandmother universe; and so on.

universe to the infinitely small bottom layer of the seed universes, there are infinite layers. Our universe is about the middle finite large layer. Above or outside our universe, there are mother universes, grandmother universes, and so on. Below or inside our universe, there are child universes, grandchild universes, and so on. In addition to the complete structure of the entire spacetime, this study has also revealed the inside of black hole or child universes. This provides us a complete new view to the inside of black holes and a unique solution of the spacetime singularity as infinite asymptotically singular spacetimes.

Acknowledgements

The work was partially supported by the NSF/REU program (Grant #: PHY-1559870). The author is also thankful to the University's Title III Program for travel support of his attending conferences.

Received on August 10, 2022

References

1. Einstein A. Die Grundlage der Allgemeinen Relativitatstheorie. *Annalen der Physik*, 1916, v. 354, 769–822.
2. Friedmann A. Über die Möglichkeit einer Welt mit konstanter negativer Krümmung des Raumes. *Zeitschrift für Physik*, 1924, v. 21, 326–332.
3. Arp H. *et al*. An Open Letter to the Scientific Community – Signed by Scientists/Engineers/Researchers. *New Scientist*, 22 May 2004.
4. Zhang T. X. A New Cosmological Model: Black Hole Universe. *American Astronomical Society 211st Meeting*, 2007, Abstract #152.04.
5. Zhang T. X. A New Cosmological Model: Black Hole Universe. *Progress in Physics*, 2009, v. 2, 3–11.
6. Zhang T. X. Principle of Spacetime and Black Hole Equivalence. *Progress in Physics*, 2016, v. 12, 353–361.
7. Zhang T. X. Cosmic Microwave Background Radiation of Black Hole Universe. *Astrophysics and Space Science*, 2010, v. 330, 157–165.
8. Zhang T. X. Quasar Formation and Energy Emission in Black Hole Universe. *Progress in Physics*, 2012, v. 3, 48–53.
9. Zhang T.X. Frederick C. Acceleration of Black Hole Universe. *Astrophysics and Space Science*, 2014, v. 349, 567–573.
10. Zhang T. X.v Gamma Ray Bursts and Black Hole Universe. *Astrophysics and Space Science*, 2015, v. 358, article.id. #14, DOI 10.1007/s10509-015-2409-1, 8 pp.
11. Zhang T. X., Wilson C. & Schamschula M P. X-ray Flares from Sagittarius A* and Black Hole Universe. *Progress in Physics*, 2016, v. 12, 61–67.
12. Zhang T. X. The Principles and Laws of Black Hole Universe. *Journal of Modern Physics*, 2018, v. 9, 1838–1859.
13. Misner C. W., Coley A. A., Ellis G. F. R., Hancock M. The Isotropy of the Universe. *The Astrophysical Journal*, 1968, v. 151, 431–457.
14. Guth A. H. Inflationary Universe: A Possible Solution to the Horizon and Flatness Problems. *Physical Review D*, 1981, v. 23, 347–356.
15. Rinaldi E. *et al*. Matrix-Model Simulations Using Quantum Computing Deep Learning and Lattice Monte Carlo. *PRX Quantum*, 2022, v. 3, 0120324.

Lamb Shift in Discrete Time

Young Joo Noh

E-mail: yjnoh777@gmail.com, Seongnam, Korea

Lamb shift is the energy difference between the two energy levels of $2S_{1/2}$ and $2P_{1/2}$ of a hydrogen atom. This cannot be explained by the existing relativistic quantum mechanics, but was explained by the interaction of electrons and vacuum in quantum field theory. However, in this paper, I tried to explain the Lamb shift as a result of the previous paper [1] that causal delay in a discrete time perspective causes the charge change. As a result, the charge change caused an additional energy change in the existing fine structure of hydrogen, and the value was approximated.

1 Introduction

In my previous paper [1], I showed that the concept of causal delay in discrete time provides a correction for minimal coupling in electromagnetic interactions, and that this correction causes energy-scale-dependent changes in the charge and mass of elementary particles. An application example of such a result was attempted to explain the anomalous magnetic moment. In this paper, I will try to explain Lamb shift as another application example.

Like the anomalous magnetic moment, the Lamb shift is not explained by the existing relativistic quantum mechanics, but by the quantum field theory, a completely different paradigm. However, the changes in charge and mass due to the concept of causal delay open the possibility that these can be explained within the scope of modified relativistic quantum mechanics.

2 Nonrelativistic approximation of the modified Dirac equation

In the previous paper [1], it was shown that the Hamiltonian of electromagnetic interacting particles in terms of causal delay and the newly defined charge and mass dependent on energy scales are as follows

$$\mathrm{H} - q'\phi = \vec{\alpha}\cdot\left(\vec{p} - q'\vec{A}\right) + \beta m' \,, \tag{1}$$

where

$$\begin{aligned} m' &= f_{1r} m \\ q' &= (1 - f_{2r})\, q \end{aligned} \tag{2}$$

$$\begin{aligned} f_{1r} &= \mathrm{Re}\,(f_1) = \frac{1}{3}\,\mathrm{Re}\left(\frac{\mathrm{e}^{-i\Delta x\cdot p}}{\mathrm{e}^{-i\Delta x\cdot p} + 2\left(\mathrm{e}^{-i\Delta x\cdot\Delta p} - 1\right)}\right) \\ f_{2r} &= \mathrm{Re}\,(f_2) = \frac{1}{3}\,\mathrm{Re}\left(\frac{2\mathrm{e}^{-i\Delta x\cdot\Delta p}}{\mathrm{e}^{-i\Delta x\cdot p} + 2\left(\mathrm{e}^{-i\Delta x\cdot\Delta p} - 1\right)}\right). \end{aligned} \tag{3}$$

The Dirac equation satisfied by the electromagnetic interacting particle with mass m' and charge q' is as follows when expressed with two-component spinors ψ_A and ψ_B

$$(H - q'\phi)\begin{pmatrix}\psi_A\\ \psi_B\end{pmatrix} = \vec{\alpha}\cdot\left(\vec{p} - q'\vec{A}\right)\begin{pmatrix}\psi_A\\ \psi_B\end{pmatrix} + \beta m'\begin{pmatrix}\psi_A\\ \psi_B\end{pmatrix}. \tag{4}$$

Eq. (4) becomes the following system of equations

$$\begin{aligned} (H - q' - m')\,\psi_A &= \vec{\sigma}\cdot\left(\vec{p} - q'\vec{A}\right)\psi_B \\ (H - q' + m')\,\psi_B &= \vec{\sigma}\cdot\left(\vec{p} - q'\vec{A}\right)\psi_A \,. \end{aligned} \tag{5}$$

Since $\vec{A} = 0$ and ϕ is static in a hydrogen atom,

$$\psi(\vec{r}, t) = \mathrm{e}^{-iEt}\psi(\vec{r}), \quad E = m' + \varepsilon \,. \tag{6}$$

Then, in the second of (5), the following expression is obtained

$$\begin{aligned} (E - q'\phi + m')\,\psi_B(\vec{r}) &= \vec{\sigma}\cdot\vec{p}\,\psi_A(\vec{r}) \\ \psi_B(\vec{r}) &= (2m' + \varepsilon - q'\phi)^{-1}\,\vec{\sigma}\cdot\vec{p}\,\psi_A(\vec{r}) \\ &\cong \frac{1}{2m'}\left(1 - \frac{\varepsilon - q'\phi}{2m'}\right)\vec{\sigma}\cdot\vec{p}\,\psi_A(\vec{r}) \,. \end{aligned} \tag{7}$$

Since m' and q' are only parameters, the first of (5) is as follows

$$\begin{aligned} (\varepsilon - q'\phi)\,\psi_A &= \vec{\sigma}\cdot\vec{p}\,\frac{1}{2m'}\left(1 - \frac{\varepsilon - q'\phi}{2m'}\right)\vec{\sigma}\cdot\vec{p}\,\psi_A \\ &= \frac{q'}{4m'^2}\,(\vec{\sigma}\cdot\vec{p}\phi)\,(\vec{\sigma}\cdot\vec{p}\psi_A) + \\ &\quad + \frac{1}{2m'}\left(1 - \frac{\varepsilon - q'\phi}{2m'}\right)(\vec{\sigma}\cdot\vec{p})^2\,\psi_A \,. \end{aligned} \tag{8}$$

Therefore, the results of the relativistic correction of the modified Dirac equation can be obtained as follows

$$\begin{aligned} \varepsilon\psi_A &= \left\{\frac{\vec{p}^2}{2m'} + q'\phi - \frac{\vec{p}^4}{8m'^3} - \frac{q'}{4m'^2}\nabla\phi\cdot\nabla + \right. \\ &\quad \left. + \frac{q'}{4m'^2}\,\vec{\sigma}\cdot(\nabla\phi\times\vec{p})\right\}\psi_A \\ &= \left\{H'_0 + H'_{rel} + H'_D + H'_{SO}\right\}\psi_A \,. \end{aligned} \tag{9}$$

Eq. (9) is the same as just replacing m and q with m' and q' in the existing equation. In Section 3, I briefly review the fine structure of hydrogen, and in Section 4, how m' and q' of each term in (9) change the fine structure will be discussed. This discussion will be limited to only $2S_{1/2}$ and $2P_{1/2}$.

3 Fine structure of hydrogen

The Hamiltonian representing the fine structure of hydrogen is as follows

$$H = \frac{\vec{p}^2}{2m} - \frac{\alpha}{r} - \frac{\vec{p}^4}{8m^3} + \frac{1}{8m^2}\nabla^2 V_C + \frac{\alpha}{2m^2}\frac{\vec{S}\cdot\vec{L}}{r^3} = H_0 + H_{rel} + H_D + H_{SO}\,. \tag{10}$$

The changes in the energy of $2S_{1/2}$ and $2P_{1/2}$ by the last three terms of (10) are known as follows. Eq. (11) is the expectation value of each Hamiltonian, and the subscripts S and P denote $2S_{1/2}$ and $2P_{1/2}$

$$\begin{aligned}\Delta_{rel} &= \langle H_{rel}\rangle_S - \langle H_{rel}\rangle_P = -\frac{1}{12}\,m\alpha^4\\ \Delta_D &= \langle H_D\rangle_S - \langle H_D\rangle_P = \langle H_D\rangle_S = \frac{1}{16}\,m\alpha^4\\ \Delta_{SO} &= \langle H_{SO}\rangle_S - \langle H_{SO}\rangle_P = -\langle H_{SO}\rangle_P = \frac{1}{48}\,m\alpha^4\,.\end{aligned} \tag{11}$$

According to (11), the relativistic correction term lowers the energy of both $2S_{1/2}$ and $2P_{1/2}$, but the energy value of $2S_{1/2}$ has a lower energy value than $2P_{1/2}$ by $m\alpha^4/12$, and the Darwin term increases only the energy of $2S_{1/2}$ by $m\alpha^4/16$, and spin-orbit term lowers the energy of only $2P_{1/2}$ by $m\alpha^4/48$. The sum of all three effects is 0, so the energies of $2S_{1/2}$ and $2P_{1/2}$ are the same as a result. In other words, the Lamb shift cannot be explained by the existing relativistic quantum mechanics.

However, as we will see in the next chapter, the change in charge due to the causal delay effect causes a slight change in the expectation value of each Hamiltonian, which may explain the Lamb shift.

4 Corrections of fine structure

4.1 Modified Coulomb potential energy

First, let's try to find the charges q'_e and q'_p of the electron and the proton interacting in a hydrogen atom from (2)

$$\begin{aligned}q'_p &= \left(1 - f^p_{2r}\right)e\\ q'_e &= -\left(1 - f^e_{2r}\right)e\,.\end{aligned} \tag{12}$$

In a reference frame where the proton is at rest, first about the proton*,

$$\begin{aligned}&p_\mu = \left(E_p = m_p, 0, 0, 0\right)\ \ ,\ \ \Delta p_\mu = 0\\ &\Delta x\cdot p = E_p\,\Delta t_p = 1.\end{aligned} \tag{13}$$

$$q'_p = \left(1 - \frac{1}{3}\,\mathrm{Re}\left(\frac{2\mathrm{e}^{-i\Delta x\cdot\Delta p}}{\mathrm{e}^{-i\Delta x\cdot p} + 2\left(\mathrm{e}^{-i\Delta x\cdot\Delta p} - 1\right)}\right)\right)e = \left(1 - \frac{2}{3}\,\cos 1\right)e \equiv de\,. \tag{14}$$

About the electron,

$$\begin{aligned}\Delta x\cdot p &= \Delta t_e\left(E - \frac{\vec{p}^2}{\gamma m_e}\right) \cong \Delta t_e\; m_e = 1\\ \Delta x\cdot\Delta p &= \Delta t_e\left(\Delta E - \frac{\vec{p}\cdot\Delta\vec{p}}{\gamma m_e}\right) = \Delta t_e\;\Delta V\,.\end{aligned} \tag{15}$$

Using (15) and $\Delta p \ll p$, we get

$$\begin{aligned}q'_e &= -\left(1 - \frac{1}{3}\,\mathrm{Re}\left(\frac{2\mathrm{e}^{-i\Delta x\cdot\Delta p}}{\mathrm{e}^{-i\Delta x\cdot p} + 2\left(\mathrm{e}^{-i\Delta x\cdot\Delta p} - 1\right)}\right)\right)e\\ &= -\frac{2 - \frac{2}{3}\,\cos(\Delta x\cdot p)}{9 - 8\,\cos(\Delta x\cdot\Delta p)}\,e = \frac{-(d+1)\,e}{9 - 8\,\cos(\Delta t_e\;\Delta V)}\,.\end{aligned} \tag{16}$$

If the potential due to the proton is defined as (17), the $q'\phi$ related to the potential energy of the electron in (9) becomes (18)

$$\phi \equiv \frac{q'_p}{r}\,. \tag{17}$$

$$\begin{aligned}q'_e\phi &= -\frac{k\alpha}{r\,(9 - 8\,\cos(\Delta t_e\;\Delta V))}\,,\\ k &\equiv d\,(d+1) = 1.049\,.\end{aligned} \tag{18}$$

What we now need to do is to find the explicit expression for ΔV in (18). In (3), Δp represents the change in the momentum of an electron due to the interaction, which means that when the momentum of a free electron is p, the electromagnetic field is "turned on" and the momentum after the interaction is $p + \Delta p$. Therefore, in (18), ΔV means the value obtained by subtracting the potential energy of the free electron from the potential energy of the electron in a hydrogen atom, that is, Coulomb potential energy $-\alpha/r$. And, since $\Delta t_e = 1/m$,

$$q'_e\phi = -\frac{k\alpha}{r\,(9 - 8\,\cos(\alpha/mr))}\,. \tag{19}$$

At (19), $q'_e\phi$ is not exactly equal to the potential energy of the electron. Eq. (19) becomes $-k\alpha/r$ for large r, so it is somewhat different from the Coulomb potential energy $-\alpha/r$. So, to be equal to the Coulomb potential energy at a large r, the modified Coulomb potential energy must be defined as follows

$$V_m \equiv \frac{q'_e\phi}{k} = -\frac{\alpha}{r\,(9 - 8\,\cos(\alpha/mr))}\,. \tag{20}$$

Eq. (20) approximates the Coulomb potential energy well at large r. For example, at Bohr radius $a_0 = 1/m\alpha$, the ratio of modified Coulomb potential energy to Coulomb potential energy is as follows

$$\frac{V_m}{V_C} = \frac{1}{9 - 8\,\cos\alpha^2} = 0.99999999\,. \tag{21}$$

However, for small r, especially around $r = b \equiv \alpha/m = a_0\,\alpha^2 = 2.82\times10^{-15}$ m, that is, the closer to the proton (proton

*See the definition of causal delay time $\Delta t \equiv 1/m$ in the previous paper [1].

radius $r_p = 0.84 \times 10^{-15}$ m), the more it deviates from the Coulomb potential energy.

Considering the potential energy in the proton, assuming that the charges are uniformly distributed, the potential energy is a linear function with respect to r^2, so the overall potential energy function is as follows

$$\begin{aligned} r < r_p : V_{in} &= \frac{\alpha}{2r_p}\left[\left(\frac{r}{r_p}\right)^2 - 1.12\right] \\ r \geq r_p : V_m &= -\frac{\alpha}{r(9 - 8\,\cos(b/r))}\,. \end{aligned} \tag{22}$$

At $r < r_p$, the effect of fine structure by (10) is negligible, and the same is true for (9).

4.2 Mass change effect

As can be seen from (2), the mass also changes according to the energy scale. We discuss how the change in mass affects the energy of the electron in hydrogen. The energy of the electron is

$$E = \sqrt{m^2 + \vec{p}^2} + V \cong m + \frac{\vec{p}^2}{2m} - \frac{\vec{p}^4}{8m^3} + V\,. \tag{23}$$

In (23), $\vec{p}^2/2m$ and V are in order of $m\alpha^2$, and $-\vec{p}^4/8m^3$ is in order of $m\alpha^4$. Meanwhile, $\vec{p}^2/2m + V$ is invariant with respect to mass change. The reason is that, when the charge is constant, $mv^2/r = -e|\vec{E}|$, the change in mass cancels out the change in velocity. Thus, the energy change due to mass change appears in the term $-\vec{p}^4/8m^3$, which is α^2 times smaller than $\vec{p}^2/2m$ or V. That is, the energy change given by the mass change is α^2 times the energy change due to the charge change, so it can be ignored. Therefore, mass will be treated as a constant from now on.

Now, let's examine how each of the terms in (9) changes the fine structure.

4.3 Nonrelativistic term

$$H_0' = \frac{\vec{p}^2}{2m} + kV_m \Rightarrow \frac{\vec{p}^2}{2m} + V_m\,. \tag{24}$$

$P^2/2m + V_m$ in (24) is used to converge to the nonrelativistic Hamiltonian H_0 at large r. This is possible because the physics is invariant to the gauge transformation of electromagnetic potential energy. Also, convergence to the nonrelativistic Hamiltonian H_0 at large r means that each term of H' can be considered as a perturbation to H_0.

Now we need to find the expectation value $\langle H_0'\rangle_{S,P}$. In (10), the expectation value of H_0 is $\langle H_0\rangle = \langle V_C\rangle/2$ by the virial theorem, which does not strictly apply to H_0'. However, since the expectation value of H_0' mostly contributes to the large r part, and $V_m \cong V_C$ in the large r, the virial theorem can be approximately applied to the expectation value of H_0'. Thus

$$\left\langle H_0'\right\rangle_{S,P} \cong \frac{\langle V_m\rangle_{S,P}}{2}\,. \tag{25}$$

What we want to calculate is

$$\Delta_0' = \left\langle H_0'\right\rangle_S - \left\langle H_0'\right\rangle_P = \frac{1}{2}\left\{\langle V_m\rangle_S - \langle V_m\rangle_P\right\}\,. \tag{26}$$

And the function of the eigenstates $2S_{1/2}$ and $2P_{1/2}$ to be used in the calculation, that is, the solution of the Schrödinger equation is as follows.

$$\begin{aligned} \psi_{n=2,l=0,m=0} &= \frac{1}{\sqrt{8\pi a_0^3}}\left(1 - \frac{r}{2a_0}\right)\mathrm{e}^{-r/2a_0} \\ \psi_{n=2,l=1,m=0} &= \frac{1}{4\sqrt{2\pi a_0^3}}\,\frac{r}{a_0}\,\mathrm{e}^{-r/2a_0}\,\cos\theta\,. \end{aligned} \tag{27}$$

Eq. (26) is calculated as follows

$$\begin{aligned} \langle V_m\rangle_S &= \int_{r_p}^{\infty} 4\pi r^2\,\frac{-\alpha}{r\,(9 - 8\,\cos(b/r))}\,\frac{1}{8\pi a_0^3}\times \\ &\quad\times\left(1 - \frac{r}{a_0} + \frac{r^2}{4a_0^2}\right)\mathrm{e}^{-r/a_0}\,dr \\ &= -\frac{m\alpha^6}{2}\int_{0.3}^{\infty}\frac{1}{9 - 8\,\cos(1/r')}\times \\ &\quad\times\left(r' - \alpha^2 r'^2 + \frac{\alpha^4}{4}r'^3\right)\mathrm{e}^{-\alpha^2 r'}\,dr'\ \ (r = br') \\ \langle V_m\rangle_P &= \int_{r_p}^{\infty} 4\pi r^2\,\frac{2}{3}\,\frac{-\alpha}{r(9 - 8\,\cos(b/r))}\times \\ &\quad\times\frac{1}{32\pi a_0^3}\,\frac{r^2}{a_0^2}\,\mathrm{e}^{-r/a_0}\,dr \\ &= -\frac{m\alpha^{10}}{24}\int_{0.3}^{\infty}\frac{1}{9 - 8\,\cos((1/r')}r'^3\mathrm{e}^{-\alpha^2 r'}\,dr' \\ \Delta_0' &= -\frac{m\alpha^6}{4}\int_{0.3}^{\infty}\frac{1}{9 - 8\,\cos(1/r')}\times \\ &\quad\times\left(r' - \alpha^2 r'^2 + \frac{\alpha^4}{6}\,r'^3\right)\mathrm{e}^{-\alpha^2 r'}\,dr'\,. \end{aligned} \tag{28}$$

Unfortunately, the integral of (28) cannot be calculated analytically, but can be approximated. In the above integral, the factor $1/(9 - 8\,\cos(b/r))$ converges to 1 at large r. Its shape resembles a step function. This means that the integral is dominant at large r, so it can be calculated with the factor $1/(9 - 8\,\cos(b/r)) \cong 1$. So

$$\begin{aligned} &\langle V_m\rangle_S \cong \langle V_C\rangle_S\,,\ \langle V_m\rangle_P \cong \langle V_C\rangle_P \\ &\therefore \Delta_0' \cong \frac{1}{2}\left\{\langle V_C\rangle_S - \langle V_C\rangle_P\right\} = 0\,. \end{aligned} \tag{29}$$

Consequently, it can be said that the energy difference between $2S_{1/2}$ and $2P_{1/2}$ by V_m is very small.

4.4 Relativistic correction term

$$H'_{rel} = -\frac{\vec{p}^4}{8m^3} = -\frac{1}{2m}(E - V_m)^2 \,. \tag{30}$$

In (30), E is the expectation value of H'_0, so the desired value is

$$\begin{aligned}\Delta'_{rel} &= \left\langle H'_{rel}\right\rangle_S - \left\langle H'_{rel}\right\rangle_P \\ &= -\frac{1}{2m}\Big\{\left(E_S^2 - E_P^2\right) - 2\left(E_S\left\langle V_m\right\rangle_S - E_P\left\langle V_m\right\rangle_P\right) + \\ &\quad + \left(\left\langle V_m^2\right\rangle_S - \left\langle V_m^2\right\rangle_P\right)\Big\} \\ &\cong -\frac{1}{2m}\left\{\left\langle V_m^2\right\rangle_S - \left\langle V_m^2\right\rangle_P\right\} \,.\end{aligned} \tag{31}$$

The first and second terms in the second line of (31) can be ignored by the results in the previous chapter $\langle V_m\rangle_S \cong \langle V_m\rangle_P, E_S \cong E_P$

$$\begin{aligned}\left\langle V_m^2\right\rangle_S &= \int_{r_p}^{\infty} 4\pi r^2 \frac{\alpha^2}{r^2\left(9 - 8\,\cos(b/r)\right)^2}\left|\psi_{200}\right|^2 dr \\ \left\langle V_m^2\right\rangle_P &= \int_{r_p}^{\infty} 2\pi r^2 \frac{2}{3}\frac{\alpha^2}{r^2\left(9 - 8\,\cos(b/r)\right)^2}\left|\psi_{210}\right|^2 dr \,.\end{aligned} \tag{32}$$

In (32), it is a rough approximation, but if we put factor $1/(9 - \cos(b/r))^2 \simeq 1$

$$\begin{aligned}&\left\langle V_m^2\right\rangle_S \simeq \left\langle V_C^2\right\rangle_S \,,\ \left\langle V_m^2\right\rangle_P \simeq \left\langle V_C^2\right\rangle_P \\ &\therefore \Delta'_{rel} \simeq -\frac{1}{2m}\left\{\left\langle V_C^2\right\rangle_S - \left\langle V_C^2\right\rangle_P\right\} = \Delta_{rel} \,.\end{aligned} \tag{33}$$

According to (33), the correction by the relativistic correction term is also expected to be small.

4.5 Spin-orbit term

$$\begin{aligned}H'_{SO} &= \frac{q'_e}{4m^2}\,\vec{\sigma}\cdot(\nabla\phi\times\vec{p}) \\ &= \frac{k\alpha}{2m^2}\,\frac{1}{9 - 8\,\cos(b/r)}\,\frac{\vec{S}\cdot\vec{L}}{r^3} \\ &= \frac{1}{2m^2}\,\frac{kV_m}{r^2}\,\vec{S}\cdot\vec{L} \,.\end{aligned} \tag{34}$$

In (34), the spin-orbit term H'_{SO} is also expressed as modified Coulomb potential energy. This means that the gauge transformation can be performed so that H'_{SO} also converges to H_{SO} at large r. Thus

$$H'_{SO} = \frac{1}{2m^2}\,\frac{V_m}{r^2}\,\vec{S}\cdot\vec{L} \,. \tag{35}$$

On the other hand, using (36),

$$\begin{aligned}&\left\langle nljm_j\left|\vec{S}\cdot\vec{L}\right|nljm_j\right\rangle = \frac{1}{2}\left\{j(j+1) - l(l+1) - \frac{3}{4}\right\} \\ &\left\langle\vec{S}\cdot\vec{L}\right\rangle_S = 0 \,,\ \left\langle\vec{S}\cdot\vec{L}\right\rangle_P = -1 \,.\end{aligned} \tag{36}$$

Expectation values are:

$$\begin{aligned}\left\langle H'_{SO}\right\rangle_S &= 0 \\ \left\langle H'_{SO}\right\rangle_P &= -\frac{\alpha}{2m^2}\left\langle\frac{1}{9 - 8\,\cos(b/r)}\,\frac{1}{r^3}\right\rangle_P \\ &\cong -\frac{\alpha}{2m^2}\left\langle\frac{1}{r^3}\right\rangle_P = \left\langle H_{SO}\right\rangle_P \,.\end{aligned} \tag{37}$$

The difference between the spin-orbit term before and after charge correction is

$$\Delta'_{SO} - \Delta_{SO} = -\left\langle H'_{SO}\right\rangle_P + \left\langle H_{SO}\right\rangle_P \cong 0 \,. \tag{38}$$

Therefore, the charge change has little contribution to the spin-orbit term.

4.6 Darwin term

$$H'_D = -\frac{q'_e}{4m^2}\,\nabla\phi\cdot\nabla \,. \tag{39}$$

If we get the expectation value of (39), we get

$$\begin{aligned}\left\langle\psi\left|H'_D\right|\psi\right\rangle &= -\frac{1}{4m^2}\int\psi^\dagger\left(q'_e\nabla\phi\cdot\nabla\right)\psi\,d^3\vec{r} \\ &= -\frac{1}{8m^2}\int q'_e\nabla\phi\cdot\nabla\left(\psi^\dagger\psi\right)d^3\vec{r} \\ &= \frac{1}{8m^2}\int\psi^\dagger\psi\nabla\cdot\left(q'_e\nabla\phi\right)d^3\vec{r} \,.\end{aligned} \tag{40}$$

Consequently

$$H'_D = \frac{1}{8m^2}\,\nabla\cdot\left(q'_e\nabla\phi\right) \,. \tag{41}$$

where

$$q'_e = -\frac{(d+1)\,e}{9 - 8\,\cos(b/r)} \,, \quad \phi = \frac{de}{r} \,. \tag{42}$$

In (41), if $q'_e = -e$ and $q'_p = e$, it becomes H_D. H'_D is

$$\begin{aligned}H'_D &= \frac{1}{8m^2}\left(\nabla q'_e\cdot\nabla\phi + q'_e\nabla^2\phi\right) \\ &= \frac{k\alpha}{8m^2}\left\{\frac{\partial}{\partial r}\frac{1}{(9 - 8\,\cos(b/r))}\,\frac{1}{r^2} + \right. \\ &\quad \left. + \frac{4\pi\delta(\vec{r})}{9 - 8\,\cos(b/r)}\right\} \,.\end{aligned} \tag{43}$$

In (43), the Darwin term is expressed as a quantity related to the second order derivative of the modified Coulomb potential energy. This means that there is no gauge degree of freedom in the Darwin term, so the value of k in the equation must be maintained.

Expectation values are:

$$\begin{aligned}
\langle H'_D\rangle_S &= \frac{k\alpha}{8m^2}\int_{r_p}^{\infty} 4\pi r^2\,\frac{\partial}{\partial r}\frac{1}{(9-8\,\cos(b/r))}\times\\
&\times\frac{1}{r^2}\left|\psi_{200}\left(\vec{r}\right)\right|^2 dr\\
&+\frac{k\alpha}{8m^2}\int_{\vec{r}_p}^{\infty}\frac{4\pi\,\delta\left(\vec{r}\right)}{9-8\,\cos(b/r)}\left|\psi_{200}\left(\vec{r}\right)\right|^2 d^3\vec{r}\\
&=\frac{4\pi k\alpha}{8m^2}\left\{\left[\frac{1}{9-8\,\cos(b/r)}\left|\psi_{200}(\vec{r})\right|^2\right]_{r_p}^{\infty}-\right.\\
&\left.-\int_{r_p}^{\infty}\frac{1}{9-8\,\cos(b/r)}\,\frac{\partial}{\partial r}\left|\psi_{200}(\vec{r})\right|^2 dr\right\} \qquad (44)\\
&+\frac{4\pi k\alpha}{8m^2}\,\frac{\left|\psi_{200}\left(\vec{r}_p\right)\right|^2}{9-8\,\cos(b/r_p)}\\
&\cong-\frac{4\pi k\alpha}{8m^2}\int_{r_p}^{\infty}\frac{\partial}{\partial r}\left|\psi_{200}\left(\vec{r}\right)\right|^2 dr\\
&=\frac{4\pi k\alpha}{8m^2}\left|\psi_{200}\left(\vec{r}_p\right)\right|^2\cong\frac{km\alpha^4}{16}\,.\\
\langle H'_D\rangle_P &\cong\frac{4\pi k\alpha}{8m^2}\left|\psi_{210}\left(\vec{r}_p\right)\right|^2=O\left(m\alpha^8\right).
\end{aligned}$$

As can be seen from (44), the Darwin term by charge correction works mostly in the $2S_{1/2}$ state. Thus

$$\Delta'_D=\langle H'_D\rangle_S-\langle H'_D\rangle_P\cong\langle H'_D\rangle_S\cong\frac{km\alpha^4}{16}\,. \qquad (45)$$

Therefore, the difference between the Darwin term before and after charge correction is

$$\Delta'_D-\Delta_D\cong(k-1)\,\frac{m\alpha^4}{16}=57.67\,m\alpha^6\,. \qquad (46)$$

In (11), the existing Darwin term acts only on the $2S_{1/2}$ state to increase its energy by $m\alpha^4/16$, and in (46), the effect of charge correction by causal delay further increases the energy of the $2S_{1/2}$ state by $57.67\,m\alpha^6$.

5 Conclusions

From a discrete time point of view, causal delay gives energy scale-dependent changes to the mass and charge of elementary particles. In this paper, as a result of applying it to the Lamb shift, it was obtained that the change in the charge value increases the energy of $2S_{1/2}$ by about $57.67\,m\alpha^6$ =1076 MHz mostly by the Darwin term. This is slightly different from the experimental value of 1057.86 MHz, but it is a good result as an approximation. If numerical integration can be done accurately, I think it will be close to the actual value.

Received on September 2, 2022

References

1. Noh Y. J. Anomalous Magnetic Moment in Discrete Time. *Progress in Physics*, 2021, v. 17, 207–209.
2. Noh Y. J. Propagation of a Particle in Discrete Time. *Progress in Physics*, 2020, v. 16, 116–122.
3. Lamb W. E., Retherford R. C. Fine Structure of the Hydrogen Atom by a Microwave Method. *Physical Review*, 1947, v. 72 (3), 241–243.
4. Bethe H. A., Jackiw R. Intermediate Quantum Mechanics. The Benjamin Cummings Publishing Company, 1986.
5. Wachter A. Relativistic Quantum Mechanics. Springer, 2011.
6. Cohen-Tannoudji C., Diu B., Laloe F. Quantum Mechanics. Hermann, Paris, France, 1977.

A Quantitative Representation of Particle Entanglements via Bohm's Hidden Variable According to Hadronic Mechanics

Ruggero Maria Santilli

The Institute for Basic Research, 35246 U. S. 19N, Suite 215, Palm Harbor, FL 34684, USA.
E-mail: research@i-b-r.org

In this note, we first recall the 1935 historical view by A. Einstein, B. Podolsky and N. Rosen according to which *"Quantum mechanics is not a complete theory"* (EPR argument), because of the inability by quantum mechanics to provide a quantitative representation of the *interactions* occurring in particle entanglements. We then show, apparently for the first time, that the completion of quantum entanglements into the covering *EPR entanglements* formulated according to hadronic mechanics provides a *quantitative representation of the interactions occurring in particle entanglements* by assuming that their continuous and instantaneous communications at a distance are due to the overlapping of the wave packets of particles, and therefore avoiding superluminal communications. According to this view, entanglement interactions result to be non-linear, non-local and not derivable from a potential, and are represented via Bohm's variable λ hidden in the quantum mechanical *associative* product of Hermitean operators $AB = A \times B$ via explicit and concrete, axiom-preserving realizations $A\hat{\times}B = A\lambda B$, with ensuing *non-unitary* structure, multiplicative unit $U1U^\dagger = \hat{I} = 1/\lambda$, $\hat{I}\hat{\times}A = A\hat{\times}\hat{I} = A$, *inapplicability'* of Bell's inequalities and consequential validity of Bohm's hidden variables. We finally introduce, also apparently for the first time, the completion of quantum computers into the broader *EPR computers* characterizing a collection of extended electronic components under continuous entanglements, and show their apparent faster computation, better cybersecurity and improved energy efficiency.

According to clear experimental evidence dating back to the early part of the past century, particles that were initially bounded together and then separated, can continuously and instantaneously influence each other at a distance, not only at the particle level (see e.g. [1, 2] and papers quoted therein), but also at the classical level [3].

The above experimental evidence is generally *assumed* to be represented by quantum mechanics and, therefore, particle entanglements are widely called *quantum entanglement* (Figure 1). However, Albert Einstein strongly criticized such an assumption because it would imply superluminal communications that violate special relativity. This occurrence motivated the 1935 historical view by A. Einstein, B. Podolsky and N. Rosen according to which *"Quantum mechanics is not a complete theory"* (EPR argument) [4].

In fact, quantum mechanics can only represent interactions derivable from a potential while *no* quantum mechanical potential is conceivably possible to represent continuous and instantaneous interactions at a distance. More explicitly, the quantum mechanical equation for two interacting particles with coordinates $r_k,\ k = 1, 2$ on a Hilbert space $\mathcal{H}$ over the field C of complex numbers is given by the familiar Schrödinger equation (for $\hbar = 1$)

$$\left[\Sigma_{k=1,2}\ \frac{1}{2m_k}\ p_k p_k + V(r)\right]\psi(r) = E\,\psi(r)\,. \tag{1}$$

When the two particles are entangled, in view of the absence of any possible potential $V(r)$, the above equation becomes

$$\begin{aligned}
&\Sigma_{k=1,2}\ \frac{1}{2m_k}\ p_k p_k \psi(r_1)\psi(r_2) = \\
&= \left[\Sigma_{k=1,2}\ \frac{1}{2m_k}\left(-i\frac{\partial}{\partial_{r_k}}\right)\left(-i\frac{\partial}{\partial_{r_k}}\right)\right]\psi(r_1)\psi(r_2) = \\
&= E\,\psi(r_1)\psi(r_2)
\end{aligned} \tag{2}$$

and *can only represent two free particles* characterized by the individual wave functions $\psi(r_k)$ without any possible or otherwise known interaction.

At the *2020 International Teleconference on the EPR argument* [5–7], R. M. Santilli proposed the new notion of *Einstein-Podolsky-Rosen entanglement* (Sect. 7.2.3, p. 61 of [6]) which is based on the sole conceivable interaction responsible for particle entanglements, that due to the overlapping of the wave packets of particles (Figure 2), thus being non-linear as first suggested by W. Heisenberg [8], non-local as first suggested by L. de Broglie and D. Bohm [9] and non derivable from a potential as first suggested by R. M. Santilli at Harvard University under DOE support [13, 14], because of contact, thus continuous and instantaneous character, by therefore voiding the need for superluminal communications.

The non-linear, non-local and non-potential character of the assumed interactions render them ideally suited for their representation via the *isotopic (i.e. axiom-preserving branch of hadronic mechanics,* [15–17]), comprising *iso-mathematics and iso-mechanics* (see [18] for an outline, [19–21] for a

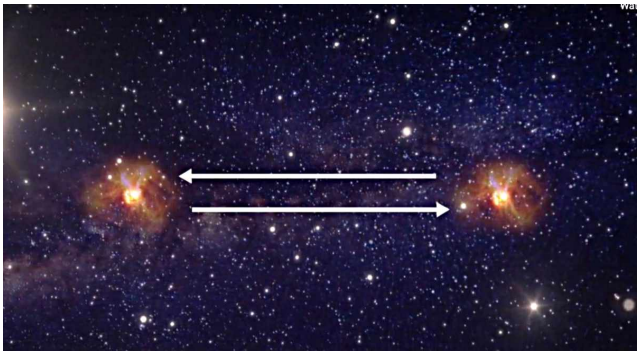

Fig. 1: In this figure, we illustrate the entanglement of particles with continuous and instantaneous interactions at a distance, and recall the argument by A. Einstein, B. Podolsky and N. Rosen on the lack of completeness of quantum mechanics due to its inability to represent said entanglement in a way compatible with special relativity [4].

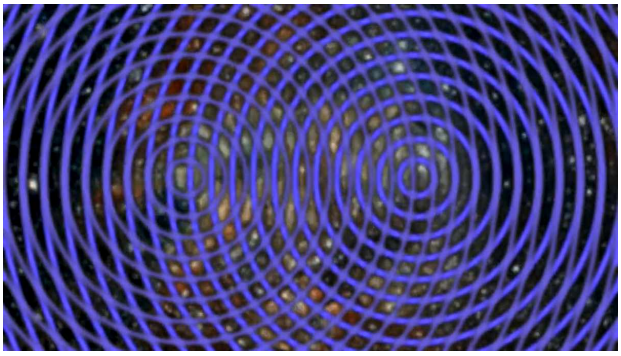

Fig. 2: In this figure, we illustrate the new Einstein-Podolsky-Rosen entanglement of particles introduced by R. M. Santilli in the 2020 overview [6] which is characterized by contact, therefore continuous and instantaneous interactions due to the overlapping of the wave packets of particles represented via Bohm's hidden variable (9), by therefore avoiding the need for superluminal interactions.

review and [22–30] for independent studies) which are characterized by the isotopy $\hat{\xi}:\{\hat{A},\hat{B},...,A\hat{\times}B\}$ of the universal enveloping associative algebra $\xi:\{A,B,...,AB=A\times B\}$ of quantum mechanical Hermitian operators $A,B,...$ with *iso-product* (first introduced in Eq. (5), p. 71 of [14])

$$\hat{A}\hat{\times}\hat{B}=\hat{A}\hat{T}\hat{B},\ \ \hat{T}>0\,, \tag{3}$$

where $\hat{T}$, called the *isotopic element,* is positive-definite but possesses otherwise an unrestricted functional dependence on coordinates, momenta, wave function and any other needed local variable, with related *iso-unit*

$$\begin{aligned}&\hat{I}=1/\hat{T}>0\,,\\ &\hat{I}\hat{\times}A=\hat{A}\hat{\times}\hat{I}=\hat{A},\ \forall\,\hat{A}\in\hat{\xi}\,,\end{aligned} \tag{4}$$

completion of Lie's theory into the *Lie-Santilli iso-theory* [14] (see [23, 28] for independent studies) with iso-brackets for an N-dimensional iso-algebra

$$[X_i\hat{,}X_j]=X_i\hat{\times}X_j-X_j\hat{\times}X_i=X_i\hat{T}X_j-X_j\hat{T}X_i=C_{ij}^kX_k\,, \tag{5}$$

iso-Heisenberg's equation (first proposed in Eq. (18), p. 163 of [14])

$$i\,\frac{dA}{dt}=[A\hat{,}H]=A\hat{\times}H-H\hat{\times}A\,, \tag{6}$$

and related *iso-Schrödinger's equation*

$$H\hat{\times}|\hat{\psi}\rangle=H\hat{T}|\hat{\psi}\rangle=E|\hat{\psi}\rangle\,. \tag{7}$$

Since the isotopic element $\hat{T}$ is *hidden* in the abstract axiom of associativity and becomes visible only in the isotopic realization (3)

$$A\hat{\times}(B\hat{\times}C)=(A\hat{\times}B)\hat{\times}C\,, \tag{8}$$

R. M. Santilli proposed in Sect. 6.8, p. 150 on, Eq. (5.8.19) in particular, of [16], as part of the isotopy of the SU(2) spin algebra and Pauli's matrices in particular, the *identification of the isotopic element $\hat{T}$ with Bohm's hidden variable λ* [31]

$$\lambda=\hat{T}(r,p,\psi,...)\,, \tag{9}$$

and consequential realization of the iso-unit $\hat{I}=1/\lambda$, with a variety of explicit and concrete realizations that, for the entanglement of two particles, are of the type [21]

$$\begin{aligned}&\lambda=\hat{T}=1/\hat{I}=\Pi_{\alpha=1,2}\,\text{Diag.}\left(\frac{1}{n_{1,\alpha}^2},\frac{1}{n_{2,\alpha}^2},\frac{1}{n_{3,\alpha}^2},\frac{1}{n_{4,\alpha}^2}\right)e^{-\Gamma},\\ &n_{\mu,\alpha}>0,\quad \Gamma>0,\ \ \mu=1,2,3,4,\ \ \alpha=1,2\,,\end{aligned} \tag{10}$$

providing:

1) A representation of the dimension and shape of particles via semi-axes $n_{k,\alpha}^2$, $k=1,2,3$ normalized to $n_{k,\alpha}=1$, $k=1,2,3$, $\alpha=1,2$ for the vacuum.

2) A representation of the density of particles via $n_{4,\alpha}^2$ normalized to the value $n_{\mu,\alpha}^2=1$ for the vacuum.

3) A representation of the non-potential character of the interactions due to the mutual penetration of particles via the exponential term e^{Γ}, where $\Gamma(\hat{r},\hat{p},\hat{\psi},...)$ is a positive-definite quantity with an unrestricted functional dependence on iso-coordinates $\hat{r}=r\hat{I}=r/\lambda$, iso-momenta $\hat{p}$, iso-wave-functions $\hat{\psi}(\hat{r})$, and other local variables.

By recalling the basic expression of the *iso-linear iso-momentum* characterized by the completion of the local Newton-Leibnitz differential calculus into the non-local *iso-differential calculus* [32] (see [29, 30] for independent studies)

$$\begin{aligned}\hat{p}\hat{\times}\hat{\psi}(\hat{r})&=\hat{p}\hat{T}(\hat{r},...)\psi(\hat{r})=-i\,\hat{\frac{\partial}{\partial_{\hat{r}}}}\hat{\psi}(\hat{r})=\\ &=-i\hat{I}(\hat{r},...)\,\frac{\partial}{\partial_{\hat{r}}}\hat{\psi}(\hat{r})=-i\,\frac{1}{\lambda}\,\frac{\partial}{\partial_{r/\lambda}}\hat{\psi}(r/\lambda)\,,\end{aligned} \tag{11}$$

the non-relativistic version of the EPR entanglement is characterized by the iso-Schrödinger equation (see [16] for the relativistic extension)

$$\begin{aligned}
&\Sigma_{k=1,2}\, \tfrac{1}{2m_k}\, \hat{p}_k \hat{\times} \hat{p}_k \hat{\times} \hat{\psi}(\hat{r}) = \\
&= \left[\Sigma_{k=1,2}\, \tfrac{1}{2m_k} \left(-i\hat{I}\tfrac{\partial}{\partial \hat{r}_k}\right)\left(-i\,\hat{I}\tfrac{\partial}{\partial \hat{r}_k}\right)\right] \hat{\psi}(\hat{r}) = \\
&= \left\{\Sigma_{k=1,2}\left[-\tfrac{\hat{I}^2}{2m_k}\left(\tfrac{\partial}{\partial \hat{r}_k}\right)\left(\tfrac{\partial}{\partial \hat{r}_k}\right) - \tfrac{\hat{I}}{2m_k}\left(\tfrac{\partial \hat{I}}{\partial \hat{r}_k}\right)\left(\tfrac{\partial}{\partial \hat{r}_k}\right)\right]\right\} \hat{\psi}(\hat{r}) = \qquad (12)\\
&= \left\{\Sigma_{k=1,2}\left[-\tfrac{\hat{I}^2}{2m_k}\left(\tfrac{\partial}{\partial \hat{r}_k}\right)\left(\tfrac{\partial}{\partial \hat{r}_k}\right) - \tfrac{\Gamma}{2m_k}\left(\tfrac{\partial \Gamma}{\partial \hat{r}_k}\right)\left(\tfrac{\partial}{\partial \hat{r}_k}\right)\right]\right\} \hat{\psi}(\hat{r}) = \\
&= \hat{E} \hat{\times} \hat{\psi}(\hat{r}) = E\hat{\psi}(\hat{r}) = E\hat{\psi}(\hat{r}_1) \hat{\times} \hat{\psi}(\hat{r}_2)\,,
\end{aligned}$$

with the following primary characteristics:

1. Iso-equation (9) characterizes a *new entanglement interaction* represented by Bohm's hidden variable $\lambda = \hat{T}$ which is absent in quantum mechanical equation (2);

2. The new entanglement interaction is manifestly *nonlinear* (in the wave-function), yet the theory is *iso-linear* [15, 16], namely, it is linear on the Hilbert-Myung-Santilli iso-space $\hat{\mathcal{H}}$ [33] with iso-states $|\psi\rangle$ and iso-normalization [12]

$$\langle \psi | \hat{\times} | \hat{\psi} \rangle = \langle \psi | \lambda | \hat{\psi} \rangle = \lambda\,, \qquad (12)$$

over Santtilli iso-field $\hat{C}$ of *iso-real, iso-complex or iso-quaternionic iso-numbers* [34]

$$\hat{n} = n\hat{I} = \frac{n}{\lambda} \qquad (13)$$

with iso-superposition principle $\psi(\hat{r}) = \hat{\psi}(\hat{r}_1 \hat{\times} \hat{\psi}(\hat{r}_2)$;

3. The new entanglement interaction is manifestly *nonlocal* in the sense of occurring in *volumes* represented by the iso-unit $\hat{I} = 1/\lambda$ and characterized by the overlapping of two volumes $V_k = (1/n^2_{1,k}, 1/n^2_{2,k}, 1/n^2_{3,k})$, $k = 1, 2$, each being on ontological grounds as big as experimental measurements can allow;

4. The new entanglement interaction is manifestly of contact, zero-range character, thus not being derivable from a potential, and therefore avoiding the need for superluminal interactions required by quantum entanglements [4];

5. The new entanglement interaction verifies, by conception and construction, the abstract axioms of relativistic quantum mechanics although realized via the indicated universal iso-associative envelope [35–37].

It should be indicated that (12) can be equally derived via a *non-unitary transformation* of quantum mechanical equation (2)

$$\begin{aligned}
&U \times 1 \times U^\dagger = \frac{1}{\lambda} = \hat{I}\,,\\
&U \times (A \times B) \times U^\dagger = A' \lambda B',\ \ \lambda = (U \times U^\dagger)^{-1}\,, \qquad (14)\\
&A' = U \times A \times U^\dagger,\ \ B' = U \times B \times U^\dagger\,.
\end{aligned}$$

The *invariance* of the numeric value of Bohm's hidden variable is then assured by the *Lorentz-Poincaré-Santilli iso-symmetry* [20] with structure [38]

$$\begin{aligned}
&U = \hat{U} \times \hat{T}^{1/2}\\
&\hat{U} \hat{\times} \hat{U}^\dagger = \hat{U}^\dagger \hat{\times} \hat{U} = \frac{1}{\lambda}\,.
\end{aligned} \qquad (15)$$

It may be of some interest to indicate the expected EPR completion of other branches of physics, such as the completion of quantum computers into new computers, here suggested under the name of *EPR computers,* for the description of extended electronic constituents in global, continuous and instantaneous communications, by therefore approaching the new notion of living organisms attempted in [39], with the following expected advances:

1) Faster computations, since all values of Bohm hidden variable λ are very small according to all available fits of experimental data [6], with ensuing rapid convergence of iso-perturbative series (see also Corollary 3.7.1, p. 128 of [20]). As a confirmation of this expectation, we recall the achievement via iso-mathematics and iso-chemistry of the first known *attractive* force between the *identical* electrons of valence coupling (see Chapter 4 of [40]), resulting in a *strong valence bond* that allowed the first known numerically exact representation of the experimental data for the hydrogen [41] and water [42] molecules with iso-perturbative calculations at least one thousand times faster than their conventional chemical counterparts.

2) Better cybersecurity, due to the formulation via iso-mathematics, with the consequential availability of iso-cryptograms equipped with an algorithm changing the numeric value of the iso-unit with such a frequency to prevent a solution within a finite period of time (Appendix 2C, p. 84 of [15] and [43]).

3) Increased energy efficiency, due to the fact that EPR entanglements are caused by *interactions without potential energy,* thus being more energy efficient than quantum computers.

The following comments are now in order:

I. Verifications of the EPR argument. In 1964, J. S. Bell [44] released a theorem according to which, under the assumption of quantum mechanics, the representation of the spin 1/2 of particles via Pauli's matrices, statistical independence and other assumptions, *a system of point-like particles with spin* 1/2 *does not admit a classical counterpart,* by therefore preventing any possibility of recovering Einstein determinism [4] under the indicated assumptions. The theorem was proved by showing that a certain expression D^{Bell} (whose explicit value depends on the relative conditions of the particles) is always *smaller* than the corresponding classical value D^{Clas},

$$D^{Bell} < D^{Clas}\,, \qquad (16)$$

for all possible values of D^{Bell}.

By assuming that nuclear forces have a non-linear, nonlocal and non-potential component represented via the isotopic element $\hat{T}$, R. M. Santilli initiated in 1981 [10] the studies on the inevitable *completion of Heisenberg's uncertainties and Bell's inequalities for strong interactions.*

Following the achievement of maturity for iso-mathematics and iso-mechanics, by representing the *extended* character of nuclear constituents via the *isotopic completion of Pauli's matrices with Bell's hidden variables* [16], today called the *Pauli-Santilli iso-matrices* formulated on a Hilbert-Myung-Sanilli iso-space [33] over Santilli iso-fields C [34] (see Eqs. (6.8.20), p. 254 of [16])

$$\hat{\sigma}_k = U\sigma_k U^\dagger, \quad UU^\dagger = \hat{I} = 1/\hat{T} = \text{Diag.}(\lambda^{-1}, \lambda),$$
$$\hat{\sigma}_1 = \begin{pmatrix} 0 & \lambda \\ \lambda^{-1} & 0 \end{pmatrix}, \quad \hat{\sigma}_2 = \begin{pmatrix} 0 & -i\lambda \\ i\lambda^{-1} & 0 \end{pmatrix}, \tag{17}$$
$$\hat{\sigma}_3 = \begin{pmatrix} \lambda^{-1} & 0 \\ 0 & -\lambda \end{pmatrix},$$

with *iso-commutation rules*

$$[\hat{\sigma}_i, \hat{\sigma}_j] = \hat{\sigma}_i \hat{\times} \hat{\sigma}_j - \hat{\sigma}_j \hat{\times} \hat{\sigma}_i = i2\epsilon_{ijk}\hat{\sigma}_k\,, \tag{18}$$

and *conventional spin* $1/2$ *iso-eigenvalues*

$$\hat{\sigma}_3 \hat{\times} |\hat{b}\rangle = \hat{\sigma}_3 \hat{T} |\hat{b}\rangle = \pm |\hat{b}\rangle\,,$$
$$\hat{\sigma}^{\hat{2}} \hat{\times} |\hat{b}\rangle = (\hat{\sigma}_1 \hat{T} \hat{\sigma}_1 + \hat{\sigma}_2 \hat{T} \hat{\sigma}_2 + \hat{\sigma}_3 \hat{T} \hat{\sigma}_3)\hat{T} |\hat{b}\rangle = 3|\hat{b}\rangle\,. \tag{19}$$

R. M. Santilli proved in 1998 the following *completion of Bell's inequalities for strong interactions* (Eq. (5.8), p. 189 of [11])

$$D^{HM} = \frac{1}{2}(\lambda_1 \lambda_2^{-1} + \lambda_1^{-1}\lambda_2)\, D^{Bell}\,, \tag{20}$$

where λ_1 and λ_2 are the hidden variables of the two particles. Additionally, Santilli proved that D^{HM} can indeed be equal to the corresponding D^{Clas} with specific examples, by therefore confirming Einstein's view on the possible recovering of classical determinism.

Finally, by combining the results of [10] and [11], in 2019 R. M. Santilli [12] (see the review in [20]) proved the following *completion of Heisenberg's uncertainties for strong interactions* (Eq. (35), p. 14 of [12])

$$\Delta r\, \Delta p \approx \frac{1}{2} \left| \langle \hat{\psi}(\hat{r}) | \hat{\times} [\hat{r}, \hat{p}] \hat{\times} | \hat{\psi}(\hat{r}) \rangle \right| \ll \frac{1}{2} \hat{T} = \frac{\lambda}{2} \tag{21}$$

establishing that *the standard deviations Δr and Δp, individually as well as their product, progressively approach Einstein's classical determinism with the increase of the density in the interior of hadrons, nuclei, and stars, and achieve a full classical determinism at the limit of Schwarzschild's horizon for which $\lambda = \hat{T} = 0$.*

In essence, verifications [10–12] of the EPR argument establish that Bell's inequalities are *valid* for the electromagnetic interactions of point-like particles, including electrons and photons, with ensuing lack of hidden variables.

By contrast, following half a century of mathematical, theoretical and experimental studies in the field, this author believes that Bell's inequalities are *inapplicable,* in favor of their completions via hadronic mechanics [10–12], for composite systems of particles at short mutual distances, including hadrons [20] and leptons [47], because the exact representation of their experimental data requires non-unitary transforms of quantum models, under which none of Bell's assumptions can be formulated, with ensuing validity of Bohm's hidden variables.

It then follows that any experiment proving the *violation* of Bell's inequalities, as defined by the above equations, is a direct experimental verification of hadronic mechanics.

II. Conditions of validity of hadronic mechanics. Recall that the wave packet of one electron is identically null only at infinity and, consequently, the universe is a single integrated structure much similar to the total EPR entanglement of living organisms [39]. Recall also that the universe will never admit one single final theory for the representation of all its complexities. Under these recollections, this author believes that the isotopic branch of hadronic mechanics can indeed provide a first axiomatically consistent representation of *stable,* thus time reversible systems, while the genotopic branch of hadronic mechanics can provide a first axiomatically consistent representation of energy-releasing processes, including nuclear fusions and fossil fuel combustion [20], and the hyperstructural branch of hadronic mechanics can at least initiate the search for an axiomatically consistent representation of life [39], here referred to a quantitative representation of the difference between organic and inorganic molecules.

III. Conditions of validity of quantum mechanics. By recalling that "point-like wave packets" do not exist in nature, and that quantum mechanics is identically and uniquely recovered by iso-mathematics and iso-mechanics for $\lambda = \hat{T} = 1$, this author believes that the Copenhagen interpretation of quantum mechanics provides an excellent representation of *stable systems of particles at mutual distances allowing their effective approximation as being point-like,* by therefore solely admitting action-at-a-distance potential interactions, with ensuing validity for atomic structures, particles in accelerators, crystals and numerous other systems. Despite these justly historical achievements, following half a century of studies in the field, this author believes that *quantum mechanics cannot be exactly valid for particle entanglements, as shown in this note, as well as for all composite systems of particles at short mutual distances, thus including leptons, hadrons, nuclei and stars* [17].

It is appropriate in the latter respect to note that the widespread assumption that a single theory, quantum mechanics, can represent all possible complexities of the universe, has

been kept for about one century in oblivion of:

A) Clear experimental evidence in various fields of *deviations* of physical reality from quantum predictions in favor of *exact* representations via hadronic mechanics, including deviations in: nuclear physics [45]; electrodynamics [46–48]; nuclear physics [45]; condensed matter physics [49]; heavy ion physics [50]; time dilation for composite particles [51]; Bose-Einstein correlation [52, 53]; cosmology [54, 55]; and other fields.

B) The insufficiencies of quantum mechanics in nuclear physics due to its inability over one century under large public funds to achieve [19–21]: a quantitative representation of the synthesis of the neutron from the hydrogen in the core of stars; an exact representation of nuclear magnetic moments; an exact representation of the spin of nuclei in their true ground state (that without the usual orbital excitations); a representation of the stability of nuclei despite the huge Coulomb repulsion between nuclear protons; a representation of the stability of neutrons when members of a nuclear structure; and other insufficiencies.

C) The inability by quantum mechanics to allow a consistent treatment of energy-releasing processes, including nuclear fusions, due to their time irreversibility compared to the known time-reversibility of quantum mechanics (e.g. because of the invariance of Heisenberg's equation under anti-Hermiticity and for other reasons). Under these conditions, the same Schrödinger equation has to be applied for both, the forward and backward time evolutions, with ensuing violation of causality due to unavoidable solutions in which the effect precedes the cause. This violation of causality may explain the lack of achievement to date of controlled nuclear fusion [56].

Consequently, the continuation of the century-old use and support of quantum mechanics for all possible conditions existing in the universe in oblivion of the teaching by Einstein, Podolsky and Rosen, in oblivion of vast opposing experimental evidence, and in oblivion of fundamental unresolved nuclear problems, may continue to have widely negative implications for our rapidly deteriorating environment.

Acknowledgements

The author would like to thank for critical comments the participants of the *2020 International Teleconference on the EPR argument*. Additional thanks are due to Mrs. Sherri Stone for linguistic control of the manuscript.

This note has been written from 9-20 to 9-30, 2022, at the Pietra Blue Resort, Polignano a Mare, Bari, Italy.

Received on October 9, 2022

References

1. Aspect A. *et al*. Experimental Realization of Einstein-Podolsky-Rosen-Bohm Gedankenexperiment: A New Violation of Bell's Inequalities. *Phys. Rev. Lett.*, 1982, v. 49, 91–94. http://ui.adsabs.harvard.edu/abs/1982PhRvL..49...91A
2. Eigen G. Measurements of the Polarization Correlation of the Two-Photon System Produced in Positron-Electron Annihilation. *Proceedings of the 2020 Teleconference on the EPR argument*, Curran Associates, New York, 823–843, 2021.
3. Berkowitz R. Macroscopic systems can be controllably entangled and limitlessly measured. *Physics Today*, July 2021, 16–18.
4. Einstein A., Podolsky B., and Rosen N. Can quantum-mechanical description of physical reality be considered complete? *Phys. Rev.*, 1935, v. 47, 777–791. http://www.eprdebates.org/docs/epr-argument.pdf
5. Beghella-Bartoli S. and Santilli R. M., eds, Proceedings of the 2020 Teleconference on the Einstein-Podolsky-Rosen argument that "Quantum mechanics is not a compete theory". Curran Associates, New York, NY, 2021. http://www.proceedings.com/59404.html (printed), 60007.html (electronic). http://www.world-lecture-series.org/level-xii-epr-teleconference-2020 (recorded lectures).
6. Santilli R. M. Overview of historical and recent verifications of the Einstein-Podolsky-Rosen argument and their applications to physics, chemistry and biology. APAV - Accademia Piceno Aprutina dei Velati, Pescara, Italy, 2021. http://www.santilli-foundation.org/epr-overview-2021.pdf
7. Dunning-Davies J. A Present Day Perspective on Einstein-Podolsky-Rosen and its Consequences. *Journal of Modern Physics*, 2021, v. 12, 887–936. http://www.scirp.org/journal/paperinformation.aspx?paperid=109219
8. Heisenberg W. *Nachr. Akad. Wiss. Gottingen*, 1953, v. IIa, 111. http://link.springer.com/chapter/10.1007/978-3-642-70079-8_23
9. Goldstein S. Bohmian (de Broglie-Bohm) Mechanics. Stanford Encyclopedia of Philosophy, 2021. http://plato.stanford.edu/entries/qm-bohm/
10. Santilli R. M. Generalization of Heisenberg's uncertainty principle for strong interactions. *Hadronic Journal*, 1981, v. 4, 642–657. http://www.santilli-foundation.org/docs/generalized-uncertainties-1981.pdf
11. Santilli R. M. Isorepresentation of the Lie-isotopic SU(2) Algebra with Application to Nuclear Physics and Local Realism. *Acta Applicandae Mathematicae*, 1998, v. 50, 177–190. http://www.santilli-foundation.org/docs/Santilli-27.pdf
12. Santilli R. M. Studies on the classical determinism predicted by A. Einstein, B. Podolsky and N. Rosen. *Ratio Mathematica*, 2019, v. 37, 5–23. http://www.eprdebates.org/docs/epr-paper-ii.pdf
13. Santilli R. M. Foundation of Theoretical Mechanics. Vol. I, The Inverse Problem in Newtonian Mechanics. Springer-Verlag, Heidelberg, Germany, 1978. http://www.santilli-foundation.org/docs/Santilli-209.pdf
14. Santilli R. M. Foundation of Theoretical Mechanics. Vol. II, Birkhoffian Generalization of Hamiltonian Mechanics. Springer-Verlag, Heidelberg, Germany, 1983. http://www.santilli-foundation.org/docs/santilli-69.pdf
15. Santilli R. M. Elements of Hadronic Mechanics. Vol. I, Mathematical Foundations. Ukraine Academy of Sciences, Kiev, 1995. http://www.santilli-foundation.org/docs/Santilli-300.pdf
16. Santilli R. M. Elements of Hadronic Mechanics. Vol. II, Theoretical Foundations. Ukraine Academy of Sciences, Kiev, 1995. http://www.santilli-foundation.org/docs/Santilli-301.pdf
17. Santilli R. M. Elements of Hadronic Mechanics. Vol. III, Experimental Verifications. Ukraine Academy of Sciences, Kiev, 2016. http://www.santilli-foundation.org/docs/elements-hadronic-mechanics-iii.compressed.pdf
18. Anderson R. Outline of Hadronic Mathematics, Mechanics and Chemistry as Conceived by R. M. Santilli. *American Journal of Modern Physics*, 2016, v. 6, 1–16. http://www.santilli-foundation.org/docs/HMMC-2017.pdf

19. Santilli R. M. Studies on A. Einstein, B. Podolsky, and N. Rosen prediction that quantum mechanics is not a complete theory. I: Basic methods. *Ratio Mathematica*, 2020, v. 38, 5–69. //eprdebates.org/docs/epr-review-i.pdf
20. Santilli R. M. Studies on A. Einstein, B. Podolsky, and N. Rosen prediction that quantum mechanics is not a complete theory. II: Apparent proof of the EPR argument. *Ratio Mathematica*, 2020, v. 38, 71–138. //eprdebates.org/docs/epr-review-ii.pdf
21. Santilli R. M. Studies on A. Einstein, B. Podolsky, and N. Rosen prediction that quantum mechanics is not a complete theory. III: Illustrative examples and applications. *Ratio Mathematica*, 2020, v. 38, 139–222. //eprdebates.org/docs/epr-review-iii.pdf
22. Aringazin A. K., Jannussis A., Lopez F., Nishioka M. and Veljanosky B. Santilli's Lie-Isotopic Generalization of Galilei and Einstein Relativities. Kostakaris Publishers, Athens, Greece, 1991. http://www.santilli-foundation.org/docs/Santilli-108.pdf
23. Sourlas D. S. and Tsagas Gr. T. Mathematical Foundation of the Lie-Santilli Theory. Ukraine Academy of Sciences, 1993. http://www.santilli-foundation.org/docs/santilli-70.pdf
24. Lohmus J., Paal E. and Sorgsepp L. Non-associative Algebras in Physics. Hadronic Press, 1994. http://www.santilli- foundation.org/docs/Lohmus.pdf
25. Kadeisvili J. V. Santilli's Isotopies of Contemporary Algebras, Geometries and Relativities, Second edition. Ukraine Academy of Sciences, Kiev, 1997. http://www.santilli-foundation.org/docs/Santilli-60.pdf
26. Jiang C.-X. Foundations of Santilli Isonumber Theory. International Academic Press, 2001. http://www.i-b-r.org/docs/jiang.pdf
27. Ganfornina R. M. F. and Valdes J. N. Fundamentos de la Isotopia de Santilli. International Academic Press, Palm Harbor, FL, 2001. www.i-b-r.org/docs/spanish.pdf. English translation: Algebras, Groups and Geometries,2015, v. 32, 135–308 (2015) http://www.i-b-r.org/docs/Aversa-translation.pdf
28. Gandzha I. and Kadeisvili J. V. New Sciences for a New Era: Mathematical, Physical and Chemical Discoveries of Ruggero Maria Santilli. Sankata Printing Press, Nepal, 2011. http://www.santilli-foundation.org/docs/RMS.pdf
29. Georgiev S. Foundations of IsoDifferential Calculus. Vol 1. – Iso-Differential and Iso-Integral Calculus for Iso-Functions in One Variable. Vol 2. – Iso-Differential and Iso-Integral Calculus for Iso-Functions in Several Variables. Vol. 3 – Iso-Ordinary Iso-Differential Equations. Vol. 4 – Iso-Difference Equations. Vol.5 – Iso-Stochastic Iso-Differential Equations. Vol. 6 – Theory of Iso-Measurable Iso-Functions. Nova Publishers, New York, NY, 2014 (I), 2014 (II), 2014 (III), 2015 (IV), 2015 (V), 2016 (VI), 2022 (I new ed.).
30. Georgiev S. Iso-Mathematics. Lambert Academic Publishing, 2022.
31. Bohm D. A Suggested Interpretation of the Quantum Theory in Terms of "Hidden Variables". *Physical Review*, 1952, v. 85, 166–182. http://journals.aps.org/pr/abstract/10.1103/PhysRev.85.166
32. Santilli R. M. Nonlocal-Integral Isotopies of Differential Calculus, Mechanics and Geometries. *Rendiconti Circolo Matematico Palermo, Suppl.*, 1996, v. 42, 7–82. http://www.santilli-foundation.org/docs/Santilli-37.pdf
33. Myung H. C. and Santilli R. M. Modular-isotopic Hilbert space formulation of the exterior strong problem. *Hadronic Journal*, 1982, v. 5, 1277–1366. http://www.santilli-foundation.org/docs/myung-santilli-1982.pdf
34. Santilli R. M. Isonumbers and Genonumbers of Dimensions 1, 2, 4, 8, their Isoduals and Pseudoduals, and "Hidden Numbers" of Dimension 3, 5, 6, 7. *Algebras, Groups and Geometries*, 1993, v. 10, 273–322. http://www.santilli-foundation.org/docs/Santilli-34.pdf
35. Santilli R. M. Lie-isotopic Lifting of Special Relativity for Extended Deformable Particles. *Lettere Nuovo Cimento*, 1983, v. 37, 545–555. http://www.santilli-foundation.org/docs/Santilli-50.pdf
36. Santilli R. M. Isotopic Generalizations of Galilei and Einstein Relativities. Intern. Academic Press, 1991. Vol. I: http://www.santilli-foundation.org/docs/Santilli-01.pdf Vol. II: http://www.santilli-foundation. org/docs/Santilli-61.pdf
37. Aringazin A. K., Jannussis A., Lopez F., Nishioka M. and Veljanosky B. Santilli's Lie-Isotopic Generalization of Galilei and Einstein Relativities. Notes from R. M. Santilli's 1990 Lectures at the ICTP, Trieste, Italy. Kostakaris Publishers, Athens, Greece, 1991. http://www.santilli-foundation.org/docs/Santilli-108.pdf
38. Santilli R. M. Invariant Lie-isotopic and Lie-admissible formulation of quantum deformations. *Found. Phys.*, 1997, v. 27, 1159–1177. http://www.santilli-foundation.org/docs/Santilli-06.pdf
39. Santilli R. M. and Vougiouklis T. New Conception of Living Organisms and its Representation via Lie-Admissible H_v-Hyperstructures. *Algebras, Groups and Geometries*, 2020, v. 37, 741–764. http://www.santilli-foundation.org/docs/Santilli-Vougiouklis-2020-epr.pdf
40. Santilli R. M. Foundations of Hadronic Chemistry, with Applications to New Clean Energies and Fuels. Kluwer Academic Publishers, 2001. http://www.santilli-foundation.org/docs/Santilli-113.pdf. Russian translation: Aringazin A. K. http://i-b-r.org/docs/Santilli-Hadronic-Chemistry.pdf
41. Santilli R. M. and Shillady D. D. A new isochemical model of the hydrogen molecule. *Intern. J. Hydrogen Energy*, 1999, v. 24, 943. http://www.santilli-foundation.org/docs/Santilli-135.pdf
42. Santilli R. M. and Shillady D. D. A new isochemical model of the water molecule. *Intern. J. Hydrogen Energy*, 2000, v. 25, 173. http://www.santilli-foundation.org/docs/Santilli-39.pdf
43. Wade M. I. and Gill T. L. Isonumbers and RGB Image Encryption. *Algebras, Groups and Geometries*, 2021, v. 37, 103–119. http://www.santilli-foundation.org/docs/wade-gill-2021.pdf
44. Bell J. S. On the Einstein Podolsky Rosen paradox. *Physics*, 1964, v. 1, 195–200. http://cds.cern.ch/record/111654/files/vol1p195-200_001.pdf
45. Santilli R. M. Iso-Representation of the Deuteron Spin and Magnetic Moment via Bohm's Hidden Variables. *Progress in Physics*, 2022, v. 18, 74–81. http://www.santilli-foundation.org/docs/PiP-paper-3-22.pdf
46. Miller J. P., de Rafael E. and Roberts B. Lee. Muon (g-2): experiment and theory. *Rep. Prog. Phys.*, 2007, v. 70, 795–881. http://news.fnal.gov/2021/04/first-results-from-fermilabs-muon-g-2-experiment-strengthen-evidence-of-new-physics/
47. Santilli R. M. Representation of the anomalous magnetic moment of the muons via the Einstein-Podolsky-Rosen completion of quantum into hadronic mechanics. *Progress in Physics*, 2021, v. 17, 210–215. http://www.santilli-foundation.org/muon-anomaly-pp.pdf
48. Santilli R. M. Representation of the anomalous magnetic moment of the muons via the novel Einstein-Podolsky-Rosen entanglement. In: Guzman J. C., ed. Scientific Legacy of Professor Zbigniew Oziewicz: Selected Papers from the International Conference "Applied Category Theory Graph-Operad-Logic". Word Scientific, in press. http://www.santilli-foundation.org/ws-rv961x669.pdf
49. Fadel M., Zibold T., Decamps B. and Treutlein Ph. Spatial entanglement patterns and Einstein-Podolsky-Rosen steering in Bose-Einstein condensates. *Science*, 2018, v. 360, 409–415. http://www.santilli-foundation.org/Basel-paper.pdf
50. Schukraft J. Heavy-ion physics with the ALICE experiment at the CERN Large Hadron Collider. *Trans. R. Soc.*, 2012, v. A370, 917–932. http://royalsocietypublishing.org/doi/10.1098/rsta.2011.0469
51. Santilli R. M. Apparent Unsettled Value of the Recently Measured Muon Magnetic Moment. *Progress in Physics*, 2022, v. 18, 15–18. http://www.santilli-foundation.org/docs/muon-meanlife-2022.pdf

52. Santilli R. M. Nonlocal formulation of the Bose-Einstein correlation within the context of hadronic mechanics. *Hadronic J.*, 1992, v. 15, 1–50 and v. 15, 81–133. http://www.santilli-foundation.org/docs/Santilli-116.pdf

53. Cardone F. and Mignani R. Nonlocal approach to the Bose-Einstein correlation. *Europ. Phys. J.*, 1998, v. C4, 705–728.

54. Ahmar H., Amato G., Kadeisvili J. V., Manuel J., West G. and Zogorodnia O. Additional experimental confirmations of Santilli's IsoRedShift and the consequential lack of expansion of the universe. *Journal of Computational Methods in Sciences and Engineering*, 2013 v. 13, 321–375. http://www.santilli-foundation.org/docs/IRS-confirmations-212.pdf

55. Santilli R. M. Experimental Verifications of IsoRedShift with Possible Absence of Universe Expansion, Big Bang, Dark Matter, and Dark Energy. *The Open Astronomy Journal* 2010, v. 3, 124. http://www.santilli-foundation.org/docs/Isoredshift-Letter.pdf

56. Santilli R. M. Apparent resolution of the Coulomb barrier for nuclear fusions via the irreversible Lie-admissible branch of hadronic mechanics. *Progress in Physcs*, 2022, in press. http://www.santilli-foundation.org/docs/hyperfusion-2022.pdf

Apparent Resolution of the Coulomb Barrier for Nuclear Fusions Via the Irreversible Lie-admissible Branch of Hadronic Mechanics

Ruggero Maria Santilli

The Institute for Basic Research, 35246 U. S. 19N, Suite 215, Palm Harbor, FL 34684, USA.
E-mail: research@i-b-r.org

In this paper, we report decades of mathematical, theoretical, experimental and industrial studies aiming at the resolution of the Coulomb barrier for nuclear fusions, here referred to the extremely big *repulsive* Coulomb force between natural nuclei that has prevented the achievement of controlled nuclear fusion to date. The studies have been done via the Lie-isotopic completion (for reversible processes) and Lie-admissible completion (for irreversible processes) of quantum mechanics into the various branches of hadronic mechanics. We first outline the prior representations via hadronic mechanics of: the synthesis of the neutron from the Hydrogen in the core of stars; the experimental data of the Deuteron in its true ground state (that with null orbital contributions); the stability of the neutron under strong nuclear forces; and the nuclear stability despite strongly repulsive protonic forces. Thanks to these preceding studies, we present apparently for the first time: 1) The prediction by hadronic mechanics of the existence of new, negatively charged, unstable nuclei, called *pseudo-nuclei* and denoted with the symbol $\tilde{N}$ (patent pending), which are characterized by a strongly attractive hadronic bond of electrons and natural nuclei, by therefore resolving the Coulomb barrier since pseudo-nuclei would be *attracted* (rather than repelled) by natural nuclei, with ensuing new conception of nuclear fusions here called *hyperfusions;* 2) The identification of engineering means for the synthesis of pseudo-nuclei which is given by the hadronic reactors for the synthesis of the neutron from the proton and the electron; 3) Laboratory evidence according to which the synthesis of pseudo-nuclei and related hyperfusions appear to be the origin of the limited, yet sustained and controlled excess energy achieved by the *Intermediate Controlled Nuclear Fusions.*

1 Introduction

As it is well known, nuclear fusions have indeed been achieved at various energies, but none of them has achieved to date the *sustainability and controllability* necessary for industrial usages, such as the production of electricity, due to a number of yet unresolved theoretical and engineering problems, such as:

Problem 1: Means to resolve the *repulsion* between natural, positively charged nuclei, called the *Coulomb barrier,* which reaches very big repulsive values of the macroscopic order of Newtons at the mutual distances of about 1 fm necessary to activate attractive strong nuclear forces,

$$F = Z\,\frac{e^2}{r^2} = \\ = Z\,(8.99\times 10^9)\,\frac{(1.60\times x10^{-19})^2}{(10^{-15})^2} = Z\times 230\,\mathrm{N}\,, \tag{1}$$

where Z represents the number of proton-proton pairs.

Problem 2: Means to control the anti-parallel coupling of nuclear spins, in which absence there would be a violation of the angular momentum conservation law with nuclear fusions solely possible at random.

Problem 3: Means to achieve "clean" nuclear fusions, ideally referring to those without the emission of harmful radiations and without the release of radioactive waste.

In this paper, we study, apparently for the first time, the possibility of synthesizing new, negatively charged, unstable nuclei, hereon called *pseudo-nuclei,* which are characterized by a strongly attractive bond between negatively charged electrons and positively charged natural nuclei.

In the event the synthesized nuclei have a sufficient mean life, pseudo-nuclei would bypass the Coulomb barrier (Problem 1) because they would be *attracted* (rather than repelled) by natural, positively charged nuclei all the way to mutual distances 10^{-13} cm = 1 fm needed to activate strong nuclear interactions.

Pseudo-nuclei also offer realistic possibilities for a resolution of Problem 2, because, in view of their opposite charges and magnetic moments, pseudo-nuclei would couple automatically with natural nuclei in anti-parallel spin alignment.

Engineering tests are expected to initiate with the synthesis of *light* pseudo-nuclei, whose fusion with natural nuclei would be the best arena for the possible resolution of Problem 3.

We shall hereon identify generic nuclei N with the familiar expression $N(Z, A, J, u)$ where Z represents the total number of protons, A represents the total number of protons and neutrons, J represents the nuclear spin, and u represents the mass in Atomic Mass Units, also denoted amu. We shall also

use tabulated symbols for individual nuclei, such as: H for Hydrogen, D for Deuteron, C for Carbon, *etc*. Measurements of nuclear data used in this paper are available from [1–4].

Our feasibility study shall initiate with the synthesis of the smallest possible pseudo-nucleus, here called the *pseudo-Deuteron-2e* and denoted with the symbol $\tilde{D}_{2e}$ (Figs. 1, 2, 3), according to the reaction

$$(\beta_{\uparrow}^{-},\beta_{\downarrow}^{-}) + D(1,2,1) \to \tilde{D}_{2e}(1,2,1)\,, \tag{2}$$

where: the subindex $2e$ represents the total number of bonded electrons; the total charge of the pseudo-nucleus is *negative,* $Z^{tot} = -1$ (since it is the result of one positive + and two negative − elementary charges); and the electron pair with antiparallel coupling is an expected image at short distances of Pauli's exclusion principle in molecular structures.

The existence of synthesis (2) would evidently imply the existence of the *pseudo-Deuteron-3e* with structure

$$(\beta_{\uparrow}^{-},\beta_{\downarrow}^{-}) + \beta_{\downarrow}^{-} + D(1,2,1_{\uparrow}) \to \tilde{D}_{3e}(1,2,1/2_{\uparrow})\,, \tag{3}$$

with intriguing characteristics due to the very big magnetic moment of the third electron for nuclear standards, and ensuing possibility of resolving Problem 2.

Following a quantitative representation of pseudo-Deuterons, in this paper we shall study the possible fusion of pseudo-nuclei and natural nuclei, called *hyperfusion* and here referred to nuclear fusions without the Coulomb barrier and with natural antiparallel spin alignments, including the following possible hyperfusion

$$\begin{aligned} &\tilde{D}_{2e}(1,2,1) + C(6,12,0) \to \to N(7,14,1) + \beta_{\uparrow}^{-} + \beta_{\downarrow}^{-} \\ &\Delta_N = 10.272\,\text{MeV}\,, \end{aligned} \tag{4}$$

and others that apparently occurred in recently measured excess heat in nuclear fusions to be reviewed in Sect. 4.

In order to conduct the indicated feasibility study, in this paper we shall adopt:

1) The 1935 historical argument by A. Einstein, B. Podolsky and N. Rosen that *Quantum mechanics is not a complete theory* [5];

2) The historical verifications of the EPR argument by W. Heisenberg [6], L. de Broglie [7] and D. Bohm [8], as well as the recent verifications by R. M. Santilli [9–11];

3) The experiments establishing deviations of quantum mechanical predictions from physical reality in various fields, including: nuclear physics [12]; electrodynamics [13–15]; condensed matter physics [16]; heavy ion physics [17]; time dilation for composite particles [18, 19]; Bose-Einstein correlation [20, 21]; cosmology [22, 23]; and various epistemological arguments [24–26].

4) The *approximate validity* of quantum mechanics in nuclear physics due to its inability over one century of achieving [27–29]: a quantitative representation of the fundamental synthesis of the neutron from a proton and an electron in the core of stars; an exact representation of nuclear magnetic moments; an exact representation of the spin of nuclei in their true ground state (that without the usual orbital excitations); a quantitative representation of the stability of neutrons when members of a nuclear structure; a quantitative representation of the stability of nuclei despite the huge Coulomb repulsion between nuclear protons; and other insufficiencies.

5) The completion of quantum mechanics into hadronic mechanics [30–32] (see [33] for an outline and [27–29] for a review); and the studies conducted during the *2020 International Teleconference on the EPR Argument* [34] (see its overviews [36,37] and monographs [38]–[47] for independent studies).

By using a language specifically intended for nuclear physicists, in Sect. 2 we review the branches of hadronic mechanics used in our study [48]–[76]; in Sect. 3, we show that hadronic mechanics allows a quantitative representation of the synthesis of the pseudo-nuclides; in Sect. 4, we show that the synthesis of pseudo-Deuterons appears to be verified by the sustainable and controllable excess energy produced by the *Intermediate Controlled Nuclear Fusions* (ICNF) [77]–[146]; and in Sect. 5 we summarize the results.

For the self-sufficiency of this presentation, in the appendices we outline preceding studies playing a crucial role for the consistent derivation and application of pseudo-nuclei. In Appendix A, we study the possible resolution of Problem 3 (nuclear fusions without harmful radiations); in Appendix B, we outline the representation via hadronic mechanics of the synthesis of the neutron from a proton and an electron (which is fundamental for the synthesis of pseudo-nuclei); and in Appendix C we present, apparently for the first time, the representation of nuclear stability permitted by hadronic mechanics despite the natural instability of the neutron and despite the strongly repulsive protonic forces in which absence no resolution of the Coulomb barrier for nuclear fusions appears to be plausible.

2 Selection of the basic methods

2.1 Basic notions of hadronic mechanics

Recall that, according to Einstein, Podolsky and Rosen [5], the primary limitation of quantum mechanics in nuclear physics is its *locality,* namely, the representation of protons and neutrons as *massive points*. Therefore, the foundations of hadronic mechanics were built in the late 1970's by R. M. Santilli at Harvard University under DOE support [48, 49] for the primary purpose of representing the actual dimension, shape and density of protons and neutrons in a form invariant over time.

Recall also that quantum mechanical point-particles can solely admit linear, local and potential interactions, hereon called *Hamiltonian interactions* (and technically identified as *variationally self-adjoint (SA) interactions* [48]).

By contrast, clear nuclear data establish that nuclear vol-

umes are generally *smaller* than the sum of the volumes of the constituent protons and neutrons. Consequently, when they are members of a nuclear structure, protons and neutrons are generally in conditions of partial mutual penetration of their dense charge distributions, resulting in additional interactions that are: *non-linear* in the wave function, as first studied by W. Heisenberg [6]; *non-local* in the sense of occurring over volumes, as first studied by L. de Broglie [7]; and of contact, thus zero-range type, *not derivable from a potential,* as first studied by R. M. Santilli [49]. The latter interactions are hereon called *non-Hamiltonian interactions* (and are technically identified as *variationally non-self-adjoint (NSA) interactions* [48]).

2.2 Lie-isotopic branch of hadronic mechanics

In Sect. 3, we shall study the representation of *stable,* thus time reversible nuclei. Their possible bonds with electrons are also reversible over time since the decay of pseudo-nuclei reproduce the original, permanently stable constituents.

In this section, we outline the branch of hadronic mechanics suggested for the consistent representation of time reversible systems, which is known as the *isotopic branch* and comprises the novel *iso-mathematics* [30] (see also [43, 47]) and *iso-mechanics* [31] (see also [38] and [45]), where the prefix "iso" is intended in the Greek meaning of denoting *preservation of the original axioms.*

By recalling that quantum mechanics is based on Lie algebras, the above methods are also known as *Lie-isotopic formulations* to indicate that they are based on the isotopies of Lie algebras not treated here for brevity [49] (see also [39]).

Recall that quantum mechanics is characterized by a universal enveloping algebra of Hermitean operators A, B, with conventional associative product $A \times B = AB$ on a Hilbert space $\mathcal{H}$ with states $|\psi\rangle$ and normalization $\langle\psi|\psi\rangle = 1$ over the field of complex numbers C, Schrödinger equation $H(r,p)|\psi\rangle = E|\psi\rangle$, canonical commutation rules and the familiar quantum mechanical methods used in nuclear physics over the past century.

Santilli achieved the first known representation of non-Hamiltonian/NSA interactions in a time-reversible way via a *new operator* called the *isotopic element* and indicated with the symbol $\hat{T}$, which is sandwiched in between all possible quantum products AB, resulting in the new, associativity-preserving product called *iso-product* (Eq. (5), p. 71 of [49])

$$A \star B = A\hat{T}B, \quad \hat{T} = \hat{T}(\hat{\psi}, ...) > 0\,, \tag{5}$$

with ensuing generalized multiplicative unit, called *iso-unit* and related identity axion

$$\begin{aligned} &\hat{I}(\hat{\psi}, ...) = 1/\hat{T}(\hat{\psi}, ...) > 0\,, \\ &I \star A = A \star I = A\,, \end{aligned} \tag{6}$$

where the dependence on $\hat{\psi}$ represents non-linearity in the appropriate iso-space of iso-mechanics.

For the case of the Deuteron as a two-body bound state according to hadronic mechanics, the isotopic element has a realization of the type [29, 36]

$$\begin{aligned} &\hat{T}(\hat{\psi}, ...) = 1/\hat{I}(\hat{\psi}, ...) = \\ &= \prod_{\alpha=1,2} \text{Diag}\left(\tfrac{1}{n_{1,\alpha}^2}, \tfrac{1}{n_{2,\alpha}^2}, \tfrac{1}{n_{3,\alpha}^2}, \tfrac{1}{n_{4,\alpha}^2}\right) e^{-\Gamma(\hat{\psi},...)}\,, \\ &n_{\mu,\alpha} > 0, \quad \Gamma > 0, \quad \mu = 1,2,3,4, \quad \alpha = 1,2\,, \end{aligned} \tag{7}$$

by therefore characterizing:

1) The dimension and shape of the proton and neutron via semi-axes $n_{k,\alpha}^2$, $k = 1, 2, 3$ (with n_3 parallel to the spin);

2) The density $n_{4,\alpha}^2$ of the proton and of the neutron with normalizations for the vacuum to the value $n_{\mu,\alpha}^2 = 1$.

3) Non-Hamiltonian/NSA interactions between the proton and the neutron caused by the mutual penetration of their dense charge distribution, which interactions are represented via the exponential term $e^{\Gamma(\hat{\psi},...)} > 0$, where Γ is positive-definite but possesses otherwise an unrestricted functional dependence on all needed local variables.

Despite their simplicity, isotopies (5)-(6) requested the step-by-step, completion of all aspects of quantum mechanics into iso-mechanics, as illustrated by the basic *Schrödinger-Santilli iso-equation* (Ch. 5, p. 182 on, [31])

$$H \star |\hat{\psi}\rangle = H(r,p)\,\hat{T}(\hat{\psi}, ...)\,|\hat{\psi}\rangle = E\,|\hat{\psi}\rangle\,, \tag{8}$$

as well as the *Heisenberg-Santilli iso-equation* for an observable A

$$\begin{aligned} i\,\frac{dA}{dt} &= [A, H]^\star = \\ &= A \star H - H \star S = A\hat{T}H - H\hat{T}A\,, \end{aligned} \tag{9}$$

whose time-reversibility is assured by the conservation of the total energy,

$$i\,\frac{dH}{dt} = [H, H]^\star \equiv 0\,, \tag{10}$$

as well as the invariance of (9) under anti-Hermiticity,

$$[A, H]^\star \equiv -[A, H]^{\star\dagger}\,. \tag{11}$$

As clearly illustrated by iso-equation (8)-(9), the representation of stable nuclei via iso-mechanics requires *two operators,* the conventional Hamiltonian H for the representation of Hamiltonian/SA interactions and the isotopic element $\hat{T}$ for the representation of the dimension, shape, density and non-Hamiltonian/NSA interactions of protons and neutrons in a nuclear structure.

To reach a preliminary understanding of the subsequent sections, interested readers should be aware that, despite their simplicity, Eqs. (5)-(6) require a step-by-step completion of *all* aspects of 20th century applied mathematics into the novel iso-mathematics, with no exception known to the author, including the new: *iso-numbers* [50] (see also [42])

$$\hat{n} = n\hat{I}\,; \tag{12}$$

iso-functions [49] (see also [38]) $\hat{f}(\hat{r}) = [f(r\hat{I})]\,\hat{I}$; and iso-differential calculus [51] (see also [46])

$$\begin{aligned} &\hat{d}\hat{r} = \hat{T}d(r\hat{I}) = dr + r\hat{T}d\hat{I}, \\ &\frac{\hat{\partial}\hat{f}(\hat{r})}{\hat{\partial}\hat{r}} = \hat{I}\,\frac{\partial\hat{f}(\hat{r})}{\partial\hat{r}}\,, \end{aligned} \tag{13}$$

that allowed the completion of the iso-Schrödinger and iso-Heisenberg representations

$$\begin{aligned} &\hat{p}\star|\,\hat{\psi}(\hat{r})\,\rangle = -\hat{i}\star\hat{\partial}_{\hat{r}}|\,\hat{\psi}(\hat{r})\,\rangle = -i\,\hat{I}\partial_{\hat{r}}|\,\hat{\psi}(\hat{r})\,\rangle\,, \\ &\left[\hat{r}_i,\hat{p}_j\right]^{\star}\star|\,\hat{\psi}(\hat{r})\,\rangle = -i\,\hat{\delta}_{ij}|\,\hat{\psi}(\hat{r})\,\rangle = -i\,\hat{I}\delta_{ij}|\,\hat{\psi}(\hat{r})\,\rangle\,, \\ &\left[\hat{r}_i,\hat{r}_j\right]^{\star}\star|\,\hat{\psi}(\hat{r})\,\rangle = [\hat{p}_i,\hat{p}_j]^{\star}\star|\,\hat{\psi}(\hat{r})\,\rangle = 0\,, \end{aligned} \tag{14}$$

as well as the completion of the Heisenberg uncertainties for point particles under electromagnetic interactions into the *Heisenberg-Santilli iso-uncertainties* for extended hadrons under strong interactions [9–12]

$$\Delta r\,\Delta p = \frac{1}{2}\,|\,\langle\,\hat{\psi}\,|\star[\hat{r},\hat{p}]^{*}\star|\,\hat{\psi}\,\rangle\,| \approx \frac{1}{2}\hat{T} \;\ll\; 1\,. \tag{15}$$

It should be finally noted that all aspects of iso-mathematics and iso-mechanics can be constructed very simply via a systematic non-unitary transformation of *all* the corresponding 20th century formulations [52], e.g.,

$$\begin{aligned} &UU^{\dagger} = \hat{I}(\hat{\psi},...) = 1/\hat{T} > 0\,, \\ &\hbar = 1 \;\to\; U\hbar U^{\dagger} = \hat{I}\,, \\ &r \;\to\; UrU^{\dagger} = \hat{r}\,, \\ &p \;\to\; UpU^{\dagger} = \hat{p}\,, \\ &U(AB)U^{\dagger} = \hat{A}\hat{T}\hat{B}\,, \\ &U(H|\,\psi\,\rangle U^{\dagger} = \hat{H}\star|\,\hat{\psi}\,\rangle = \\ &\quad = \left[\frac{1}{\hat{2}\star\hat{m}}\sum_{k=1,2,3}\hat{p}_k\star\hat{p}_k + \hat{V}(\hat{r})\right]\star|\,\hat{\psi}\,\rangle = \\ &\quad = \hat{E}\star|\,\hat{\psi}\,\rangle = E|\,\hat{\psi}\,\rangle\,. \end{aligned} \tag{16}$$

The invariance over time of the numeric values of the isotopic element and of the iso-unit is finally assured by the reformulation of conventional non-unitary transformations (15) into the *iso-unitary iso-transformations* of hadronic mechanics [52]

$$\begin{aligned} &WW^{\dagger} = \hat{I}, \quad W = \hat{W}\hat{T}^{1/2}\,, \\ &WW^{\dagger} = \hat{W}\star\hat{W}^{\dagger} = \hat{W}^{\dagger}\star\hat{W} = \hat{I}\,, \end{aligned} \tag{17}$$

under which

$$\begin{aligned} &\hat{I}\to\hat{I}' = \hat{W}\star\hat{I}\star\hat{W}^{\dagger}\equiv\hat{I}\,, \\ &\hat{A}\star\hat{B}\to\hat{W}\star(\hat{A}\star\hat{B})\star\hat{W}^{\dagger} = \\ &\quad = \hat{A}'\star\hat{B}' = \hat{A}'\hat{T}\hat{B}'\,, \\ &\hat{A}' = \hat{W}\star A\star\hat{W}^{\dagger}),\;\hat{B}' = \hat{W}\star\hat{B}\star\hat{W}^{\dagger}\,, \\ &\hat{T} = (W^{\dagger}\star\hat{W})^{-1}\,. \end{aligned} \tag{18}$$

The invariance of isotopic formulation then follows (see [29] for a technical review via *iso-symmetries,* namely, the isotopic completion of 20th century space-time symmetries).

2.3 Lie-admissible branch of hadronic mechanics

In Sect. 4, we shall study apparent nuclear fusions that are permitted by pseudo-Deuterons without Coulomb barrier and with a natural antiparallel alignment of nuclear spins. The primary difference between stable nuclei and nuclear fusions is that the former constitute time reversible systems, thus allowing their treatment via time reversible isotopic methods, while the latter are *irreversible over time* by therefore requiring for their consistent treatment the *irreversible branch of hadronic mechanics* known as *Lie-admissible or genotopic formulations* [53]–[70] (see [30–32] for a general treatment), where the prefix "geno" is intended this time in the Greek sense of *inducing new axioms.*

In the author's view, an important problem of nuclear fusions, that has remained essentially unaddressed for about one century, is that *the representation of nuclear fusions via quantum mechanics generally violates causality,* because the same Schrödinger equation applies for both, the fusion process as well as its time reversal image which requires the spontaneous disintegration of the synthesized nucleus, resulting in solutions that generally admit effects preceding their cause.

The primary objective of Santilli's research in the late 1970's at Harvard University under DOE support was the construction of the EPR completion of time reversible quantum mechanics into an irreversible form representing nuclear fusions without causality problems. The study was essentially along the Ph. D. thesis at the University of Torino, Italy, on the time irreversible, Lie-admissible generalization of quantum mechanics [53, 54, 56].

The need for new clean nuclear energies to contain the deterioration of our environment (that was already visible in the late 1970's), joint with the lack of controlled nuclear fusions, stimulated a considerable volume of research in the period 1977–1985 under DOE support, including papers [57]–[61] five *Workshops on Lie-admissible formulations* [61], the *First International Conference on Nonpotential Interactions and their Lie-Admissible Treatment* [62], the first *Workshops on Hadronic Mechanics* [63, 64], and various reprint volumes, such as [65]. The post-1985 references on Lie-admissible

mathematics and mechanics are too numerous for comprehensive quotations. We here merely quote *The third international conference on the Lie-admissible treatment of non-potential interactions* [66] and special contributions [67]–[70].

As a main aspect in the representation of nuclear fusions via irreversible genotopic methods let us recall that quantum mechanics is a time reversible theory beginning with its axiomatic structure. In particular, the right modular action of the Hermitean Hamiltonian on a Hilbert state, $H|\psi\rangle = E|\psi\rangle$, is equivalent to the corresponding left modular action, $\langle\psi|H = -\langle\psi|E'$, $E' \equiv E$, and the same holds for isotopic methods in view of the Hermiticity of the isotopic element $\hat{T} = \hat{T}^\dagger$.

Following extensive studies, the foundations of irreversible formulations were achieved in the 1979 Harvard University paper [57] via the following inequivalent right and left modular actions of a Hamiltonian on a Hilbert state. The right modular action (indicated with the symbol >) is assumed to represent *motion forward in time,* while the left modular action (indicated with the symbol <) is assumed to represent *motion backward in time,* with forward ("for") and backward ("bac") geno-Schödinger equations

$$\begin{aligned} &\hat{H} \equiv \hat{H}^\dagger, \\ &\hat{H} > |\psi\rangle = \hat{H}\hat{R}|\psi\rangle = E^{for}|\psi\rangle, \\ &\langle\psi| < \hat{H} = \langle\psi|\hat{S}\hat{H} = \langle\psi|E^{bac}, \end{aligned} \tag{19}$$

which assure irreversibility whenever the *genotopic operators* $\hat{R}, \hat{S}$ are different

$$\hat{R} \neq \hat{S}, \quad E^{for} \neq E^{bac}, \tag{20}$$

isotopic formulations being a particular case for $\hat{R} = \hat{S} = \hat{T}$.

Note that *genotopic formulations maintain the observability of the total energy* [31], by therefore avoiding the use of complex-valued Hamiltonians to represent irreversibility with the consequential loss of observability.

According to the above assumptions, geno-mathematics (geno-mechanics) essentially consists of *two* inequivalent iso-mathematics (iso-mechanics), one with *all* products ordered to the right and the other ordered to the left.

By using (19), the *genotopic time evolution* (for the simple case $\hat{t} = t$) is given by (Eqs. (19), p. 153 of [49])

$$\begin{aligned} \hat{A}(t) = e^{Hti}_{>} > \hat{A}(0) < e_{<}e^{-itH} = \\ = e^{H\hat{S}ti}\hat{A}(0)\, e^{-it\hat{S}H}, \end{aligned} \tag{21}$$

with infinitesimal form

$$\begin{aligned} i\frac{\hat{d}\hat{A}}{\hat{d}t} = (\hat{A}, \hat{H}) = \\ = \hat{A} < \hat{H} - \hat{H} > \hat{A} = \hat{A}\hat{S}\hat{H} - \hat{H}\hat{R}\hat{A} = \\ = (\hat{A}\hat{T}\hat{H} - \hat{H}\hat{T}\hat{A}) + (\hat{A}\hat{J}\hat{H} - \hat{H}\hat{J}\hat{A}), \\ \hat{S} = \hat{T} + \hat{J}, \quad \hat{R} = -\hat{T} + \hat{J}. \end{aligned} \tag{22}$$

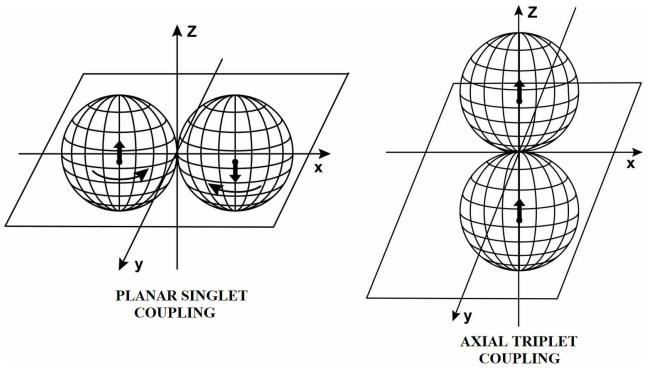

Fig. 1: In this figure, we illustrate the two stable bound states of particles with spin predicted by hadronic mechanics, which are given by the "planar singlet coupling" on the left and the "axiom triplet coupling" on the right.

The important methodological, as well as historical feature of genotopic formulations is that their brackets (A, H) are *jointly Lie-admissible and Jordan-admissible* according to the American mathematician A. A. Albert [71], in the sense that the antisymmetric brackets $[A, B]^\star$ verify the Lie algebra axioms, while the symmetric brackets $\{A, B\}^\star$ verify the Jordan axioms.

Intriguingly, the symmetric term of brackets (21) provides a representation of the *external terms* $\hat{F}^{NSA}$ of Lagrange's and Hamilton's equations as one can see for the particular case

$$\begin{aligned} &\hat{S} = 1, \quad \hat{R} = -1 + \frac{\hat{F}}{\hat{H}}, \\ &i\frac{\hat{d}\hat{A}}{\hat{d}t} = (\hat{A}, \hat{H}) = \hat{A}\hat{H} - \hat{H}\hat{A} + \hat{A}\hat{F}, \end{aligned} \tag{23}$$

by therefore realizing Jordan's wish that his symmetric algebra may, one day, see physical applications (for details, see Sect. 2 of [27]).

Recall that iso-mathematics and iso-mechanics can be constructed with the sole use of *one*, single, non-unitary transformation of the conventional applied mathematics and quantum mechanics, Eqs. (16). Similarly, geno-mathematics and geno-mechanics can be constructed, this time, via *two* different non-unitary transformations of conventional applied mathematics and quantum mechanics, and this includes the lifting of quantum mechanical nuclear models with sole potential interactions into their covering hadronic models with potential, as well as contact, non-potential interactions (see [52] for brevity).

3 Negatively charged pseudo-Deuterons

3.1 Basic assumptions

As indicated in Sect. 1, no study of pseudo-nuclei, with ensuing resolution of the Coulomb barrier for nuclear fusions, appears to be plausible without the prior resolution of a number of basic problems in nuclear physics, beginning with the

resolution of the *locality* of quantum mechanics via the invariant representation of the dimension, shape and density of protons and neutrons outlined in Sect. 2.

In this section, we outline the second necessary requirement for the indicated task, the numerically exact and time invariant representation of the experimental data of the Deuteron in its true ground state (that with null orbital contributions) under the assumption that the neutron is an extended structureless neutral particle with spin 1/2.

The indicated task additionally requires the representation according to hadronic mechanics (outlined in Appendix B) of the synthesis of the neutron from a proton and an electron in the core of stars. In fact, the neutron synthesis is prohibited by quantum mechanics for numerous technical reasons, despite the huge proton-electron Coulomb *attraction,* with ensuing expectation that pseudo-nuclei are not possible because not allowed by quantum mechanics.

The latter view is quickly dispelled by the century old evidence that the neutron is indeed synthesized in the core of stars from a proton and an electron, by therefore confirming the Einstein-Podolsky-Rosen argument that *Quantum mechanics is not a complete theory* [5].

In turn, the representations of *all* characteristics of the neutron during its synthesis from the proton and the electron have allowed the resolution of the last nuclear problems needed for the study of pseudo-nuclei, which are given by the understanding of nuclear stability despite the neutron natural instability and despite the huge repulsive protonic forces. The latter resolutions are presented apparently for the first time in Appendix C.

3.2 Representation of the Deuteron experimental data

As it is well known, the only stable bound state between a proton and a neutron predicted by quantum mechanics (qm) is the singlet coupling

$$D = (p_\uparrow, n_\downarrow)_{qm}\,, \tag{24}$$

for which the total spin would be zero, $J_D = 0$, contrary to clear experimental evidence for which the spin of the Deuteron is $J_D = 1$.

For the intent of maintaining quantum mechanics as an exact discipline in nuclear physics, the spin of the Deuteron is generally associated to a collection of *orbital states* $L_D = 1$ (see e.g. [75]), which association is however contrary to the experimental evidence for which *the spin of the Deuteron has the value* $J_D = 1$ *in the true ground state,* namely, a state for which all excited orbital contributions are null.

Following the non-relativistic and relativistic representations of all characteristics of the neutron in its synthesis from the proton and the electron [84]–[103], the numerically exact and time invariant representation of all the experimental data of the Deuteron in its true ground state has been achieved by R. M. Santilli [29, 77, 78, 83] (see also [79–81]).

Under the assumption that the neutron is an extended structureless particle, the representation of the spin $J_D = 1$ was achieved via the notion of *hadronic spin* (first introduced in Sect. 6.8, p. 250 of [31] and [10]) which is given by iso-unitary, iso-irreducible iso-representations of the Lie-Santilli iso-algebra $\widehat{\mathrm{SU}}(2)$ whose iso-fundamental iso-representation can be constructed quite easily via the following *non-unitary* transformation of Pauli's matrices

$$UU^\dagger = \hat{I} = \mathrm{Diag}\,(\lambda^{-1}, \lambda)\,,\ \ \hat{T} = \mathrm{Diag}\,(\lambda, \lambda^{-1})\,, \tag{25}$$

including an explicit and concrete realization of Bohm's *hidden variables* λ [8], first introduced in Eqs. (6.8.20), p. 254 of [31], and resulting in the *iso-Pauli matrices* generally called *Pauli-Santilli iso-matrices*

$$\begin{aligned}
&\hat{\Sigma}_k = U\Sigma_k U^\dagger,\ \ \Sigma_k = \sigma_k \hat{I}\,,\\
&\hat{\sigma}_1 = \begin{pmatrix} 0 & \lambda \\ \lambda^{-1} & 0 \end{pmatrix},\ \ \hat{\sigma}_2 = \begin{pmatrix} 0 & -i\lambda \\ i\lambda^{-1} & 0 \end{pmatrix},\\
&\hat{\sigma}_3 = \begin{pmatrix} \lambda^{-1} & 0 \\ 0 & -\lambda \end{pmatrix},
\end{aligned} \tag{26}$$

and then used in various works (see e.g. [10]).

As one can see, the iso-Pauli matrices verify the iso-commutation rules

$$\begin{aligned}
[\hat{\sigma}_i, \hat{\sigma}_j]^* &= \hat{\sigma}_i \star \hat{\sigma}_j - \hat{\sigma}_j \star \hat{\sigma}_i = \\
&= \hat{\sigma}_i \hat{T} \hat{\sigma}_j - \hat{\sigma}_j \hat{T} \hat{\sigma}_i = i2\epsilon_{ijk}\hat{\sigma}_k\,,
\end{aligned} \tag{27}$$

showing the clear iso-morphism $\widehat{\mathrm{SU}}(2) \approx \mathrm{SU}(2)$, as well as the iso-eigenvalue equations on an iso-state $|\hat{b}\rangle$ of the *Hilbert-Myung-Santilli iso-space* $\hat{\mathcal{H}}$ [76] over the iso-field of iso-complex iso-numbers $\hat{C}$ [50]

$$\begin{aligned}
&\hat{S}_k = \frac{\hat{1}}{2} \star \hat{\sigma}_k = \frac{1}{2}\hat{\sigma}_k\,,\\
&\hat{\sigma}_3 \star |\,\hat{b}\,\rangle = \hat{\sigma}_3 \hat{T}\,|\,\hat{b}\,\rangle = \pm\,|\,\hat{b}\,\rangle\,,\\
&\hat{\sigma^2} \star |\,\hat{b}\,\rangle = (\hat{\sigma}_1 \hat{T} \hat{\sigma}_1 + \hat{\sigma}_2 \hat{T} \hat{\sigma}_2 + \hat{\sigma}_3 \hat{T} \hat{\sigma}_3)\hat{T}\,|\,\hat{b}\,\rangle = 3\,|\,\hat{b}\,\rangle.
\end{aligned} \tag{28}$$

The addition of hadronic spins (Sect. 6.11, p. 265 of [31]) allowed the identification of two stable couplings of spin 1/2 *extended* particles called *planar singlet coupling* and *axial triplet coupling* which are illustrated in Fig. 1.

The configuration of the Deuteron allowing the representation of the spin $J_D = 1$ in its true ground state is evidently the axial triplet coupling, first identified in Fig. 13, p 91 of [36] (Fig. 2)

$$\tilde{D} = \begin{pmatrix} \hat{p}_\uparrow \\ \star \\ \hat{n}_\uparrow \end{pmatrix}. \tag{29}$$

Two complementary, numerically exact and time invariant representations of the Deuteron magnetic moment

$$\mu_D^{ex} = 0.85647\,\mu_{\mathrm{N}}\,, \tag{30}$$

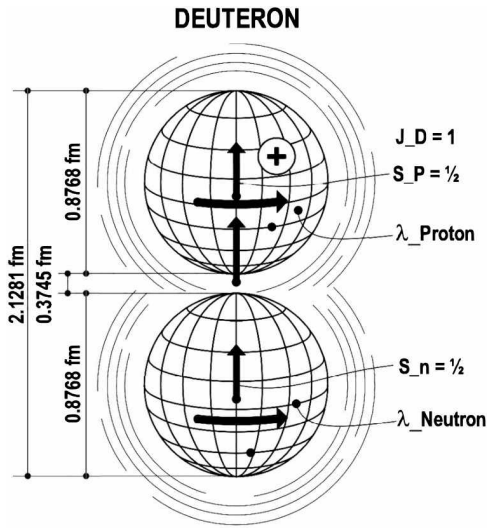

Fig. 2: In this figure, we reproduce known experimental data on the dimensions of the Deuteron [2] and its constituent proton and neutron [4], as well as their interpretation as a hadronic bound state in axial triplet coupling (Fig. 1), thus representing for the first time the spin of the Deuteron $S_D = 1$ in its ground state, that with null angular contributions $L_D = 0$ [83].

were achieved via hadronic mechanics. The first representation was reached in Eq. (3.6), p. 124 of the 1994 paper [77] (see also the 1998 monograph [78]) via the following numeric values of the characteristic quantities of isotopic element (26)

$$\begin{aligned} b_1 &= \frac{1}{n_1} = b_2 = \frac{1}{n_2} = 1.0028\,, \\ b_3 &= \frac{1}{n_3} = 1.662, \;\; b_4 = \frac{1}{n_4} = 1.653\,. \end{aligned} \tag{31}$$

The second representation of the magnetic moment of the Deuteron (35) was reached in the recent paper [83] via the realization of Bohm's hidden variable λ

$$\lambda = e^{\phi} \geq 0\,, \tag{32}$$

and the factorization (from Eq. (6.8.18), p. 254 of [31]),

$$\hat{\sigma}_3|\,\hat{b}\,\rangle = \sigma_3\hat{|}\,\hat{b}\,\rangle = \sigma_3 e^{\phi\sigma_3}|\,\hat{b}\,\rangle\,, \tag{33}$$

resulting in the relation

$$\mu_{hm}|\,\hat{b}\,\rangle = e^{\phi\sigma_3}\mu_{qm}|\,\hat{b}\,\rangle = e^{\phi\sigma_3} gS\,|\,\hat{b}\,\rangle\,, \tag{34}$$

from which the magnetic moment (35) is exactly represented via the following numeric value of Bohm's hidden variable λ [83]

$$\lambda = e^{\phi} = e^{0.97666} = 2.65557\,. \tag{35}$$

The invariance over time of the representations follows from the derivation of iso-Pauli matrices (31) from the isotopies of the Poincaré symmetry (see the general review [29] for brevity).

The representation of the rest energy and charge radius of the Deuteron (Fig. 2) were first achieved via the iso-Schrödinger equation of hadronic mechanics for a two-body, proton-neutron system (Fig. 12) [78] and then extended to a *restricted three-body system* comprising two protons and an electron (Fig. 13 and reviews [79–81]). The stability of the Deuteron despite the natural instability of the neutron is studied in Appendix C.

3.3 Predicted characteristics of the pseudo-Deuteron-2e

In this section, we study the possible bound state (2) of an electron pair and the Deuteron into a negatively charged unstable nucleus called *pseudo-Deuteron-2e* and denoted with the symbol $\tilde{D}_{2e}(1,2,1)$ (Sect. 1), conceptually proposed in Sect. 8.2.8, p. 96 of [36], and here studied at the non-relativistic level with the structure according to hadronic mechanics (hm)

$$[(\beta^-_{\uparrow},\beta^-_{\downarrow})_{hm} + D(1,2,1)]_{hm} = \tilde{D}_{2e}(1,2,1)\,, \tag{36}$$

where:

3.1.1) The bond between the electron pair and the Deuteron is primarily due to their very big *attractive* Coulomb force of 460 N at the mutual distance of 10^{-13} cm, Eq. (1), as well as non-Hamiltonian/NSA interactions caused by the motion of the electron pair within the wave packet of the Deuteron here presented as an example of the *Einstein-Podolsky-Rosen (EPR) entanglement* [12].

3.1.2) The electron pair in synthesis (36) is the valence electron bond represented via hadronic chemistry under the name of *isoelectronium* (see Chapter 4 on, [72] and applications [73, 74]) which is the sole valence electron pair with an *attractive force* known to this author despite their equal charges.

3.1.3) The electron pair and the Deuteron are assumed, for simplicity, to constitute single bodies in structure equations.

3.1.4) Synthesis (36) is assumed in first approximation to be reversible over time with spontaneous decay

$$\tilde{D}_{2e}(1,2,1) \;\to\; D(1,2,1) + \beta^-_{\uparrow} + \beta^-_{\downarrow}\,. \tag{37}$$

3.1.5) Synthesis (36) is studied via the iso-mathematics and iso-mechanics of hadronic mechanics outlined in Sect. 2.2 under the sole assumption of the following non-relativistic form of isotopic element (7) [29, 36]

$$\begin{aligned} &\hat{T}(\hat{\psi},...) = 1/\hat{I}(\hat{\psi},...) = \\ &= \prod_{\alpha=1,2} \text{Diag}\left(\frac{1}{n^2_{1,\alpha}}, \frac{1}{n^2_{2,\alpha}}, \frac{1}{n^2_{3,\alpha}}\right) e^{-\Gamma(\hat{\psi},...)}, \\ &n_{\mu,\alpha} > 0, \quad \Gamma > 0, \;\; \mu = 1,2,3 \;\; \alpha = 1,2\,. \end{aligned} \tag{38}$$

3.1.6) We assume that both the electron pair and the Deuteron are spherical with characteristic quantities $n_\mu = 1$, $\mu = 1,2,3$, by therefore reducing isotopic element (36) to its exponential term

$$\hat{T}(\hat{\psi},...) = 1/\hat{I}(\hat{\psi},...) = e^{-\Gamma(\hat{\psi},...)}. \tag{39}$$

3.1.7) To avoid insidious instabilities, the orbit of the electron pair around the Deuteron is assumed to be in a plane and a perfect circle on iso-spaces over iso- fields.

Following the study of synthesis (36) with two electrons, we shall study the synthesis with a bigger number of electrons, such as the *pseudo-Deuteron-3e* (Fig. 4).

A generic hyperfusion between a pseudo-nucleus $\tilde{N}_{ke}(Z_1, A_1, J_1)$ with k bonded electrons and a natural nucleus $N(Z_2, A_2, J_2)$ will be denoted

$$\begin{aligned} &\tilde{N}_{ke}(Z_1, A_1, J_1) + N(Z_2, A_2, J_2) \to \\ &\to N(Z_1 + Z_2, A_1 + A_2, J_1 + J_2) + k\beta^- \,. \end{aligned} \tag{40}$$

With reference to Fig. 3, we consider now the quantum mechanical Schrödinger equation for the bond of an electron pair with rest energy $M_{2e} = 1.022$ MeV to the Deuteron with rest energy $M_D = 1875.6129$ MeV

$$\left[-\frac{1}{2m} \sum_{k=1,2,3} p_k p_k + V_c(r) \right] | \psi(r) \rangle = E \, | \psi(r) \rangle \,, \tag{41}$$

where m is the reduced mass

$$m = \frac{M_D \times 2m_e}{M_d + 2M_e} \approx M_{2e} = 1.022 \text{ MeV} \,, \tag{42}$$

and the attraction is that of the Coulomb force between the electron pair and the proton

$$V_c = \frac{(+e) \times (-2e)}{r} = -2 \, \frac{e^2}{r} \,. \tag{43}$$

We now assume that the considered bond is characterized by a second interaction due to the overlapping of the wave packets of the electrons with that of the Deuteron (illustrated with the dashed area of Fig. 2), resulting in a deep EPR entanglement (Sect. 3 of [15]) with ensuing contact, non-Hamiltonian/NSA interactions represented by isotopic element (27).

In order to achieve an interaction in the iso-Schrödinger equation which is *additive* to the Coulomb interaction, we select the following simplified form of the isotopic element that has produced various numerically exact representations of experimental data [29]

$$\hat{T} = 1/\hat{I} = e^{+V_h(\hat{r})/V_c(\hat{r})} \,, \tag{44}$$

where $V_h(\hat{r})$ is the *Hulten potential* in the hadronic system of iso-coordinates $\mathrm{v}\hat{r} = r\hat{I}$

$$V_h(\hat{r}) = -K_h \, \frac{e^{b\hat{r}}}{1 - e^{b\hat{r}}} \,, \tag{45}$$

b represents the charge radius of the pseudo-Deuteron here assumed to be of the order of 2 fm,

$$R_{\tilde{D}} = b \approx 2 \, \text{fm} = 2 \times 10^{-13} \, \text{cm}, \tag{46}$$

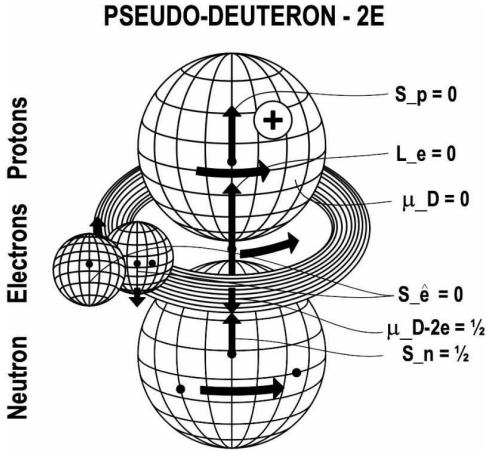

Fig. 3: In this figure, we illustrate the structure of the pseudo-Deuteron-2e predicted by hadronic mechanics as a bound state of an electron pair and a Deuteron (Sect. 3).

and K_h is the Hulten constant.

Under the above assumptions, the iso-Schrödinger equation in the structure of the pseudo-Deuteron is uniquely characterized by the following *non-unitary* transformation of the quantum mechanical description

$$\begin{aligned} &UU^\dagger = \hat{I} = 1/\hat{T} = e^{[-V_h(\hat{r})]/[-V_c(\hat{r})]} \approx 1 + \tfrac{\hat{V}_h(\hat{r})}{V_c(\hat{r})} + ... \\ &(UU^\dagger)^{-1} = \hat{T} = e^{V_h(\hat{r})/V_c(\hat{r})} \approx 1 - \tfrac{V_h(\hat{r})}{V_c(\hat{r})} + ... \end{aligned} \tag{47}$$

when applied to (41) (first studied in Sect. 5.1, p. 827 on, of the 1978 Harvard University memoir [82] and upgraded in Sect. 2.7.2 of [29]) with final result

$$\left[-\frac{1}{2m} \hat{\Delta}_{\hat{r}} - V_c(\hat{r}) - V_h(\hat{r}) \right] | \hat{\psi}(\hat{r}) \rangle = E_h \, | \hat{\psi}(\hat{r}) \rangle \,. \tag{48}$$

Recall that the Hulten potential behaves like the Coulomb potential at short distances (see Eq. (5.1.15), p. 885 of [82]),

$$V_h(\hat{r}) \approx \frac{k_h}{b\hat{r}} \,. \tag{49}$$

Consequently, the strongly attractive Hulten potential *absorbs* the attractive Coulomb potential with a mere redefinition K_h', of the constant K_h, resulting in the iso-Schrödinger equation

$$\left[-\frac{1}{2m_e} \hat{\Delta}_{\hat{r}} - K_h' \, \frac{e^{b\hat{r}}}{1 - e^{b\hat{r}}} \right] | \hat{\psi}(\hat{r}) \rangle = E_{be} \, | \hat{\psi}(\hat{r}) \rangle, \tag{50}$$

where E_{be} is the binding energy of the Hulten potential and $\bar{m}_e$ is the iso-renormalized mass of the electron, that is, the renormalization of the mass caused by non-Hamiltonian interactions.

For our initial feasibility study, we assume that the pseudo-Deuteron has the mass $m_{\tilde{D}} \approx 2m_e + m_D = 1.876 \, \text{MeV} - E_{be}$,

the mean life of $\tau_{\tilde{D}} \approx 1\,\text{s}$ and the charge radius $R_{\tilde{D}} = b^{-1} = 2 \times 10^{-13}\,\text{cm}$.

By following the structure model of pions as hadronic bound states of electrons and positrons of Eqs. (5.1.14), p. 836, [82], we reach the following *non-relativistic structure equations of the pseudo-Deuteron-2e*

$$\begin{aligned} &\left[\frac{1}{r^2}\left(\frac{d}{dr}r^2\frac{d}{dr}\right) + \tilde{2}\bar{m}_e\left(E_{be} + K'_h\frac{e^{-br}}{1-e^{-br}}\right)\right] = 0\,,\\ &m_{\tilde{D}} = 2m_e + m_D - E_{be}\,,\\ &\tau_{\tilde{D}}^{-1} = 2\pi\lambda^2\,|\hat{\psi}(0)|^2\,\frac{\alpha^2 E_1}{\hbar} = 1\,\text{s}\,,\\ &R_{\tilde{D}} = b^{-1} = 2\times 10^{-13}\,\text{cm}\,. \end{aligned} \tag{51}$$

The solution of the above equations was reduced (see Eqs. (5.1.32a) and (5.1.32b), p. 840 of [82]) to the numeric values of two parameters denoted k_1 and k_2 that, in our case, become

$$k_1[1-(k_2-1)2] = \frac{1}{2\hbar c}\left(m_{\tilde{D}}b^{-1}\right) = 2.5\times 10^{-2} m_{\tilde{D}}\,, \tag{52}$$

$$\frac{(k_2-1)^3}{k_1} = 2.9\times 10^{-6}\left(\tau_{\tilde{D}}^{-1}b^{-1}\right) = 1.45\times 10^{-19}\,, \tag{53}$$

whose numeric solutions are given by

$$k_2 \approx 1\,,\quad k_1 \approx 1.45\,. \tag{54}$$

As it is well known, the binding energy is represented by the familiar *finite* spectrum of the Hulten potential (Eq. (5.1.20), p. 837, [82]) that in our case has the null value

$$\begin{aligned} &E_{be} = -\frac{1}{4K_h k_2}\left(\frac{k_2}{N} - N\right)^2 = 0\,,\\ &k_2 = K_h\,\frac{m_{\tilde{D}}}{\hbar^2 b^2} = 1\,, \end{aligned} \tag{55}$$

suggesting the existence of *one and only one energy value* that with $N = 1$ and $E_{be} = 0$ as expected because contact interactions have no potential.

In conclusion, the use of non-Hamiltonian/NSA interactions yields structure model (54) of the pseudo-Deuteron-2e predicting the following rest energy

$$m_{\tilde{D}} \approx 2m_e + m_D = 1.876\,\text{MeV}, \tag{56}$$

with the evident understanding that the above value needs a correction via hadronic mechanics of the Coulomb binding energy which is currently under study.

3.4 Spin of the pseudo-Deuteron-2e

Evidently, the total spin of the electron pair in structure (36) is identically null, while the Deuteron-2e is represented in its ground state, thus implying that the orbital angular momentum of the electron pair has the value $L_{2e} = 0$. Consequently, the total angular momentum of the electron pair is null and *the spin of the pseudo-Deuteron-2e coincides with that of the conventional Deuteron.*

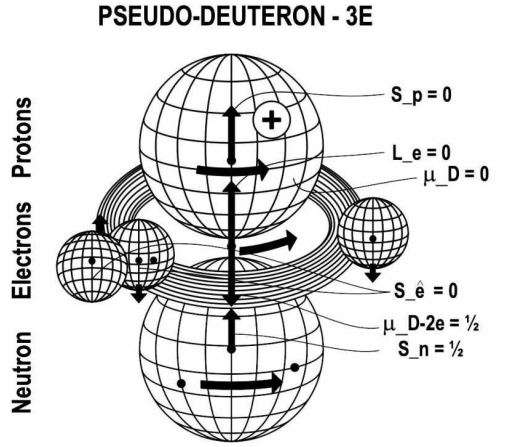

Fig. 4: In this figure, we illustrate the structure of the pseudo-Deuteron-3e predicted by hadronic mechanics as a bound state of an electron and a pseudo-Deuteron-2e (Sect. 3).

3.5 Magnetic moment of the pseudo-Deuteron-2e

Evidently, the magnetic moment of the electron pair in structure (36) is identically null. However, the *rotation* of the two elementary charges in the ground state creates a rather big magnetic moment (per nuclear standards) in the direction opposite that of the Deuteron magnetic moment.

In fact, the magnetic moment of the electron is given by

$$\begin{aligned} \mu_e^{spin} &= -9.284764\times 10^{-24}\,\text{J/T} =\\ &= 1838.2851\,\mu_{\text{N}}, \end{aligned} \tag{57}$$

(where J/T stands for Joules per Tesla and μ_{N} is the nuclear magnetron) thus being 2,162-times *bigger* than the magnetic moment of the Deuteron.

Direct calculations of the magnetic moment of elementary charges rotating within a dense hadronic medium are unknown at this writing. To have an order of magnitude of the magnetic moment of the pseudo-Deuteron-2e, we use the orbital magnetic moment of the electron in the synthesis of the neutrons from the Hydrogen in the core of star done in [84]–[97] (see also reviews [98]–[103]) which, in order to counter magnetic moment (57) to reach the neutron magnetic moment of $-1.9130\,\mu_{\text{N}}$, is given from (84) by $\mu_e = 1833.5801\,\mu_{\text{N}}$, resulting in the tentative prediction of the *magnetic moment of the pseudo-Deuteron-2e*

$$\mu_{\tilde{D}-2e} = -3.666\,\mu_{\text{N}}. \tag{58}$$

Evidently, a much bigger magnetic moment is predicted for the pseudo-Deuteron-3e.

4 Hyperfusion

4.1 Basic assumptions

In this section, we show that, according to our best understanding and documentation, the *Intermediate Controlled Nu-*

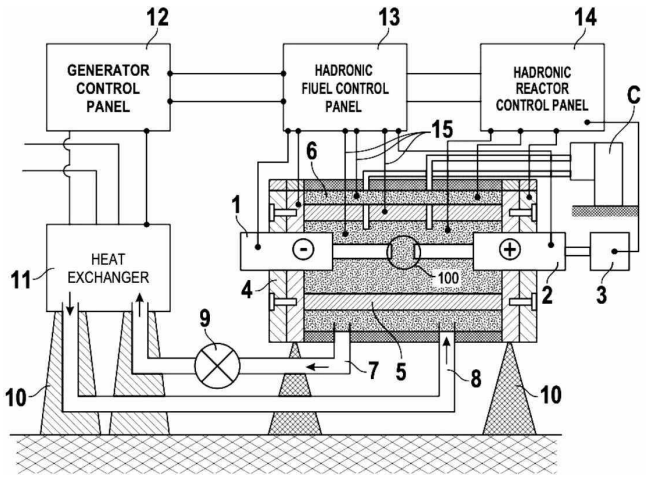

Fig. 5: In this figure, we provide a conceptual rendering of the main features of the hadronic reactor for the engineering realization of Intermediate Controlled Nuclear Fusions described in Sect. 4.3 according to Laws I-V of hadronic mechanics, including: 1. Stationary cathode; 2. Controllable anode; 3. Servomotor for the remote control of the electrode gap; 4. High pressure metal vessel; 5. External flanges; 6. Gaseous hadronic fuel, pump and tank; 7. Liquid coolant; 8. Outlet and inlet ports for the liquid coolant; 9. Liquid coolant pump; 10. Heat exchanger; 11. Electric power released to the grid; 12-13. Separate stands for the hadronic reactor and for the heat exchanger; 14. Electric power in; 15. DC power cables; 16. DC generator; 17. Variety of detectors for temperature, pressure, radiation, *etc*.; 18-20. Integrated remote and automatic control panels for the electric generator (19), hadronic fuel (20) and hadronic reactor (21), with automatic disconnect for any pre-set values for: outlet power; hadronic fuel temperature, pressure and flow; liquid coolant temperature, pressure and flow; *etc*; 21. Area in which the nuclear fusion occurs (for technical details see U. S. patents [129–131]).

clear Fusions (ICNF) tested from 2005 to 2016 [78] [104]–[128]: 1) Produce fully controlled energy without harmful radiations in excess of the used energy; 2) The production of excess energy via ICNF hadronic reactors has been limited to a few minutes for safety reasons, but it is expected to be continuous under sufficient funding and engineering; 3) The primary origin of the sustainable and controlled production of clean excess energy, here studied for the first time, appears to be primarily due to the capability by the ICNF technology of turning the nuclei of at least one of the two hadronic fuels into pseudo-nuclei (Sect. 3).

As done in the ICNF tests here considered, we assume that the hadronic fuels are *light, natural and stable elements* in their solid, liquid or gaseous form. The selection of their form is made following the engineering realization of the hadronic laws for nuclear fusions reviewed below.

Since ICNF are irreversible over time, in order to avoid the causality problems in the use of quantum mechanics or iso-mechanics identified earlier, all elaborations of ICNF are tacitly assumed to be done via the Lie-admissible geno-mathematics and geno-mechanics of Sect. 2.3.

4.2 Physical laws of controlled nuclear fusions according to hadronic mechanics

Following the quantitative representation of the neutron synthesis and its use for the exact representation of deuteron data, the physical laws of new clean nuclear energies predicted by hadronic mechanics have been presented for the first time in the 1998 monograph [78], specialized in the 2007 paper [104] and then developed at the scientific and industrial levels in subsequent years [105]–[128] according to the following classification:

Class I: Clean nuclear energies predicted via stimulated nuclear transmutations (Sect. III-4, p. 127 of [78]);

Class II: Clean nuclear energies predicted via controlled nuclear fusions (Sect. IV-3, p. 183 of [78]);

Class III: Clean energies predicted at the atomic-molecular level via contributions from energies of Class I and II (Sect. V-4, p. 287 of [78]).

In this section, we adopt the physical laws of Class II presented in Sect. 8, p. 149 of [104] and here specialized for the engineering realization of ICNF:

HADRONIC LAW I: Hadronic fusion reactors should have means for the systematic and controlled exposure of nuclei out of their electronic clouds. In the absence of such engineering means, it is assumed that nuclear fusions may indeed occur, but only at random.

HADRONIC LAW II: Whenever the nuclei of hadronic fuels have non-null spins, hadronic fusion reactors should have means for the systematic and controlled coupling of nuclear spins either in planar singlet or in axial triplet coupling (Fig. 1). In the absence of said engineering means, it is assumed that nuclear fusions may occur, but again, only at random.

HADRONIC LAW III: Hadronic fusion reactors should have means for the systematic and controlled transmutation of the nuclei of at least one of the two hadronic fuels into pseudo-nuclei (Sect. 3). In the absence of said engineering means, nuclear fusions remain possible but at a smaller efficiency rate.

HADRONIC LAW IV: The search for ICNF without the emission of harmful radiation or the release of radioactive waste should use light, natural and stable elements as hadronic fuels. Hadronic mechanics predicts that the use of heavy natural elements as hadronic fuels creates such instantaneous energy surges to trigger processes that may inevitably emit neutrons (see Appendix A for details).

HADRONIC LAW V: The energy used by hadronic reactors to achieve a desired energy output should be the minimal possible for the operation of all engineering components of the reactors. The Lie-admissible branch of hadronic mechanics predicts that any energy in excess of the indicated minimum creates instabilities with ensuing decrease of efficiency.

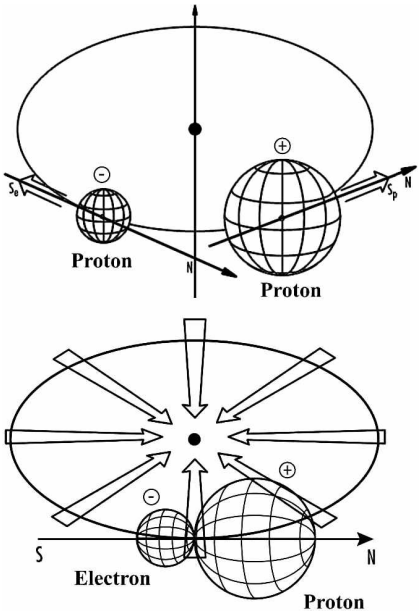

Fig. 6: In this figure, we illustrate the action of an electric DC arc between carbon electrodes submerged within a Hydrogen gas. The top view illustrates the ionization of the gas and the orientation of the proton and electron along a magnetic line, which occurs during the activation of the arc. The bottom view illustrates the compression of the plasma surrounding the arc in all radial directions toward its symmetry axis, which occurs during the disconnection of the arc [104].

4.3 Engineering realization and test of hadronic reactors for ICNF

The main principle for the engineering realization of ICNF according to Laws I-V suggested by decades of tests is the use of *DC arcs between carbon electrodes submerged within a gas.* This assumption implies that the first recommendable hadronic fuel is given by *Carbon C*$(6, 12, 0)$, while the second hadronic fuel is a properly selected, commercially available *gaseous fuel* flown through the arc to control its temperature and maximize efficiency (see U. S. patents [129–131]). Note that *Carbon nuclei have spin zero,* by therefore avoiding the need for the engineering realization of Hadronic Law II.

The action of submerged DC arcs on the gaseous hadronic fuel is the following:

1) Following their activation, DC arcs consume the point of the carbon electrode where they occur, with consequential disconnection and reconnection between points with the shortest distance. Hence, when activated, DC arcs consist of a continuous sequence of connection and disconnections generally occurring in [ms].

2) During their activation and under sufficient DC power (generally of a minimum of 40 kW), DC arcs ionize the gas, by creating a plasma in their surroundings comprising electrons, nuclei and atoms (left view of Fig. 6).

3) During their reconnection, DC arcs have been proved by the technology for the neutron synthesis (Fig. 11, 12 and Appendix B) to *compress* the surrounding plasma in all radial directions toward its symmetry axis (right view of Fig. 6).

Fig. 7: In the top figure, we show the main components of the Nitrogen hadronic reactor [105]; in the bottom left picture, we show the team of experimentalists from Princeton Gamma Spectroscopy Corporation [118]–[121] headed by L. Ying, President, who confirmed all results of [105]; in the bottom right picture, we show the confirmation of the lack of neutron or other harmful radiations by R. Brenna [110].

Consequently, to the author's best knowledge, submerged DC arcs provide the best known means for the verification of Hadronic Laws I-V, with particular reference to the synthesis of pseudo-nuclei (Hadronic Law III).

Hadronic reactors for the engineering realization of ICNF consist of: a metal vessel containing a gaseous hadronic fuel at pressure traversed by internal electrodes with remote means for the monitoring and control of the arc power, arc gap, gas pressure, gas temperature, vessel temperatures, gas flow through the arc, heat exchanger; a variety of neutrons and other detectors; interconnected, remote, monitoring and control panels of the various functions with automatic disconnect of all systems in the event of any deviation of the data from pre-set values (for details, see Fig. 5 and U. S. patents [129–131]).

In regards to manufacturing data, tests [104]–[109] were done via hadronic reactors comprising: cylindrical metal vessels with outside diameters ranging from 1 foot to 2 feet and length ranging from 2 feet to 6 feet, said vessels being certified to withstand internal pressures at least up to three times the expected operating pressure; electrodes fabricated form cylindrical graphite rods ranging from 1 to 2 inches diame-

ter with the non-consuming anode generally being 4 inches long and the consuming cathode generally being a minimum 6 inches long; a metal jacket surrounding said vessel containing a coolant (such as water) which is recirculated through a heat exchanger; specially designed control panels for the various functions; and other engineering means (Fig. 5).

All tests [104]–[109] were done via a 50 kW Miller Electric Dimension 1000, AC-DC converter operating at 40 kW by therefore supplying 0.866 kWh per minute. The reader should be aware that the use (in lieu of a commercially available AC-DC converter) of the special DC power unit for the neutron synthesis (Appendix B) provides a significant increase of the energy output due to special features of the DC arc not outlined here for brevity. All ICNF tests conducted from 2005 to 2019 by the U. S. publicly traded company *Thunder Energies Corporation,* now the private company *Hadronic Technologies Corporation* which owns all intellectual rights on ICNF. All ICNF tests were done from 2005 to 2016 with *private funds.*

Samples of the solid and gaseous hadronic fuels where taken for all ICNF tests outlined in Sects. 4.4, 4.5, 4.6, under the Trail of Custody by the technician Jim Alban before and after the tests and sent out for analysis by independent companies.

More specifically, laboratory bottles were filled up with the gaseous hadronic fuel at ambient temperature of about $80^{o}\,\mathrm{F} = 26^{o}\,\mathrm{C}$ before and after the activation of the reactor. Said samples were individually marked and shipped to *Oneida Research Services* (ORS) of Whitebnodo, New York, for the *two* different analyses of reports [118]–[124], the first for *molecular* counts and the second for *nuclear* counts with Atomic Mass Units from 2 u to 400 u, which were done via an Internal Vapor Analyzer, model 110-s operated with SOP MEL-1070. The generally low pressure of the various laboratory bottles were also marked and are reported in the individual ORS reports.

The following information is important for the proper interpretation of ORS reports: 1) The molecular and nuclear counts are inequivalent due to molecular anomalies caused by the DC arc discussed in Sect. 4.7; 2) The total number of nuclear counts before and after the tests are not the same because the Avogadro number is not conserved under nuclear fusions; 3) Reported nuclear counts generally refer to primary counts out of possible counts from 2 u to 400 u, thus implying that the sum of all counts per given sample does not necessarily add to 100; 4) The type of gas was not generally disclosed to ORS, thus implying that the used gaseous hadronic fuel is generally identified in a given report by the biggest number of reported counts; 5) The approximate character of the analyses is unquestionable, yet sufficient to establish the *existence* of an excess clean energy produced by ICNF, with the understanding that readers interested in the utmost possible accuracy should wait for proper funding.

Also under the Trail of Custody by Jim Alban, samples of the graphite used for the electrodes were taken before and after each test, marked and shipped to *Constellation Technology* of Largo, Florida, for analyses available in reports [125]–[128]. It should be noted that the latter analyses are for *solid* traces of new elements in the electrodes following tests, that confirm *some* of the nuclear fusions detected by the ORS analyses, but not all, since the primary nuclear fusions occur at the gaseous level.

Fig. 8: In this figure, we show the Oxygen hadronic reactor for the ICNF of Helium and Carbon into Oxygen (Sect. 4.5) with the structure outlined in Fig. 5, including: in the top view, the engineer Chris Lynch, the reactor, its control panel and the power unit; in the bottom left view, the scorching of the cathode despite its continuous cooling by the flow of the Helium; in the bottom right view, the production of steam operated by the author.

4.4 ICNF with the Nitrogen hadronic reactor [105]

The *Nitrogen hadronic reactor* ([105]–[107] and Fig. 7) was built according to the specifications described in Sect. 4.3 and in Fig. 5. In particular, the metal vessel was built out of Schedule 40 steel tube 1 foot $\times$ 2 feet with 1/2 inch thickness weighting 325 lbs plus side flanges weighting 125 lbs each for a total of 575 lbs certified to withstand 300 psi. All tests were done with gaseous hadronic fuels at 100 psi and for a maximum of *two minutes* due to the rapidity of the temperature surge.

Among the variety of tests with the Nitrogen hadronic reactor from 2005 to 2016, we outline below the following tests with the understanding that, to avoid an excessive length, all technical details are referred to [105]–[107]:

4.4.1 ICNF with Deuterium and Carbon

The Nitrogen hadronic reactor was filled up with a commercial grade Deuterium gas at 100 psi pressure under 40 kW DC power. Following two minutes of operation, the external temperature of the reactor went from 26° C to 150° C. Two laboratory bottles before and after the activation of the reactor were filled up with the gas at the pressure indicated in the reports, market HCN1 and HCN2, respectively and shipped to ORS. The results are available in [118] and will be analyzed for nuclear fusions in Sect. 4.7.

4.4.2 ICNF with Hydrogen and Carbon

The preceding results were confirmed by tests in the Nitrogen hadronic reactor with a commercial grade Hydrogen at 100 psi pressure and 40 kW DC power, as reported in Sect. 6 of [105] and in ORS report [120] for bottles market HC1 and HC2 (see Sect. 4.7 for their study). An important result of this test is that, under the same conditions of pressure, power, electrodes, *etc*. of the preceding test with Deuterium and Carbon, the operation with a hydrogen gas produced an energy excess bigger than that with Deuterium gas, since in two minutes of operation the temperature of the exterior wall of the reactor went from 26° C to 254° C with about 1.72% *increase* of the temperature compared to the test with Deuterium.

4.4.3 ICNF with Magnegas and Carbon

The most successful tests with the Nitrogen hadronic reactor occurred with the use as hadronic fuel of *magnegas,* the gaseous fuel with the new magnecular structure [72, 131] (Fig. 10). The results of the ORS analyses are reported in [120] for bottles marked MG1 and MG2. A main result of various tests is that the Nitrogen hadronic reactor operating with magnegas at 100 psi pressure under 40 kW power went from 26° C to 254° C in *one minute,* rather than the two minutes as for then Hydrogen-Carbon tests, thus implying a 3.44 increase of efficiency of the Deuteron-Carbon tests.

We should indicate the conduction of additional tests with the Nitrogen hadronic reactor by using various gaseous fuels whose analyses are available from [119].

4.5 ICNF with the Oxygen hadronic reactor

The Oxygen hadronic reactor (see [106]–[107], independent studies in [113], ORS reports [121, 122] and Fig. 8 in the present paper) was built in 2010 for testing the ICNF of Helium and Carbon into Oxygen, by therefore using Helium as the gaseous hadronic fuel.

The hadronic reactor comprised: a vertical 1 foot × 4 feet Schedule 40 steel cylinder certified to withstand 500 psi; a chamber surrounding said vessel for flowing water as coolant; the flow of the gaseous hadronic fuel through the electrodes for its cooling; and the remaining engineering component illustrated in Fig. 5.

The reactor was additionally built to test the feasibility of the new principle of combustion subsequently released in 2018 under the name of *HyperCombustion* [145] which is intended to achieve the full combustion of fossil fuels via a combination of a conventional combustion plus ICNF in Parts Per Million by Volume, ppmv.

For the test done in April 2010, the laboratory bottles prior and after the test were filled up with the internal gas at the pressure indicated in the reports, market HT1 and HT2 and shipped to ORS for analysis whose results are available from [121]. The tests were repeated in February 2011, market HE1 and HE2 and sent to ORS for analyses whose results are available from [122] (see Sect. 4.7 for their analysis).

The primary result of the tests was the proof under various eyewitnesses that, when filled up with Helium at 100 psi and operated with a 40 kW AC-DC converter, the Oxygen hadronic reactor did indeed produce a steam sustainable for two minutes after which the cooling system was insufficient to maintain the reactor at a constant temperature.

During additional tests done on May 15, 2011, with the Helium hadronic fuel at 150 psi, in two minutes of operation the mixture of Helium and synthesized Oxygen sent the internal temperature gauge off the 10 000° C limit and melted the top Helium recirculation port, with an impressive release of the incandescent interior gas after which all tests with the Oxygen hadronic reactor were terminated for safety. The technicians (who eyewitnessed the discharge at a distance) nicknamed *Dragons* the hadronic reactors (Dragons I, II and III for the Nitrogen, Oxygen and Silicon reactors, respectively).

4.6 ICNF with the Silicon hadronic reactor

The Silicon hadronic reactor ([106]–[108], video [109] and Fig. 9) was built to test the ICNF of Oxygen and Carbon into Silicon via the use of *air* as hadronic fuel, instead of pure Oxygen, because the natural mixture of 78% Nitrogen and 21% Oxygen is known to quench the Oxygen reactance experienced in Section 4.5.

The hadronic reactor consisted of a Schedule 40 steel tube with 1 foot diameter and 6 feet long certified to withstand a 5 000 psi pressure. Air was continuously pumped through the reactor at 1 000 psi. The arc was powered by a 50 kW AC-DC converter. The reactor was surrounded by a jacket as in Fig. 5 in which water was continuously pumped at ambient pressure. The superheated air and cooling water from the reactor were mixed to power an electricity producing turbine whose data are analyzed in Sect. 4.7. To avoid an excessive length, we suggest interested readers to view video [109] for a detailed description of this third hadronic reactor including the identification of the various members of the experimental team.

The analyses for the gaseous part of the test are available from ORS [123, 124], and the analyses for the solid part are

Fig. 9: In this figure, we illustrate the hadronic reactor for the ICNF of Oxygen and Carbon into Silicon (Sect. 4.6), with a structure outlined in Fig. 5 and described in detail in the video [109], including: in the top row, a front and rear view; in the middle view, the reactor and the touch screen for remote control; in the bottom view, one of control panels and some of the technicians (from the left) Chrys Lynch, Jim Alban and Michael Rodriguez eye-witnessing the sustainable and controllable production of steam from the turbine for the duration of 15 min.

available from Constellation Technology [125]–[128]. Independent studies are available from [110]–[117].

The main result of the tests with the Silicon hadronic reactor is that, under various eyewitness (see Fig. 9 and [109]), *the Silicon hadronic reactor did prove the capability by ICNF to produce clean excess energy for* 15 min *(fifteen minutes),* after which the remote monitoring and control panels automatically disconnected the operation for the inability of the cooling system to maintain the reactor temperature within a pre-set safety value. No additional tests were done with the Silicon hadronic reactor due to lack of funds for the construction of a properly engineered *prototype hadronic power plant.*

4.7 Representation of ICNF excess energy via hyperfusions

The ICNF tests conducted from 2015 to 2016 via the Nitrogen, Oxygen and Silicon hadronic reactors [104]–[109] were conceived, conducted and reported under the assumption that the Hadronic Laws for nuclear fusions available at that time [78] were verified by the processing, via a submerged DC arc, of the gaseous hadronic fuel into the new chemical species

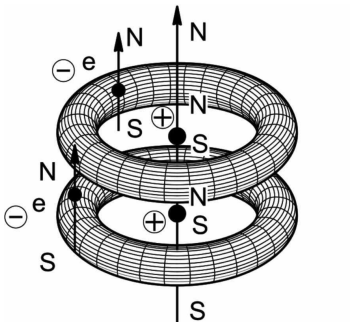

Fig. 10: In this figure, we illustrate the simplest possible case of the new chemical species of magnecules [72–74, 131], which is characterized by two atoms with a toroid polarization of their orbits caused by a DC arc which atoms are bonded together according to an axial triplet coupling thanks to their newly acquired magnetic field which does not exist in natural atomic configurations.

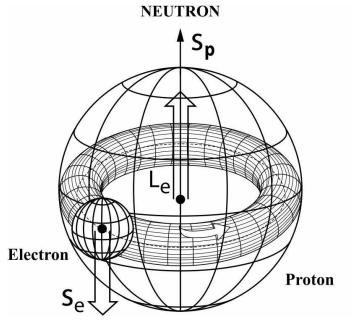

Fig. 11: In this figure, we illustrate the synthesis of the neutron from a proton and an electron in the core of stars according to hadronic mechanics reviewed in Appendix B [84]–[103].

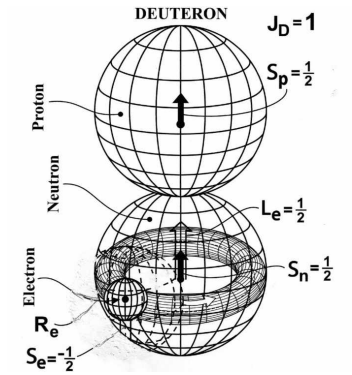

Fig. 12: A view of the structure of the Deuteron according to the synthesis of the neutron from a proton and an electron in the core of Stars ([83] and Appendix B).

of *magnecules* [72, 131] (see the MG1 counts in [120] for a sample of its anomalous chemical structure), due to the verification by magnecules such as $C \times D$ (Fig. 10) of Hadronic Laws I and II. The fusion $C \times D \to N$ was then supposed to be permitted by the compression of the magnecules during the disconnection of the DC arc (Fig. 6).

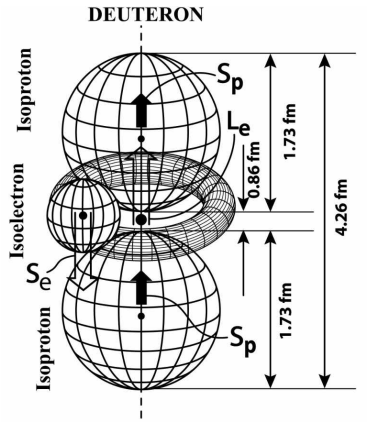

Fig. 13: In this figures, we illustrate the representation by hadronic mechanics of the stability of natural nuclei despite the natural instability of their neutrons. Said representation is intrinsic in the hadronic synthesis of the neutron from a proton and an electron (Appendix B), and it is given by the decoupling of the electron to assure a symmetric position between the two attracting protons (Appendix C). Note that the model implies the reduction of all matter in the universe to protons and electrons.

Subsequent studies have revealed that the sole creation of a magnecular structure for gaseous hadronic fuels is insufficient for a consistent representation of the nuclear fusions reported in the ORS nuclear counts for various reasons, including:

1) As shown below, the representation of ORS data on the fusion of Oxygen, Silicon and higher nuclei requires the prior fusion of two Deuterons into the Helium, which has not been achieved to date in a sustainable form via conventional engineering means;

2) Deuterium atoms are ionized by the DC current of the ICNF tests, by therefore resulting in Deuterons and electrons;

3) Explicit calculations done via the Ampere law have shown that the compression caused by the disconnection of the DC arc is unable to overcome the *extremely big Coulomb repulsion* between two Deuterons at 1 fm mutual distance, Eq. (1), by therefore rendering impossible their fusions into the Helium.

To the author's knowledge, the best possibility for two Deuterons to fuse into the Helium is that one of them acquires the form of pseudo-Deuteron (Sect. 3) since in that case all Hadronic Laws I-V are verified due to opposite charges and magnetic moments, including the planar spin coupling, under an extremely big Coulomb *attraction,* and the consequential inevitable activation of strong nuclear forces under which the fusion is inevitable. In this section, we study the excess clean energy produced by the ICNF [104]–[109] to illustrate the plausibility of their being in reality hyperfusions.

The excess energy produced by the Nitrogen hadronic reactor (Sect. 4.4.1) over the used energy in two minutes of 1.333 kWh was tentatively appraised in Sect. 4. Eq. (4.3) of [105] resulting in the value

$$\Delta E = E^{out} - E^{in} = \\ = 2.203 - 1.333\,\text{kWh} = 0.87\,\text{kWh}\,. \tag{59}$$

These preliminary appraisals were confirmed by the independent analysis [113]. By using a different method, Sect. 3.3 of the independent study [110] reached the value

$$\Delta E = 2.88\,\text{MJ} = 0.138\,\text{kWh}\,. \tag{60}$$

The tests of Sect. 4.4.2 then imply a clean excess energy of 1.73% bigger then that of (59), i.e.,

$$\Delta E = E^{out} - E^{in} = \\ = 2.823 - 1.333\,\text{kWh} = 1.49\,\text{kWh}\,. \tag{61}$$

For the case of magnegas as hadronic fuel (Sect. 4.4.3) we would then have an excess clean energy 3.44 times bigger that that of (59) in only one minute,

$$\Delta E = E^{out} - E^{in} = \\ = 23.656 - 0.666\,\text{kWh} = 2.99\,\text{kWh}\,. \tag{62}$$

It should be noted that the above preliminary appraisals are significantly *below* the excess energy actually produced by the hadronic reactors because said appraisals used the *external temperature* of the hadronic reactors, rather than the actual *internal temperature*. As an example, calculations done for the tests indicated in Section 4.1.2 with the Helium as hadronic fuel at 150 psi and the temperature of the internal gas in excess of 10 000° C in two minutes of operation we would have a multiple of value (62). The same large thermal values can be obtained from the tests of Section 4.6 with the Silicon hadronic reactor operating at 1 000 psi.

In view of the indicated insufficiencies of thermal calculations of excess clean energy produced by the hadronic reactors, in this section we present, apparently for the first time, an alternative approximate calculation of excess energy output based on the energy produced by the primary nuclear fusions reported in the ORS counts. Along these lines, [118] reports the following primary increased counts Δu among numerous other counts that are omitted in this first study for brevity,

$$\begin{aligned}
&(a)\ \ \Delta 2u : 18,550,801 - 16,075,402 = \\
&\qquad = 2,475,399\,\text{ppmv}\,, \\
&(b)\ \ \Delta 3u : 41,165 - 30,269 = 10,896\,\text{ppmv}\,, \\
&(c)\ \ \Delta 4u : 76 - 0 = 76\,\text{ppmv}\,, \\
&(d)\ \ \Delta 14u : 3,555 - 2,841 = 714\,\text{ppmv}\,, \\
&(e)\ \ \Delta 16u : 3,010 - 1,205 = 1,805\,\text{ppmv}\,, \\
&(f)\ \ \Delta 18u : 2,949 - 2,718 = 231\,\text{ppmv}\,, \\
&(g)\ \ \Delta 28u : 30,171 - 24,684 = 3,687\,\text{ppmv}\,.
\end{aligned} \tag{63}$$

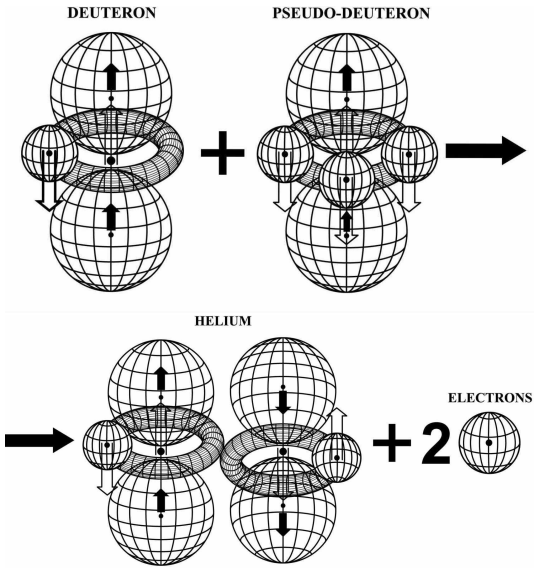

Fig. 14: In this figure, we illustrate the hyperfusion of a natural Deuteron and a pseudo-Deuteron-2e into the Helium plus the emission of an electron pair (Sects. 3 and 4).

Recall the following tabulated values (see e.g. [1])

$$\begin{aligned} &E_e = 0.511\,\text{MeV}\,,\\ &E_p = 938.272\,\text{MeV}\,,\quad E_n = 939.565\,\text{MeV}\,,\\ &E_D = 2.014102\,\text{u}\,,\quad E_{He} = 4.002603\,\text{u}\,,\\ &E_C = 12.00000\,\text{u}\,,\quad E_N = 14.003074\,\text{u}\,,\\ &E_O = 15.994915\,\text{u}\,,\quad E_{Si} = 27.976927\,\text{u}\,,\\ &1\,u = 931.5\,\text{MeV}\,. \end{aligned} \tag{64}$$

Recall also that the commercial grade Deuterium gas used for the tests contained a considerable percentage of Hydrogen. From our studies on the neutron synthesis (Appendix B), we expect that the reactor first synthesized the neutron according to the *endothermic* reaction (82)

$$\hat{e}^- + \hat{a} + p^+ \to n\,,\quad \Delta E_n = -0.782\,\text{MeV}\,. \tag{65}$$

Immediately following their synthesis, neutrons are compressed by the arc against the protons, by therefore synthesizing the Deuterium. This would explain the considerable increase of counts (a) in (63)

$$n + p \to D(1,2,1)\,,\quad \Delta E_D = 1.7045\,\text{MeV}\,. \tag{66}$$

Count (b) of (63) is interpreted as the synthesis of the Tritium with an energy balance here assumed, for simplicity, to be similar to that for the Deuterium. Count (c) of (63) is evidently the synthesis of the Helium from two Deuterons which, according to our view, can be best interpreted as the hyperfusion between a pseudo-Deuteron-2e and a natural Deuteron according to the general rule of (28) (Fig. 14),

$$\begin{aligned} &\tilde{D}_{2e}(1,2,1_\uparrow) + D(1,2,1_\downarrow) \to He(2,4,0) + \beta^-_\uparrow + \beta^-_\downarrow\,,\\ &\Delta E_{4\,u} = 23.8473315\,\text{MeV}\,. \end{aligned} \tag{67}$$

Count (d) of Eq. (63) is interpreted via the synthesis of the Nitrogen,

$$\begin{aligned} &\tilde{D}_{2e}(1,2,1) + C(6,12,0) \to N(7,14,1) + 2\beta^-\,,\\ &\Delta E_{14\,u} = 10.272582\,\text{MeV}\,. \end{aligned} \tag{68}$$

Count (e) is interpreted as due to the synthesis of the Oxygen

$$\begin{aligned} &\tilde{He}_{ke}(2,4,0) + C(6,12,0) \to O(8,16,0) + k\beta^-\,,\\ &\Delta E_{16\,u} = 7.161372\,\text{MeV}\,. \end{aligned} \tag{69}$$

Count (f) of (63) is evidently due to the synthesis of the Silicon

$$\begin{aligned} &\tilde{O}_{ke}(8,16,0) + C(6,12,0) \to Si(14,28,0) + k\beta^-\,,\\ &DeltaE_{15\,u} = 16.755822\,\text{MeV}\,. \end{aligned} \tag{70}$$

Even though incomplete, the above ICNF are sufficient to illustrate the sustainable and controllable production of clean energy by ICNF.

By using the data from (63) to (70), we have the following energy output for the counts of (63):
Deuterium synthesis: 2, 283, 555 MeV in ppmv which is given by the energy released by the Deuterium synthesis 2,475,399 ppmv $\times$ 1.7045 MeV = 4, 219, 317 MeV in ppmv *less* the energy needed for the neutron synthesis $2,475,399 \times 0.782 = 1,935,762$ MeV;
Helium synthesis: 76 ppmv $\times$ 23.8 MeV = 1, 808.8 MeV in ppmv;
Nitrogen synthesis: 714 ppmv $\times$ 10.3 MeV = 7, 354.2 MeV in ppmv;
Oxygen synthesis: $1,805 \times 7.2$ MeV = 12, 996 MeV in ppmv;
Silicon synthesis: 3, 687 ppmv $\times$ 16.7 MeV = 61, 573 MeV;
resulting in the total energy output of 54, 546, 518 MeV in ppmv corresponding to the total energy output of

$$54,546,518\,\text{MeV} = 2.43 \times 10^{-12}\,\text{kWh}\,. \tag{71}$$

By assuming that the gas in the reactor is a perfect gas, by assuming the related law

$$PV = nRT\,, \tag{72}$$

and by recalling that one mole contains 6.02×10^{23} particles, that is, 6.02×10^{17} *millions* of particles, the total energy output for data (63) is given by

$$\begin{aligned} &\Delta E = E^{out} - E^{in} =\\ &= 2.43 \times 10{-}12 \times n \times 6.02 \times 10^{17} - 1.333\,\text{kwh} \approx\\ &\approx n \times 14.628 \times 10^5\,\text{kwh}\,. \end{aligned} \tag{73}$$

For a first approximation of the number of moles n, we assume the conversions for: pressure 100 psi = 6.8 atm; length 1 foot = 2.54 cm; radius of the cylinder r = 1 foot = 13.97 cm; height of the cylinder h = 2 ft = 60.85 cm; and volume of the gas $V = \pi \times r^2 h = 3.14 \times 196 \times 60.85 = 37,455\,\text{cm}^3 = 37.45\,\text{L}$. Consequently, $PV = 6.8 \times 37.45 = 254.66$. Since the gas constant is given (in our units) by $R = 0.0821$, we have $PV/R = 254.66/0.0821 = 3,101.827$. Consequently, an approximate value of the total number of moles under the indicated assumptions is given by

$$n = 3 \times 10^3 \times \frac{1}{T}. \tag{74}$$

We now assume that the internal gas is Hydrogen and that its temperature varies from the expected 1 000 000° C in the small area of the nuclear fusions all the way to temperatures of the order of 1 000° C in the back of the reactor wall, resulting in an average temperature of the order of 10^5 C. A similar temperature value is reached via calculations based on the transmission of from 26° C to 150° C through a 1/2 inch steel wall within a period of time of the order of sixty seconds via a gas, such as Hydrogen, with the smallest possible density.

By using the equivalency 0° C ≡ 273.15 K, we have 150° C ≡ 423.15 K, our approximate value of the number of moles is given by

$$\begin{aligned} n = 3 \times 10^3 \times \frac{1}{T} = 3 \times 10^3 \times \frac{1}{423} \times 10^{-5} = \\ = 0.00704 \times 10^{-2} = 7.04 \times 10^{-4}\,. \end{aligned} \tag{75}$$

Corrections of the above value for the total number of moles of a Deuterium gas reduce the above value to

$$n \approx 7 \times 10^{-5}\,. \tag{76}$$

The approximate total output of controlled clean energy of the considered ICNF is then given by

$$\begin{aligned} \Delta E = E^{out} - E^{in} = \\ = 7 \times 10^{-5} \times 15 \times 10^5 - 1.333\,\text{kWh} \approx 100\,\text{kWh}\,. \end{aligned} \tag{77}$$

It is easy to see that, for the case of the tests of the Silicon hadronic reactor (Section 4.6) done at 1,000 psi of the gaseous hadronic fuel, the repetition of the above analysis yields a total sustainable and controllable, clean energy output of the order of 1,000 kWh, out of which the surplus electric energy released by a turbine operated electric generator is expected to be of the order of 100 kWh.

The author has no words to indicate again the approximate character of the above appraisal. More accurate calculations are planned for the forthcoming paper [146].

5 Concluding remarks

In this paper, we have recalled the generally forgotten insufficiencies of quantum mechanics in nuclear physics in view of its inability in about one century of achieving: A) A quantitative representation of the fundamental synthesis of the neutron from a proton and an electron in the core of stars; B) An exact representation of nuclear magnetic moments; C) An exact representation of the spin of nuclei in their true ground state (that without the usual orbital excitations); D) A quantitative representation of the stability of neutrons when members of a nuclear structure; E) A quantitative representation of the stability of nuclei despite the huge Coulomb repulsion between positive nuclear charges; and other insufficiencies.

We then recalled the largely forgotten experiments establishing deviations of quantum mechanical predictions from physical reality in various fields, including: electrodynamics; condensed matter physics; heavy ion physics; time dilation for composite particles; Bose-Einstein correlation; propagation of light within physical media; and in other fields.

We additionally recalled that *quantum mechanics is reversible over time* due to the invariance of Heisenberg's equation under anti-Hermiticity and for other reasons. Consequently, quantum mechanics cannot provide a consistent representation of energy-releasing processes such as nuclear fusion due to their *irreversibility over time.* In particular, we have shown that the treatment of nuclear fusions via quantum mechanics may violate causality laws (e.g., because of solutions in which effects precede the cause), because the same Schrödinger equation applies for nuclear fusions forward as well as backward in time.

We then recalled that the axiomatic origin of the above insufficiencies of quantum mechanics has been first identified in 1935 by A. Einstein, B. Podolsky and N. Rosen and rests in the *locality* of the theory (EPR argument) [5], beginning at the level of the Newton-Leibnitz calculus, due to the sole possibility of characterizing particles and nuclei as massive points, thus creating conceptual and technical difficulties in fusing two points into a third point.

We then briefly reviewed the EPR completion of quantum mechanics into hadronic mechanics for the characterization of particles and nuclei as *extended, thus deformable and hyperdense* under conventional, Hamiltonian interactions plus contact, thus zero-range, non-Hamiltonian interactions caused by mutual penetrations, with an elementary review of:

i) The Lie-isotopic (i.e. axiom-preserving) branch of hadronic mechanics including *iso-mathematics and iso-mechanics* (Sect. 2.2) for the representation of extended particles and their non-Hamiltonian interactions via the isotopic element $\hat{T} = \hat{T}^\dagger > 0$ of the universal enveloping iso-associative algebra of Hermitean operators with product $A \star B = A\hat{T}B$ and ensuing iso-Schrödinger equation $H \star |\psi\rangle = H\hat{T}|\psi\rangle = E|\psi\rangle$ with apparent resolution of quantum mechanical insufficiencies for *stable* nuclei.

ii) The Lie-admissible branch of hadronic mechanics, also called genotopic branch, including *geno-mathematics and geno-mechanics* (Sect. 2.3) based on forward enveloping algebra with ordered products to the right $A > b = ARB$, R-

> 0 representing motion forward in time, and backward enveloping algebra with ordered products to the left $A < B = ASB, S > 0$ representing motion backward in time, with the corresponding forward and backward geno-Schrödinger equations $H > |\psi^{for}\rangle = HR|\psi^{for}\rangle = E^{for}|\psi^{for}\rangle$, $\langle\psi^{bac}| < H = \langle\psi^{bac}|S\,H = E^{bac}\langle\psi^{bac}|$, and axiomatically consistent resolution of the quantum mechanical causality problems for irreversible processes whenever $R \neq S$.

Thanks to half a century preparatory studies on the above issues, in this paper we have presented apparently for the first time:

1) The prediction by hadronic mechanics of the existence of new, negatively charged, unstable nuclei, called *pseudo-nuclei,* which are characterized by a hadronic bond of negatively charged electrons and positively charged natural nuclei, by therefore resolving the Coulomb barrier since pseudo-nuclei would be *attracted* (rather than repelled) by natural nuclei, with ensuing new conception of nuclear fusions between pseudo-nuclei and natural nuclei, here called *hyperfusions* (Section 3);

2) The identification of engineering means for the synthesis of pseudo-nuclei which is given by the hadronic reactors for the synthesis of the neutron from the proton and the electron (Sects. 4.1-4.6 and Appendix B);

3) Laboratory evidence according to which the synthesis of pseudo-nuclei and related hyperfusions appear to be the origin of the limited, yet sustained and controlled excess energies achieved by the *Intermediate Controlled Nuclear Fusions* (Section 4.7).

In view of the inability by quantum mechanics in about one century under large public funds to achieve industrially applicable nuclear fusions, and the consequential, rapidly increasing deterioration of our environment, the author hopes that appropriate academic and governmental entities initiate the implementation of a true scientific democracy for qualified inquiries, which requires the continuation of the search for clean nuclear energies along quantum mechanical lines, *jointly* with the search based on new vistas, such as the forgotten EPR argument.

Appendices

A Is neutron radiation truly necessary for nuclear fusions?

As it is well known, it has been generally assumed for about one century that the emission of harmful neutrons is necessary for nuclear fusions (see e.g. [132]), as it is the case for the *Tokamak nuclear fusion* of Deuterium and Tritium into Helium plus neutron [133, 134]

$$\begin{aligned} &D(1,2,1) + D(1,3,1/2) \to He(2,4,0) + n\,,\\ &\Delta E = +17.6\,\text{MeV}\,. \end{aligned} \tag{78}$$

The author respectfully suggests the conduction of *experimental verifications* of the need for the emission of neutrons in Deuteron-type fusions prior to its systematic use under public support, in view of the following opposing evidence:

A.1. The need for the emission of neutrons in nuclear fusions was historically established for the fusions of *heavy nuclei* but, to the author's best knowledge, no quantitative study is currently available on a similar need for the fusion of *light nuclei,* such as the Deuterium and the Tritium.

A.2. It is known that, in the core of stars, Deuterons fuse into the Helium without neutron emission,

$$\begin{aligned} &D(1,2,1_\uparrow) + D(1,2,1_\downarrow) \to He(2,4,0)\,,\\ &\Delta E = +29.523\,\text{MeV}\,, \end{aligned} \tag{79}$$

since the Coulomb barrier is overcome by the extreme local pressures, while collective fusions leading to the explosion of the star are prohibited by the random spin alignment of fusion (79).

A.3. There exists valid evidence of excess heat creation in condensed matter due to nuclear fusions of light nuclei without the emission of neutrons [135–137].

A.4. The assumption of the necessary emission of neutrons in the fusion of light nuclei is based on a theory, quantum mechanics, which is only *approximately valid* in nuclear physics due to its inability in one century of achieving exact representations of basic nuclear data (Sect. 1).

A.5. Clear experimental evidence achieved in major physics laboratories has established the existence of deviations of quantum mechanical predictions from physical reality in various fields [12]–[26].

A.6. The unverified assumption of the necessary emission of neutrons in nuclear fusion is made in oblivion of the Einstein-Podolsky-Rosen argument that *Quantum mechanics is not a complete theory* [5].

A.7. The totality of the *intermediate Controlled Nuclear Fusions* occurred with the independently certified absence of any neutron emission [104]–[128].

Since sustainability has not been achieved in about one century for nuclear fusions with neutron emission, nuclear fusions without neutron emission should deserve the same scientific process.

B The synthesis of the neutron in a star

In 1920, E. Rutherford [138] suggested that the hydrogen atom in the core of stars is "compressed" into a new particle that he called the *neutron*

$$e^- + p^+ \to n\,. \tag{80}$$

In 1932, J. Chadwick [139] provided an experimental confirmation of the existence of the neutron.

In 1933, W. Pauli [140] pointed out that synthesis (80) violates the conservation of angular momentum.

In 1935, E. Fermi [141] submitted the hypothesis that the synthesis of the neutron occurs with the joint *emission* of a

neutral and massless particle ν with spin 1/2 that he called the *neutrino* (meaning "little neutron" in Italian)

$$e^- + p^+ \ \rightarrow \ n + \nu \, . \tag{81}$$

In 1978, R. M. Santilli [82] (see also the 2021 update [29]) identified various arguments according to which quantum mechanics is *inapplicable* to (rather than violated by) the neutron synthesis, beginning with the fact that the rest energy of the neutron is *bigger* than the sum of the rest energies of the proton and the electron,

$$\begin{aligned} &E_p = 938.272 \, \text{MeV} \, , \ \ E_e = 0.511 \, \text{MeV} \, , \\ &E_n = 939.565 \, \text{MeV} \, , \\ &\Delta E = E_n - (E_p + E_e) = 0.782 \, \text{MeV} > 0 \, , \end{aligned} \tag{82}$$

by therefore requiring a *positive binding energy* and resulting in a *mass excess* for which the Schrödinger and Dirac equations admit no physically meaningful solutions.

Consequently, when he was at Harvard University under support of the U.S. Department of Energy, R. M. Santilli proposed [49] the construction of the non-unitary Einstein-Podolski-Rosen completion of quantum mechanics into a new mechanics called *hadronic mechanics* (Sect. 2).

Following the achievement of mathematical and physical maturity [51] (see [30, 31] for detailed treatment), the Lie-isotopic branch of hadronic mechanics allowed the representation of *all* characteristics of the neutron at the non-relativistic and relativistic levels via a structure model of the neutron consisting of an electron e^- totally compressed inside the extended and dense proton p^+ in singlet coupling [84]–[89] (Figs. 11, 12 and 13).

At the non-relativistic level, the exact representation of the **mass, mean life and charge radius of the neutron** were achieved via structure equations of type (51) [84].

The exact representation of the **spin of the neutron** was achieved thanks to the appearance of the *internal orbital motion* of the electron within the extended and dense proton with angular momentum $L_e = 1/2$ (which is necessary to avoid major resistive forces), resulting in the following realization of Rutherford's original conception of the neutron, Eq. (80),

$$\begin{aligned} &\hat{e}^- + \hat{p}^+ \rightarrow \hat{e}^-_{spin} + \hat{e}^-_{orb} + \hat{p}^+ \rightarrow n \, , \\ &S^{spin}_{\hat{e}} + S^{orb}_{\hat{e}} + S^{spin}_{\hat{p}} = -\frac{1}{2} + \frac{1}{2} + \frac{1}{2} = \frac{1}{2} \, , \end{aligned} \tag{83}$$

(where the "hat" denotes treatment via hadronic mechanics) according to which *the spin of the neutron coincides with that of the proton,* as expected since the proton is assumed to be at rest in synthesis (80) and its mass is about 1 800 times that of the electron. Note that the internal orbital motion of the electron is impossible for quantum mechanics due to the representation of the proton as a point.

Recall that, in Rutherford's synthesis (80), we have the following tabulated magnetic moments of the electron, the proton and the neutron all considered in nuclear magnetrons

$$\begin{aligned} &\mu^{spin}_{\hat{e}} = +1838.285 \, \mu_{\text{N}}, \ \ \mu^{spin}_{\hat{p}} = +2.7/92 \, \mu_{\text{N}} \, , \\ &\mu^{spin}_{n} = -1.913 \, \mu_{\text{N}} \, , \end{aligned} \tag{84}$$

where one should note that the direction of the magnetic moment of the electron is the same as that of the proton because of the double inversion of the spin and of the charge. One should also note the very big value of the intrinsic magnetic moment of the electron for nuclear standards which is intrinsic in the synthesis of the neutron from the Hydrogen.

The exact representation of the **anomalous magnetic moment of the neutron** was achieved thanks to the indicated internal orbital motion of the electron with the value

$$\mu^{orb}_{\hat{e}} = -1842.990 \, \mu_{\text{N}} \, , \tag{85}$$

by keeping in mind that the orbital magnetic moment of the electron is opposite that of the proton due to opposite charges. The exact representation of the anomalous magnetic moment of the neutron was then reached via the sum [84]

$$\begin{aligned} &\mu^{spin}_{e} + \mu^{orb}_{e} + \mu^{spin}_{p} = \\ &= +1838.285 - 1842.990 + +2.792 \, \mu_{\text{N}} = \\ &= -1.913 \, \mu_{\text{N}} \, . \end{aligned} \tag{86}$$

The above representation is considered to be a confirmation of the internal orbital motion of the electron in synthesis (80) because of the representation of the *negative* value of the neutron magnetic moment.

The **relativistic representation** of all characteristics of the neutron in synthesis (80) was reached in the 1995 paper [89] (see review [28]) via the isotopies $\hat{\mathcal{P}}(3.1)$ of the spinorial covering of the Lorentz-Poincaré symmetry and cannot be reviewed here for brevity.

Following the mathematical and physical understanding of the neutron synthesis in the core of stars, Santilli and his associates conducted systematic experimental and industrial tests on the laboratory synthesis of the neutron from a commercial grade Hydrogen gas [90]–[97] (see also independent studies [98]–[103]). These tests eventually lead to the production and sale by the U.S. publicly traded company *Thunder Energies Corporation* (now the private company *Hadronic Technologies Corporation* http://www.hadronictechnologies.com) of the *Directional Neutron Source* (DNS) producing on demand a flux of low energy neutrons in the desired direction (Fig. 15).

In regard to the mass excess of synthesis (80), we should recall that the missing energy of 0.782 MeV cannot be provided by the relative kinetic energy between the electron and the proton because, at that energy, the electron-proton cross section is essentially null, thus prohibiting any synthesis.

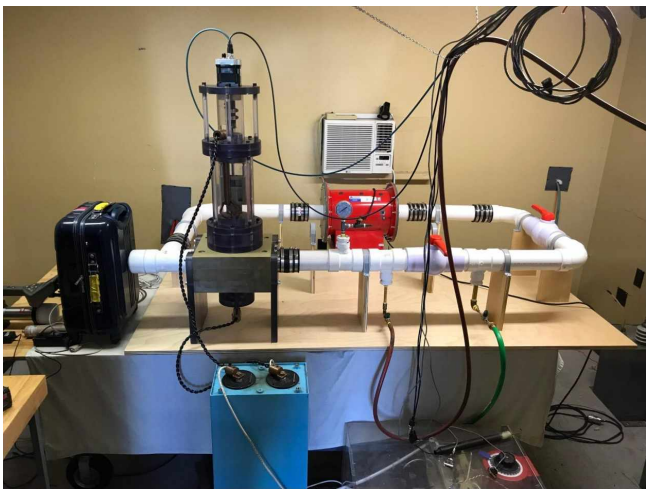

Fig. 15: In this figure, we illustrate the Directional Neutron Source (DNS) produced and sold by the U. S. publicly traded company Thunder Energies Corporation* which produces on demand a flux of low energy, directional neutrons synthesized from a commercial-grade Hydrogen gas contained in the loop of the hadronic reactor.
*Now www.hadronictechnologies.com

Similarly, said missing energy cannot be provided by a star such as our Sun, because the Sun synthesizes about 10^{38}–10^{39} neutrons *per second,* that would require such a big amount of energy (about 10^{38} MeV/s) to prevent a star from producing light due to insufficient internal temperature.

For these and other reasons, Santilli [142] proposed in 2007 the hypothesis that *the missing energy in the neutron synthesis is provided by space as a universal substratum with an extremely big energy density* needed for the characterization and propagation of electromagnetic waves and elementary particles. The missing energy is transferred from space to the neutron by a massless, chargeless and spinless longitudinal impulse called *etherino* and denoted with the letter $\hat{a}$ (from the Latin *aether*), according to the synthesis

$$\hat{e}^- + \hat{a} + \hat{p}^+ \to n\,, \tag{87}$$

where one should note that, contrary to the case of the neutrino in synthesis (81), the etherino is on the *left* of the synthesis as a condition to supply the missing energy.

Independently from the above studies, the Sun releases into light 2.3×10^{38} MeV/s [143], corresponding to about 4.3×10^6 t/s. Since in a Gregorian year there are 10^7 seconds, the loss of mass by the Sun ΔM_S per year due to light emission is given by

$$\Delta M_S = 10^{23} \text{ metric tons per year}\,. \tag{88}$$

This loss of mass is of such a size to cause a decrease of planetary orbits detectable in astrophysical laboratories, contrary to centuries of measurements on the stability of planetary orbits.

Therefore, Santilli proposed the etherino hypothesis [142] for the intent of representing the gravitational stability of the Sun via a return to the historical cosmological model based on the continuous creation of matter in the universe. In fact, the energy needed for the star to synthesize neutrons 10^{38} MeV/s is essentially equal to the energy needed for the neutron synthesis, by therefore representing the stability of the star with intriguing cosmological implications [22, 23], e.g. for supernova explosions and neutron stars.

Note that the *permanently stable* protons and electrons cannot possibly disappear from the universe during the neutron synthesis to be replaced by the hypothetical quarks. Note also that the neutron is naturally unstable (when isolated) and decays into the original stable constituents. The above features imply new recycling nuclear waste via their stimulated decay caused by photon irradiation with a suitable resonating frequency $\gamma^{res} = 1.293$ MeV and transmutations of the type [78, 95]

$$M\gamma^{res} + N(Z, A, J) \;\to\; N'(Z + M, A, J + K) + M\beta^-\,, \tag{89}$$

(where K is the spin corrections due to the emission of electrons) under which transmutations the long mean lives of nuclear waste can be reduced in a way proportional to the intensity of the gamma irradiation.

Additionally, we should mention that, following the compression of the electron within the proton, hadronic mechanics predicts the subsequent compression (evidently with a smaller probability) of an electron, this time, within a neutron, resulting in a *new negatively charged particle* called *pseudo-proton* $\tilde{p}^-$ [144] with an additional possibility of recycling nuclear waste via pseudo-proton irradiation and ensuing transmutations

$$M\tilde{p}^- + N(Z, A, J) \;\to\; N'(Z - M, A, J + K)\,, \tag{90}$$

under which long mean lives (calculated via hadronic mechanics) can be reduced to seconds.

C Representation of nuclear stability

We close this paper with an outline of the representation of nuclear stability according to hadronic mechanics.

C.1 Representation of nuclear stability despite the instability of the neutron

According to quantum mechanics, no stable nuclei should exist in nature because nuclei are assumed to be quantum mechanical bound states of protons, which are permanently stable, and neutrons which are naturally unstable, with a mean life of 879.6 ± 0.8 s and spontaneous decay [1]

$$n \;\to p^+ + e^- + \bar{\nu}\,. \tag{91}$$

Following decades of study of the problem, this author was unable to *formulate,* let alone solve, the above problem due to

the lack of any possible quantum mechanical representation of the synthesis of the neutron in a star.

Following a conceptual suggestion in [36], we here indicate, apparently for the first time, that the quantitative representation of nuclear stability despite the natural instability of the neutron is an intrinsic feature of the hadronic synthesis of the neutron from the proton and the electron because, starting from the hadronic structure of the neutron (Fig. 11 and Appendix B) with ensuing hadronic structure of the Deuteron as a two-body bound state of a proton and a neutron in axial triplet coupling (Fig. 12 and Sect. 3), the electron naturally decouples from the proton to acquire a position intermediate between the two protons (Fig. 13). Consequently, the decoupled electron assumes an intermediate position between the two attracting protons by occupying the distance between their charge distributions of 0.3745 fm, which would otherwise be empty according to available experimental data (Fig. 2, [2]). Intriguingly, the suggested decoupling allows a novel representation of the known *exchange forces* in nuclear physics because the transition of the decoupled electron from one proton to the other evidently implies a proton-neutron exchange.

Note that the indicated decoupling of the neutron is impossible for 20^{th} century physics. Note also that, in the preceding Deuteron model based on planar singlet couplings of Sect. IV-2.5, p. 171 of [78], the decoupling here considered is impossible while, for the axial triplet coupling the decoupled electron remains with null total angular momentum due to its motion within the nuclear medium, by therefore confirming the uniqueness and importance of the axial triplet coupling (Fig. 1). Note finally that the decoupling of nuclear neutrons into protons and electrons implies the reduction of all matter in the universe to protons and electrons.

C.2 Representation of nuclear stability despite repulsive protonic forces

Additionally, stable nuclei should not exist in nature according to quantum mechanics because equal charge nuclear protons *repel* each other with an extremely big Coulomb force of the order of hundreds of Newtons Eq. (1).

We here indicate, also apparently for the first time, that hadronic mechanics can indeed represent this second problem of nuclear stability via a mechanism similar to the achievement by quantum chemistry of a strongly *attractive* force between the *identical* electrons of valence couplings [72–74].

Let us consider the nucleus with the minimal number of proton pairs, which is evidently given by the Helium $He(2,4,0)$ [1]. Various measurements [3] have established that the Helium has a charge radius of 1.678 fm, against the radius of two protons and two neutrons each having the value of 0.841 fm [4] with the total radius of 1.678 fm .

The above measurements confirm the primary assumption of hadronic mechanics, according to which nuclei are composed by extended protons and neutrons in conditions of partial mutual penetration of their dense charge distributions with ensuing non-Hamiltonian interactions (Sect. 2).

Let us assume in first approximation that the Helium is a quantum mechanical (qm) bound state of two Deuterons with anti-parallel spins

$$He(2,4,0) = [\, D(1,2,1_\uparrow), D(1,2,1_\downarrow)\,]_{qm}\,. \tag{92}$$

We assume the representation of the non-Hamiltonian interactions via non-unitary transform (47) of the quantum model (92) thus yielding the expression

$$\begin{aligned} & U\left[\frac{1}{2m}\,\delta^{ij}p_ip_j + V_c(r)\right]|\,\psi(r)\,\rangle\,U^\dagger = \\ & = \left\{-\frac{1}{m}\,\hat\partial_{\hat r}\hat\partial_{\hat r} + V_c(\hat r)\left[1 - \frac{V_h(\hat r)}{V_c(\hat r)}\right]\right\}|\,\hat\psi(\hat r)\,\rangle = \\ & = \left[-\frac{1}{m}\,\hat\Delta_{\hat r} - K_h'\,\frac{e^{b\hat r}}{1-e^{b\hat r}}\right]|\,\hat\psi(\hat r)\,\rangle = E_h\,|\,\hat\psi(\hat r)\,\rangle\,, \end{aligned} \tag{93}$$

where the last expression has been reached by "absorbing" the Coulomb potential into the Hulten potential as in (50).

Consequently, the above analysis confirms that non-linear, non-local and non-potential nuclear interactions due to the mutual penetration of nucleons can be so strongly attractive to overcome repulsive Coulomb force between protons.

It is easy to see that the hadronic conversion of the repulsive Coulomb into a strongly attractive Hulten-type or other potentials also applies for other nuclear potentials, such as the *Yukawa potential* [147], the *Woods-Saxon potential* [148] and other potentials or their combination [149].

C.3 Representation of the Helium data

We now show that, following the overcoming of the repulsive ptotonic forces, non-Hamiltonian interactions remain so strong to represent the characteristics of Helium.

Note that the representation of the spin and magnetic moment of Helium follows from the antiparallel Deuteron spins of model (92). The representation of the rest energy, mean life and charge radius of Helium can be done via the hadronic structure model of the pion (Sect. 5.1, p. 827 on, [82]) and of the Deuteron (Sect. IV-2.5, p. 171 on, [78])

$$\begin{aligned} & \left[\frac{1}{r^2}\left(\frac{d}{dr}r^2\frac{d}{dr}\right) + \tilde m_d\left(E + K_h'\frac{e^{-br}}{1-e^{-br}}\right)\right] = 0\,, \\ & E_{he} = 2E_d - E_{be} = 3.7284\times 10^3\,\text{MeV}\,, \\ & \tau^{-1} = 2\pi\lambda^2\,|\hat\psi(0)|^2\,\frac{\alpha^2 E_1}{\hbar} = \infty\,, \\ & R = b^{-1} = 1\,\text{fm}, \end{aligned} \tag{94}$$

where $\hat m = m/\rho$ is the *iso-renormalized mass* of the Deuteron, that is, the mass renormalized from non-Hamiltonian interac-

tions (Eq. (5.1.7b), p. 833, of [82]) here adjusted for Helium

$$\tilde{m} = \tilde{E}_d = \frac{E_d}{\rho} = \frac{E_{he}}{2} = 1.8542 \times 10^3 \,\mathrm{MeV}\,, \qquad \rho = 1.0188 > 1\,, \tag{95}$$

The solution of Eqs. (94) was studied in all details in Sect. 5.1, p. 836 on, [82] (see also the recent review in [29]) and reduced to the numeric values of two parameters denoted k_1 and k_2, Eqs. (5.1.32a) and (5.1.32b), p. 840 [82], that become in our case

$$\tau = \frac{48 \times (137)^2}{4\pi bc} \frac{k_1}{(k_2 - 1)^3} = \infty\,, \tag{96}$$

$$E_{he} = k_1[1 - (k_2 - 1)2] \frac{2\bar{h}c}{b} = 3.7284 \times 10^3 \,\mathrm{MeV}\,, \tag{97}$$

with numeric solutions

$$k_2 = 1\,, \quad k_1 = 4.9\,, \tag{98}$$

that should be compared with the numeric solutions for the meson octet of [29, 82].

Intriguingly, the known finite spectrum of the Hulten potential (see Eq. (5.1.20), p. 837, [82])

$$BE_h = -\frac{1}{4K_h k_2} \left(\frac{k_2}{n} - n\right)^2\,, \quad k_2 = K_h \frac{\tilde{E}_d}{\hbar^2 b^2} = 1\,, \tag{99}$$

admits *only one value, Helium*, for $n = 1$, with null value of the binding energy, $BE_h = 0$, as expected for the sole *non-potential* interactions of model (94), since the representation of the Helium binding energy requires the addition of a *potential* force here left to interested readers.

In conclusion, the above model confirms that nuclear forces are some of the most complex forces in nature, since they include a linear, local and potential component represented by the Hamiltonian which is responsible for nuclear binding energies, plus a non-linear, non-local and non-potential component represented by the isotopic element which is responsible for the nuclear stability.

Acknowledgements

The author would like to thank for penetrating critical comments the participants of the *2020 International Teleconference on the EPR argument* and the *2021 International Conference on Applied Category Theory and Graph-Operad-Logic*. Additional thanks are due to the technicians Micahel Rodriguez, Jim Alban, Ray Jones and Chris Lynch for the recollection of 2005-2019 ICNF tests. Special thanks are due to Eng. S. Beghella-Bartoli for a critical reading of the manuscript, and to Mrs. Sherri Stone for linguistic control of the manuscript. The author is solely responsible for the content of this paper due to inevitable final controls of the manuscript.

Received September 29, 2022

References

1. KAERI Table of Nuclide, website. http://pripyat.mit.edu/KAERI/
2. Rau S., *et al*. Penning Ttrap measurements of the deuteron and the HD^+ molecular ion. *Nature*, 2020, v. 585, 43–47. http://doi.org/10.1038/s41586-020-2628-7
3. Krauth J. J., Schuhmann K. and Kottmann F, Measuring the α-particle charge radius with muonic helium-4 ions. *Nature*, 2021, v. 589, 527–531. http://www.nature.com/articles/s41586-021-03183-1
4. Pohl R. Antognini A. and Kottmann F. The size of the proton. *Nature*, 2010, v. 466, 213–216. http://www.nature.com/articles/nature09250
5. Einstein A., Podolsky B. and Rosen N. Can quantum-mechanical description of physical reality be considered complete? *Phys. Rev.*, 1935, v. 47, 777–780. http://www.eprdebates.org/docs/epr-argument.pdf
6. Heisenberg W. *Nachr. Akad. Wiss.* Gottingen, Germany, 1953, v. IIa, 111. http://link.springer.com/chapter/10.1007/978-3-642-70079-8-23
7. Geoldtesin S. Stanford Encyclopedia of Philosophy, Bohmian (de Broglie-Bohm) Mechanics, 2021. http://plato.stanford.edu/entries/qm-bohm/
8. Bohm D. A Suggested Interpretation of the Quantum Theory in Terms of "Hidden Variables". *Physical Review*, 1952, v. 85, 166–182. http://journals.aps.org/pr/abstract/10.1103/PhysRev.85.166
9. Santilli, R. M. Generalization of Heisenberg's uncertainty principle for strong interactions. *Hadronic Journal*, 1981, v. 4, 642–657. http://www.santilli-foundation.org/docs/generalized-uncertainties-1981.pdf
10. Santilli R. M. Isorepresentation of the Lie-isotopic SU(2) Algebra with Application to Nuclear Physics and Local Realism. *Acta Applicandae Mathematicae*, 1998, v. 50, 177–190. http://www.santilli-foundation.org/docs/Santilli-27.pdf
11. Santilli R. M. Studies on the classical determinism predicted by A. Einstein, B. Podolsky and N. Rosen. *Ratio Mathematica*, 2019, v. 37, 5–23. http://www.eprdebates.org/docs/epr-paper-ii.pdf
12. Santilli R. M. A quantitative representation of particle entanglements via Bohm's hidden variables according to hadronic mechanics. *Progress in Physics*, 2022, v. 18, 131–137. http://www.santilli-foundation.org/docs/pip-entanglement-2022.pdf
13. Miller J P., de Rafael E. and Roberts B. Lee. Muon (g2): experiment and theory. *Rep. Prog. Phys.*, 2007, v. 70, 795–881. http://news.fnal.gov/2021/04/first-results-from-fermilabs-muon-g-2-experiment-strengthen-evidence-of-new-physics/
14. Santilli R. M. Representation of the anomalous magnetic moment of the muons via the Einstein-Podolsky-Rosen completion of quantum into hadronic mechanics. *Progress in Physics*, 2021, v. 17, 210–215. http://www.santilli-foundation.org/muon-anomaly-pp.pdf
15. Santilli R. M. Representation of the anomalous magnetic moment of the muons via the novel Einstein-Podolsky-Rosen entanglement. In: Guzman J. C., ed. Scientific Legacy of Professor Zbigniew Oziewicz: Selected Papers from the International Conference "Applied Category Theory Graph-Operad-Logic". World Scientific, in press. http://www.santilli-foundation.org/ws-rv961x669.pdf
16. Fadel M., Zibold T., Decamps B. and Treutlein Ph. Spatial entanglement patterns and Einstein-Podolsky-Rosen steering in BoseEinstein condensates. *Science*, 2018, v. 360, 409–415. http://www.santilli-foundation.org/Basel-paper.pdf
17. Schukraft J. Heavy-ion physics with the ALICE experiment at the CERN Large Hadron Collider. *Trans. R. Soc.*, 2012, v. A370, 917–932. royalsocietypublishing.org/doi/10.1098/rsta.2011.0469
18. Cardone F., Mignani R. and Santilli, R. M. On a possible energy-dependence of the K^0 lifetime. Paper I *J. Phys. G: Part. Phys.*, 1992, v. 18, L61–L65. Paper II *J. Phys. G: Part. Phys.*, 1992, v. 18, L141–L144. http://www.santilli-foundation.org/docs/Santilli-32.pdf

19. Santilli R. M. Apparent Unsettled Value of the Recently Measured Muon Magnetic Moment. *Progress in Physics*, 2022, v. 18, 15–18. http://www.santilli-foundation.org/docs/muon-meanlife-2022.pdf
20. Santilli R. M. Nonlocal formulation of the Bose-Einstein correlation within the context of hadronic mechanics. *Hadronic J.*, 1992, v. 15, 1–50 and v. 15, 81–133. www.santilli-foundation.org/docs/Santilli-116.pdf
21. Cardone F. and Mignani R. Nonlocal approach to the Bose-Einstein correlation. . *Phys. J.*, 1998, v. C4, 705–728.
22. Ahmar H., Amato G., Kadeisvili J. V., Manuel J., West G. and Zogorodnia O. Additional experimental confirmations of Santilli's IsoRedShift and the consequential lack of expansion of the universe. *Journal of Computational Methods in Sciences and Engineering*, 2013, v. 13, 321–375. http://www.santilli-foundation.org/docs/IRS-confirmations-212.pdf
23. Santilli R. M. Experimental Verifications of IsoRedShift with Possible Absence of Universe Expansion, Big Bang, Dark Matter, and Dark Energy. *The Open Astronomy Journal*, 2010, v. 3, 124. http://www.santilli-foundation.org/docs/Isoredshift-Letter.pdf
24. Saldanha P. L. Inconsistency of a Realistic Interpretation of Quantum Measurements: a Simple Example. *Braz. J. Phys.*, 2020, v. 50, 438–441. http://doi.org/10.1007/s13538-020-00757-8
25. Svensson E. Y. Logical inconsistencies in quantum mechanics. arXiv: 1803.06162, 2018. http://arxiv.org/abs/1803.06162
26. Myrvold W. Philosophical Issues in Quantum Theory. *The Stanford Encyclopedia of Philosophy*, 2022. http://plato.stanford.edu/entries/qt-issues
27. Santilli R. M. Studies on A. Einstein, B. Podolsky, and N. Rosen prediction that quantum mechanics is not a complete theory. I: Basic methods. *Ratio Mathematica*, 2020, v. 38, 5–69. http://eprdebates.org/docs/epr-review-i.pdf
28. Santilli R. M. Studies on A. Einstein, B. Podolsky, and N. Rosen prediction that quantum mechanics is not a complete theory. II: Apparent proof of the EPR argument. *Ratio Mathematica*, 2020, v. 38, 71–138. http://eprdebates.org/docs/epr-review-ii.pdf
29. Santilli R. M. Studies on A. Einstein, B. Podolsky, and N. Rosen prediction that quantum mechanics is not a complete theory. III: Illustrative examples and applications. *Ratio Mathematica*, 2020, v. 38, 139–222. http://eprdebates.org/docs/epr-review-iii.pdf
30. Santilli, R. M. Elements of Hadronic Mechanics, Vol. I. *Mathematical Foundations. Ukraine Academy of Sciences, Kiev*, 1995. http://www.santilli-foundation.org/docs/Santilli-300.pdf
31. Santilli R. M. Elements of Hadronic Mechanics, Vol. II, *Theoretical Foundations. Ukraine Academy of Sciences, Kiev*, 1995. http://www.santilli-foundation.org/docs/Santilli-301.pdf
32. Santilli R. M. Elements of Hadronic Mechanics, Vol. III, *Experimental Verifications. Ukraine Academy of Sciences, Kiev*, 2016. http://www.santilli-foundation.org/docs/elements-hadronic-mechanics-iii.compressed.pdf
33. Anderson R. Outline of Hadronic Mathematics, Mechanics and Chemistry as Conceived by R. M. Santilli. *American Journal of Modern Physics*, 2016, v. 6, 1–16. http://www.santilli-foundation.org/docs/HMMC-2017.pdf
34. Beghella-Bartoli S. and Santilli R. M., eds. Proceedings of the 2020 Teleconference on the Einstein-Podolsky-Rosen argument that "Quantum mechanics is not a complete theory". Curran Associates, New York, 2021. http://www.proceedings.com/59404.html (printed). http://www.proceedings.com/60007.html (electronic). http://www.world-lecture-series.org/level-xii-eprteleconference-2020 (recorded lectures).
35. Santilli R. M. Overview of historical and recent verifications of the Einstein-Podolsky-Rosen argument and their applications to physics, chemistry and biology. APAV - Accademia Piceno Aprutina dei Velati, Pescara, Italy, 2021. http://www.santilli-foundation.org/epr-overview-2021.pdf
36. Santilli R. M. Overview of historical and recent verifications of the Einstein-Podolsky-Rosen argument and their applications to physics, chemistry and biology. APAV - Accademia Piceno Aprutina dei Velati, Pescara, Italy, 2021.
37. Dunning-Davies J. A Present Day Perspective on Einstein-Podolsky-Rosen and its Consequences. *Journal of Modern Physics*, 2021, v. 12, 887–936. www.scirp.org/journal/paperinformation.aspx?paperid=-109219
38. Aringazin A. K., Jannussis A., Lopez F., Nishioka M. and Vel-janosky B. Santilli's Lie-Isotopic Generalization of Galilei and Einstein Relativities. Notes from R. M. Santilli's 1990 Lectures at the ICTP, Trieste, Italy. Kostakaris Publishers, Athens, Greece, 1991. http://www.santilli-foundation.org/docs/Santilli-108.pdf
39. Sourlas D. S. and Tsagas Gr. T. Mathematical Foundation of the Lie-Santilli Theory. *Ukraine Academy of Sciences*, 1993. http://www.santilli-foundation.org/docs/santilli-70.pdf
40. Lohmus J., Paal E. and Sorgsepp L. Non-associative Algebras in Physics. Hadronic Press, 1994. http://www.santilli- foundation.org/docs/Lohmus.pdf
41. Kadeisvili J. V. Santilli's Isotopies of Contemporary Algebras, Geometries and Relativities, Second edition. *Ukraine Academy of Sciences*, Kiev, 1997. http://www.santilli-foundation.org/docs/Santilli-60.pdf
42. Jiang C.-X. Foundations of Santilli Isonumber Theory. *International Academic Press*, 2001. http://www.i-b-r.org/docs/jiang.pdf
43. Ganfornina R. M. F. and Valdes J. N. Fundamentos de la Isotopia de Santilli. International Academic Press, Palm Harbor, FL, 2001. http://www.i-b-r.org/docs/spanish.pdf
English translation: *Algebras, Groups and Geometries*, 2015, v. 32, 135–308, 2015. http://www.i-b-r.org/docs/Aversa-translation.pdf
44. Davvaz B. and Vougiouklis Th. A Walk Through Weak Hyperstructures and H_v-Structures. World Scientific, 2018.
45. Gandzha I. and Kadeisvili J. V. New Sciences for a New Era: Mathematical, Physical and Chemical Discoveries of Ruggero Maria Santilli. Printing Press, Nepal, 2011. http://www.santilli-foundation.org/docs/RMS.pdf
46. Georgiev S. Foundations of IsoDifferential Calculus. Vol 1. IsoDifferential and Iso-Integral Calculus for Iso-Functions in One Variable. Vol 2. Iso-Differential and Iso-Integral Calculus for IsoFunctions in Several Variables. Vol. 3 Iso-Ordinary Iso-Differential Equations. Vol. 4 Iso-Difference Equations. Vol. 5 Iso-Stochastic Iso-Differential Equations. Vol. 6 Theory of Iso-Measurable IsoFunctions. Nova Publishers, New York, NY, 2014 (I), 2014 (II), 2014 (III), 2015 (IV), 2015 (V), 2016 (VI), 2022 (I new ed.)
47. Georgiev S. Iso-Mathematics. Lambert Academic Publishing, 2022.
48. Santilli R. M. Foundation of Theoretical Mechanics. Vol. I The Inverse Problem in Newtonian Mechanics. Springer-Verlag, Heidelberg, Germany, 1978. http://www.santilli-foundation.org/docs/Santilli-209.pdf
49. Santilli R. M. Foundation of Theoretical Mechanics. Vol. II Birkhoffian Generalization of Hamiltonian Mechanics. Springer-Verlag, Heidelberg, Germany, 1983. http://www.santilli-foundation.org/docs/santilli-69.pdf
50. Santilli R. M. Isonumbers and Genonumbers of Dimensions 1, 2, 4, 8, their Isoduals and Pseudoduals, and "Hidden Numbers" of Dimension 3, 5, 6, 7. *Algebras, Groups and Geometries*, 1993, v. 10, 273–322. http://www.santilli-foundation.org/docs/Santilli-34.pdf
51. Santilli R. M. Nonlocal-Integral Isotopies of Differential Calculus, Mechanics and Geometries. *Circolo Matematico Palermo, Suppl.*, 1996, v. 42, 7–82. http://www.santilli-foundation.org/docs/Santilli-37.pdf
52. Santilli R. M. Invariant Lie-isotopic and Lie-admissible formulation of quantum deformations. *Found. Phys.*, 1997, v. 27, 1159–1177. http://www.santilli-foundation.org/docs/Santilli-06.pdf

53. Santilli R. M. Embedding of Lie-algebras into Lie-admissible algebras. *Nuovo Cimento*, 1967, v. 51, 570-585. http://www.santilli-foundation.org/docs/Santilli-54.pdf
54. Santilli R. M. Dissipativity and Lie-admissible algebras. *Meccanica*, 1969, v. 1, 3–12.
55. Santilli R. M. An introduction to Lie-admissible algebras. *Suppl. Nuovo Cimento*, 1968, v. 6, 1225.
56. Santilli R. M. On a possible Lie-admissible covering of Galilei's relativity in Newtonian mechanics for nonconservative and Galilei form-non-invariant systems. *Hadronic J.*, 1978, v. 1, 223–423. http://www.santilli-foundation.org/docs/Santilli-58.pdf
57. Santilli R. M. Initiation of the representation theory of Lie-admissible algebras of operators on bimodular Hilbert spaces. *Hadronic J.*, 1978, v. 3, 440–467. http://www.santilli-foundation.org/docs/santilli-1978-paper.pdf
58. Santilli R. M. Lie-Admissible Approach to the Hadronic Structure. International Academic Press, Vol. I, 1978. http://www.santilli-foundation.org/docs/Santilli-71.pdf Vol. II, 1982. http://www.santilli-foundation.org/docs/Santilli-72.pdf
59. Fronteau J., Tellez-Arenas A. and Santilli R. M. Lie-admissible structure of statistical mechanics. *Hadronic Journal*, 1979, v. 3, 130–176. http://www.santilli-foundation.org/docs/arenas-fronteau-santilli-1981.pdf
60. Myung H. C. and Santilli R. M., Eds. Proceedings of the Second Workshop on Lie-Admissible formulations.
Part A: Review Papers. *Hadronic Journal*, 1979, v. 2 (6). http://www.santilli-foundation.org/docs/hj-2-6-1979.pdf
Part B: Research Papers. *Hadronic Journal*, 1979, v. 3 (1). http://www.santilli-foundation.org/docs/hj-3-1-1979.pdf
61. Myung H. C. and Santilli R. M., Eds. Proceedings of the Third Workshop on Lie-Admissible Formulations. Part A: Mathematics. *Hadronic Journal*, 1981, v. 4 (2). http://www.santilli-foundation.org/docs/hj-4-2-1981.pdf Part B: Theoretical Physics. *Hadronic Journal*, 1981, v. 4 (3). http://www.santilli-foundation.org/docs/hj-4-3-1981.pdf Part C: Experimental Physics, and Bibliography. *Hadronic Journal*, 1981, v. 4 (4). http://www.santilli-foundation.org/docs/hj-4-4-1981.pdf
62. Arenas T., Fronteau J. and Santilli R. M., Eds. Proceedings of the First International Conference on Nonpotential Interactions and their Lie-Admissible Treatment.
Part A: Invited Papers. *Hadronic Journal*, 1982, v. 5 (2). http://www.santilli-foundation.org/docs/hj-5-2-1982.pdf
Part B: Invited Papers. *Hadronic Journal*, 1982, v. 5 (3). http://www.santilli-foundation.org/docs/hj-5-3-1982.pdf
Part C: Contributed Papers. *Hadronic Journal*, 1982, v. 5 (4). http://www.santilli-foundation.org/docs/hj-8-4-1982.pdf
Part D: Contributed Papers. *Hadronic Journal*, 1982, v. 5 (5). http: http://www.santilli-foundation.org/docs/hj-5-5-1982.pdf
63. Myung H. C. and Santilli R.M., Eds. Proceedings of the First Workshop on Hadronic Mechanics. *Hadronic Journal*, 1983, v. 6 (6). http://www.santilli-foundation.org/docs/hj-6-6-1983.pdf
64. Myung H. C. and Santilli R. M., Eds. Proceedings of the Second Workshop on Hadronic Mechanics. Vol. I. *Hadronic Journal*, 1984, v. 7 (5). http://www.santilli-foundation.org/docs/hj-7-5-1984.pdf Vol. II. *Hadronic Journal*, 1984, v. 7 (6). http://www.santilli-foundation.org/docs/hj-7-6-1984.pdf
65. Schoeber A., Ed. Irreversibility and Non-potentiality in Statistical Mechanics. Hadronic Press, 1984.
http://www.santilli-foundation.org/docs/Santilli-110.pdf
66. Tuladhar Bhadra Man, Ed. , Proceedings of the third international conference on the Lie-admissible treatment of non-potential interactions. Kathmandu University, Nepal, 2011.
Vol. I: http://www.santilli-foundation.org/docs/2011-nepal-conference-vol-1.pdf Vol. II: http://www.santilli-foundation.org/docs/2011-nepal-conference-vol-2.pdf
67. Dunning-Davies J. The Thermodynamics Associated with Santilli's Hadronic Mechanics. *Progress in Physics*, 2006, v. 4, 24–26. http://www.santilli-foundation.org/docs/Dunning-Davies-Thermod.PDF
68. Bhalekar A. A. Santilli's Lie-Admissible Mechanics. The Only Option Commensurate with Irreversibility and Nonequilibrium Thermodynamics. *AIP Conf. Proc.*, 2013, v. 1558, 702–722. http://www.santilli-foundation.org/docs/bhalekar-lie-admissible.pdf
69. Vougiouklis T. The Santilli theory 'invasion' in hyperstructures. *Algebras, Groups and Geometries*, 2011, v. 28, 83–104. http://www.santilli-foundation.org/docs/santilli-invasion.pdf
70. Santilli R. M. Lie-admissible invariant representation of irreversibility for matter and antimatter at the classical and operator levels. *Nuovo Cimento B*, 2006, v. 121, 443–485. http://www.santilli-foundation.org/docs http://Lie-admiss-NCB-I.pdf
71. Albert A. A. *Trans. Amer. Math. Soc.*, 1948, v. 64, 552–585.
72. Santilli R. M. Foundations of Hadronic Chemistry, with Applications to New Clean Energies and Fuels. Kluwer Academic Publishers, 2001. http: http://www.santilli-foundation.org/docs/Santilli-113.pdf Russian translation: Aringazin A. K. http: http://i-b-r.org/docs/Santilli-Hadronic-Chemistry.pdf
73. Santilli R. M. and Shillady D. D. A new isochemical model of the hydrogen molecule. *Intern. J. Hydrogen Energy*, 1999, v. 24, 943. http://www.santilli- foundation.org/docs/Santilli-135.pdf
74. Santilli R. M. and Shillady D. D. A new isochemical model of the water molecule. *Intern. J. Hydrogen Energy*, 2000, v. 25, 173. http://www.santilli-foundation.org/docs/Santilli-39.pdf
75. Blatt J. M. and Weisskopf V. F. Theoretical Nuclear Physics. Wiley and Sons, 1952.
76. Myung H. C. and Santilli R. M. Modular-isotopic Hilbert space formulation of the exterior strong problem. *Hadronic Journal*, 1982, v. 5, 1277–1366.
http://www.santilli-foundation.org/docs/myung-santilli-1982.pdf
77. Santilli R. M. A quantitative isotopic representation of the Deuteron magnetic moment. In: Proceedings of the International Symposium "Dubna Deuteron-3e". Joint Institute for Nuclear Research, Dubna, Russia, 1994. http://www.santilli-foundation.org/docs/Santilli-134.pdf
78. Santilli R. M. The Physics of New Clean Energies and Fuels According to Hadronic Mechanics. Special issue of the Journal of New Energy, 1998. http://www.santilli-foundation.org/docs/Santilli-114.pdf
79. Dhondge S. S. Santilli's Hadronic Mechanics Formation for the Deuteron. AIP Conference Proceedings 1648, 510009, 2015. doi: 10.1063/1.4912714.
http://www.santilli-foundation.org/docs/1.4912714(SS-Dhondge).pdf
80. Dhondge S. S. Studies on Santilli Three-Body Model of the Deuteron According to Hadronic Mechanics. *American Journal of Modern Physics*, 2016, V. 5 (2-1), 46–55.
http://www.santilli-foundation.org/docs/deuteron-2018.pdf
81. Muktibodh Arun S. Studies on Santilli Three-Body Model of the Deuteron According to Hadronic Mechanics. *American Journal of Modern Physics*, 2016, v. 5 (2-1), 17–36. http://www.santilli-foundation.org/docs/pdf4.pdf
82. Santilli R. M. Need of subjecting to an experimental verification the validity within a hadron of Einstein special relativity and Pauli exclusion principle. *Hadronic J.*, 1978, v. 1, 574–901. http://www.santilli-foundation.org/docs/santilli-73.pdf
83. Santilli R. M. Iso-Representation of the Deuteron Spin and Magnetic Moment via Bohm's Hidden Variables. *Progress in Physics*, 2022, v. 18, 74–81. http://www.santilli-foundation.org/docs/PiP-paper-3-22.pdf
84. Santilli R. M. Apparent consistency of Rutherford's hypothesis on the neutron as a compressed hydrogen atom. *Hadronic J.*, 1990, v. 13, 513–533. http://www.santilli-foundation.org/docs/Santilli-21.pdf

85. Santilli R. M. The notion of non-relativistic isoparticle. ICTP release IC/91/265, 1991. www.santilli-foundation.org/docs/Santilli-145.pdf

86. Santilli R. M. Apparent consistency of Rutherford's hypothesis on the neutron structure via the hadronic generalization of quantum mechanics, nonrelativistic treatment. ICTP communication IC/91/47, 1992. http://www.santilli-foundation.org/docs/Santilli-150.pdf

87. Santilli R. M. The synthesis of the neutron according to hadronic mechanics and chemistry. *Journal Applied Sciences*, 2006, v. 5, 32–47.

88. Santilli R. M. Recent theoretical and experimental evidence on the synthesis of the neutron. Communication of the Joint Institute for Nuclear Research, Dubna, Russia, No. E4-93-252, 1993.

89. Santilli R. M. Recent theoretical and experimental evidence on the synthesis of the neutron. *Chinese J. System Eng. and Electr.*, 1995, v. 6, 177–195. http://www.santilli-foundation.org/docs/Santilli-18.pdf

90. Santilli R. M. Apparent confirmation of Don Borghi's experiment on the laboratory synthesis of neutrons from protons and electrons. *Hadronic J.*, 2007, v. 30, 29–41. http://www.i-b-r.org/NeutronSynthesis.pdf

91. Santilli R. M. Confirmation of Don Borghi's experiment on the synthesis of neutrons. arXiv: physics/0608229v1. http://arxiv.org/pdf/physics/0608229v1.pdf

92. Santilli R. M. Documentation of scans from the Polimaster and SAM 935 detectors. http://www.neutronstructure.org/neutron-synthesis-3.htm http://www.neutronstructure.org/neutron-synthesis-2.htm

93. Burande C. S. On the experimental verification of Rutherford-Santilli neutron model. *AIP Conf. Proc.*, 2013, v. 158, 693–721. http://www.santilli-foundation.org/docs/Burande-2.pdf

94. Santilli R. M. and Nas A. Confirmation of the Laboratory Synthesis of Neutrons from a Hydrogen Gas. *Journal of Computational Methods in Sciences and Eng.*, 2014, v. 14, 405–414. http://www.hadronictechnologies.com/docs/neutron-synthesis-2014.pdf

95. Santilli R. M. Apparent Nuclear Transmutations without Neutron Emission Triggered by Pseudoprotons. *American Journal of Modern Physics*, 2015, v. 4, 15–18. http://www.sciencepublishinggroup.net/journal/paperinfo?journalid=122&doi=10.11648/j.ajmp.20150401.13

96. de Haan V. Possibilities for the Detection of Santilli Neutroids and Pseudo-protons. *American Journal of Modern Physics*, 2015, v. 5, 131–136. http://sciencepublishinggroup.com/journal/paperinfo?journalid=122

97. Norman R., Bartoli S. B., Buckley B., Dunning-Davies J., Rak J. and Santilli R. M. Experimental Confirmation of the Synthesis of Neutrons and Neutroids from a Hydrogen Gas. *American Journal of Modern Physics*, 2017, v. 6, 85–104. http://www.santilli-foundation.org/docs/confirmation-neutron-synthesis-2017.pdf

98. Driscoll R. B. Bohrs Atom Completed: the Rutherford-Santilli Neutron. APS Conf. Proc., April 5-8, 2003. http://ui.adsabs.harvard.edu/abs/2003APS..APR.D1009D/abstract

99. Chandrakant S. B. On the Rutherford-Santilli Neutron Model. AIP Conf. Proc., 2015, 1648, 510006, 10.1063/1.4912711. http://www.santilli-foundation.org/docs/1.4912711(CS-Burande(1)).pdf

100. Kadeisvili J. V. The Rutherford-Santilli Neutron. *Hadronic J.*, 2008, v. 31, 1–125. http://www.i-b-r.org/Rutherford-Santilli-II.pdf

101. Burande C. S. Santilli Synthesis of the Neutron According to Hadronic Mechanics. *American Journal of Modern Physics*, 2016, v. 5, 17–36. http://www.santilli-foundation.org/docs/pdf3.pdf

102. Burande C. S. Santilli Synthesis of the Neutron According to Hadronic Mechanics. *American Journal of Modern Physics*, in press, 2015. http://www.santilli-foundation.org/docs/

103. Bartoli S. B. Significance for the EPR Argument of the Neutron Synthesis from Hydrogen and of a New Controlled Nuclear Fusion without Coulomb Barrier. Proceedings of the 2020 Teleconference on the EPR argument, Curran Associates Conference Proceedings, New York, USA, 2021, 459–466.

104. Santilli R. M. The novel Intermediate Controlled Nuclear fusions, a report for its industrial realization. *Hadronic Journal*, 2008, v. 31, 15–42. http://www.santilli-foundation.org/docs/CNF-HJ.pdf

105. Santilli R. M. Experimental Confirmation of Nitrogen Synthesis from Deuterium and Carbon without harmful radiations. *New Advances in Physics*, 2010, v. 4, 17–41. http://www.santilli-foundation.org/docs/Nitrogen-synthesis-2010.pdf

106. Santilli R. M. Additional Confirmation of the Intermediate Controlled Nuclear Fusions without harmful radiation or waste. Proceedings of the Third International Conference on the Lie-Admissible Treatment of Irreversible Processes, Kathmandu University, 2011, 163–177. http://www.santilli-foundation.org/docs/ICNF-3.pdf

107. Santilli R. M. Intermediate Controlled Nuclear Fusions without the emission of radiations and without the release of radioactive waste, Lecture. http://www.world-lecture-series.org/level-v

108. Santilli R. M. Third Hadronic Reactor for Intermediate Controlled Nuclear Fusions without Radiations. Lecture. http://www.world-lecture-series.org/lecture-vc

109. Santilli R. M. Video presentation of the third hadronic reactor for the Nitrogen and Silicon syntheses. 2011. http://www.world-lecture-series.org/dragon-iii

110. Brenna R., Kuliczkowski T. and Ying L. Verification of Santilli intermediate Controlled Nuclear Fusions without harmful radiations and the production of magnecular clusters. *New Advances in Physics*, 2011, v. 5, 9–18. http://www.santilli-foundation.org/docs/ICNF-2.pdf

111. Brenna R., Kuliczkowski T. and Ying L. Report on Test for Silicon on the Nitrogen synthesis. Princeton Gamma Technologies report dated April 6, 2011. http://www.santilli-foundation.org/docs/PGTI-Anal-test1.pdf

112. Ying L., Cai W., J., Lynch C., Marton, Elliot S. and Yang Y. Experimental verification for Intermediate Controlled Nuclear Fusion. City College of New York, Preprint 2012, unpublished. http://www.santilli-foundation.org/docs/ICNF-Cai-paper-Ying.pdf

113. Kadeisvili J. V., Lynch C. and Yang Y. Confirmation of Santilli's intermediate controlled nuclear fusion of Deuterium and Carbon into Nitrogen without harmful radiation. *The Open Physical Chemistry Journal*, 2013, v. 5, 17–27. http://www.santilli-foundation.org/docs/ICNF-Conf-2013.pdf

114. Abundo U. Interpretation and enhancement of the excess energy of Rossi's reactor via Santilli neutroids and nucleoids. *Hadronic J.*, 2014, v. 37, 697–737. http://www.santilli-foundation.org/docs/abundo-paper-2014.pdf

115. Lanjewar R. B. A Brief Review of Intermediate Controlled Nuclear Syntheses (ICNS) without Harmful Radiations. *AIP Conference Proceedings*, 2015, v. 1648, 510–515. 10.1063/1.4912717. http://www.santilli-foundation.org/docs/1.4912717(RB-Lanjewar).pdf

116. Das Sarma I. B. Hadronic Nuclear Energy: An Approach Towards Green Energy. *American Journal of Modern Physics*, 2016, v. 5, 119–130. http://www.santilli-foundation.org/docs/pdf6.pdf

117. Ying L. Verification of Santilli's Intermediate Nuclear Harmful Radiation and the Production of Magnecular Clusters. Lecture, 2012 http://www.world-lecture-series.org/lecture-vd

118. Rossiter D., Director. IVA Report 184727-001 on comparative Nitrogen counts on samples of the Nitrogen synthesis. http://www.santilli-foundation.org/docs/nitrogen-tests-2010.pdf

119. Rossiter D., Director. IVA Report 200010 on comparative Nitrogen counts. http://www.santilli-foundation.org/docs/Oneida-analyses-2013.zip

120. Rossiter D., Director. IVA Report 184033-001 on comparative hydrogen and magnegas tests. http://www.santilli-foundation.org/docs/hydrogen-magnegas-2010.pdf

121. Rossiter D., Director. IVA Report 189920 on comparative Oxygen counts. http://www.santilli-foundation.org/docs/helium-carbon-fusion-I.pdf

122. Rossiter D., Director. IVA Report 189920 on comparative Oxygen counts. http://www.santilli-foundation.org/docs/helium-carbon-fusion-II.pdf

123. Rossiter D., Director. IVA Report 189920 on comparative Silicon counts. http://www.santilli-foundation.org/docs/IVAReport.189920.pdf

124. Rossiter D., Director. IVA Report 189920 on comparative Silicon count. http://www.santilli-foundation.org/docs/IVAReport.189920.pdf

125. Swartz D. Constellation Technologies first report on comparative Silicon counts. http://www.santilli-foundation.org/docs/Constellation-Si-10-13.zip

126. Swartz D. Constellation Technologies second report on comparative Silicon counts. http://www.santilli-foundation.org/docs/Constellation-Rep-Si-2.zip

127. Swartz D. Constellation Technologies third report on comparative Silicon counts. http://www.santilli-foundation.org/docs/Constell-Si-3.pdf

128. Swartz D. Constellation technologies Third report on comparative Silicon counts. http://www.santilli-foundation.org/docs/Constell-Silicon-10-14.pdf

129. Santilli R. M. Apparatus and method for recycling contaminated liquids. U. S. patent No. 6,540,966. http://pdfpiw.uspto.gov/.piw?docid=06540966

130. Santilli R. M. Durable and efficient equipment for the production of a combustible and non-pollutant gas from underwater arcs and method therefore. U. S. patent No. 6,183,604. http://patentimages.storage.googleapis.com/4c/ad/2b/8-74b5ffe4a2f12/US6183604.pdf

131. Santilli R. M. Method and Apparatus for the industrial production of new hydrogen-rich fuels. U. S. patent No. 9,700,870,B2. http://www.santilli-foundation.org/docs/Magnecule-patent.pdf

132. Eriksson J. Neutron Emission Spectrometry for Fusion Reactor Diagnosis Method Development and Data Analysis. *Acta Universitatis Upsalensis, Uppsala*, 2015. http://uu.diva-portal.org/smash/get/diva2:798599/FULLTEXT01.pdf

133. Wesson J. Tokamak, Oxford Science Publ., 2011.

134. Saxena Y. C. Tokamak: Q device for nuclear fusion. *Indian Journal fr Cryogenics*, 2016, v. 41, 2–18. http://www.researchgate.net/publication/306373246

135. Ke H. B., Wen P. and Wang W. H. The Excess Heat Capacity in Glass-forming Liquid Systems Containing Molecules. arXiv 1111.4826. http://arxiv.org/abs/1111.4826

136. Mizuno T. and Rothwell J. Increased Excess Heat from Palladium Deposited on Nickel in the 22nd International Conference for Condensed Matter Nuclear Science ICCF-22 Assisi, Italy, 2019. http://fdocuments.net/document/mizuno-increased-excess-mizuno-t-and-j-rothwell-increased-excess-heat-from-palladium.html?page=1

137. Iwamura Y., Itoh T. and Kasagi Ji. Research Article Excess Energy Generation using a Nano-sized Multilayer Metal Composite and Hydrogen Gas. *J. Condensed Matter Nucl. Sci.*, 2020, v. 33, 1–13. http://www.cleanplanet.co.jp/wp-content/uploads/J-Condensed-Matter-Nucl-Sci-33-2020-1.pdf

138. Rutherford E. Bakerian Lecture: Nuclear Constitution of Atoms. *Proc. Roy. Soc. A*, 1920, v. 97, 374–382. http://royalsocietypublishing.org/doi/10.1098/rspa.1920.0040

139. Chadwick J. *Proc. Roy. Soc. A*, 1932, v. 136, 692–723.

140. Rapports du Septième Conseil de Physique Solvay, Gauthier-Villars, Paris, 1933, 324.

141. Fermi E. Nuclear Physics. University of Chicago Press, 1949.

142. Santilli R. M. The etherino and/or the neutrino Hypothesis? *Found. Phys.*, 2007, v. 37, 670–695. http://www.santilli-foundation.org/docs/EtherinoFoundPhys.pdf

143. American Chemical Society. Energy from the Sun. http://www.acs.org/content/acs/en/climatescience/energybalance/energyfromsun.html

144. Santilli R. M. Apparent Experimental Confirmation of Pseudoprotons and their Application to New Clean Nuclear Energies. *International Journal of Applied Physics and Mathematics*, 2019, v. 9, 72–100. http://www.santilli-foundation.org/docs/pseudoproton-verification-2018.pdf

145. Santilli R. M. The Novel Hyper Combustion for the Complete Combustion of Fossil Fuels. *Intern. Journal of Chemical Engineering and Applications*, 2019, v. 10, 16. http://www.santilli-foundation.org/docs/hypercombustion-2019.pdf

146. Bartoli S. B. and Santilli R. M. Studies on the engineering realization of Intermediate Controlled Nuclear Fusions. to appear.

147. Yukawa, H. On the interaction of elementary particles. *Proc. Phys. Math. Soc. Jpn*, 1935, v. 17, 48–57.

148. Woods R. D. and Saxon D. S. Diffuse Surface Optical Model for Nucleon-Nuclei Scattering. *Physical Review*, 1954, v. 95, 577–578.

149. Reid R. V. Local phenomenological nucleon–nucleon potentials. *Annals of Physics*, 1962, v. 50, 411–448.

On the Nature of Some Cosmic Radiations

Anatoly V. Belyakov

Tver, Russia. E-mail: belyakov.lih@gmail.com

Frequency distributions of the spectrum of hydrogen and hydrogen-like elements help to determine the most probable excited elements spectral radio lines in outer space. Based on the geometrodynamic concept of J. Wheeler, the reason for the appearance of recombination radio lines is explained, and the background cosmic radiation maximum nature is established. The hydrogen atom limiting quantum number is calculated. It has been established that the wavelength during proton-electron recombination at the limiting quantum level coincides with the known 21 cm cold atomic hydrogen wavelength.

1 Introduction

Space is filled with various types of radiation, and some of them, such as the background cosmic (relic) radiation, recombination radio lines (RRL) and atomic hydrogen radiation at a wavelength of 21.1 centimeters, are of particular interest to researchers. The study of radio lines of excited atoms is the most effective method of astrophysical research to obtain the important information about various galactic and extragalactic objects. The spectrum of the relic radiation filling the Universe corresponds to the completely black body radiation spectrum with a temperature of 2.73 K. Its maximum falls at a wavelength of 1.9 mm.

The conditions for the occurrence of this kind of radiation exist in a cold rarefied interstellar medium. Under such conditions, in the process of electrons and ions recombination, some highly excited stable hydrogen atoms and other light elements can be formed with a quantum number theoretically possible up to $n = 1000$, where the electronic levels are still distinguishable; the atom limiting size is limited by the background nonthermal radio emission of the Galaxy and $n_{lim} = 1600$ [1].

High electronic levels are inhabited mainly due to recombinations, and radio lines most often manifest themselves during electron transitions between neighboring electronic levels. The spectral RRLs emitted during the transitions fall in the radio range. To date, the recombination radio lines of hydrogen have been registered in the scale from the infrared to the metre scale at $n = 10 \ldots 300$. At higher excitation levels, radio lines were observed in the process of absorption only [2–4].

Atomic hydrogen in the interstellar medium is observed due to emission and absorption in the 21 cm line. The hydrogen radio line is an effective means of studying the Universe, because there is about half the mass of galactic interstellar matter in the atomic hydrogen ground state form. It is assumed this spectral line to be the result of transitions between sublevels of the hyperfine structure of the hydrogen atom ground energy level. The reason for hyperfine splitting is the interaction of the nucleus spin and the electron spin, since these spins can be parallel or antiparallel. When the electron spin orientation is reversed, emission (or absorption) of quanta with the frequency of 1420 MHz occurs [5, 6].

2 On the shape of the spectra of frequency distributions

The presence and spectral lines intensity of specific sources depend on various factors, and usually a small part of the spectrum is realized. However, the averaging with respect to many sources in large space and time scales (infinite scales as an ultimate case) of all possible hydrogen atom electron transitions and the spectral lines corresponding to these transitions gives characteristic *frequency distributions* in accordance with the Balmer-Rydberg formula

$$W = \frac{m^2 n^2}{m^2 - n^2}\,, \tag{1}$$

where $m, n = 1, 2, 3 \ldots$ Moreover, in the range of $n, m = 10 \ldots 300$ (in radiation), the characteristic frequency distribution will correspond to the completely black body radiation spectrum with a temperature of about 3 K, and the characteristic frequency distribution over all remaining levels at $n, m = 300 \ldots 500$ will take a similar shape with a maximum of about 21 cm, see Fig. 1. Such a result to some extent explains the nature of these radiations. For example, the shape of the background radiation curve could be explained

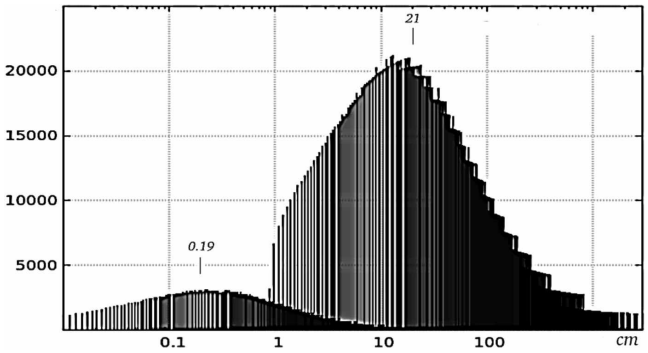

Fig. 1: Frequency distribution of the Balmer-Rydberg formula for $n, m = 10 \ldots 300$ (left) and for $n, m = 300 \ldots 1500$ (right).

by natural factors currently taking place. Details about frequency distributions and methods for their construction are given in [7, 8].

The radio lines of excited atoms provide information about the electron temperature, density, composition of the interstellar medium, and about other important parameters. However, finding useful RRL is a laborious task, because building even one spectrum for a single observed point at decameter waves requires many days of observations. Frequency distributions help solve this problem.

Fig. 2 shows the characteristic frequency distribution of the Balmer-Rydberg formula in the decameter range. The currently recorded radio links according to the data of [1] and [3] are also shown there. Although these lines belong to carbon, its atoms under these conditions are hydrogen-like. Designations, for example, $427\,\alpha$ means transition $428 \rightarrow 427$. At $n = 1530$ (this value, as will be shown below, is equal to the limiting value of n), good agreement with the experimental data is achieved.

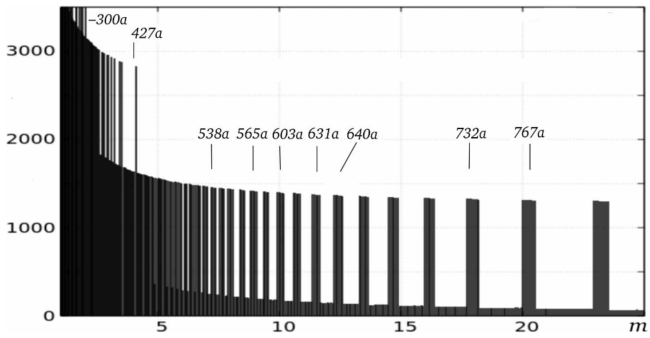

Fig. 2: Frequency distribution for hydrogen-like atoms at $n, m = 300 \ldots 1530$. The designated a-lines belong to carbon.

Not all lines are observable in practice, and not only and not so much for external reasons. As follows from the analysis of the characteristic frequency distributions, the most active radio lines are in fact a superposition (combination) of closely spaced spectral lines, when the electrons make a variety of transitions. Of course, the spectrograms constructed under the condition of the equiprobability of all possible electron transitions cannot completely coincide with the real radiation spectrum, but where the combinatorial factor is significant, the important spectral lines should be sought in the areas of concentration of spectral lines of the frequency distribution. The strong *widening* of radio links at large n [3] can also be explained by the summation, superposition, and combination of close frequencies.

3 Proton-electron contour and the nature of RRL

Recombination radio lines were recorded starting from $n \approx 10$, moreover, at $n \approx 100$ and more, only RRLs are observed. These features, as well as the recombination phenomenon itself, can be explained by considering the atom from the point of view of *J. Wheeler's geometrodynamic concept* [9].

According to Wheeler's concept, charged microparticles are singular points on a topologically non-unitary coherent and fractalized two-dimensional surface of our world, connected by a "wormhole", a vortex tube or a force current line of the drain-source type in an additional dimension, forming a closed *contour*. According to the adopted model [10], the vortex tube (contour) has mass M, radius r_e, and it is helically filled with some medium in the triple vortex thread form with radius r, circulating along the contour at a velocity v.

The parameters of an arbitrary proton-electron contour are defined in dimensionless units of the electron mass m_e, its classical radius r_e, and the speed of light c:

$$M = (an)^2 , \tag{2}$$

$$v = \frac{c_0^{1/3}}{(an)^2} , \tag{3}$$

$$r = \frac{c_0^{2/3}}{(an)^4} , \tag{4}$$

where a and c_0 are the reciprocal fine structure constant and the dimensionless speed of light c divided by [m/sec].

It is assumed the contour to be structured into ordered units (let's call them photons for short), and their number z is determined by the contour total length to the wavelength ratio. As a result, the formula is obtained:

$$z = \frac{n^6}{k\,W} , \tag{5}$$

where $k = 1.7 \ldots 1$ depending on the parameter n, and for large n can be accepted $k \approx 1$. The contour unit mass corresponding to one photon is equal to

$$m = \frac{M}{z} . \tag{6}$$

It is clear, a unit mass kinetic energy's changing during an electron transition from n_i to n_k orbit is:

$$E_k = \left(m_i v_i^2 - m_k v_k^2\right) \tag{7}$$

or, bearing in mind (2), (3), (5), and (6) and setting $n = n_i$ and $m = n_k$ in the Balmer formula, we obtain in units of $m_e c^2$:

$$E_k = k\,W\,c_0^{2/3}\left(\frac{1}{n_i^8} - \frac{1}{n_k^8}\right)\frac{1}{a^2} . \tag{8}$$

At the same time, the energy of the corresponding photon is:

$$E_h = \frac{hc}{\lambda} , \tag{9}$$

where Planck's constant is:

$$h = 2\pi\alpha m_e c r_e , \tag{10}$$

wavelength is:

$$\lambda = \frac{W}{R_\infty}\,, \tag{11}$$

and the Rydberg constant is:

$$R_\infty = \frac{1}{4\pi\alpha^3 r_e}\,. \tag{12}$$

Then the photon energy, taking into account (10), (11) and (12), in units of $m_e c^2$ is:

$$E_h = \frac{1}{2Wa^2}\,. \tag{13}$$

The ratio of a unit mass energy and a photon energy, bearing in mind (8) and (13), in units of $m_e c^2$ takes the form:

$$\frac{E_k}{E_h} = 2kW^2 c_0^{2/3}\left(\frac{1}{n_i^8} - \frac{1}{n_k^8}\right), \tag{14}$$

and for large n and for neighboring levels, when $W \approx n^3/2$

$$\frac{E_k}{E_h} = \frac{1}{2}\,kn^6 c_0^{2/3}\left(\frac{1}{n_i^8} - \frac{1}{n_k^8}\right), \tag{15}$$

where $n \approx \frac{1}{2}(n_i + n_k)$.

As the quantum number n grows, i.e. as the contour increases when an electron passes from the n_k level to the n_i level, there comes a moment when the increment of kinetic energy of a unit mass per photon is not enough to form the corresponding photon, and additional energy is required through external influence. In these cases the emission is preceded by an act of *recombination* – the capture of a free electron by an ion to one of the high levels, for example, photorecombination. Free electrons recombine with a proton or ions. An excess of energy equal to the difference between the electron energy and its binding energy in the atom is carried away with the quantum. During subsequent downward cascade transitions, RRL radiation occurs with frequencies $\nu \sim \Delta n/n^3$. Thus, from (15) it follows that for $n > 110$ the ratio E_k/E_h is always less than 1, and *all radio lines will already be recombination*. Moreover, the electron-proton recombination according to the type $\infty \to n$ at n close to 110 just forms quanta, with a frequency equal to the frequency of the relic radiation maximum.

At $n < 110$, in the millimeter range, there are possible transition where electrons can spontaneously move to lower levels, forming the corresponding spectral lines. These lines in the hydrogen spectrum are observed experimentally [1], and they are well revealed when the restriction $E_k/E_h > 1$ is introduced into the program for calculating the characteristic frequency distributions, Fig. 3. Without this condition, it is difficult to isolate them in the full spectrum. If one builds a frequency distribution with an inverse constraint $E_k/E_h < 1$, then one can make sure that RRLs can occur starting from $\lambda = 0.1$ mm, i.e. at $n \approx 10$.

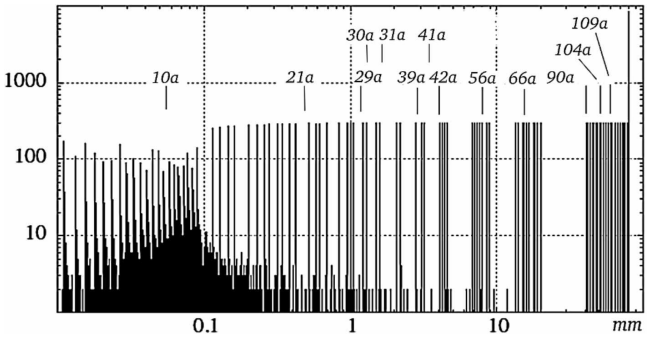

Fig. 3: Frequency distribution for hydrogen in the millimeter range at $n, m = 1 \ldots 130$ under the condition $E_k/E_h > 1$.

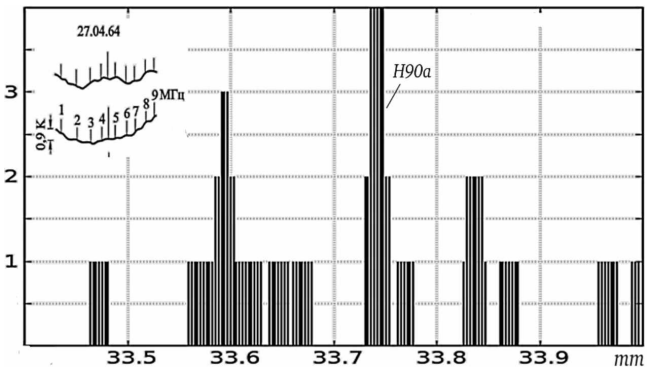

Fig. 4: Frequency distribution of the H90a line at $n, m = 50 \ldots 250$; 207 intervals per range. Top left – the line of hydrogen according to observations in Pushchino in the direction of the Omega Nebula compared with the control spectrogram with the antenna retracted from the source.

It is obvious that the detected radio lines in the range $n = 10 \ldots 110$ can be the result of the superposition of close spectral lines, both recombination and non-recombination ones, for example, the 33.76 mm radio line [11]. This line was one of the first to be discovered in space, perhaps because it is the combination of several very close lines, Fig. 4, and the central peak in the figure is not RRL. That is, the peak does not disappear when the restriction $E_k/E_h > 1$ is imposed. If there are other known restrictions or conditions, they can also be entered into the program for calculating the characteristic frequency distributions.

These distributions explain the features of some spectra noted by some authors. Thus, in [1], the profiles of the H29a, H30a, and H31a lines are given, which turned out to be two-humped, which the authors have given an exotic explanation to. However, the analysis of the spectrum in Fig. 5 narrow part shows that the two-humped profile of the mentioned lines is due to the presence of two closely spaced spectral lines.

In another case, the reason for the unusually low intensity of the H41a line, namely, more than 50 times lower than the intensity of the above lines, is clear from Fig. 3. Indeed, the H41a line height is 60 times lower than the neighboring lines height (in arbitrary units).

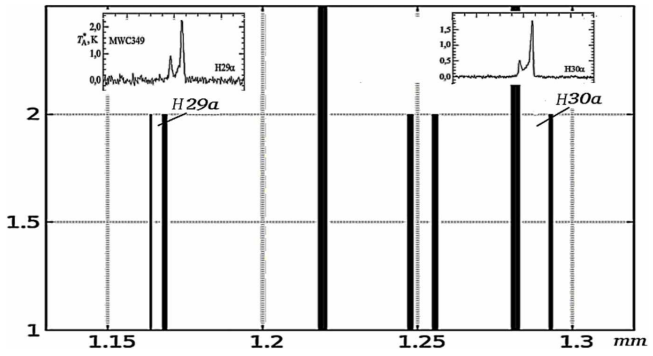

Fig. 5: Frequency distribution in the millimeter range of the H29a and H30a lines at $n, m = 30 \dots 70$, provided $E_k/E_h > 1$; 341 intervals per range. Above: RRL spectra obtained from the MWC349 source.

4 The hydrogen atom limiting size and the 21 centimeters line

It is believed the atom limiting size to be limited by the background non-thermal Galaxy radio emission and n cannot be more than 1500–1600. But the background radiation is not a constant, and more fundamental parameters are needed to accurately determine the limiting level.

In the adopted model based on Wheeler's geometrodynamics, the vortex thread radius r, which fills the proton-electron contour like a spiral, decreases as the contour increases according to (4). On the whole, the thread consists of three unit threads, and each of them can in the limit have the Planck size r_h [12]. Then, under the condition of their dense packing and based on geometric considerations, the vortex thread size (circumferential diameter) will be:

$$r_0 = \left(1 + 2/\sqrt{3}\right) r_h = 2.1547\, r_h\,, \tag{16}$$

where the Planck size is:

$$r_h = \left(\frac{\hbar\gamma}{c^3}\right)^{1/2} = 1.616 \times 10^{-35}\,\text{m} \;\text{ or }\; 5.735 \times 10^{-21}\, r_e\,, \tag{17}$$

where $\hbar = h/2\pi$, and γ is the gravitational constant.

Let us assume that in the limit the thread fills the contour in the spiral form, having turns being twisted into the last (tertiary) spiral structure, then the thread (by the Bohr atom general analogy) has the size:

$$r = a^2 r_0\,. \tag{18}$$

Then, when taking into account (4), (16), (17), and (18), one obtains the limiting quantum number value:

$$n_{lim} = \frac{c_0^{1/6}}{\left(1 + 2/\sqrt{3}\right)^{1/4} r_h^{1/4} a^{3/2}}\,. \tag{19}$$

Further, substituting the dimensionless value r_h in units of r_e, one obtains the limiting quantum number $n_{lim} = 1530$ and the proton-electron recombination wavelength for the transition $\infty \to n_{lim}$:

$$\lambda = \frac{n_{lim}^2}{R_\infty} = 21.3\,\text{cm}\,. \tag{20}$$

Thus, the recombination wavelength for the $\infty \to n_{lim}$ transition turned out to be actually equal to the hydrogen radio line 21.1 cm.

It is assumed some mechanism for the atomic hydrogen radiation appearance to exist in which when the atoms are impacting, there is their electron with different directions of spins exchanging [5, 6]. The very same transitions between the hyperfine structure sublevels of the hydrogen atom main energy level, as quantum calculations show, occur with a negligible probability of $2.85 \times 10^{-15}\,\text{sec}^{-1}$. Moreover, although there are analogs of the 21 cm line for atoms of hydrogen isotopes as well as for some other atoms whose nuclei have a nonzero spin moment, such lines are not found in astrophysical sources [5]. Therefore, the low probability and the absence of analogues of this radiation in other atoms make it possible to doubt the main reason for the radiation at 21 cm. It is logical to assume the recombination radiation to be the main reason. Its energy coincides with the spin reorientation energy, that in general creates radiation in a relatively narrow range of about 21 cm.

Thus, the situation with recombination at $n = 10$, where the photon energy is compared with the energy of a unit mass, which forms the background radiation maximum, is reproduced symmetrically at a higher level at $n = 1530$, where the photon energy is compared with the spin reorientation energy, which forms the recombination radiation maximum. This situation seems to be harmonious and logical.

5 Conclusion

It is shown that the frequency distributions make it possible to use the combinatorics factor to identify spectral regions with the most intense spectral lines of excited elements in outer space. In general, the range of cosmic radiation can be divided into two subranges: at $n = 1 \dots 300$ (mainly in radiation), which has a total maximum coinciding with the background (relic) radiation maximum and at $n = 300 \dots 1530$ (in mainly in absorption), which has a total maximum coinciding with the atomic hydrogen wavelength.

It has been established that the transition to recombination radiation is due to the equality of the recombination photon energy and the energy of a unit mass of the contour per one photon at $n \approx 110$, which corresponds to the background radiation maximum during the transition $\infty \to n$.

The limiting quantum level for hydrogen has been determined and it has been found that the photon recombination energy is at this level equal to the electron spin reorientation energy with respect to the atomic hydrogen nuclear spin.

Received on November 30, 2022

References

1. Sorochenko R. L., Gordon M. A. Recombination of Radio Lines. Physics and Astronomy. Fizmatlit, Moscow, 2003.
2. Pedlar A. *et al*. *Mon. Not. R. Astron. Soc.*, 1978, v. 182, 473.
3. Konovalenko A. A. Decametric astrospectroscopy. *Earth and Universe*, 1986, v. 5, 26–34.
4. Gordon M. A. and Sorochenko R. L., eds. Radio Recombination Lines: 25 Years of Investigation. 1990, *Proceeding of the IAU Colloquium 125*, Kluwer Academic Publishers.
5. http://ns1.andynet.org/~gmr/course/5.htm.
6. http://12apr.su/books/item/f00/s00/z0000038/st025.shtml.
7. Belyakov A. V. Finding the fine structure of the solutions of complicate logical probabilistic problems by the frequent distributions. *Progress in Physics*, 2010, v. 6 (4), 36–39.
8. Belyakov A. V. Combinatorics and frequency distributions as the determining factors of electron and nuclear spectra. *Progress in Physics*, 2022, v. 18 (1), 15–20.
9. Dewitt B. S. Quantum gravity. *Scientific American*, December 1983, v. 249, 112–129.
10. Belyakov A. V. Macro-analogies and gravitation in the microworld: further elaboration of Wheeler's model of geometrodynamics. *Progress in Physics*, 2012, v. 8 (2), 47–57.
11. http://www.prao.ru/History/history_6.html
12. Belyakov A. V. Determination of the neutrino mass. *Progress in Physics*, 2016, v. 12 (1), 34–38.

On the Nature of the Spacetime Continuum

Pierre A. Millette

E-mail: pierre.millette@uottawa.ca, Ottawa, Canada

In this paper, we summarize the nature of the Spacetime Continuum (STC) as provided by the Elastodynamics of the Spacetime Continuum (*STCED*). We note that, in addition to providing a physical explanation for inertial mass and for wave-particle duality, *STCED* covers the Physics of the Spacetime Continuum. We show that the dimensionality of the Spacetime Continuum could be deduced mathematically if the value of the Lamé elastic constants $\bar{\kappa}_0$, $\bar{\mu}_0$ and $\bar{\lambda}_0$ of the Spacetime Continuum could be determined experimentally. From Einstein's field equation for an isotropic and homogeneous STC, we derive the value of the Spacetime Continuum bulk modulus $\bar{\kappa}_0$ in terms of elementary constants. Understanding the nature of the Spacetime Continuum as provided by *STCED* provides a better understanding of the general relativistic spacetime.

1 Introduction

In this paper, we summarize the nature of the Spacetime Continuum (*STC*) as provided by the Elastodynamics of the Spacetime Continuum (*STCED*) [1–3]. *STCED* is a natural extension of Einstein's General Theory of Relativity which blends continuum mechanical and general relativistic descriptions of the Spacetime Continuum. The introduction of strains in the Spacetime Continuum as a result of the energy-momentum stress tensor allows us to use, by analogy, results from continuum mechanics, in particular the stress-strain relation, to provide a better understanding of the general relativistic spacetime.

2 Elastodynamics of the Spacetime Continuum

The stress-strain relation for an isotropic and homogeneous Spacetime Continuum is given by [1, 3]

$$2\bar{\mu}_0\,\varepsilon^{\mu\nu} + \bar{\lambda}_0\,g^{\mu\nu}\varepsilon = T^{\mu\nu} \tag{1}$$

where $\bar{\lambda}_0$ and $\bar{\mu}_0$ are the Lamé elastic constants of the Spacetime Continuum: $\bar{\mu}_0$ is the shear modulus (the resistance of the Spacetime Continuum to *distortions*) and $\bar{\lambda}_0$ is expressed in terms of $\bar{\kappa}_0$, the bulk modulus (the resistance of the Spacetime Continuum to *dilatations*):

$$\bar{\lambda}_0 = \bar{\kappa}_0 - \tfrac{1}{2}\,\bar{\mu}_0 \tag{2}$$

in a four-dimensional continuum. $T^{\mu\nu}$ is the general relativistic energy-momentum stress tensor, $\varepsilon^{\mu\nu}$ the Spacetime Continuum strain tensor resulting from the stresses, and

$$\varepsilon = \varepsilon^{\alpha}{}_{\alpha}\,, \tag{3}$$

the trace of the strain tensor obtained by contraction, is the volume dilatation ε defined as the change in volume per original volume [4, see pp. 149–152] and is an invariant of the strain tensor. It should be noted that the structure of (1) is similar to that of the field equations of General Relativity,

$$R^{\mu\nu} - \tfrac{1}{2}\,g^{\mu\nu}R = -\varkappa\,T^{\mu\nu} \tag{4}$$

where $R^{\mu\nu}$ is the Ricci curvature tensor, R is its trace, $\varkappa = 8\pi G/c^4$ and G is the gravitational constant (see [2, Ch. 2] for more details).

In *STCED*, as shown in [1, 3], energy propagates in the spacetime continuum (*STC*) as wave-like *deformations* which can be decomposed into *dilatations* and *distortions*. *Dilatations* involve an invariant change in volume of the Spacetime Continuum which is the source of the associated rest-mass energy density of the deformation. On the other hand, *distortions* correspond to a change of shape (shearing) of the Spacetime Continuum without a change in volume and are thus massless.

Thus deformations propagate in the Spacetime Continuum by longitudinal (*dilatation*) and transverse (*distortion*) wave displacements. This provides a natural explanation for wave-particle duality, with the massless transverse mode corresponding to the wave aspects of the deformations and the massive longitudinal mode corresponding to the particle aspects of the deformations.

The rest-mass energy density of the longitudinal mode is given by [1, see Eq. (32)]

$$\rho c^2 = 4\bar{\kappa}_0\varepsilon \tag{5}$$

where ρ is the rest-mass density, c is the speed of light, $\bar{\kappa}_0$ is the bulk modulus of the *STC* as seen previously, and ε is the volume dilatation given by (3).

3 The physicality of four-dimensional spacetime

Minkowski [5,7] first introduced the concept of a four-dimensional spacetime and the description of particles in this spacetime as worldlines in 1908. This has given rise to the question whether four-dimensional spacetime is real or a mathematical abstraction. Eddington [7] considered this question in 1921:

> It was shown by Minkowski that all these fictitious spaces and times can be united in a single continuum of four dimensions. The question is often raised whether this four-dimensional space-time is real, or merely a mathematical construction; perhaps it is sufficient to

> reply that it can at any rate not be less real than the fictitious space and time which it supplants.

Petkov [6, 7] provides a cogent summary of Minkowski's paper. Worldlines of particles at rest are vertical straight lines in a *space−ct* diagram, while particles moving at a constant velocity v are oblique lines and accelerated particles are curved lines. This provides a physical explanation for length contraction as a manifestation of the reality of a particle's extended worldline, where the cross-section measured by an observer moving relative to it (i.e. at an oblique line in the *space−ct* diagram), creates the difference in perceived length between a body at rest and one in movement. This is explored in greater detail in [8, 9]. Minkowski's work demonstrates the physicality of four-dimensional spacetime, and that indeed, four-dimensional physics is spacetime geometry.

The relation (2) between κ, and μ and λ can be generalized to N dimensions, and is given by [10, p. 769]

$$\kappa = \frac{2\mu + N\lambda}{N} \,. \tag{6}$$

The dimensionality of the Spacetime Continuum could thus be deduced mathematically if the value of the Lamé elastic constants $\bar{\kappa}_0$, $\bar{\mu}_0$ and $\bar{\lambda}_0$ of the Spacetime Continuum could be determined experimentally.

4 Physics of the Spacetime Continuum

From General Relativity and *STCED*, one can deduce the properties of the Spacetime Continuum, as *STCED* includes the physics of the Spacetime Continuum as an underlay of the theory.

The Spacetime Continuum is modelled as a four-dimensional differentiable manifold [11] endowed with a metric $g_{\mu\nu}$. It is a continuum that can undergo deformations and support the propagation of such deformations. A continuum that is deformed is strained.

An infinitesimal element of the unstrained continuum is characterized by a four-vector x^μ, where $\mu = 0, 1, 2, 3$. The time coordinate is $x^0 \equiv ct$.

A *deformation* of the Spacetime Continuum corresponds to a state of the *STC* in which its infinitesimal elements are displaced from their unstrained positions. Under deformation, the infinitesimal element x^μ is displaced to a new position $x^\mu + u^\mu$, where u^μ is the displacement of the infinitesimal element from its unstrained position x^μ.

The Spacetime Continuum is approximated by a deformable linear elastic medium that obeys Hooke's law. Under those conditions, for a general anisotropic continuum in four dimensions [12, see pp. 50–53],

$$E^{\mu\nu\alpha\beta}\varepsilon_{\alpha\beta} = T^{\mu\nu} \tag{7}$$

where $\varepsilon_{\alpha\beta}$ is the strain tensor, $T^{\mu\nu}$ is the energy-momentum stress tensor, and $E^{\mu\nu\alpha\beta}$ is the elastic moduli tensor.

The Spacetime Continuum is further assumed to be isotropic and homogeneous. This assumption is in agreement with the conservation laws of energy-momentum and angular momentum as expressed by Noether's theorem [13, see pp. 23–30]. For an isotropic medium, the elastic moduli tensor simplifies to [12]:

$$E^{\mu\nu\alpha\beta} = \bar{\lambda}_0(g^{\mu\nu}g^{\alpha\beta}) + \bar{\mu}_0(g^{\mu\alpha}g^{\nu\beta} + g^{\mu\beta}g^{\nu\alpha}) \tag{8}$$

where $\bar{\lambda}_0$ and $\bar{\mu}_0$ are the Lamé elastic constants of the Spacetime Continuum as seen previously in Section 2. Substituting (8) into (7), we obtain the stress-strain relation (1) seen previously in Section 2, for an isotropic and homogeneous Spacetime Continuum. The Spacetime Continuum is thus modelled as an elastic medium (see [3, pp. 16–18,24]).

Blair [14, p. 3–4] writes Einstein's field equation as

$$\mathbf{T} = \frac{c^4}{8\pi G}\,\mathbf{G}\,, \tag{9}$$

where $\mathbf{T}$ is the stress energy tensor, $\mathbf{G}$ is the Einstein curvature tensor and G is the universal gravitational constant. He notes the very large value of the proportionality constant. This leads him to point out that spacetime is an elastic medium that can support waves, but its extremely high stiffness means that extremely small amplitude waves have a very high energy density. He notes that the coupling constant $c^4/8\pi G$ can be considered as a modulus of elasticity (K) for spacetime. In similarity to the acoustic case, where the specific impedance $z = K/v$, he identifies the quantity c^3/G with the characteristic impedance of spacetime [14, p. 45].

Substituting for the Einstein curvature tensor in (9), the equation becomes

$$T^{\mu\nu} = \frac{c^4}{8\pi G}\,G^{\mu\nu} = \frac{c^4}{8\pi G}\left[R^{\mu\nu} - \tfrac{1}{2}\,g^{\mu\nu}R\right]. \tag{10}$$

For *STCED*, as seen in (7), the single modulus of elasticity of (10) is replaced by the elastic moduli tensor $E^{\mu\nu\alpha\beta}$ of rank 4, consisting of 256 components. For an isotropic and homogeneous Spacetime Continuum, the elastic moduli tensor is given by (8) and simplifies to two moduli, the shear modulus $\bar{\mu}_0$ for transverse waves and the bulk modulus $\bar{\kappa}_0$ for longitudinal waves, as seen previously in (1):

$$T^{\mu\nu} = 2\bar{\mu}_0\,\varepsilon^{\mu\nu} + \bar{\lambda}_0\,g^{\mu\nu}\varepsilon\,. \tag{11}$$

As shown in [2, §2.5], (10) and (11) can be combined and separated into a longitudinal relation

$$\frac{c^4}{8\pi G}\,R = 2(\bar{\mu}_0 + 2\bar{\lambda}_0)\,\varepsilon = 4\,\bar{\kappa}_0\,\varepsilon = \rho c^2 \tag{12}$$

where ρ is the rest-mass energy density present in the Spacetime Continuum, and a transverse relation

$$\frac{c^4}{8\pi G}\,R^{\mu\nu} = 2\bar{\mu}_0\,\varepsilon^{\mu\nu} - (\bar{\lambda}_0 + \bar{\mu}_0)\,g^{\mu\nu}\varepsilon \tag{13}$$

which becomes

$$\frac{c^4}{8\pi G}\, R^{\mu\nu} = 2\bar{\mu}_0 \left(\varepsilon^{\mu\nu} - \frac{1}{2}\, \frac{\bar{\lambda}_0 + \bar{\mu}_0}{\bar{\mu}_0}\, g^{\mu\nu}\varepsilon \right) \tag{14}$$

where $(\bar{\lambda}_0 + \bar{\mu}_0)/\bar{\mu}_0$ is a numerical factor.

We can derive the relationship between the Spacetime Continuum bulk modulus $\bar{\kappa}_0$ and known constants from relation (12) as follows:

$$\frac{c^4}{8\pi G}\, R = 4\,\bar{\kappa}_0\, \varepsilon\,, \tag{15}$$

where the constant $c^4/8\pi G$ has dimensions of [N], R has dimensions of $[\mathrm{m}^{-2}]$, $\bar{\kappa}_0$ has dimensions of $[\mathrm{N\,m}^{-2}]$ or $[\mathrm{J\,m}^{-3}]$, and ε is dimensionless. We need to express R as a dimensionless quantity and combine its constant factor with constant $c^4/8\pi G$. Curvature R is expressed in $[\mathrm{m}^{-2}]$. As shown in [15], the smallest Spacetime Continuum Burgers vector b_0 is equal to Planck's length

$$\ell_P = \sqrt{\frac{\hbar G}{c^3}}\,. \tag{16}$$

The curvature of this smallest surface element will be constant, such that we can write the curvature R as

$$R = \frac{\bar{R}}{\ell_P^2} \tag{17}$$

where $\bar{R}$ is the dimensionless curvature number in terms of the smallest surface element ℓ_P^2.

Substituting (17) and (16) into (15), we obtain

$$\frac{c^7}{8\pi\hbar G^2}\, \bar{R} = 4\,\bar{\kappa}_0\, \varepsilon\,, \tag{18}$$

where the units are $[\mathrm{N\,m}^{-2}]$. The dimensionless curvature $\bar{R}$ and, as seen in Section 2, the dimensionless volume dilatation ε corresponding to the change in volume per original volume $(\Delta V/V)$ [4, see pp. 149–152], result from the applied stresses leading to the deformation of the Spacetime Continuum.

The latter corresponds to the definition of the bulk modulus. The numerical factors can be included in the definition of the dimensionless curvature $\bar{R}$ and the dimensionless volume dilatation ε to obtain

$$\frac{c^7}{\hbar G^2}\, \frac{\bar{R}}{8\pi} = \bar{\kappa}_0\, (4\varepsilon)\,. \tag{19}$$

One option is to equate the terms having dimensions of $[\mathrm{N\,m}^{-2}]$ to obtain the Spacetime Continuum bulk modulus, with the understanding that there may be a numerical factor on the R.H.S. of (20):

$$\bar{\kappa}_0 = \frac{c^7}{\hbar G^2}\,. \tag{20}$$

From one of my previous articles [1, Eq. (150)], we then have

$$\bar{\mu}_0 = 32\bar{\kappa}_0 = 32\, \frac{c^7}{\hbar G^2}\,. \tag{21}$$

Numerically, $\bar{\kappa}_0 = 4.6\times10^{113}\,\mathrm{J/m^3}$ and $\bar{\mu}_0 = 1.5\times10^{115}\,\mathrm{J/m^3}$.

With these constants, we are now in a position to calculate the density of the Spacetime Continuum $\bar{\rho}_0$. Using the relation [1]

$$c = \sqrt{\frac{\bar{\mu}_0}{\bar{\rho}_0}}, \tag{22}$$

the density of the spacetime continuum is

$$\bar{\rho}_0 = 1.7 \times 10^{98}\,\mathrm{kg/m^3}. \tag{23}$$

This value is in the same ballpark as the vacuum energy density calculated by Carroll [16, see p. 173] ($\sim 10^{112}\,\mathrm{ergs/cm^3}$) from quantum mechanical considerations.

5 Mass in the Spacetime Continuum

We have considered the origin of inertial mass in the Spacetime Continuum in [17], where we showed that integrating (5) over the 3-D space volume,

$$\int_{V_3} \rho c^2\, \mathrm{d}V_3 = 4\bar{\kappa}_0 \int_{V_3} \varepsilon\, \mathrm{d}V_3\,, \tag{24}$$

and using

$$m = \int_{V_3} \rho\, \mathrm{d}V_3 \tag{25}$$

in (24), where m is the rest mass of the deformation, we obtain

$$mc^2 = 4\bar{\kappa}_0 \int_{V_3} \varepsilon\, \mathrm{d}V_3\,. \tag{26}$$

This demonstrates that mass is not independent of the Spacetime Continuum, but rather mass is part of the Spacetime Continuum fabric itself. Hence mass results from the dilatation of the Spacetime Continuum in the longitudinal propagation of energy-momentum in the Spacetime Continuum. Matter does not warp spacetime, but rather, matter *is* warped spacetime (i.e. dilated spacetime). The missing link in General Relativity is the understanding that the trace of the energy-momentum stress tensor is related to the trace of the Spacetime Continuum strain tensor and is proportional to the mass of matter as given by (5) and (26).

6 Discussion and conclusion

In this paper, we have summarized the nature of the Spacetime Continuum (*STC*) as provided by the Elastodynamics of the Spacetime Continuum (*STCED*), which provides a better understanding of general relativistic spacetime. We have shown that the dimensionality of the Spacetime Continuum could be deduced mathematically if the value of the Lamé elastic constants $\bar{\kappa}_0$, $\bar{\mu}_0$ and $\bar{\lambda}_0$ of the Spacetime Continuum

could be determined experimentally. From Einstein's field equation for an isotropic and homogeneous STC, we derive the value of the Spacetime Continuum bulk modulus $\bar{\kappa}_0$ in terms of elementary constants.

STCED provides a physical model of the nature of inertial mass, which also includes an explanation for wave-particle duality. Mass is shown to be the invariant change in volume of spacetime in the longitudinal propagation of energy-momentum in the spacetime continuum. Hence mass is not independent of the spacetime continuum, but rather mass is part of the spacetime continuum fabric itself.

Received on December 23, 2022

References

1. Millette P. A. Elastodynamics of the Spacetime Continuum. *The Abraham Zelmanov Journal*, 2012, vol. 5, 221–277.
2. Millette P. A. Elastodynamics of the Spacetime Continuum: A Spacetime Physics Theory of Gravitation, Electromagnetism and Quantum Physics. American Research Press, Rehoboth, NM, 2017.
3. Millette P. A. Elastodynamics of the Spacetime Continuum, Second Expanded Edition. American Research Press, Rehoboth, NM, 2019.
4. Segel L. A. Mathematics Applied to Continuum Mechanics. Dover Publications, New York, 1987.
5. Minkowski H. Space and Time. 80^{th} *Assembly of German Natural Scientists and Physicians*. Cologne, 21 September 1908. English translation reprinted in Lorentz H. A., Einstein A., Minkowski H, and Weyl H. The Principle of Relativity: A Collection of Original Memoirs on the Special and General Theory of Relativity. Dover Publications, New York, 1952, pp. 73–91.
6. Petkov V. Relativity and the Nature of Spacetime, 2^{nd} ed. Springer, New York, 2009, pp. 111–114.
7. Petkov V. Inertia and Gravitation: From Aristotle's Natural Motion to Geodesic Worldlines in Curved Spacetime. Minkowski Institute Press, Montreal, 2012, pp. 78–82.
8. Millette P. A. On Time Dilation, Space Contraction, and the Question of Relativistic Mass. *Progress in Physics*, 2017, vol. 13 (4), 202–255.
9. Millette P. A. On the Question of Acceleration in Special Relativity. *Progress in Physics*, 2017, vol. 13 (4), 215–219.
10. Kleinert H. Gauge Fields in Condensed Matter, Vol. II Stresses and Defects. World Scientific Publishing, Singapore, 1989.
11. Millette P. A. The Elastodynamics of the Spacetime Continuum as a Framework for Strained Spacetime. *Progress in Physics*, 2013, vol. 9 (1), 55–59.
12. Flügge W. Tensor Analysis and Continuum Mechanics. Springer-Verlag, New York, 1972.
13. Kaku M. Quantum Field Theory: A Modern Introduction. Oxford University Press, Oxford, 1993.
14. Blair D. G., ed. The Detection of Gravitational Waves. Cambridge University Press, Cambridge, 1991.
15. Millette P. A. The Burgers Spacetime Dislocation Constant b_0 and the Derivation of Planck's Constant. *Progress in Physics*, 2015, vol. 11 (4), 313–316.
16. Carroll S. M. Spacetime and Geometry: An Introduction to General Relativity. Addison Wesley, San Francisco, 2004.
17. Millette P. A. The Origin of Inertial Mass in the Spacetime Continuum. *Progress in Physics*, 2019, vol. 15 (2), 86–91.

Progress in Physics is an American scientifc journal on advanced studies in physics, registered with the Library of Congress (DC, USA): ISSN 1555-5534 (print version) and ISSN 1555-5615 (online version). The journal is peer reviewed.

Electronic version of this journal: http://www.ptep-online.com

Postal address:
Department of Mathematics and Science, University of New Mexico,
705 Gurley Avenue, Gallup, NM 87301, USA